

Structural and functional analysis of the *E. coli* cell division proteins

FtsL and FtsB

By

Samuel James Craven

A dissertation submitted in partial fulfillment of

the requirements for the degree of

Doctor of Philosophy

(Biochemistry)

at the

UNIVERSITY OF WISCONSIN-MADISON

2020

Date of final oral examination: 04/23/2020

The dissertation is approved by the following members of the Final Oral Committee:

Alessandro Senes, Associate Professor, Biochemistry

Ivan Rayment, Professor, Biochemistry

Michael Cox, Professor, Biochemistry

Katherine Henzler-Wildman, Associate Professor, Biochemistry

Richard Gourse, Professor, Bacteriology

Table of contents

Acknowledgments.....	iv
Abstract.....	viii
Abbreviations.....	x
Chapter 1: Introduction.....	1
1.1 Bacterial cell division.....	2
1.2 Bacterial cell division requires multiple membrane proteins.....	5
1.3 The <i>E. coli</i> divisome.....	7
1.3.1 The early divisome components establish the site of division.....	9
1.3.2 The late divisome components regulate cytokinesis.....	12
1.3.3 Regulators of the Z-ring.....	17
1.3.4 Disassembly of the divisome and the multi-ring model.....	20
1.3.5 Advances in our understanding of divisome structure.....	21
1.4 Major unanswered questions of cell division.....	26
1.5 Review of dissertation chapters and appendices.....	28
1.6 References.....	31
Chapter 2: The FtsLB subcomplex of the bacterial divisome is a tetramer with an uninterrupted FtsL helix linking the transmembrane and periplasmic regions.....	46
2.1 Abstract.....	47
2.2 Introduction.....	48
2.3 Results and Discussion.....	54
2.3.1 Co-evolutionary analysis identifies potential quaternary contacts consistent with an extended helical bundle.....	54
2.3.2 A continuous FtsL helix and a discontinuous FtsB.....	56
2.3.3 FtsLB is a higher oligomer, likely an L_2B_2 tetrameric complex.....	57
2.3.4 Molecular modeling of the FtsLB helical bundle.....	60
2.3.5 Molecular dynamics suggest a stable TM region with an intricate network of hydrogen bonding.....	64
2.3.6 A continuous FtsL helix and a dynamic coiled coil.....	67
2.3.7 Functional analysis: the effect of mutations in the TM region is consistent with the predicted interface.....	69
2.3.8 The juxtamembrane and coiled coil of FtsB are tolerant to mutation.....	74
2.3.9 Integrity of the juxtamembrane and coiled-coil regions of FtsL is essential for function.....	76
2.4 Conclusions.....	78
2.5 Experimental Procedures.....	80
2.5.1 Co-evolutionary analysis.....	80
2.5.2 Modeling the TM region of FtsLB.....	80
2.5.3 Modeling the coiled-coil domains of FtsL and FtsB.....	83
2.5.4 Modeling the juxtamembrane regions of FtsL and FtsB.....	83
2.5.5 All-atom molecular dynamic simulations.....	84
2.5.6 Cloning, expression, purification and labeling of FtsLB constructs for FRET measurements.....	85
2.5.7 FRET measurements.....	88
2.5.8 Fitting of experimental FRET data to obtain the number of subunits.....	89

2.5.9 Bacterial strains, plasmids and media for <i>in vivo</i> experiments.....	91
2.5.10 Depletion strain experiments.....	91
2.5.11 Microscopy and cell length measurement.....	92
2.5.12 Whole-cell lysate preparation and Western Blotting.....	92
2.6 Supplemental information.....	94
2.7 Acknowledgments.....	113
2.8 Author contributions.....	113
2.9 References.....	114
Chapter 3: Structural and functional analysis of the <i>E. coli</i> FtsLB periplasmic domain.....	123
3.1 Abstract.....	124
3.2 Introduction.....	125
3.3 Results.....	132
3.3.1 The periplasmic domains of FtsL and FtsB contain multiple conserved polar and charged residues.....	132
3.3.2 Nonideal amino acids at the coiled-coil interface are important for function.....	133
3.3.3 The charge identity of nonideal FtsL residues has functional relevance..	137
3.3.4 Circular dichroism spectra reveal structural effects of the nonideal coiled-coil interface.....	140
3.3.5 Remodeling the FtsLB coiled coils to accommodate nonideal residues..	142
3.3.6 The FtsB flexible juxtapamembrane linker is constrained for length.....	144
3.3.7 Snapshots of the FtsLB MD trajectories are tolerant of deletions.....	146
3.3.8 A potential FtsB alanine interface is not crucial for function.....	147
3.4 Conclusions.....	149
3.5 Experimental Procedures.....	150
3.5.1 Plasmid cloning.....	150
3.5.2 Bacterial strains, plasmids, and media for <i>in vivo</i> experiments.....	151
3.5.3 Depletion strain experiments.....	151
3.5.4 Microscopy and cell length measurements.....	152
3.5.5 Western blots.....	152
3.5.6 Protein expression and purification for CD.....	153
3.5.7 CD experiments.....	154
3.5.8 Bioinformatic analyses.....	155
3.5.9 Modeling the FtsLB complex.....	155
3.5.10 Modeling the effect of loop deletions in FtsB.....	156
3.6 Supplemental information.....	157
3.7 References.....	170
Chapter 4: Identification of interaction sites between the essential cell division proteins FtsL and FtsW.....	178
4.1 Abstract.....	179
4.2 Introduction.....	180
4.3 Results and discussion.....	184
4.3.1 Identification of the FtsW-interaction site in FtsL.....	184
4.3.2 Identification of the FtsL-interaction site in FtsW.....	189
4.3.3 In vitro binding between FtsLB and FtsW.....	195

4.3.4 The length and flexibility of an FtsL linker region may impact the interaction with FtsW.....	199
4.4 Conclusions.....	203
4.5 Materials and methods.....	205
4.5.1 Plasmid cloning.....	205
4.5.2 Bacterial strains, plasmids, and media for <i>in vivo</i> experiments.....	205
4.5.3 Depletion strain experiments.....	206
4.5.4 Microscopy and cell length measurements.....	207
4.5.5 Protein expression and purification for on-column binding.....	207
4.5.6 On-column binding experiments.....	209
4.6 Supplemental information.....	210
4.7 References.....	217
Chapter 5: Future directions and continuing work.....	222
5.1 Summary of dissertation: What have we learned?.....	223
5.2 What comes next?.....	224
5.2.1 Construction of dual-depletion strains.....	225
5.2.2 Obtaining better FtsLB thermodynamic data.....	227
5.2.3 Further characterization of FtsW interactions and function.....	228
5.2.4 X-ray crystallography and NMR spectroscopy studies of FtsLB structure.....	228
5.2.5 Cryo-EM on a subset of divisome proteins.....	231
5.3 Conclusion.....	231
5.4 References.....	232
Appendix 1 – FtsLB expression and purification.....	234
Appendix 2 – X-ray crystallography trials.....	241

Acknowledgments

Many people have impacted my journey through graduate school and my Madison life in general, so I want to take a few pages to acknowledge them here. First off, I would like to thank the current members of the Senes lab. Alessandro has been an excellent mentor and has challenged me to grow into the scientist that I am today. He has provided me with enough direct guidance to help keep me on track without micromanaging my work and stifling my independence as a researcher. Samson Condon has been my friend since we joined the IPiB program, and he has been one of my main outlets for discussing interests and hobbies outside of lab work. Samantha Anderson has provided me with a voice of reason and critical “outsider” observations about my projects, so I want to thank her for that as well as for continuing the “Sam” trend in the Senes lab (though I might be the only one who finds this more hilarious than annoying). Among all the Senes lab members, I know I can count on Gladys Díaz-Vázquez to provide honest feedback, so I would like to thank her for not pulling punches during group meeting. Gilbert Loiseau has been my bay mate for over two years now, so I am grateful to him for fun conversations and for dealing with my incessant distractions. Finally, I would like to thank the newer lab members – Joshua Choi, Tyler Peterson, and Samridhi Garg – for contributing to the friendly and collaborative atmosphere that has become a hallmark of the Senes lab. It is likely that I will be working directly with Tyler and Samridhi in the near future, so I would also like to thank them in advance for helping me move the various divisome projects forward.

There are also many former members of the Senes lab that deserve acknowledgment. Drs. Loren LaPointe and Ambalika Khadria helped train me on

various techniques and protocols for working with FtsLB, so I would like to thank them for patiently dealing with my constant questioning (especially Loren, who was my bay mate for a few years). Drs. Benjamin Mueller and Sabareesh Subramaniam also provided helpful insights and guidance during my early graduate school career. Deena Al Mahbuba had to leave the Senes lab earlier than we would have liked, but during her time here, she helped advance our divisome work greatly and also cooked us some excellent Bangladeshi cuisine (even if she did not properly warn me how spicy those green peppers were). Drs. Elizabeth Caselle and Kai Cai were both postdoctoral researchers who I interacted with regularly, so I would like to thank them for their expertise and insights into my research. Claire Armstrong was my bay mate during what was probably the most difficult years of graduate school for me, and I appreciate her letting me vent about research problems or just talk about anything not relating to my work. Claire Holesovsky was an undergraduate student who worked with me on various projects, and I never had to worry about the quality of her research or her work ethic, which made my job much easier. Finally, Xiangyang Liu was a previous undergraduate student who moved next door to my lab, and he is now my go-to friend when I want to play hooky from my research.

Outside of the Senes lab, there are various others who have greatly helped my research. I would like to thank my current and past committee members – Drs. Ivan Rayment, Mike Cox, Katie Henzler-Wildman, Rick Gourse, and Doug Weibel – for constantly challenging me and helping me to set ambitious but realistic goals for my research. I am also grateful to the various members of the Raman, Craig, Ntambi, Henzler-Wildman, Cox, Rayment, and Weibel labs for letting me use their equipment,

providing me with materials, and overall sharing their expertise with me whenever I wandered over to them for help. Specifically, I collaborated with Becky Phillips and Michael Andreas from the Rayment lab as well as John Crooks from the Weibel lab, each of whom spent significant time training me with various techniques. Finally, I would like to thank the IPiB class of 2013 for the time we spent complaining about our research, eating chicken wings, playing flong, and generally doing graduate school together.

I would not have been able to make it through graduate school without my network of Madison friends, so I feel the need to recognize them as well. There are too many people that deserve individual mention though, so I will have to group most of them by the different circles through which we interacted. To Aeli, you told me not to acknowledge you in my dissertation, so obviously I am going to; thank you for helping me deal with the stress of completing a PhD and for, in general, putting up with my snarky comments these past few months. To Zach, you also told me not to acknowledge you in my dissertation, so I won't. To my various roommates, thank you for intriguing conversations and for generally not destroying the apartment. To my friends from Blackhawk Church, thank you for helping me grow as a person and for supporting me during my many ups and downs. To my ultimate frisbee team (the aptly-named "Discertators"), thank you for tolerating my poor passing accuracy and my love of hammer throws; I plan to keep playing as long as I am in Madison, so you have not gotten rid of me just yet (Go Tots!). To my D&D party members, thank you for picking me up whenever I fall and for letting me experience just how ridiculous your imaginations can get. To my MTG group, I am sorry about the Mindslaver lock, but I never claimed to

be a good person. To the random friends who do not quite fit into a convenient group, thank you for enriching my life in your own unique way. Finally, to the various pets of my Madison friends, you are all good boys/girls, and I want you to know that you are the real MVP's of this dissertation.

Most importantly, I need to thank my family for their love and support through my life. To my parents, Jim and Carla Craven, thank you for always having my back; ultimately, I am who I am today due to the examples you set for me and your constant guidance from day one. To my sisters, Carly and Rita, thank you for teaching me the value of patience and always (lovingly) reminding me to keep humble. To my adorable nibblings, Joel, Rowan, and Kyan, thank you for making every Nashville visit exciting and unpredictable. To my grandmother, Juanita Adduci, thank you for being an all-around awesome grandma; I only hope I can have some measure of your fire when I become a grandparent. To my late grandfathers, Bill Kuduk and Nick Adduci, thank you for your unique (and sometimes confusing) senses of humor; life is not the same without you. Finally, to my numerous aunts, uncles, and cousins, thank you for making my life interesting (in a good way); now you can finally stop asking me when I will be done with school.

And to whoever is actually reading this dissertation, thank you for taking an interest in my work. This represents what is probably the largest endeavor of my life to this point, but ultimately, I believe I am a better scientist and person because of it.

Abstract

Cell division in bacteria is mediated by a multiprotein machine called the divisome, which is responsible both for directing constrictive force and remodeling the cell wall into a septum at midcell. In *Escherichia coli*, an essential component of the divisome is the FtsLB complex, which is necessary for recruiting other proteins to the division site and is involved with triggering the final constriction event. The structural arrangement, specific functions, and interaction network of FtsLB are still poorly understood, and improved insights into the roles this essential complex plays would lead to a more complete understanding of cell division as a whole. In this dissertation, I will discuss a series of investigations from myself and collaborators that address how different structural aspects of FtsLB relate to its function. First, we establish via FRET that FtsLB forms a likely 2:2 heterotetramer and use a combination of co-evolutionary analysis and computational modeling to produce a structural model for the complex. These results suggest that the coiled coil of FtsLB is marginally stable due to an abundance of non-hydrophobic interfacial residues. To address a functional role for these residues, we use *in vivo* complementation experiments and incorporate our results into an alternative structural model. We also provide *in vivo* evidence that FtsB contains a flexible linker region, whereas FtsL is a continuous, rigid helix. Finally, we identify potential binding sites between FtsL and the essential cell wall synthase FtsW using both *in vivo* complementation and *in vitro* binding assays. Together, these studies suggest that distinct structural features of FtsLB – namely its tetrameric arrangement, marginally stable coiled coil, and site of interaction with FtsW – are critical components of divisome regulation. This has important implications for the study of bacterial cell division, as

improving our understanding of such a key regulatory component will ultimately lead to a better comprehension of the divisome as a whole.

Abbreviations

ABC: ATP-binding cassette

aBPB: class A penicillin-binding protein

ACN: acetonitrile

ATP: adenosine triphosphate

bBPB: class B penicillin-binding protein

bEBL: backbone-dependent Energy-Based Conformer Library

β ME: β -mercaptoethanol

CC: coiled coil

CCD: constriction control domain

CD: circular dichroism

CRISPRi: CRISPR interference

cryo-EM: cryogenic electron microscopy

DDM: *n*-dodecyl- β -D-maltopyranoside

DM: *n*-decyl- β -D-maltopyranoside

DPC: dodecylphosphocholine

EDTA: Ethylenediaminetetraacetic acid

FRET: Förster (fluorescence) resonance energy transfer

Fts: filamentous temperature sensitive

GFP: green fluorescent protein

GlcNAc: *N*-acetylglucosamine

GTase: glycosyltransferase

GTP: guanosine triphosphate

HEPES: 4-(2-hydroxyethyl)-1-piperazineethanesulfonic acid

HSQC: heteronuclear single quantum coherence

IM: inner membrane

IMP: integral membrane protein

IPTG: isopropyl- β -D-1-thiogalactoside

LB: lysogeny broth

LDAO: lauryldimethylamine oxide

MCS: multiple cloning site

MD: molecular dynamics

MP: membrane protein

MSA: multiple sequence alignment

MSL: Molecular Software Library

MurNAc: *N*-acetylmuramic acid

NMR: nuclear magnetic resonance

NTA: nitrilotriacetic acid

OD₆₀₀: optical density at 600 nm

PAGE: polyacrylamide gel electrophoresis

PBP: penicillin-binding protein

PDB: Protein Data Bank

PEG: polyethylene glycol

PG: peptidoglycan

PMSF: phenylmethylsulfonyl fluoride

RMSD: root mean square deviation

rTEV: recombinant tobacco etch virus

SDS: sodium dodecyl sulfate

SEDS: shape, elongation, division, and sporulation

sfGFP: superfolder green fluorescent protein

TCEP: tris(2-carboxyethyl)phosphine

TFA: trifluoroacetic acid

TFE: 2,2,2-trifluoroethanol

TM: transmembrane

TMD: transmembrane domain

TPase: transpeptidase

WT: wild type

Chapter 1: Introduction

1.1 Bacterial cell division

In the most basic terms, bacterial cell division can be described as the process by which a single mother cell splits in half to form a pair of genetically identical daughter cells. On the surface, cell division seems rather straightforward, but its apparent simplicity belies an incredibly complex process involving interactions between the chromosome, the cell envelope, and an ever-expanding list of essential and nonessential proteins. Even the decision of where and when to divide requires extensive cellular coordination, as misregulated division events can have disastrous results for the cell. For example, if the mother cell were to divide before the chromosome completed replication and segregation into the daughter cells, then the closing septum would shear the chromosome in half and one or both of the new daughter cells would meet an untimely death. The same would happen if the septum were established over one of the newly replicated chromosomes instead of between them. Alternatively, if the division site were to form at the pole of the mother cell, then the replicated chromosomes would not be partitioned into new daughter cells, leading to energetically wasteful division events. Due to the importance of proper positioning and timing of cell division, bacterial cells have evolved multiple systems to tightly regulate both; however, knowing where and when to divide is only half the battle. The bacterial cell must also undergo extensive reorganization of the cell envelope for cytokinesis (the physical process of cell division) to occur. Depending on the bacterial species, this involves coordination of various events at the cell wall and one or two lipid membranes, each of which must invaginate at the division site and eventually pinch off to form poles for the new daughter cells. Finally, numerous environmental factors such as nutrient

availability, pH, and osmolarity influence cell division as well (1), which further increases the requirement for comprehensive regulatory mechanisms.

The centrality of cell division to the bacterial life cycle necessitates detailed research into its various aspects. The better we understand the intricacies of cell division, the better we understand how cells grow in general, which has important implications for all research involving bacteria. Cell division research also has major clinical relevance, specifically within the realm of antibiotic drug development. For example, discovery of the penicillin family of antibiotics was a major leap forward in the arms race against bacterial infection, and these antibiotics are known to target certain cell division proteins. Unfortunately, many pathogens have developed resistance to penicillins (and other antibiotics as well), and we are constantly in need of novel antibacterial strategies. Since a wide range of bacterial species rely on similar machinery for division, each of the essential cell division proteins provides an excellent potential target for novel drug studies. This is further compounded by the fact that eukaryotic cells divide by completely different mechanisms from bacterial cells, and therefore drugs targeting these bacterial proteins are less likely to have unintended side effects on the host. Furthermore, many of the bacterial division proteins are positioned towards the cell exterior, and this localization greatly facilitates drug targeting as many drugs either are excluded from entering the cell interior (the cytoplasm) or are quickly pumped back out. Altogether, the cell division machinery represents one of the most promising current directions for antibiotic development, but rational drug design requires further research into the structures and functions of the various proteins involved.

At the heart of bacterial cell division lies the multiprotein divisome complex, which assembles into a ring-like structure at the division site (2). This complex can take on a variety of forms depending on the bacterial species, but for the most part, all bacteria with cell walls (as well as some archaea, mitochondria, and chloroplasts) have a divisome of some sort (3, 4). For the purposes of this dissertation, I will focus primarily on cell division within *Escherichia coli* and will use the nomenclature adopted for the *E. coli* divisome components. I will also describe these various components according to their known roles within *E. coli* specifically, even though certain components may not exist or may have different characteristics within other bacterial species. Before I can discuss the *E. coli* divisome, however, some basic information on the bacterium itself is needed. *E. coli* is one of the most widely employed model organisms for microbiology research, and indeed, the majority of cell division research has been performed within this bacterium. However, much of our understanding of cell division has also come from studies within other bacteria, including *Bacillus subtilis* and *Caulobacter crescentus* (5, 6). *E. coli* is a rod-shaped, Gram-negative bacterium, which means it contains both an inner and outer membrane, as compared to Gram-positive bacteria, which only have a single cytoplasmic membrane. Gram-negative bacteria have a relatively thin cell wall or peptidoglycan (PG) layer (compared to a much thicker PG in Gram-positive bacteria), which resides in the space between the two membranes (the periplasm). The various *E. coli* divisome components largely exist within the inner membrane or associate with it from either the cytoplasmic or periplasmic side; in other words, cell division is primarily mediated by membrane proteins.

1.2 Bacterial cell division requires multiple membrane proteins

Although the multitude of proteins within bacteria can be categorized by a near-limitless number of criteria, a common way to distinguish proteins is to group them by the environment in which they reside. Soluble proteins are those that float freely in either the cytoplasm or periplasm or are secreted into the extracellular environment. These proteins largely fold by burying hydrophobic residues in the interior of their tertiary structure, whereas hydrophilic residues are exposed to the surface to interact with the surrounding water-filled environment. Membrane proteins, on the other hand, are those that associate with a membrane in some way and can be further classified as integral membrane proteins (IMPs) or peripheral membrane proteins. IMPs pass through both leaflets of the membrane bilayer via one or more hydrophobic alpha helices or a barrel-like arrangement of beta strands (referred to as a beta barrel). Peripheral membrane proteins, on the other hand, interact with a single leaflet of the membrane in an often-reversible manner via amphipathic helices or through interactions with other membrane proteins. Both types of membrane proteins often contain soluble domains, but they are defined by their hydrophobic regions that enable favorable interactions with the membrane.

By spanning the lipid bilayer, IMPs are capable of bridging the two soluble environments separated by the membrane. For this reason, IMPs often function as transporters or signaling proteins that pass molecules or signals, respectively, across membranes. Not all IMPs function in this manner though, and numerous other enzymatic and structural roles are performed, which may or may not directly involve the transmembrane (TM) region of the protein. In these cases, the TM regions may facilitate

interactions within and between proteins or merely serve as anchors to sequester the protein to the membrane. Many IMPs have essential functions for cell survival, and obtaining detailed structural information of a wide range of IMPs is critically important. Unfortunately, a disproportionately low number of structures has been solved for IMPs (as compared to soluble proteins). Despite IMPs accounting for approximately 20-30% of genes within the average genome (7), less than 4% of structures within the Protein Data Bank are for IMPs (Feb. 2020 data from the PDB). This structural gap is not due to lack of effort, however, as IMPs and membrane proteins in general tend to be more recalcitrant to *in vitro* analyses such as X-ray crystallography and nuclear magnetic resonance (NMR) spectroscopy.

The difficulty in applying IMPs to *in vitro* experiments stems from several issues (8, 9). IMPs tend to be expressed at lower levels than soluble proteins, which is at least in part due to bottlenecking at the point of insertion into the membrane via the SEC translocon. This can result in a large fraction of the expressed protein forming inclusion bodies, which may or may not be recoverable for later use. IMPs also tend to have a higher density of hydrophobic residues, which can result in an increased tendency towards aggregation, especially when overexpressed for purification. Possibly the biggest problem for *in vitro* handling of IMPs, however, is the requirement for a membrane mimetic to keep the protein in solution. Common membrane mimetics include a wide range of detergents, spherical bilayers of lipids (liposomes), small disc-shaped lipid bilayers (bicelles), and bilayers wrapped by amphipathic proteins (nanodiscs), among other less common systems. The variety of options for membrane mimetics provides near-limitless potential to optimize the system for the protein under

study, but simply put, membrane mimetics are not the native membrane environment and therefore can lead to any number of defects on the structure and function of the protein. Combined with these potential defects, the mere presence of membrane mimetics tends to interfere with any downstream application of the protein. Regardless, we are constantly improving our methods to handle these problematic proteins, and the structural gap between soluble and membrane proteins will likely decrease in the years to come.

As discussed in the following sections, the majority of the essential divisome proteins are either single-pass or multi-pass IMPs. This has largely hampered extensive *in vitro* work with these proteins, which is evidenced by the primarily genetic nature of early divisome research and the general lack of complete structures for many of the components. Nevertheless, an abundance of detailed work over the past decades has provided us with an ever-growing understanding of how these proteins enable cell division. In the sections that follow, I will cover some of this divisome literature, focusing primarily on major topics that should serve as an entry point for those new to this specific field.

1.3 The *E. coli* divisome

Bacterial cell division has been a recognized process for as long as we have studied bacterial growth, but we have only known about many of the specific players involved for less than 30 years (6). These proteins were primarily discovered in *E. coli* through genetic screens that identified essential genes in which mutations disrupted the cell's ability to divide at elevated temperatures, eventually resulting in cell lysis and death.

Disrupting cell division does not immediately disrupt growth as a whole, however, and these mutations therefore resulted in cells that could continue DNA replication and lateral elongation but were unable to divide into distinct daughter cells. This phenotype of long, multinucleated cell filaments gave rise to the *fts* (filamentous temperature sensitive) nomenclature assigned to the various genes identified by the genetic screens. Currently, we have identified 12 essential divisome proteins (Fig. 1.1) along with a variety of others with redundant or accessory functions.

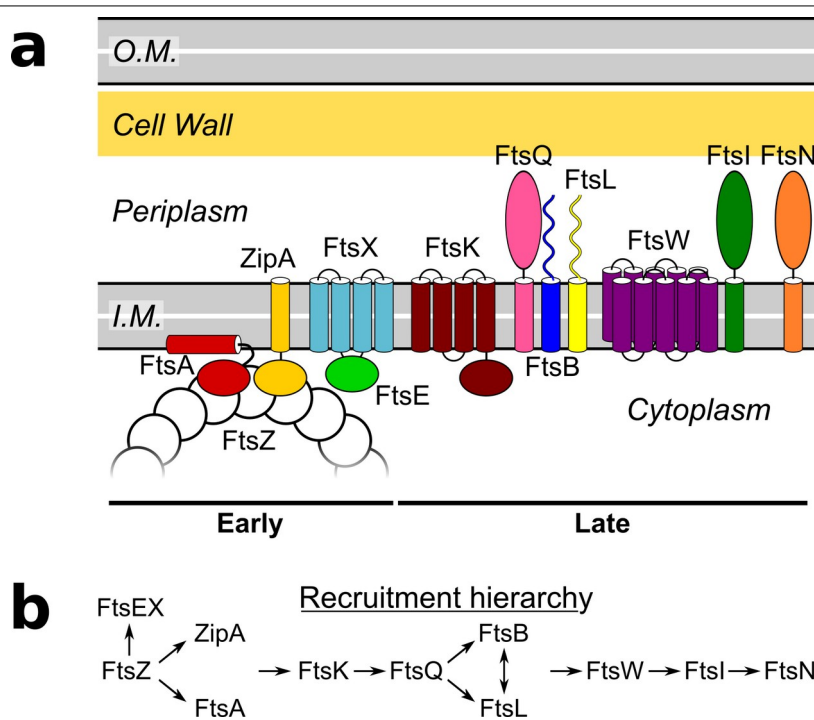


Figure 1.1. The *E. coli* divisome. a) Schematic representation of the essential proteins of the *E. coli* divisome separated by early and late components. Stoichiometries shown are not necessarily representative of the actual divisome. O.M. indicates the outer membrane; I.M. indicates the inner membrane. b) The divisome assembles in a roughly hierarchical manner, with arrows representing order of dependence for localization to the division site.

Localization of the essential divisome proteins to the division site occurs in a roughly hierarchical manner and can be split into two distinct steps (10): assembly of the early components to form the proto-ring (also called the FtsZ-ring or Z-ring) followed by recruitment of the late components to form a septum at the division site and complete cell division. The hierarchy of divisome assembly was largely determined through a variety of two-hybrid, co-immunoprecipitation, and fluorescence localization experiments (11–35), which revealed a somewhat linear dependency of recruitment (Fig. 1.1). In this hierarchy, localization of a divisome protein to the division site enables recruitment of the next protein, which in turn enables further recruitment of the downstream proteins. This is not a strict mode of recruitment, however, and certain proteins (e.g., FtsN) can localize earlier than indicated by the hierarchy.

1.3.1 The early divisome components establish the site of division

FtsZ is the first protein to localize in the divisome hierarchy and thus establishes the future site of division (36). As a tubulin homologue (37), FtsZ polymerizes into protofilaments at the cytoplasmic face of the inner membrane in a manner dependent on guanosine triphosphate (GTP) (38, 39). FtsZ filaments are extremely dynamic (40, 41) due largely to treadmilling activity (42, 43), in which individual FtsZ monomers assemble and disassemble at opposite ends of a filament. This results in directional movement of the entire filament without movement of the individual monomers within the filament. These FtsZ filaments can also laterally associate or bundle with each other (44) to form a semi-continuous ring around the circumference of the cell at the division site. This Z-ring serves as the primary scaffold upon which the rest of the divisome assembles, and it was initially proposed to provide the constrictive force that drives

cytokinesis at the division site (45). Indeed, *in vitro* experiments have shown that FtsZ is sufficient (in the presence of GTP) to cause constrictions in liposomes when anchored to the membrane directly via an amphipathic helix fusion or indirectly via the membrane-associated protein FtsA (46–48). However, though sufficient to constrict and potentially even divide liposomes (47), the Z-ring is now largely considered not to be the primary driving force behind cytokinesis within live cells. In fact, FtsZ leaves the division site before cytokinesis is completed (49, 50), which indicates that other divisome components must be responsible for the ending stages of division. Instead, the rate of septum closure seems largely dependent on cell wall synthesis activity (51, 52), which suggests that it is the inward growth of new PG at the septum that drives completion of cell division. This, of course, does not imply that the Z-ring provides no constrictive force to cytokinesis but that any force likely plays a more supportive role such as directing a switch from lateral to inward PG synthesis at the division site (53).

On its own, FtsZ is unable to interact with the membrane, so other divisome components are required to assemble FtsZ protofilaments at the division site. This tethering role is provided by the membrane-associated protein FtsA (54) and the IMP ZipA (55, 56), either of which alone is sufficient to attach FtsZ to the membrane (12, 13, 57, 58). FtsA and ZipA are not mere FtsZ anchors, however, as both proteins have important regulatory roles as well. A member of the actin family (54, 59), FtsA can self-associate into polymers dependent on adenosine triphosphate (ATP) (60–62), and its oligomerization state is a key aspect of cell division regulation (63–65). In current models, polymeric FtsA serves to help organize the Z-ring but prevents cell division from proceeding to the later stages (64). This occurs in part because polymeric FtsA inhibits

tight bundling of FtsZ protofilaments (62) and because the FtsA-FtsA interaction buries its 1C domain, which is necessary for recruiting late divisome components to midcell (25, 26, 66–69). Interactions with other divisome components (e.g., ZipA, FtsEX, and FtsN, as explained later) result in a switch from polymeric FtsA to monomeric (or less polymeric (62)) FtsA (70). This enables FtsZ protofilaments to reorganize into tight bundles and late divisome components to localize to midcell, resulting in a shift to active septal PG synthesis (62). ZipA is an important factor for this shift as it disfavors FtsA polymerization (64); however, the essentiality of ZipA can be bypassed by overexpression or mutation of other divisome components that generally promote FtsZ protofilament bundling or inhibit FtsA polymerization (64, 66, 69–72). ZipA may also function in protecting FtsZ from degradation (73) or in general Z-ring stability, but the ease of bypassing the essentiality of ZipA combined with its relatively poor conservation (compared to FtsA) throughout bacterial species (13) implies that ZipA plays a supporting role whereas FtsA is more central to cell division regulation.

The last of the essential components to form the early divisome is an ATP-binding cassette (ABC) transporter-like complex, which consists of the cytoplasmic ATP-binding protein FtsE and the IMP FtsX (74–76). Only recently have we begun to appreciate the varied roles that the FtsEX complex plays in cell division, as it was originally assumed to merely be involved in stabilizing the divisome and assisting in its assembly (27). This was largely due to the ease of bypassing FtsEX essentiality, seeing as osmoprotectants, low temperature, and overexpression or mutation of various other divisome components are each known to allow division in the absence of FtsEX (27, 76–78). Recent models have emerged, however, in which FtsEX acts in both the

cytoplasm and periplasm to coordinate divisome assembly with septal PG remodeling. During the early stages of cell division, FtsEX interacts with FtsA to inhibit its polymerization and thereby promote recruitment of downstream divisome proteins, and this interaction may also inhibit triggering of cytokinesis until the appropriate time (78). When cell division is ready to be completed, the ATPase activity of FtsE drives conformational changes in FtsX that both relieves the cytokinesis inhibition and activates nonessential PG hydrolases (AmiA and AmiB) in the periplasm via interactions with the regulatory protein EnvC (78–80). How exactly these various roles are accomplished in the absence of FtsEX is still unclear, but the complex interaction network within the divisome and functional redundancy among its various members likely explains at least part of this, especially in the optimal conditions for divisome stability (i.e., high osmolarity and/or low temperature) in which FtsEX becomes nonessential (77).

1.3.2 The late divisome components regulate cytokinesis

After the early divisome components form the Z-ring and establish the site of division, the remainder of the complex localizes to the division site to mediate reorganization of septal PG and trigger cytokinesis. The first of these late divisome components is the IMP FtsK, which is recruited to midcell via interactions with FtsZ and/or FtsA (15, 24, 57, 81, 82). Some of the functions of FtsK are known, but its overall role in cell division remains enigmatic. The C-terminal, cytoplasmic domain of FtsK has DNA translocase activity, which is involved with partitioning chromosomes into daughter cells and thereby preventing obstruction of the closing septum (83–86). DNA-based septal obstructions (e.g., chromosome dimers) only form in a small proportion of cells,

however, so this FtsK activity is not essential for survival of the population (83, 85). The N-terminus of FtsK consists of four TM helices followed by a cytoplasmic linker region that together provide the essential function of the protein (15, 16, 83, 87–90). The exact details of this function are still poorly understood, but it at least partly involves recruitment of downstream proteins to the division site (21). As is the case with FtsEX, the essentiality of the FtsK N-terminus can be bypassed relatively easily (87, 90–92), which suggests some functional redundancy with other divisome components. Overall, the combined functions of the N-terminal and C-terminal regions of FtsK have been proposed to provide a checkpoint of sorts for coordinating cytokinesis with chromosome partitioning (90, 93, 94), though mechanistic details for such a function are still lacking.

The next step in the recruitment hierarchy involves localization of a complex comprising the essential single-pass TM proteins FtsQ, FtsL, and FtsB (23, 95, 96). The first of these to arrive is technically FtsQ, which can localize to midcell in an FtsK-dependent manner (21, 33) apart from FtsL and FtsB (19, 23), but the FtsQLB complex can also assemble independent of the rest of the divisome and presumably localize to midcell all at once (28). Originally, the FtsQLB complex was assumed to merely act as a scaffold enabling recruitment of downstream proteins (97), but recent advances in our understanding of the late cell division stages have clarified a more nuanced role for this complex in divisome regulation. The major paradigm shift for FtsQLB function came in 2015, when two separate groups identified gain-of-function mutations within FtsL and FtsB that enabled survival in the absence of the normally essential divisome protein FtsN (65, 72). This led to a model in which FtsQLB (or potentially just FtsLB) exists in either an “off” or “on” state, which determines when the final stages of cell division will

trigger (98). FtsN is normally required to convert FtsQLB from the “off” to “on” state (among its other functions, as discussed later), and the gain-of-function mutations in FtsL and FtsB force the complex into the “on” state so that cell division occurs prematurely (65, 72). Exactly what constitutes the difference between the “off” and “on” states of FtsQLB is still unclear; however, recent findings have implicated derepression of septal PG synthases as a possibility. Specifically, individual components of FtsQLB were shown *in vitro* to repress the activities of two divisome PG synthases, PBP1b and FtsI (99), and removal of this repression may be an aspect of FtsQLB-mediated regulation. In addition, FtsQLB may physically sequester PG synthases away from sites of active synthesis. This could occur through a recently-proposed mechanism (100, 101) in which PG synthases (presumably through interactions with FtsQLB in the “off” state) track along the depolymerizing ends of treadmilling FtsZ protofilaments until FtsN disrupts the interaction (by converting FtsQLB to the “on” state) and enables the synthases to instead localize to sites of active PG synthesis. Further clarification of this FtsQLB-mediated regulation will require a detailed understanding of the complex itself, which is why the structure and function of FtsL and FtsB are the major focuses of this dissertation. As such, these proteins will be discussed in greater detail in the chapters to come.

In order to remodel the cell wall into a septum that will separate the nascent daughter cells, three distinct enzymatic activities are required. These enzyme types have been reviewed in detail elsewhere (5, 102, 103), but in short, glycosyltransferases (GTases) and transpeptidases (TPases) function as synthases to construct new PG layers, whereas hydrolases break down old PG so new material can be inserted. Each

of these PG layers consists of a meshwork of polysaccharide chains linked together via short peptides. The precursor molecule for these chains is lipid II, which comprises a disaccharide of an *N*-acetylmuramic acid (MurNAc) pentapeptide linked to *N*-acetylglucosamine (GlcNAc) and anchored to the membrane via a lipid tail. Lipid II molecules are polymerized into chains via GTase enzymes (104), and the resulting chains are crosslinked by their pentapeptides via TPases. To make room for new PG material, various hydrolases like amidases, peptidases, and lytic transglycosylases are needed to break down portions of the old PG layer. This PG turnover activity is necessary for cell division to complete, but the redundancy of the various enzymes involved means that no individual hydrolase is considered an essential divisome component.

The major PG synthase activities during cell division are primarily relegated to three late divisome proteins: FtsW, FtsI, and PBP1b. FtsW is an essential ten-pass IMP (105, 106) that is recruited to the division site primarily through an interaction with the cytoplasmic tail of FtsL (35). FtsW is a member of the recently characterized SEDS (shape, elongation, division, and sporulation) family of proteins (107, 108) and was originally proposed to be a lipid II flippase (109–111) (an enzyme that flips lipids from the inner to outer leaflet of the membrane bilayer). Our understanding of FtsW function has shifted greatly within the past few years though, as it is now largely considered to be the primary division-specific GTase (107, 112). FtsW GTase activity is stimulated through interactions with the essential single-pass IMP FtsI (PBP3) (112). As a class B penicillin-binding protein (bPBP), FtsI contains a periplasmic TPase domain that partners with the GTase activity of FtsW to synthesize septal PG (113–116). FtsI TPase

activity can be repressed *in vitro* by FtsQ (99), which suggests that FtsQLB-mediated regulation of cell division occurs in part through FtsI (and possibly FtsW, as well). Such inhibition of PG synthase activity may be at the core of the “off” to “on” switch during late cell division, as the GTase activity of the third major divisome PG synthase, PBP1b (117), can also be repressed *in vitro* by FtsLB (99). As a class A penicillin-binding protein (aPBP), PBP1b contains distinct periplasmic GTase and TPase domains (118), but despite this dual functionality, it is actually considered a nonessential divisome protein. This is due to the presence of another nonessential aPBP, called PBP1a, which allows survival in the absence of PBP1b (with some mild defects) (119, 120). Lack of both PBP1b and PBP1a is lethal (120), however, which indicates that at least one aPBP is required in addition to the FtsWI complex. It is unclear how exactly the synthase activities of PBP1b are implemented during cell division relative to those of FtsWI, but PBP1b may enable PG synthesis at midcell prior to septum formation (121) (and therefore prior to midcell localization of FtsWI) or may otherwise provide polymerization/crosslinking events that are spatially distinct but coordinated with those performed by FtsWI (102, 122). This is supported by the knowledge that PBP1b interacts with FtsWI (111, 115, 123), but more detailed analyses of these proteins in complex are required before we can understand how the various PG synthases are coordinated during cell division.

The last essential protein to localize to the division site is the single-pass IMP FtsN (124, 125). This designation as “last” is slightly inaccurate, seeing as FtsN is known to interact with various upstream divisome components (24, 29, 33, 67, 126, 127) and is likely to localize in small amounts throughout the course of divisome assembly (68).

Regardless, the upstream divisome components can normally localize to midcell without FtsN (21), whereas efficient FtsN accumulation requires the other components (22, 125), so it is referred to as the last component. FtsN contains three distinct domains of importance for its function within cell division (128): 1) an N-terminal, cytoplasmic domain that interacts with the 1C domain of FtsA and likely inhibits FtsA oligomerization (25, 26, 67, 68), 2) a periplasmic, juxtamembrane E-domain that provides the essential function of FtsN (129), possibly by promoting the “on” state of FtsQLB (65, 72), and 3) a C-terminal SPOR domain that binds to cleaved PG produced at the septum during active cell division (129–131). FtsN also functions in recruiting nonessential PG amidases and amidase-regulating proteins to midcell (132, 133), though this may be an indirect effect due to activation of PG synthesis. The varied interactions between FtsN and other divisome proteins as well as the identification of mutations within specific divisome proteins that enable bypass of FtsN function (65, 71, 72, 78) have resulted in a model in which FtsN acts as part of a positive feedback loop to trigger completion of cell division (65, 69, 72, 129). In this model, both the inhibition of FtsA oligomerization by the FtsN cytoplasmic tail and the activation of FtsQLB by the FtsN E-domain result in septal PG remodeling that provides new substrate for SPOR domain binding. This in turn recruits more FtsN to midcell which strengthens the “on” state of the late divisome and propels cytokinesis forward.

1.3.3 Regulators of the Z-ring

As discussed earlier, serious complications for a bacterium (e.g., death) can result if cell division is not properly regulated in terms of both timing and location within the cell. It is therefore not surprising that *E. coli* has evolved multiple systems that regulate when

and where the divisome forms. This regulation is generally performed at the level of Z-ring assembly as this enables control at the earliest stages of the divisome hierarchy. However, despite the importance of these systems for proper divisome assembly, they are considered nonessential to survival as their removal only causes complications in a portion of the total bacterial population and because each system has some functional overlap with the others (134).

One of the primary reasons to regulate Z-ring formation is that cytokinesis cannot safely occur through a region of the cell otherwise occupied by a chromosome. Completing cytokinesis in this case would entail shearing the chromosome in half, so division must be inhibited wherever DNA is present. This form of regulation is referred to as nucleoid occlusion, and it is mediated primarily through the cytoplasmic protein SlmA (135). SlmA binds to specific sites within the chromosome and acts as a potent Z-ring inhibitor by promoting depolymerization of FtsZ protofilaments (136). Before chromosome replication completes, DNA-bound SlmA resides at midcell and prevents Z-ring formation there (135). Following replication and segregation of the new chromosomes, a DNA-less void is produced at midcell, and the corresponding lack of SlmA enables Z-ring formation and subsequent cell division to occur there.

DNA is generally absent from the cell poles as well, and therefore another system besides nucleoid occlusion is needed to prevent wasteful polar division events. This is primarily accomplished through the actions of MinC, MinD, and MinE, which together act to prevent Z-ring formation away from midcell. In this Min system (134, 137), MinC disrupts both FtsZ polymerization and interactions between FtsZ and other divisome components. MinD and MinE do not directly interfere with the Z-ring but instead function

to accumulate MinC at the cell poles. This occurs through a complex oscillatory mechanism in which the membrane anchor MinD sequesters MinC at one pole while MinE releases MinCD from the membrane, causing migration to the other pole. The pattern of this oscillation results in a low average concentration of MinC at midcell, which allows Z-ring formation there.

Recently, a third system was identified that promotes Z-ring formation specifically at midcell. Referred to as Ter linkage, this system employs another DNA-binding protein, MatP, which binds to multiple sites within the Ter region of the chromosome (138). MatP also coordinates interactions with the Z-ring via the nonessential divisome components ZapB and ZapA (139). The Zap proteins are generally involved with Z-ring organization (140), and the midcell positioning of Ter regions combined with MatP-ZapAB interactions are thought to promote Z-ring formation at midcell even in the early stages of chromosome segregation (141). Together with the nucleoid occlusion and Min systems, Ter linkage promotes efficient midcell positioning of the Z-ring; however, at least one more unknown system is likely involved, seeing as Z-rings can still form to some extent at the proper location within cells missing all three of the other systems discussed (141).

Along with the midcell-positioning systems described above, two other more general systems – the SOS response and ClpXP protease complex – also regulate FtsZ as one of their many targets. The SOS response is triggered following DNA damage in the cell, and this invokes widespread changes in the expression of various proteins in order to fix the damage or prevent further harm before the damage is fixed (142). One such response protein is SulA, which inhibits the GTPase activity of FtsZ (143), thereby

preventing Z-ring formation and cell division in general from occurring (144). This provides the cell with extra time to fix the DNA damage before chromosome partitioning and cell separation need to be completed. On the other hand, the ClpXP protease complex is able to regulate Z-ring function by degrading FtsZ molecules (145). Excess FtsZ can disrupt cell division (146), and so proper regulation of FtsZ levels (specifically in relation to FtsA levels (147)) is a crucial aspect of Z-ring function.

1.3.4 Disassembly of the divisome and the multi-ring model

As our ability to visualize the finer details of the cell has improved, so too have we gained a deeper understanding of the spatiotemporal dynamics of the divisome. In particular, we now know that the divisome not only follows an assembly hierarchy, but it disassembles in an ordered manner as well. Presumably, the various divisome components have to eventually leave the division site anyways so they can be recycled for future use, and it follows that many of the early components in particular may become unnecessary as cell division progresses to the later stages. Residual cytoplasmic components could even occlude the closing septum, so their disassembly may be required before division can be completed. These ideas led to localization studies of the order of divisome disassembly, which revealed that the first components to localize to the division site are generally also the first to leave (49, 50, 148). For the early components, FtsZ and ZapA delocalize from the division site first, and this occurs well before cytokinesis completes (49, 50). FtsA and ZipA remain at the septum during closure but depart before the late components (50, 148). The FtsQLB complex is next in the disassembly pathway, and FtsI follows after (148). To mirror its recruitment to the division site, FtsN is last to leave, though it delocalizes in part with the earlier

components (148). These studies have not placed other core components like FtsEX, FtsK, FtsW, and PBP1b in the disassembly hierarchy, but it is reasonable to assume they also follow a similar pattern to the assembly hierarchy.

The disassembly order of the divisome supports a few models for its function and arrangement. The first model is that cytokinesis is driven forward primarily by PG synthesis instead of Z-ring contraction (51), as has already been discussed. The second model presents the divisome as multiple independent yet related rings instead of as a single cohesive complex. This idea is supported by super-resolution imaging experiments, which show spatial distinction between various divisome components (148–152). In current models (153, 154), three concentric rings exist as discrete structures with independent functions. The innermost ring contains at least ZapB and MatP and plays a nonessential role in regulating Z-ring function through interactions with ZapA. The middle ring contains cytoplasmic components (at least FtsZ, FtsA, ZipA, and ZapA) and provides the essential functions associated with the early divisome, including establishing the site of division, providing a scaffold for divisome assembly, and guiding cytokinesis. Finally, the outermost ring comprises the late periplasmic components (at least FtsQ, FtsL, FtsI, and FtsN), which regulate septal PG synthesis and drive cell division to completion. Details of how these rings interact within a dynamic divisome are still forthcoming, and these models will likely be updated in the near future.

1.3.5 Advances in our understanding of divisome structure

As discussed earlier, a major hurdle in cell division research is the overall lack of structural data for the various divisome components. This is largely due to the difficulty in determining structures for integral membrane proteins (IMPs), which compose the

majority of the essential divisome. Multiple partial structures and some full-length structures have been obtained from a variety of bacterial and archaeal species, however, and these data have provided invaluable clues for our understanding of divisome function. Below, I will present some divisome structures obtained via X-ray crystallography, NMR spectroscopy, cryogenic electron microscopy (cryo-EM), and computational modeling, and I will discuss how these structures have furthered the field of cell division research.

The early focus for structural divisome research centered on the components of the Z-ring, which is unsurprising considering their centrality to division initiation and their more soluble nature. A full-length crystal structure for FtsZ was solved over 20 years ago using the sequence from the extremophilic archaean *Methanocaldococcus jannaschii* (37). This structure provided a crucial step forward in our understanding of FtsZ function, as it clearly revealed homology to the tubulin family of GTPases. This resemblance had been previously suggested (155, 156) as FtsZ and tubulin share some sequence homology and have other similar attributes (e.g., GTP binding/hydrolysis and protofilament formation), but it was not until the actual structure was solved that accurate comparisons could be made between the two proteins (157). A few years later, a full-length FtsA crystal structure from *Thermotoga maritima* was obtained (54), which similarly confirmed its homology to actin (59). The same group later solved a crystal structure for an FtsA dimer in complex with a C-terminal peptide of FtsZ (61). For ZipA, two research groups determined partial structures for the C-terminal region (lacking the TM domain) of the *E. coli* variant. The first group solved crystal structures for ZipA alone and in complex with a C-terminal peptide of FtsZ (55), whereas the second group

produced a solution NMR structure for ZipA and mapped its interactions with FtsZ using NMR peak shifts (56). Overall, these structures for FtsZ, FtsA, and ZipA greatly advanced our understanding of the organization and dynamics of the Z-ring.

Since the last of the early divisome components, FtsEX, was only recently recognized as essential (158), its structural data are currently limited. Specifically, partial structures for the FtsX extracellular domain were obtained from *Mycobacterium tuberculosis* (159) (X-ray crystallography) and from *Streptococcus pneumonia* (160) (X-ray crystallography and NMR). These structures have important implications for understanding how FtsEX interacts with extracellular/periplasmic PG remodeling enzymes, but detailed structures of the full complex are still needed to elucidate the mechanisms behind its complex regulatory roles in cell division. In lieu of such structures, a computational model for *E. coli* FtsEX was built using homology modeling to other ABC transporters (161). This enabled identification of critical residues within the complex, but further validation of the model is still required.

A variety of structures have been solved for many of the late divisome components as well. Although the essential function of FtsK resides in its N-terminal TM region (87), more success has been achieved with determining structures for the soluble C-terminal DNA translocase domain. Various FtsK structures were obtained from *E. coli* and *Pseudomonas aeruginosa* using X-ray crystallography, NMR spectroscopy, and cryo-EM, and these structures provide important details on how the motor domain assembles alone and in complex with DNA (162–165). Crystal structures have also been solved for the periplasmic domain of FtsQ either alone (166) (*E. coli* and *Yersinia enterocolitica*) or in complex with the C-terminal tail of FtsB (167, 168) (*E. coli*). A crystal structure for the

coiled-coil region of *E. coli* FtsB is also available (169), but no structures have been solved for any region of FtsL. The mechanistic details behind the FtsQLB “off/on” switch that triggers cytokinesis are currently unclear (65, 72), and complete structures of these proteins (especially in complex) are sorely needed to clarify the events of late cell division. In the absence of such structures, computational models of full-length FtsLB have been proposed through a combination of co-evolutionary analyses and molecular dynamics (MD) simulations (170) (see Chapters 2 and 3), and these models provide an excellent basis for further experimentation.

The bacterial PG synthesis machinery contains some of the most prominent targets for established antibiotics, and improved structural information for these proteins will likely lead to development of novel antibacterial strategies. As targets for the penicillin family of antibiotics, FtsI and other penicillin-binding proteins (PBPs) like PBP1b are especially important candidates for structural studies. For this reason, numerous crystal structures have been solved from a variety of bacterial species for FtsI (116, 171–174) and PBP1b (117, 175–177) either alone or in complex with different antibiotics. Effective PBP antibiotics generally only target the TPase domains, however, and the rapid development of bacterial resistance demands that other avenues be addressed. Studies to develop antibiotics targeting the GTase domains of aPBPs are still ongoing and quite promising (178), and the recent identification of FtsW as the essential GTase for cell division (107, 112) introduces even more options for drug design. Although no structures have been solved yet for FtsW, a computational model has been proposed for *E. coli* FtsW in complex with the TM region of FtsI (179). This model was based on co-evolutionary analyses and structure prediction, and it is in good agreement with a

crystal structure (181) obtained for RodA (the elongation-specific GTase homologue of FtsW (107, 108, 180)) from *Thermus thermophilus*. Further structural validation is still required, but the computational model of FtsW represents a starting point for developing antibiotics that target this essential enzyme.

Finally, NMR spectroscopy revealed a structure for the C-terminal region of *E. coli* FtsN, which forms a commonly seen $\beta\alpha\beta\beta\alpha\beta$ topology (128). This region was later identified as a PG-binding SPOR domain, and other proteins have since been discovered to share similar functions based on the presence of their own SPOR domains (129). The structure for the remainder of FtsN is largely unclear, however, and obtaining a full-length structure (particularly in complex with other divisome components) would greatly aid our understanding of how the E-domain and N-terminal tail of FtsN function in coordinating the late stages of PG synthesis.

Eventually, we will likely obtain detailed structures for all the major divisome components, especially considering how far techniques for membrane protein structure determination have come within the past few decades. The recent cryo-EM boom (182), in particular, is extremely promising as this technique enables determination of high-resolution structures for large complexes of proteins. The divisome consists of multiple interacting protein complexes, and determining structures for such complexes would provide more detailed insights into divisome function than would individual structures in isolation. A major question in this regard is which proteins can form complexes stable enough for structural characterization. Certain divisome complexes like FtsQLB (28) and FtsWI/PBP1b (111) have already been purified *in vitro*, and even a larger complex comprising at least FtsZ, ZipA, FtsK, FtsQLB, and FtsN has been demonstrated via

native gel electrophoresis (183). Whether such complexes are conducive to structural determination still remains an open question, but the potential for obtaining crucial information on divisome arrangement and function warrants further research.

1.4 Major unanswered questions of cell division

As discussed throughout the preceding sections, there are still many holes remaining in our understanding of the divisome and cell division in general. The advent of super-resolution imaging has provided major progress in our models for the overall organization of the early divisome, but the extreme complexity and dynamic nature of the Z-ring have ensured that much remains to be clarified. Specifically, detailed insight into how FtsZ dynamics relate to Z-ring function and regulation of the late divisome components is sorely needed. FtsZ treadmilling has been shown to correlate to the spatiotemporal organization of PG synthases (42, 43, 100, 101), but further work is required to develop clear models explaining the mechanisms behind this regulation. Similarly, we are still lacking a complete understanding of the regulation of Z-ring placement and timing. Multiple regulatory systems have been characterized so far (i.e., the nucleoid occlusion, Min, and Ter linkage systems), but seeing as these systems are not completely necessary for proper Z-ring placement, it is likely that others remain to be identified (141).

Another hot topic in the divisome field (and the one I am personally most invested in) is how cytokinesis is regulated during the late stages of cell division. The proposal of distinct “off” and “on” states for FtsQLB and FtsA (65, 72) has opened numerous paths of inquiry, and we are only beginning to understand how all the various factors are

intertwined. Although the “off/on” nature of FtsA is generally presumed to involve changes in its oligomeric state (64), we do not yet have solid evidence as to how the FtsQLB complex manifests these states. Somehow, recruitment of FtsN to midcell triggers the activity of various PG enzymes through FtsQLB, but which factors are involved and the specific roles for each are still largely unclear at this point. Much of the confusion is due to the large number of completely or partially redundant PG remodeling enzymes for which we have a limited understanding, but even the major synthases like FtsW, FtsI, and PBP1b are still far from solved questions.

Another major cell division riddle is how the cell pinches off its envelope to form the new poles of the daughter cells after division has completed. It is likely that this process would require membrane fission and fusion proteins for both the inner and outer membranes, but the critical factors providing these functions have yet to be identified. The FtsK homologue SpolIIIE has been implicated in membrane fission during *B. subtilis* sporulation (184), which suggests that FtsK may play a similar role in cell division membrane fission. However, the ease of bypassing FtsK essentiality (87, 90, 91) indicates that it probably does not have such a unique role and may instead just enable proper divisome assembly.

Finally, as mentioned earlier, bacterial cell division studies have been largely performed within a select few species, and therefore our understanding of the diverse methods bacteria use to divide is relatively limited. Certain divisome components that are essential in *E. coli* are completely lacking in multiple other species (e.g., ZipA and FtsN), and various other species have their own essential proteins that are absent from the *E. coli* divisome. Obviously, *E. coli* is not the only important bacterium for study

(though it is probably the most well-characterized and therefore one of the easiest to manipulate), and the multitude of other bacterial species provides near-limitless opportunities for engaging cell division research.

1.5 Review of dissertation chapters and appendices

The majority of my graduate research has focused on obtaining a better understanding of the structure and function of the *E. coli* FtsLB complex. When I started graduate school in 2013, relatively little was known about this essential divisome complex, and it was largely assumed to merely have a scaffolding role in divisome assembly and enable recruitment of downstream components. Within the past five years, my field has gained a much stronger appreciation for the intricate role that FtsLB plays in regulating initiation of cytokinesis. However, as our understanding of FtsLB deepens, we become increasingly in need of detailed information explaining how the various aspects of the complex function within itself and in relation to the rest of the divisome. To address these questions, I have primarily taken an *in vivo* approach using complementation experiments to identify FtsLB mutations that disrupt cell division. These experiments are supported by biophysical and biochemical techniques using purified protein as well as by computational modeling to predict structure.

In Chapter 2, I present work published from my group in 2018 within The Journal of Biological Chemistry. In this paper, we used co-evolutionary analyses to identify interfaces within the FtsLB TM and coiled-coil regions and rationalized the need for a non-helical, juxtamembrane region in FtsB to properly align the TM and coiled-coil registries. We also established a likely 2:2 heterotetrameric arrangement for the FtsLB

complex using *in vitro* Förster resonance energy transfer (FRET) and modeled such an arrangement using structural prediction algorithms and MD simulations. Finally, we performed *in vivo* complementation experiments to validate our predicted FtsLB models and to provide more information on the function of the complex, specifically pertaining to flexibility in the juxtamembrane FtsB region and rigidity throughout FtsL.

In Chapter 3, I present my research that further addresses questions raised by our 2018 paper. This work is almost complete and will be submitted for publication in the near future. I show that multiple nonideal amino acids exist within the coiled-coil region of FtsL and FtsB, and I use *in vivo* complementation experiments to demonstrate that these residues are important for FtsLB function. I also explore the relevance of charge identity within the nonideal FtsL residues. I further address the function of the flexible juxtamembrane linker region in FtsB and show that it is constrained for length. I also present work that incorporates these results to further refine our computational models and develop alternative structural arrangements for FtsLB. Specifically, I propose that the nonideal coiled-coil residues of FtsLB may favor a pair of two-helix coiled coils for the periplasmic domain, which contrasts to the four-helix arrangement we had previously proposed.

In Chapter 4, I present my research that focuses on the interaction between FtsL and FtsW. This work is still in progress and will be submitted for publication during my postdoctoral training in the Senes lab. Through implementation of *in vivo* complementation experiments, I identified the likely FtsW-interaction site within the N-terminal, cytoplasmic tail of FtsL. I also identified potential residues in FtsW that may compose the corresponding FtsL-binding site. I also discuss the importance of a specific

cytoplasmic loop region in FtsW that is necessary for some function of FtsW aside from its interaction with FtsL. I present my ongoing research to demonstrate an FtsL-FtsW interaction *in vitro*, which would validate the binding sites identified *in vivo*. Finally, I discuss evidence that the length and flexibility of a linker region between the TM domain and FtsW-binding site of FtsL are important for proper cell division regulation.

In Chapter 5, I briefly summarize the preceding chapters, highlighting what I think to be the major findings from each. I also discuss future directions for my research, which includes projects currently underway as well as some that are still in their infancy. As I plan to remain in the Senes lab as a postdoctoral researcher after graduation, I will be personally attending to some of these projects and relegating others to some of our newer graduate students.

In Appendix 1, I provide a protocol I developed for expression and purification of FtsL and FtsB. Since both proteins are IMPs, they tend to express relatively poorly (especially when expressed alone), so finding optimal expression conditions was not as straightforward as could be expected. Similarly, isolating high-purity FtsLB requires some unconventional techniques, especially if FtsL and FtsB are to be separated from each other.

In Appendix 2, I present my *in vitro* work with soluble FtsB, FtsL, and FtsQ constructs. The bulk of this work was aimed at obtaining structures for FtsLB and/or FtsQLB via X-ray crystallography, but I also performed binding experiments to identify important residues within the C-terminal tails of FtsL and FtsB.

1.6 References

1. Haeusser DP, Levin PA. The great divide: coordinating cell cycle events during bacterial growth and division. *Curr Opin Microbiol.* 2008 Apr;11(2):94–9.
2. Du S, Lutkenhaus J. Assembly and activation of the *Escherichia coli* divisome. *Mol Microbiol.* 2017 Jul;105(2):177–87.
3. Cabeen MT, Jacobs-Wagner C. Bacterial cell shape. *Nat Rev Microbiol.* 2005 Aug;3(8):601–10.
4. Margolin W. FtsZ and the division of prokaryotic cells and organelles. *Nat Rev Mol Cell Biol.* 2005 Nov;6(11):862–71.
5. Egan AJF, Vollmer W. The physiology of bacterial cell division. *Ann N Y Acad Sci.* 2013 Jan;1277:8–28.
6. den Blaauwen T, Hamoen LW, Levin PA. The divisome at 25: the road ahead. *Curr Opin Microbiol.* 2017 Apr;36:85–94.
7. Wallin E, von Heijne G. Genome-wide analysis of integral membrane proteins from eubacterial, archaean, and eukaryotic organisms. *Protein Sci Publ Protein Soc.* 1998 Apr;7(4):1029–38.
8. Seddon AM, Curnow P, Booth PJ. Membrane proteins, lipids and detergents: not just a soap opera. *Biochim Biophys Acta.* 2004 Nov 3;1666(1–2):105–17.
9. Link AJ, Georgiou G. Advances and challenges in membrane protein expression. *AIChE J.* 2007;53(4):752–6.
10. Aarsman MEG, Piette A, Fraipont C, Vinkenvleugel TMF, Nguyen-Distèche M, den Blaauwen T. Maturation of the *Escherichia coli* divisome occurs in two steps. *Mol Microbiol.* 2005 Mar;55(6):1631–45.
11. Addinall SG, Lutkenhaus J. FtsA is localized to the septum in an FtsZ-dependent manner. *J Bacteriol.* 1996 Dec;178(24):7167–72.
12. Wang X, Huang J, Mukherjee A, Cao C, Lutkenhaus J. Analysis of the interaction of FtsZ with itself, GTP, and FtsA. *J Bacteriol.* 1997 Sep;179(17):5551–9.
13. Hale CA, de Boer PA. Direct binding of FtsZ to ZipA, an essential component of the septal ring structure that mediates cell division in *E. coli*. *Cell.* 1997 Jan 24;88(2):175–85.
14. Weiss DS, Pogliano K, Carson M, Guzman LM, Fraipont C, Nguyen-Distèche M, et al. Localization of the *Escherichia coli* cell division protein FtsI (PBP3) to the division site and cell pole. *Mol Microbiol.* 1997 Aug;25(4):671–81.

15. Wang L, Lutkenhaus J. FtsK is an essential cell division protein that is localized to the septum and induced as part of the SOS response. *Mol Microbiol*. 1998 Aug;29(3):731–40.
16. Yu XC, Tran AH, Sun Q, Margolin W. Localization of cell division protein FtsK to the *Escherichia coli* septum and identification of a potential N-terminal targeting domain. *J Bacteriol*. 1998 Mar;180(5):1296–304.
17. Liu Z, Mukherjee A, Lutkenhaus J. Recruitment of ZipA to the division site by interaction with FtsZ. *Mol Microbiol*. 1999 Mar;31(6):1853–61.
18. Hale CA, de Boer PA. Recruitment of ZipA to the septal ring of *Escherichia coli* is dependent on FtsZ and independent of FtsA. *J Bacteriol*. 1999 Jan;181(1):167–76.
19. Ghigo JM, Weiss DS, Chen JC, Yarrow JC, Beckwith J. Localization of FtsL to the *Escherichia coli* septal ring. *Mol Microbiol*. 1999 Jan;31(2):725–37.
20. Chen JC, Weiss DS, Ghigo JM, Beckwith J. Septal localization of FtsQ, an essential cell division protein in *Escherichia coli*. *J Bacteriol*. 1999 Jan;181(2):521–30.
21. Chen JC, Beckwith J. FtsQ, FtsL and FtsI require FtsK, but not FtsN, for co-localization with FtsZ during *Escherichia coli* cell division. *Mol Microbiol*. 2001 Oct;42(2):395–413.
22. Hale CA, Boer PAJ de. ZipA Is Required for Recruitment of FtsK, FtsQ, FtsL, and FtsN to the Septal Ring in *Escherichia coli*. *J Bacteriol*. 2002 May 1;184(9):2552–6.
23. Buddelmeijer N, Judson N, Boyd D, Mekalanos JJ, Beckwith J. YgbQ, a cell division protein in *Escherichia coli* and *Vibrio cholerae*, localizes in codependent fashion with FtsL to the division site. *Proc Natl Acad Sci U S A*. 2002 Apr 30;99(9):6316–21.
24. Di Lallo G, Fagioli M, Barionovi D, Ghelardini P, Paolozzi L. Use of a two-hybrid assay to study the assembly of a complex multicomponent protein machinery: bacterial septosome differentiation. *Microbiol Read Engl*. 2003 Dec;149(Pt 12):3353–9.
25. Rico AI, García-Ovalle M, Mingorance J, Vicente M. Role of two essential domains of *Escherichia coli* FtsA in localization and progression of the division ring. *Mol Microbiol*. 2004 Sep;53(5):1359–71.
26. Corbin BD, Geissler B, Sadavivam M, Margolin W. Z-ring-independent interaction between a subdomain of FtsA and late septation proteins as revealed by a polar recruitment assay. *J Bacteriol*. 2004 Nov;186(22):7736–44.

27. Schmidt KL, Peterson ND, Kustusch RJ, Wissel MC, Graham B, Phillips GJ, et al. A predicted ABC transporter, FtsEX, is needed for cell division in *Escherichia coli*. *J Bacteriol.* 2004 Feb;186(3):785–93.
28. Buddelmeijer N, Beckwith J. A complex of the *Escherichia coli* cell division proteins FtsL, FtsB and FtsQ forms independently of its localization to the septal region. *Mol Microbiol.* 2004 Jun;52(5):1315–27.
29. Karimova G, Dautin N, Ladant D. Interaction network among *Escherichia coli* membrane proteins involved in cell division as revealed by bacterial two-hybrid analysis. *J Bacteriol.* 2005 Apr;187(7):2233–43.
30. Goehring NW, Gueiros-Filho F, Beckwith J. Premature targeting of a cell division protein to midcell allows dissection of divisome assembly in *Escherichia coli*. *Genes Dev.* 2005 Jan 1;19(1):127–37.
31. Goehring NW, Gonzalez MD, Beckwith J. Premature targeting of cell division proteins to midcell reveals hierarchies of protein interactions involved in divisome assembly. *Mol Microbiol.* 2006 Jul;61(1):33–45.
32. Corbin BD, Wang Y, Beuria TK, Margolin W. Interaction between cell division proteins FtsE and FtsZ. *J Bacteriol.* 2007 Apr;189(8):3026–35.
33. D'Ulisse V, Fagioli M, Ghelardini P, Paolozzi L. Three functional subdomains of the *Escherichia coli* FtsQ protein are involved in its interaction with the other division proteins. *Microbiol Read Engl.* 2007 Jan;153(Pt 1):124–38.
34. Gonzalez MD, Beckwith J. Divisome under construction: distinct domains of the small membrane protein FtsB are necessary for interaction with multiple cell division proteins. *J Bacteriol.* 2009 Apr;191(8):2815–25.
35. Gonzalez MD, Akbay EA, Boyd D, Beckwith J. Multiple interaction domains in FtsL, a protein component of the widely conserved bacterial FtsLBQ cell division complex. *J Bacteriol.* 2010 Jun;192(11):2757–68.
36. Bi EF, Lutkenhaus J. FtsZ ring structure associated with division in *Escherichia coli*. *Nature.* 1991 Nov 14;354(6349):161–4.
37. Löwe J, Amos LA. Crystal structure of the bacterial cell-division protein FtsZ. *Nature.* 1998 Jan 8;391(6663):203–6.
38. Mukherjee A, Lutkenhaus J. Guanine nucleotide-dependent assembly of FtsZ into filaments. *J Bacteriol.* 1994 May;176(9):2754–8.
39. Bramhill D, Thompson CM. GTP-dependent polymerization of *Escherichia coli* FtsZ protein to form tubules. *Proc Natl Acad Sci U S A.* 1994 Jun 21;91(13):5813–7.

40. Stricker J, Maddox P, Salmon ED, Erickson HP. Rapid assembly dynamics of the *Escherichia coli* FtsZ-ring demonstrated by fluorescence recovery after photobleaching. *Proc Natl Acad Sci U S A.* 2002 Mar 5;99(5):3171–5.
41. Anderson DE, Gueiros-Filho FJ, Erickson HP. Assembly dynamics of FtsZ rings in *Bacillus subtilis* and *Escherichia coli* and effects of FtsZ-regulating proteins. *J Bacteriol.* 2004 Sep;186(17):5775–81.
42. Yang X, Lyu Z, Miguel A, McQuillen R, Huang KC, Xiao J. GTPase activity-coupled treadmilling of the bacterial tubulin FtsZ organizes septal cell wall synthesis. *Science.* 2017 17;355(6326):744–7.
43. Bisson-Filho AW, Hsu Y-P, Squyres GR, Kuru E, Wu F, Jukes C, et al. Treadmilling by FtsZ filaments drives peptidoglycan synthesis and bacterial cell division. *Science.* 2017 17;355(6326):739–43.
44. Fu G, Huang T, Buss J, Coltharp C, Hensel Z, Xiao J. In vivo structure of the *E. coli* FtsZ-ring revealed by photoactivated localization microscopy (PALM). *PLoS One.* 2010 Sep 13;5(9):e12682.
45. Li Z, Trimble MJ, Brun YV, Jensen GJ. The structure of FtsZ filaments in vivo suggests a force-generating role in cell division. *EMBO J.* 2007 Nov 14;26(22):4694–708.
46. Osawa M, Anderson DE, Erickson HP. Reconstitution of contractile FtsZ rings in liposomes. *Science.* 2008 May 9;320(5877):792–4.
47. Osawa M, Erickson HP. Liposome division by a simple bacterial division machinery. *Proc Natl Acad Sci U S A.* 2013 Jul 2;110(27):11000–4.
48. Szwedziak P, Wang Q, Bharat TAM, Tsim M, Löwe J. Architecture of the ring formed by the tubulin homologue FtsZ in bacterial cell division. *eLife.* 2014 Dec 9;3:e04601.
49. Wang X, Possoz C, Sherratt DJ. Dancing around the divisome: asymmetric chromosome segregation in *Escherichia coli*. *Genes Dev.* 2005 Oct 1;19(19):2367–77.
50. Söderström B, Skoog K, Blom H, Weiss DS, von Heijne G, Daley DO. Disassembly of the divisome in *Escherichia coli*: evidence that FtsZ dissociates before compartmentalization. *Mol Microbiol.* 2014 Apr;92(1):1–9.
51. Coltharp C, Buss J, Plumer TM, Xiao J. Defining the rate-limiting processes of bacterial cytokinesis. *Proc Natl Acad Sci U S A.* 2016 Feb 23;113(8):E1044-1053.
52. Daley DO, Skoglund U, Söderström B. FtsZ does not initiate membrane constriction at the onset of division. *Sci Rep.* 2016 09;6:33138.

53. Nguyen LT, Oikonomou CM, Ding HJ, Kaplan M, Yao Q, Chang Y-W, et al. Simulations suggest a constrictive force is required for Gram-negative bacterial cell division. *Nat Commun.* 2019;10(1):1259.
54. van den Ent F, Löwe J. Crystal structure of the cell division protein FtsA from *Thermotoga maritima*. *EMBO J.* 2000 Oct 16;19(20):5300–7.
55. Mosyak L, Zhang Y, Glasfeld E, Haney S, Stahl M, Seehra J, et al. The bacterial cell-division protein ZipA and its interaction with an FtsZ fragment revealed by X-ray crystallography. *EMBO J.* 2000 Jul 3;19(13):3179–91.
56. Moy FJ, Glasfeld E, Mosyak L, Powers R. Solution structure of ZipA, a crucial component of *Escherichia coli* cell division. *Biochemistry.* 2000 Aug 8;39(31):9146–56.
57. Pichoff S, Lutkenhaus J. Unique and overlapping roles for ZipA and FtsA in septal ring assembly in *Escherichia coli*. *EMBO J.* 2002 Feb 15;21(4):685–93.
58. Pichoff S, Lutkenhaus J. Tethering the Z ring to the membrane through a conserved membrane targeting sequence in FtsA. *Mol Microbiol.* 2005 Mar;55(6):1722–34.
59. Bork P, Sander C, Valencia A. An ATPase domain common to prokaryotic cell cycle proteins, sugar kinases, actin, and hsp70 heat shock proteins. *Proc Natl Acad Sci U S A.* 1992 Aug 15;89(16):7290–4.
60. Lara B, Rico AI, Petruzzelli S, Santona A, Dumas J, Biton J, et al. Cell division in cocci: localization and properties of the *Streptococcus pneumoniae* FtsA protein. *Mol Microbiol.* 2005 Feb;55(3):699–711.
61. Szwedziak P, Wang Q, Freund SMV, Löwe J. FtsA forms actin-like protofilaments. *EMBO J.* 2012 May 16;31(10):2249–60.
62. Krupka M, Rowlett VW, Morado D, Vitrac H, Schoenemann K, Liu J, et al. *Escherichia coli* FtsA forms lipid-bound minirings that antagonize lateral interactions between FtsZ protofilaments. *Nat Commun.* 2017 11;8:15957.
63. Shiomi D, Margolin W. Dimerization or oligomerization of the actin-like FtsA protein enhances the integrity of the cytokinetic Z ring. *Mol Microbiol.* 2007 Dec;66(6):1396–415.
64. Pichoff S, Shen B, Sullivan B, Lutkenhaus J. FtsA mutants impaired for self-interaction bypass ZipA suggesting a model in which FtsA's self-interaction competes with its ability to recruit downstream division proteins. *Mol Microbiol.* 2012 Jan;83(1):151–67.

65. Liu B, Persons L, Lee L, de Boer PAJ. Roles for both FtsA and the FtsBLQ subcomplex in FtsN-stimulated cell constriction in *Escherichia coli*. *Mol Microbiol*. 2015 Mar;95(6):945–70.
66. Goehring NW, Petrovska I, Boyd D, Beckwith J. Mutants, suppressors, and wrinkled colonies: mutant alleles of the cell division gene ftsQ point to functional domains in FtsQ and a role for domain 1C of FtsA in divisome assembly. *J Bacteriol*. 2007 Jan;189(2):633–45.
67. Busiek KK, Eraso JM, Wang Y, Margolin W. The early divisome protein FtsA interacts directly through its 1c subdomain with the cytoplasmic domain of the late divisome protein FtsN. *J Bacteriol*. 2012 Apr;194(8):1989–2000.
68. Busiek KK, Margolin W. A role for FtsA in SPOR-independent localization of the essential *Escherichia coli* cell division protein FtsN. *Mol Microbiol*. 2014 Jun;92(6):1212–26.
69. Pichoff S, Du S, Lutkenhaus J. The bypass of ZipA by overexpression of FtsN requires a previously unknown conserved FtsN motif essential for FtsA-FtsN interaction supporting a model in which FtsA monomers recruit late cell division proteins to the Z ring. *Mol Microbiol*. 2015 Mar;95(6):971–87.
70. Geissler B, Elraheb D, Margolin W. A gain-of-function mutation in ftsA bypasses the requirement for the essential cell division gene zipA in *Escherichia coli*. *Proc Natl Acad Sci U S A*. 2003 Apr 1;100(7):4197–202.
71. Bernard CS, Sadasivam M, Shiomi D, Margolin W. An altered FtsA can compensate for the loss of essential cell division protein FtsN in *Escherichia coli*. *Mol Microbiol*. 2007 Jun;64(5):1289–305.
72. Tsang M-J, Bernhardt TG. A role for the FtsQLB complex in cytokinetic ring activation revealed by an ftsL allele that accelerates division. *Mol Microbiol*. 2015 Mar;95(6):925–44.
73. Pazos M, Natale P, Vicente M. A specific role for the ZipA protein in cell division: stabilization of the FtsZ protein. *J Biol Chem*. 2013 Feb 1;288(5):3219–26.
74. Gill DR, Hatfull GF, Salmond GP. A new cell division operon in *Escherichia coli*. *Mol Gen Genet MGG*. 1986 Oct;205(1):134–45.
75. Gibbs TW, Gill DR, Salmond GP. Localised mutagenesis of the fts YEX operon: conditionally lethal missense substitutions in the FtsE cell division protein of *Escherichia coli* are similar to those found in the cystic fibrosis transmembrane conductance regulator protein (CFTR) of human patients. *Mol Gen Genet MGG*. 1992 Jul;234(1):121–8.

76. de Leeuw E, Graham B, Phillips GJ, ten Hagen-Jongman CM, Oudega B, Luirink J. Molecular characterization of *Escherichia coli* FtsE and FtsX. *Mol Microbiol*. 1999 Feb;31(3):983–93.
77. Reddy M. Role of FtsEX in cell division of *Escherichia coli*: viability of ftsEX mutants is dependent on functional SufI or high osmotic strength. *J Bacteriol*. 2007 Jan;189(1):98–108.
78. Du S, Pichoff S, Lutkenhaus J. FtsEX acts on FtsA to regulate divisome assembly and activity. *Proc Natl Acad Sci U S A*. 2016 23;113(34):E5052-5061.
79. Yang DC, Peters NT, Parzych KR, Uehara T, Markovski M, Bernhardt TG. An ATP-binding cassette transporter-like complex governs cell-wall hydrolysis at the bacterial cytokinetic ring. *Proc Natl Acad Sci U S A*. 2011 Nov 8;108(45):E1052-1060.
80. Arends SJR, Kustusch RJ, Weiss DS. ATP-binding site lesions in FtsE impair cell division. *J Bacteriol*. 2009 Jun;191(12):3772–84.
81. Grenga L, Luzi G, Paolozzi L, Ghelardini P. The *Escherichia coli* FtsK functional domains involved in its interaction with its divisome protein partners. *FEMS Microbiol Lett*. 2008 Oct;287(2):163–7.
82. Berezuk AM, Roach EJ, Seidel L, Lo R, Khursigara C. FtsA G50E Mutant Suppresses the Essential Requirement for FtsK During Bacterial Cell Division in *Escherichia coli*. *Can J Microbiol*. 2020 Jan 23;
83. Liu G, Draper GC, Donachie WD. FtsK is a bifunctional protein involved in cell division and chromosome localization in *Escherichia coli*. *Mol Microbiol*. 1998 Aug;29(3):893–903.
84. Yu XC, Weihe EK, Margolin W. Role of the C terminus of FtsK in *Escherichia coli* chromosome segregation. *J Bacteriol*. 1998 Dec;180(23):6424–8.
85. Steiner W, Liu G, Donachie WD, Kuempel P. The cytoplasmic domain of FtsK protein is required for resolution of chromosome dimers. *Mol Microbiol*. 1999 Jan;31(2):579–83.
86. Männik J, Bailey MW, O'Neill JC, Männik J. Kinetics of large-scale chromosomal movement during asymmetric cell division in *Escherichia coli*. *PLoS Genet*. 2017;13(2):e1006638.
87. Draper GC, McLennan N, Begg K, Masters M, Donachie WD. Only the N-terminal domain of FtsK functions in cell division. *J Bacteriol*. 1998 Sep;180(17):4621–7.
88. Dorazi R, Dewar SJ. Membrane topology of the N-terminus of the *Escherichia coli* FtsK division protein. *FEBS Lett*. 2000 Jul 28;478(1–2):13–8.

89. Bigot S, Corre J, Louarn J-M, Cornet F, Barre F-X. FtsK activities in Xer recombination, DNA mobilization and cell division involve overlapping and separate domains of the protein. *Mol Microbiol*. 2004 Nov;54(4):876–86.
90. Dubarry N, Possoz C, Barre F-X. Multiple regions along the *Escherichia coli* FtsK protein are implicated in cell division. *Mol Microbiol*. 2010 Dec;78(5):1088–100.
91. Geissler B, Margolin W. Evidence for functional overlap among multiple bacterial cell division proteins: compensating for the loss of FtsK. *Mol Microbiol*. 2005 Oct;58(2):596–612.
92. Mueller EA, Westfall CS, Levin PA. pH-dependent activation of cytokinesis modulates *Escherichia coli* cell size. *PLoS Genet*. 2020 Mar;16(3):e1008685.
93. Grainge I. FtsK--a bacterial cell division checkpoint? *Mol Microbiol*. 2010 Dec;78(5):1055–7.
94. Berezuk AM, Goodyear M, Khursigara CM. Site-directed fluorescence labeling reveals a revised N-terminal membrane topology and functional periplasmic residues in the *Escherichia coli* cell division protein FtsK. *J Biol Chem*. 2014 Aug 22;289(34):23287–301.
95. Begg KJ, Hatfull GF, Donachie WD. Identification of new genes in a cell envelope-cell division gene cluster of *Escherichia coli*: cell division gene ftsQ. *J Bacteriol*. 1980 Oct;144(1):435–7.
96. Guzman LM, Barondess JJ, Beckwith J. FtsL, an essential cytoplasmic membrane protein involved in cell division in *Escherichia coli*. *J Bacteriol*. 1992 Dec;174(23):7716–28.
97. Natale P, Pazos M, Vicente M. The *Escherichia coli* divisome: born to divide. *Environ Microbiol*. 2013 Dec;15(12):3169–82.
98. Weiss DS. Last but not least: new insights into how FtsN triggers constriction during *Escherichia coli* cell division. *Mol Microbiol*. 2015 Mar;95(6):903–9.
99. Boes A, Olatunji S, Breukink E, Terrak M. Regulation of the Peptidoglycan Polymerase Activity of PBP1b by Antagonist Actions of the Core Divisome Proteins FtsBLQ and FtsN. *mBio*. 2019 08;10(1).
100. McCausland JW, Yang X, Lyu Z, Söderström B, Xiao J, Liu J. Treadmilling FtsZ polymers drive the directional movement of sPG-synthesis enzymes via a Brownian ratchet mechanism. *bioRxiv*. 2019 Nov 28;857813.
101. Yang X, McQuillen R, Lyu Z, Phillips-Mason P, Cruz ADL, McCausland JW, et al. FtsW exhibits distinct processive movements driven by either septal cell wall synthesis or FtsZ treadmilling in *E. coli*. *bioRxiv*. 2019 Nov 21;850073.

102. Sauvage E, Kerff F, Terrak M, Ayala JA, Charlier P. The penicillin-binding proteins: structure and role in peptidoglycan biosynthesis. *FEMS Microbiol Rev.* 2008 Mar;32(2):234–58.
103. Booth S, Lewis RJ. Structural basis for the coordination of cell division with the synthesis of the bacterial cell envelope. *Protein Sci Publ Protein Soc.* 2019 Dec;28(12):2042–54.
104. Barrett D, Wang T-SA, Yuan Y, Zhang Y, Kahne D, Walker S. Analysis of glycan polymers produced by peptidoglycan glycosyltransferases. *J Biol Chem.* 2007 Nov 2;282(44):31964–71.
105. Boyle DS, Khattar MM, Addinall SG, Lutkenhaus J, Donachie WD. *ftsW* is an essential cell-division gene in *Escherichia coli*. *Mol Microbiol.* 1997 Jun;24(6):1263–73.
106. Lara B, Ayala JA. Topological characterization of the essential *Escherichia coli* cell division protein *FtsW*. *FEMS Microbiol Lett.* 2002 Oct 29;216(1):23–32.
107. Meeske AJ, Riley EP, Robins WP, Uehara T, Mekalanos JJ, Kahne D, et al. SEDS proteins are a widespread family of bacterial cell wall polymerases. *Nature.* 2016 29;537(7622):634–8.
108. Cho H, Wivagg CN, Kapoor M, Barry Z, Rohs PDA, Suh H, et al. Bacterial cell wall biogenesis is mediated by SEDS and PBP polymerase families functioning semi-autonomously. *Nat Microbiol.* 2016 Sep 19;1:16172.
109. Mohammadi T, van Dam V, Sijbrandi R, Vernet T, Zapun A, Bouhss A, et al. Identification of *FtsW* as a transporter of lipid-linked cell wall precursors across the membrane. *EMBO J.* 2011 Apr 20;30(8):1425–32.
110. Mohammadi T, Sijbrandi R, Lutters M, Verheul J, Martin NI, den Blaauwen T, et al. Specificity of the transport of lipid II by *FtsW* in *Escherichia coli*. *J Biol Chem.* 2014 May 23;289(21):14707–18.
111. Leclercq S, Derouaux A, Olatunji S, Fraipont C, Egan AJF, Vollmer W, et al. Interplay between Penicillin-binding proteins and SEDS proteins promotes bacterial cell wall synthesis. *Sci Rep.* 2017 24;7:43306.
112. Taguchi A, Welsh MA, Marmont LS, Lee W, Sjödt M, Kruse AC, et al. *FtsW* is a peptidoglycan polymerase that is functional only in complex with its cognate penicillin-binding protein. *Nat Microbiol.* 2019;4(4):587–94.
113. Botta GA, Park JT. Evidence for involvement of penicillin-binding protein 3 in murein synthesis during septation but not during cell elongation. *J Bacteriol.* 1981 Jan;145(1):333–40.

114. Mercer KLN, Weiss DS. The *Escherichia coli* cell division protein FtsW is required to recruit its cognate transpeptidase, FtsI (PBP3), to the division site. *J Bacteriol.* 2002 Feb;184(4):904–12.
115. Fraipont C, Alexeeva S, Wolf B, van der Ploeg R, Schloesser M, den Blaauwen T, et al. The integral membrane FtsW protein and peptidoglycan synthase PBP3 form a subcomplex in *Escherichia coli*. *Microbiol Read Engl.* 2011 Jan;157(Pt 1):251–9.
116. Sauvage E, Derouaux A, Fraipont C, Joris M, Herman R, Rocaboy M, et al. Crystal structure of penicillin-binding protein 3 (PBP3) from *Escherichia coli*. *PLoS One.* 2014;9(5):e98042.
117. Sung M-T, Lai Y-T, Huang C-Y, Chou L-Y, Shih H-W, Cheng W-C, et al. Crystal structure of the membrane-bound bifunctional transglycosylase PBP1b from *Escherichia coli*. *Proc Natl Acad Sci U S A.* 2009 Jun 2;106(22):8824–9.
118. Nakagawa J, Tamaki S, Matsuhashi M. Purified Penicillin Binding Proteins 1Bs from *Escherichia coli* Membrane Showing Activities of Both Peptidoglycan Polymerase and Peptidoglycan Crosslinking Enzyme. *Agric Biol Chem.* 1979 Jun;43(6):1379–80.
119. Suzuki H, Nishimura Y, Hirota Y. On the process of cellular division in *Escherichia coli*: a series of mutants of *E. coli* altered in the penicillin-binding proteins. *Proc Natl Acad Sci U S A.* 1978 Feb;75(2):664–8.
120. Yousif SY, Broome-Smith JK, Spratt BG. Lysis of *Escherichia coli* by beta-lactam antibiotics: deletion analysis of the role of penicillin-binding proteins 1A and 1B. *J Gen Microbiol.* 1985 Oct;131(10):2839–45.
121. Pazos M, Peters K, Casanova M, Palacios P, VanNieuwenhze M, Breukink E, et al. Z-ring membrane anchors associate with cell wall synthases to initiate bacterial cell division. *Nat Commun.* 2018;30;9(1):5090.
122. Nguyen LT, Gumbart JC, Beeby M, Jensen GJ. Coarse-grained simulations of bacterial cell wall growth reveal that local coordination alone can be sufficient to maintain rod shape. *Proc Natl Acad Sci U S A.* 2015 Jul 14;112(28):E3689-3698.
123. Bertsche U, Kast T, Wolf B, Fraipont C, Aarsman MEG, Kannenberg K, et al. Interaction between two murein (peptidoglycan) synthases, PBP3 and PBP1B, in *Escherichia coli*. *Mol Microbiol.* 2006 Aug;61(3):675–90.
124. Dai K, Xu Y, Lutkenhaus J. Topological characterization of the essential *Escherichia coli* cell division protein FtsN. *J Bacteriol.* 1996 Mar;178(5):1328–34.
125. Addinall SG, Cao C, Lutkenhaus J. FtsN, a late recruit to the septum in *Escherichia coli*. *Mol Microbiol.* 1997 Jul;25(2):303–9.

126. Müller P, Ewers C, Bertsche U, Anstett M, Kallis T, Breukink E, et al. The essential cell division protein FtsN interacts with the murein (peptidoglycan) synthase PBP1B in *Escherichia coli*. *J Biol Chem.* 2007 Dec 14;282(50):36394–402.
127. Alexeeva S, Gadella TWJ, Verheul J, Verhoeven GS, den Blaauwen T. Direct interactions of early and late assembling division proteins in *Escherichia coli* cells resolved by FRET. *Mol Microbiol.* 2010 Jul;77(2):384–98.
128. Yang J-C, Van Den Ent F, Neuhaus D, Brevier J, Löwe J. Solution structure and domain architecture of the divisome protein FtsN. *Mol Microbiol.* 2004 May;52(3):651–60.
129. Gerdung MA, Liu B, Bendezú FO, Hale CA, Bernhardt TG, de Boer PAJ. Self-enhanced accumulation of FtsN at Division Sites and Roles for Other Proteins with a SPOR domain (DamX, DedD, and RlpA) in *Escherichia coli* cell constriction. *J Bacteriol.* 2009 Dec;191(24):7383–401.
130. Ursinus A, van den Ent F, Brechtel S, de Pedro M, Höltje J-V, Löwe J, et al. Murein (peptidoglycan) binding property of the essential cell division protein FtsN from *Escherichia coli*. *J Bacteriol.* 2004 Oct;186(20):6728–37.
131. Yahashiri A, Jorgenson MA, Weiss DS. Bacterial SPOR domains are recruited to septal peptidoglycan by binding to glycan strands that lack stem peptides. *Proc Natl Acad Sci U S A.* 2015 Sep 8;112(36):11347–52.
132. Bernhardt TG, de Boer PAJ. The *Escherichia coli* amidase AmiC is a periplasmic septal ring component exported via the twin-arginine transport pathway. *Mol Microbiol.* 2003 Jun;48(5):1171–82.
133. Peters NT, Dinh T, Bernhardt TG. A fail-safe mechanism in the septal ring assembly pathway generated by the sequential recruitment of cell separation amidases and their activators. *J Bacteriol.* 2011 Sep;193(18):4973–83.
134. Lutkenhaus J, Du S. *E. coli* Cell Cycle Machinery. *Subcell Biochem.* 2017;84:27–65.
135. Bernhardt TG, de Boer PAJ. SlmA, a nucleoid-associated, FtsZ binding protein required for blocking septal ring assembly over Chromosomes in *E. coli*. *Mol Cell.* 2005 May 27;18(5):555–64.
136. Cho H, McManus HR, Dove SL, Bernhardt TG. Nucleoid occlusion factor SlmA is a DNA-activated FtsZ polymerization antagonist. *Proc Natl Acad Sci U S A.* 2011 Mar 1;108(9):3773–8.
137. Rowlett VW, Margolin W. The Min system and other nucleoid-independent regulators of Z ring positioning. *Front Microbiol.* 2015;6:478.

138. Mercier R, Petit M-A, Schbath S, Robin S, El Karoui M, Boccard F, et al. The MatP/matS site-specific system organizes the terminus region of the *E. coli* chromosome into a macrodomain. *Cell*. 2008 Oct 31;135(3):475–85.
139. Espéli O, Borne R, Dupaigne P, Thiel A, Gigant E, Mercier R, et al. A MatP-divisome interaction coordinates chromosome segregation with cell division in *E. coli*. *EMBO J*. 2012 May 11;31(14):3198–211.
140. Ortiz C, Natale P, Cueto L, Vicente M. The keepers of the ring: regulators of FtsZ assembly. *FEMS Microbiol Rev*. 2016 Jan;40(1):57–67.
141. Bailey MW, Bisicchia P, Warren BT, Sherratt DJ, Männik J. Evidence for divisome localization mechanisms independent of the Min system and SlmA in *Escherichia coli*. *PLoS Genet*. 2014 Aug;10(8):e1004504.
142. Walker GC. SOS-regulated proteins in translesion DNA synthesis and mutagenesis. *Trends Biochem Sci*. 1995 Oct;20(10):416–20.
143. Trusca D, Scott S, Thompson C, Bramhill D. Bacterial SOS checkpoint protein SulA inhibits polymerization of purified FtsZ cell division protein. *J Bacteriol*. 1998 Aug;180(15):3946–53.
144. Huisman O, D'Ari R, Gottesman S. Cell-division control in *Escherichia coli*: specific induction of the SOS function SfiA protein is sufficient to block septation. *Proc Natl Acad Sci U S A*. 1984 Jul;81(14):4490–4.
145. Camberg JL, Hoskins JR, Wickner S. ClpXP protease degrades the cytoskeletal protein, FtsZ, and modulates FtsZ polymer dynamics. *Proc Natl Acad Sci U S A*. 2009 Jun 30;106(26):10614–9.
146. Ward JE, Lutkenhaus J. Overproduction of FtsZ induces minicell formation in *E. coli*. *Cell*. 1985 Oct;42(3):941–9.
147. Dai K, Lutkenhaus J. The proper ratio of FtsZ to FtsA is required for cell division to occur in *Escherichia coli*. *J Bacteriol*. 1992 Oct;174(19):6145–51.
148. Söderström B, Mirzadeh K, Todd S, von Heijne G, Skoglund U, Daley DO. Coordinated disassembly of the divisome complex in *Escherichia coli*. *Mol Microbiol*. 2016;101(3):425–38.
149. Galli E, Gerdes K. Spatial resolution of two bacterial cell division proteins: ZapA recruits ZapB to the inner face of the Z-ring. *Mol Microbiol*. 2010 Jun;76(6):1514–26.
150. Rowlett VW, Margolin W. 3D-SIM super-resolution of FtsZ and its membrane tethers in *Escherichia coli* cells. *Biophys J*. 2014 Oct 21;107(8):L17–20.

151. Buss J, Coltharp C, Shtengel G, Yang X, Hess H, Xiao J. A multi-layered protein network stabilizes the *Escherichia coli* FtsZ-ring and modulates constriction dynamics. *PLoS Genet.* 2015 Apr;11(4):e1005128.
152. Söderström B, Chan H, Shilling PJ, Skoglund U, Daley DO. Spatial separation of FtsZ and FtsN during cell division. *Mol Microbiol.* 2018;107(3):387–401.
153. Söderström B, Daley DO. The bacterial divisome: more than a ring? *Curr Genet.* 2017 May;63(2):161–4.
154. Söderström B, Chan H, Daley DO. Super-resolution images of peptidoglycan remodelling enzymes at the division site of *Escherichia coli*. *Curr Genet.* 2019 Feb;65(1):99–101.
155. Erickson HP. FtsZ, a prokaryotic homolog of tubulin? *Cell.* 1995 Feb 10;80(3):367–70.
156. Erickson HP. FtsZ, a tubulin homologue in prokaryote cell division. *Trends Cell Biol.* 1997 Sep;7(9):362–7.
157. Nogales E, Downing KH, Amos LA, Löwe J. Tubulin and FtsZ form a distinct family of GTPases. *Nat Struct Biol.* 1998 Jun;5(6):451–8.
158. Pichoff S, Du S, Lutkenhaus J. Roles of FtsEX in cell division. *Res Microbiol.* 2019 Dec;170(8):374–80.
159. Mavrici D, Marakalala MJ, Holton JM, Prigozhin DM, Gee CL, Zhang YJ, et al. *Mycobacterium tuberculosis* FtsX extracellular domain activates the peptidoglycan hydrolase, RipC. *Proc Natl Acad Sci U S A.* 2014 Jun 3;111(22):8037–42.
160. Rued BE, Alcorlo M, Edmonds KA, Martínez-Caballero S, Straume D, Fu Y, et al. Structure of the Large Extracellular Loop of FtsX and Its Interaction with the Essential Peptidoglycan Hydrolase PcsB in *Streptococcus pneumoniae*. *mBio.* 2019 29;10(1).
161. Du S, Henke W, Pichoff S, Lutkenhaus J. How FtsEX localizes to the Z ring and interacts with FtsA to regulate cell division. *Mol Microbiol.* 2019;112(3):881–95.
162. Massey TH, Mercogliano CP, Yates J, Sherratt DJ, Löwe J. Double-stranded DNA translocation: structure and mechanism of hexameric FtsK. *Mol Cell.* 2006 Aug;23(4):457–69.
163. Sivanathan V, Allen MD, de Bekker C, Baker R, Arciszewska LK, Freund SM, et al. The FtsK gamma domain directs oriented DNA translocation by interacting with KOPS. *Nat Struct Mol Biol.* 2006 Nov;13(11):965–72.

164. Löwe J, Ellonen A, Allen MD, Atkinson C, Sherratt DJ, Grainge I. Molecular mechanism of sequence-directed DNA loading and translocation by FtsK. *Mol Cell.* 2008 Aug 22;31(4):498–509.
165. Jean NL, Rutherford TJ, Löwe J. FtsK in motion reveals its mechanism for double-stranded DNA translocation. *bioRxiv.* 2019 Nov 1;828319.
166. van den Ent F, Vinkenvleugel TMF, Ind A, West P, Veprintsev D, Nanninga N, et al. Structural and mutational analysis of the cell division protein FtsQ. *Mol Microbiol.* 2008 Apr;68(1):110–23.
167. Kureisaite-Ciziene D, Varadajan A, McLaughlin SH, Glas M, Montón Silva A, Luirink R, et al. Structural Analysis of the Interaction between the Bacterial Cell Division Proteins FtsQ and FtsB. *mBio.* 2018 11;9(5).
168. Choi Y, Kim J, Yoon H-J, Jin KS, Ryu S, Lee HH. Structural Insights into the FtsQ/FtsB/FtsL Complex, a Key Component of the Divisome. *Sci Rep.* 2018 24;8(1):18061.
169. LaPointe LM, Taylor KC, Subramaniam S, Khadria A, Rayment I, Senes A. Structural organization of FtsB, a transmembrane protein of the bacterial divisome. *Biochemistry.* 2013 Apr 16;52(15):2574–85.
170. Condon SGF, Mahbuba D-A, Armstrong CR, Diaz-Vazquez G, Craven SJ, LaPointe LM, et al. The FtsLB subcomplex of the bacterial divisome is a tetramer with an uninterrupted FtsL helix linking the transmembrane and periplasmic regions. *J Biol Chem.* 2018 02;293(5):1623–41.
171. Han S, Zaniewski RP, Marr ES, Lacey BM, Tomaras AP, Evdokimov A, et al. Structural basis for effectiveness of siderophore-conjugated monocarbams against clinically relevant strains of *Pseudomonas aeruginosa*. *Proc Natl Acad Sci U S A.* 2010 Dec 21;107(51):22002–7.
172. Han S, Caspers N, Zaniewski RP, Lacey BM, Tomaras AP, Feng X, et al. Distinctive attributes of β -lactam target proteins in *Acinetobacter baumannii* relevant to development of new antibiotics. *J Am Chem Soc.* 2011 Dec 21;133(50):20536–45.
173. Sainsbury S, Bird L, Rao V, Shepherd SM, Stuart DI, Hunter WN, et al. Crystal structures of penicillin-binding protein 3 from *Pseudomonas aeruginosa*: comparison of native and antibiotic-bound forms. *J Mol Biol.* 2011 Jan 7;405(1):173–84.
174. Bellini D, Koekemoer L, Newman H, Dowson CG. Novel and Improved Crystal Structures of *H. influenzae*, *E. coli* and *P. aeruginosa* Penicillin-Binding Protein 3 (PBP3) and *N. gonorrhoeae* PBP2: Toward a Better Understanding of β -Lactam Target-Mediated Resistance. *J Mol Biol.* 2019 Aug 23;431(18):3501–19.

175. Contreras-Martel C, Amoroso A, Woon ECY, Zervosen A, Inglis S, Martins A, et al. Structure-guided design of cell wall biosynthesis inhibitors that overcome β -lactam resistance in *Staphylococcus aureus* (MRSA). *ACS Chem Biol.* 2011 Sep 16;6(9):943–51.
176. King AM, King DT, French S, Brouillet E, Asli A, Alexander JAN, et al. Structural and Kinetic Characterization of Diazabicyclooctanes as Dual Inhibitors of Both Serine- β -Lactamases and Penicillin-Binding Proteins. *ACS Chem Biol.* 2016 Apr 15;11(4):864–8.
177. King DT, Wasney GA, Nosella M, Fong A, Strynadka NCJ. Structural Insights into Inhibition of *Escherichia coli* Penicillin-binding Protein 1B. *J Biol Chem.* 2017 20;292(3):979–93.
178. Sauvage E, Terrak M. Glycosyltransferases and Transpeptidases/Penicillin-Binding Proteins: Valuable Targets for New Antibacterials. *Antibiot Basel Switz.* 2016 Feb 17;5(1).
179. Ovchinnikov S, Kinch L, Park H, Liao Y, Pei J, Kim DE, et al. Large-scale determination of previously unsolved protein structures using evolutionary information. *eLife.* 2015 Sep 3;4:e09248.
180. Emami K, Guyet A, Kawai Y, Devi J, Wu LJ, Allenby N, et al. RodA as the missing glycosyltransferase in *Bacillus subtilis* and antibiotic discovery for the peptidoglycan polymerase pathway. *Nat Microbiol.* 2017 Jan 13;2:16253.
181. Sjödt M, Brock K, Dobihal G, Rohs PDA, Green AG, Hopf TA, et al. Structure of the peptidoglycan polymerase RodA resolved by evolutionary coupling analysis. *Nature.* 2018 05;556(7699):118–21.
182. Nogales E. The development of cryo-EM into a mainstream structural biology technique. *Nat Methods.* 2016 Jan;13(1):24–7.
183. Trip EN, Scheffers D-J. A 1 MDa protein complex containing critical components of the *Escherichia coli* divisome. *Sci Rep.* 2015 Dec 8;5:18190.
184. Fleming TC, Shin JY, Lee S-H, Becker E, Huang KC, Bustamante C, et al. Dynamic SpolIIIE assembly mediates septal membrane fission during *Bacillus subtilis* sporulation. *Genes Dev.* 2010 Jun 1;24(11):1160–72.

Chapter 2: The FtsLB subcomplex of the bacterial divisome is a tetramer with an uninterrupted FtsL helix linking the transmembrane and periplasmic regions

This chapter was prepared for publication as:

Condon, S. G. F., Mahbuba, D. A., Armstrong, C. R., Diaz-Vazquez, G., Craven, S. J., LaPointe, L. M., Khadria, A. S., Chadda, R., Crooks, J. A., Rangarajan, N., Weibel, D. B., Hoskins, A. A., Robertson, J. L., Cui, Q., & Senes, A. (2018). The FtsLB subcomplex of the bacterial divisome is a tetramer with an uninterrupted FtsL helix linking the transmembrane and periplasmic regions. *Journal of Biological Chemistry*, 293(5), 1623-1641.

My contributions to this chapter are the development of the FtsLB expression and purification schemes used in the FRET experiments; the production of constructs, data collection, and data analysis for *in vivo* mutations made within the FtsLB linker regions and transmembrane domains; and writing and editing the manuscript.

2.1 Abstract

In *Escherichia coli*, FtsLB plays a central role in the initiation of cell division, possibly transducing a signal that will eventually lead to the activation of peptidoglycan remodeling at the forming septum. The molecular mechanisms by which FtsLB operates in the divisome, however, are not understood. Here we present a structural analysis of the FtsLB complex – performed with biophysical, computational, and *in vivo* methods – that establishes the organization of the transmembrane region and proximal coiled coil of the complex. FRET analysis *in vitro* is consistent with formation of a tetramer composed of two FtsL and two FtsB subunits. We predicted subunit contacts through co-evolutionary analysis and used them to compute a structural model of the complex. The transmembrane region of FtsLB is stabilized by hydrophobic packing and by a complex network of hydrogen bonds. The coiled-coil domain likely terminates near the critical Constriction Control Domain, which might correspond to a structural transition. The presence of strongly polar amino acids within the core of the tetrameric coiled coil suggests that the coil may split into two independent FtsQ-binding domains. The helix of FtsB is interrupted between the transmembrane and coiled-coil regions by a flexible Gly-rich linker. Conversely, the data suggest that FtsL forms an uninterrupted helix across the two regions, and that integrity of this helix is indispensable for the function of the complex. The FtsL helix is thus a candidate for acting as a potential mechanical connection to communicate conformational changes between periplasmic, membrane, and cytoplasmic regions.

2.2 Introduction

The cell envelope of Gram-negative bacteria, such as *Escherichia coli*, consists of three layers: a cytoplasmic membrane, an outer membrane, and a rigid cell wall formed by a mesh of peptidoglycan located in the intervening periplasmic space. Cell division requires mechanisms for the separation of these three layers. The first step is the establishment of a division site and the segregation of the duplicated chromosome. This allows for the beginning of constriction, during which the coordinated activities of numerous peptidoglycan synthases and hydrolases remodel the cell wall. Finally, the process leads to membrane fusion and to the separation of two daughter cells. The large multiprotein complex that supports a majority of these functions is called the divisome.

At least three dozen proteins are known to participate in cell division in *E. coli*, but the essential components of the divisome consist of a core of twelve proteins. Their recruitment to midcell follows a hierarchical order of dependency (FtsZ → FtsA/ZipA → FtsE/FtsX → FtsK → FtsQ → FtsL/FtsB → FtsW → FtsI → FtsN, Fig. 2.1a), which also reflects, in part, the timing and interactions that occur in the complex assembly (1–12). The divisome assembles around the tubulin homologue FtsZ, which forms a ring-like structure at midcell (the Z-ring) (13–15). FtsZ protofilaments treadmill around the circumference of the cell, providing a scaffold for the recruitment and movement of the components around the cell, and ultimately leading to incorporation of new peptidoglycan around the forming septum (16, 17). FtsZ is tethered to the plasma membrane by the cooperative action of ZipA, a single-pass transmembrane (TM) protein (18, 19), and of FtsA, an actin homologue and peripheral membrane protein able

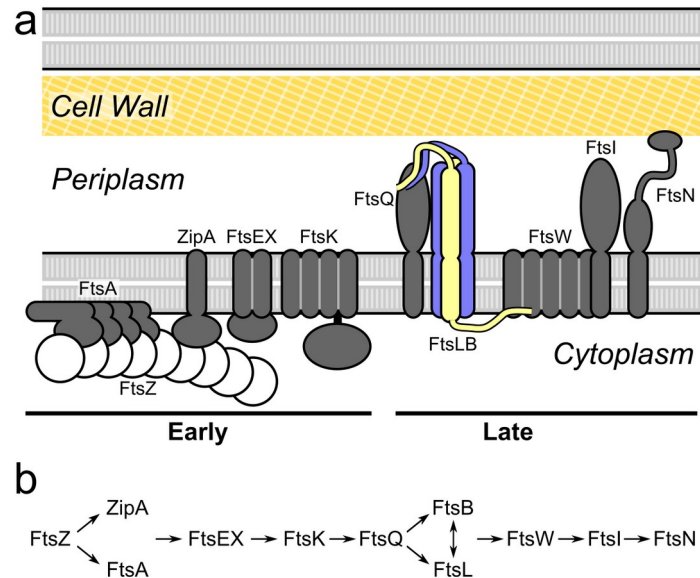


Figure 2.1. The essential proteins of the divisome. a) Schematic representation of the divisome of *E. coli*. The complex assembles around a polymeric scaffold formed by FtsZ. With a few exceptions (FtsZ, FtsA, FtsE), all essential components are integral membrane proteins. As reported in this article, the FtsLB complex is a hetero-tetramer formed by two FtsL subunits (yellow) and two FtsB subunits (blue). The complex forms an extended helical bundle that comprises the transmembrane helices and the periplasmic coiled coil. The C-terminal periplasmic tails of FtsLB mediate the binding to FtsQ. The cytoplasmic tail of FtsL has been hypothesized to bind to FtsW. Description of the function of the various components is provided in the main text. b) The divisome of *E. coli* displays a characteristic hierarchy of recruitment at the division site, with the arrows indicating a dependency of a component from the one that precedes it in the sequence. The hierarchy also roughly corresponds to the order of recruitment, which can be subdivided into early and late components.

to form protofilaments (20). Other early components of the divisome include FtsEX, an ABC transporter-like complex that controls cell wall hydrolysis and possibly divisome assembly (21, 22), as well as FtsK, a DNA translocase important for chromosome segregation (23).

The late components of the divisome (FtsQ, FtsB, FtsL, FtsW, FtsI, and FtsN) localize approximately at the beginning of constriction (24). FtsQ, FtsB, and FtsL are three bitopic (single-pass) membrane proteins that form a complex whose exact function is not well understood (6). The FtsQLB complex is required for the recruitment of FtsW, a large multi-span membrane protein, and FtsI, a bitopic protein. FtsW and FtsI work in coordination to synthesize septal cell wall (8): FtsI is a Penicillin Binding Protein (PBP3) with transpeptidase activity (25), and FtsW is most likely its cognate glycosyltransferase (26–28) (FtsW has also been proposed to be a flippase for peptidoglycan precursors (29, 30)). The last protein in the recruitment hierarchy is FtsN, a bitopic protein with an N-terminal TM domain, a predicted disordered region, and a C-terminal domain capable of recognizing septal peptidoglycan (31). The precise role of FtsN is not understood, but its accumulation at the septal ring represents a key event for triggering constriction. This activation may be mediated by some of the interactions that have been postulated for FtsN, which include FtsA, the peptidoglycan synthase complex (FtsW, FtsI, and PBP1B), and the FtsQLB complex (32–36).

Because the divisome consists primarily of integral membrane proteins, its structural characterization has been lagging and limited to fragments of water-soluble domains (31, 37–40). Here we focus on the structural organization of the FtsL/FtsB sub-complex (FtsLB) which has been implicated as a critical player in triggering constriction (41, 42). Topologically, FtsL and FtsB are both small bitopic proteins with a nearly identical domain organization, which suggests that they may derive from a common evolutionary ancestor. Both proteins have short (or absent) N-terminal cytoplasmic tails, one TM domain, a juxtamembrane coiled coil, and C-terminal tails in the periplasm (Fig. 2.1a).

Peptides corresponding to the TM helices form a stable higher-order oligomer *in vitro*, with an equal number of FtsL and FtsB subunits, indicating that the TM region is an important contributor to the stability of the complex (43). This is consistent with the observation that the TM domains are biologically important (6, 44, 45). FtsL and FtsB associate *in vivo* even in the absence of FtsQ (11, 46), although FtsQ is required for their recruitment to midcell (6). The association with FtsQ to form the FtsQLB complex is primarily mediated by the C-terminal tails of FtsLB, which bind to the C-terminal end of FtsQ, as evidenced from truncation functional analysis (45, 47) as well as cross-linking performed *in vivo* (48). The periplasmic domains of the three proteins are sufficient to form soluble complexes with sub-micromolar binding affinities, as established for *E. coli* (49) and *Streptococcus pneumoniae* (50, 51) proteins. Notably, these studies have been performed using solubilized FtsLB constructs that were fused to a stable hetero-dimeric coiled coil and thus forced into a dimeric state. However, FtsLB is likely to be a higher-order oligomer (such as a tetramer) as evidenced by biophysical analysis of their TM helices in isolation (43). The tight binding affinity of these 1:1:1 FtsQLB soluble constructs, therefore suggests that independent FtsQ-binding sites exist in FtsLB, each formed by one FtsL and one FtsB subunit.

The precise function of FtsLB has not yet been determined. It was originally hypothesized that FtsLB could have a structural role in stabilizing the divisome (45, 47). The finding that FtsL is subject to active degradation unless it is stabilized by interaction with FtsB in *Bacillus subtilis* (52–54) and *E. coli* (45), suggested that FtsL levels may be rate-limiting for division (54). More recent evidence indicates that FtsLB is an active participant in the decision-making that controls the cell division process, playing a

central role in triggering of septal peptidoglycan synthesis. This hypothesis is supported by observations that point mutations in a particular region of FtsL and FtsB alter the tightly regulated cell division process, allowing it to proceed even in situations in which normally it would not occur (41, 42). Tsang and Bernhardt discovered that a single point mutation in FtsL (E88K) allows the cells to bypass the normally strict requirements for other division proteins, namely FtsK, ZipA, FtsN, and FtsA (although residual levels of FtsA expression appear to be still necessary) (41). Independently, de Boer and colleagues identified a series of mutants that bypass the need for FtsN. These mutants map to two short regions of the coiled coil of FtsL (88-94) and FtsB (55-59). These regions, which are located approximately 30 residues past the TM domain, were named the “Constriction Control Domain” (CCD) (42).

The observed properties of these CCD mutants are consistent with a conformational change in FtsLB that has become deregulated. In other words, an OFF/ON structural transition in FtsLB may be part of the events that control the beginning of cell constriction. This transition may be triggered allosterically by FtsN itself, as suggested by the observation that the essential region of FtsN (^EFtsN, a short stretch of sequence that is separated by ~20 amino acids from the C-terminal side of the TM domain) is in a position that is topologically equivalent with the location of the CCD in FtsLB (41, 42).

To elucidate the effect of the CCD mutants and the overall function of the FtsQLB complex in molecular detail, it is necessary to understand its structural organization. So far, two partial structures have been obtained. The structure of the periplasmic domain of FtsQ has been solved by X-ray crystallography, without the TM and cytoplasmic domains (39). Additionally, we previously determined the crystal structure of the coiled-

coil domain of FtsB and also produced a computational model of the TM domain of the same protein, based on mutagenesis data (38). Both structures were obtained in the absence of FtsL and in a homo-dimeric form. In addition, computational models of the FtsQLB periplasmic region (both in trimeric and hexameric state) have also been reported (55). These models were based on available experimental data regarding contacts between FtsQ and FtsLB, whereas the FtsLB component was predicted *ab initio*. Additionally, these models lacked the TM region.

Here, we present a structural analysis of the TM domain and periplasmic coiled coil of FtsLB, based on a combination of biophysical and computational methods with *in vivo* validation. The work includes *in vitro* FRET to determine the oligomerization state of FtsLB; a co-evolutionary analysis of sequence alignments to provide an extensive set of predicted contacts between positions in FtsL and FtsB; molecular modeling to compute a tri-dimensional structural model of the complex; molecular dynamics in lipid bilayers to evaluate stability and dynamics of the model; and a functional analysis of mutants *in vivo* to experimentally test the model and investigate the biological relevance of the predicted structural features.

Our results confirm that FtsLB is a higher oligomer, and point to an L₂B₂ tetramer. Overall, the phenotypic analysis is in good agreement with structural features identified computationally. The distribution of deleterious phenotypes among the TM region mutants is consistent with the predicted interface. We confirm that the helix of FtsB breaks between the TM and periplasmic regions, with the formation of a flexible linker, as previously hypothesized (38). In contrast, we show that FtsL forms a continuous helix and that the integrity of this helix is crucial for function. We also found indications that

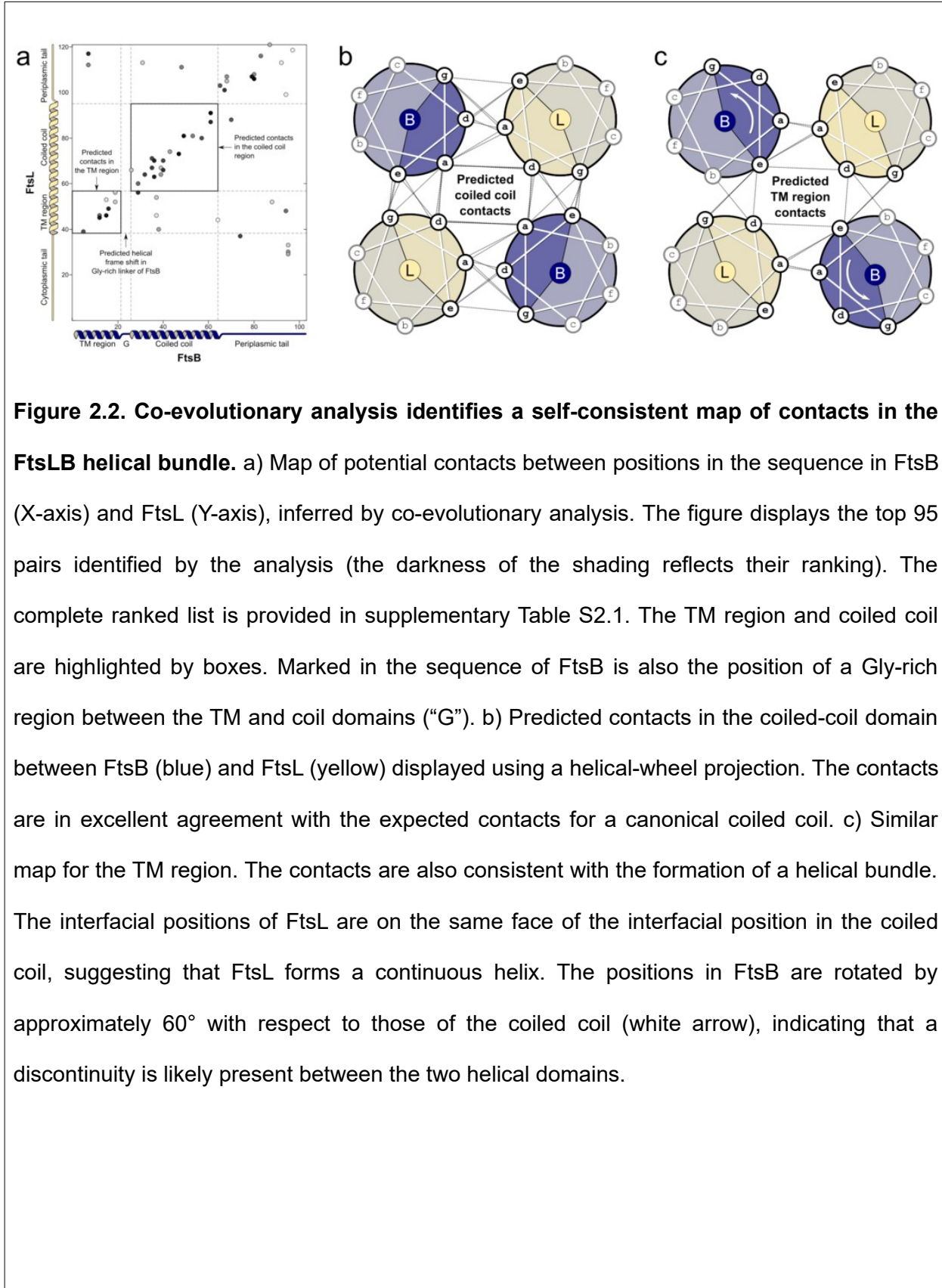
the coiled coil might not be built for structural stability, at least not in the form of a canonical tetrameric helical bundle assembly, suggesting that the coil may either serve as a dynamic structural unit or else split into two independent domains.

2.3 Results and Discussion

2.3.1 Co-evolutionary analysis identifies potential quaternary contacts consistent with an extended helical bundle

To predict the positions that mediate the association of the FtsLB complex, we analyzed a paired alignment of FtsL and FtsB sequences from proteobacteria species using the EV-Couplings algorithm (56). EV-Couplings uses a maximum-entropy model of the evolutionary history of a protein (or protein complex) to infer potential tertiary (56) and quaternary (57) contacts in their structure. It is based on the notion that, in order to maintain complementary interactions, amino acid changes influence the variation of positions that are in close proximity. The results of our EV-Couplings analysis are shown in Fig. 2.2a. The figure displays the top 95 pairs of positions identified between FtsL and FtsB. The complete ranked list is provided in supplementary Table S2.1. FtsB-FtsB and FtsL-FtsL pairs are displayed in supplementary Fig. S2.1.

A notable diagonal pattern of co-evolving positions starts in the TM region of both proteins and continues in the coiled-coil region, which is consistent with the contact map expected for an extended parallel helical bundle. As shown in the helical wheel diagram of Fig. 2.2b, the co-evolving positions in the periplasmic region are also consistent with the expected geometry of a coiled coil (7, 50, 58), occurring at positions of the “heptad repeat” (*abcdefg*) that are interfacial, at either the buried “*a*” and “*d*” positions, or at the



partially solvent exposed “e” and “g” positions. Moreover, these predicted contacts occur between pairs that are in proximity in a canonical coiled coil (for example, *a-a*, *a-d*, *g-e*, but not *a-e*). The pattern of connectivity remains in good agreement with a coiled-coil contact map until positions 61 in FtsB and 91 in FtsL, after which it loses this periodicity. This range covers approximately five heptad repeats, which for FtsB is approximately 10-20 amino acids shorter than the consensus of the sequence-based predictors Paircoil (59), Multicoil (60), Marcoil (61), and Coils (62, 63) (inferring the length of the coiled coil of FtsL with the same methods is difficult because it is poorly predicted (58)). The coiled coil predicted by the evolutionary analysis approximately reaches the CCD (55-59 in FtsB, 88-94 in FtsL, highlighted in yellow in Fig. 2.2a and d), suggesting that it is possible that this critical regulatory region occurs toward the end of the coil and thus in proximity of a structural transition.

2.3.2 A continuous FtsL helix and a discontinuous FtsB

As illustrated in the helical wheel diagram of Fig. 2.2c, the TM region also displays a pattern of predicted contacts consistent with a bundle of parallel helices. The co-evolving positions are clustered toward the C-terminal side of the TM domains. Remarkably, the interfacial positions of the TM domain FtsB are in excellent agreement with those identified previously from their sensitivity to mutagenesis in a self-association assay (38).

Comparison of the contact maps (Fig. 2.2b and c) indicates that, in FtsL, the predicted interfaces of coiled-coil and TM domains occur on the same face of the helix (involving “*a*”, “*d*”, “*g*” positions in the TM domain, and “*a*”, “*d*”, “*e*”, “*g*” positions in the coil). This pattern indicates that FtsL forms a continuous helix across the membrane and

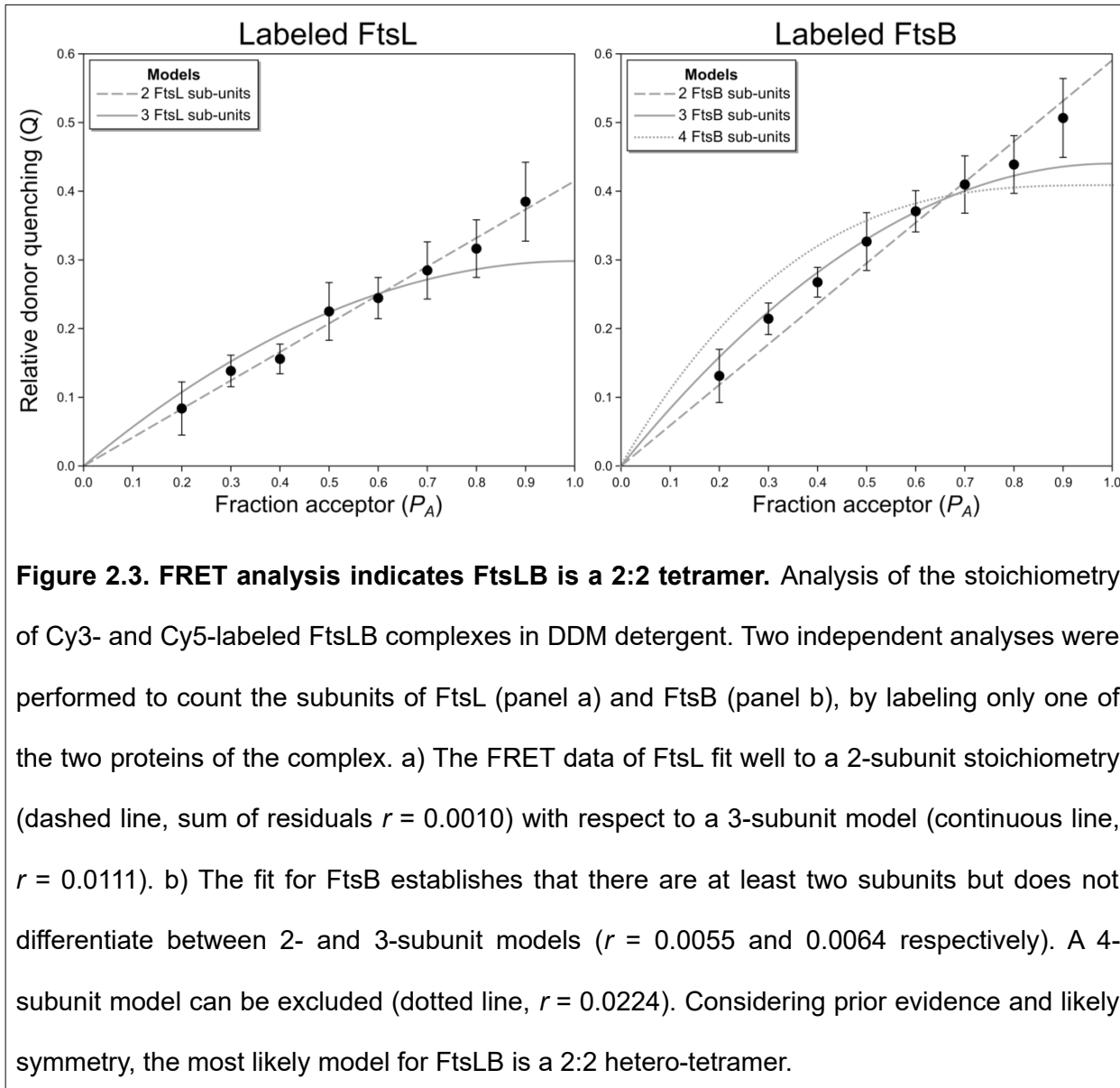
the periplasmic region. A different outcome is observed for FtsB, for which the TM domain interface involves “a” and “e”, but also “b” positions (versus “a”, “d”, “e”, “g” positions in the coil) and thus appears rotated by approximately 60° with respect to each other (as indicated by the arrow in Fig. 2.2c). This rotation suggests the presence of a helical break. Rearrangements of the periodicity from the canonical heptad repeat are not uncommon in long coils. The 60° shift of the relative orientation of the interface between the TM and coiled-coil regions of FtsB would correspond to the insertion of four amino acids (*abcdabcde*fg), which is designated as a “stutter” (64, 65). Such mismatches influence the coil’s local structure and can possibly facilitate conformational changes necessary for function (66, 67). In this particular case, however, the presence of a conserved Gly-rich region (22-GKNG-25 in *E. coli*, and 22-GKGG-25 in the consensus sequence of α-, β-, and γ-proteobacteria (38)) suggests that the juxtamembrane linker of FtsB is more likely to adopt a flexible and extended conformation, instead of a local distortion of the helix.

2.3.3 FtsLB is a higher oligomer, likely an L_2B_2 tetrameric complex

In order to build a structural model for the FtsLB complex based on the evolutionary constraints, it was necessary to establish its oligomeric state. In previous work, we demonstrated that the isolated TM region of the FtsLB complex assembles to form a higher-order oligomer consisting of an equal number of FtsL and FtsB subunits, but we were unable to distinguish between hetero-tetrameric (L_2B_2), hetero-hexameric (L_3B_3), or even higher oligomeric forms (43). Here, we assessed the stoichiometry of a construct that includes both periplasmic and TM domains by FRET analysis *in vitro*.

The FtsLB complex was overexpressed in *E. coli*, consisting of an N-terminally His-tagged FtsB and an N-terminally Strep-tagged FtsL. FtsL and FtsB were co-expressed. The proteins co-purify over sequential Ni-NTA and streptavidin columns in DM and DDM detergents, indicating that they form a stable complex with a density over coomassie staining compatible with a 1:1 stoichiometric ratio (supplementary Fig. S2.2a). A C-terminal Cys residue was introduced in either FtsB or FtsL, and protein samples were separately labeled with either donor (Cy3) or acceptor (Cy5) fluorophores. Since the stoichiometric analysis is performed separately for the two proteins, to further confirm interaction between FtsL and FtsB in the experimental conditions, we mixed and equilibrated $\text{FtsL}_{\text{unlabelled}}/\text{FtsB}_{\text{Cy3}}$ and $\text{FtsL}_{\text{Cy5}}/\text{FtsB}_{\text{unlabelled}}$ samples, which produced a distinct FRET signal (supplementary Fig. S2.2b).

We analyzed the stoichiometry of FtsLB by adopting a FRET method based on changing the relative fraction of donor- and acceptor-labeled molecules while the total protein concentration was maintained constant (68). In these conditions, the theoretical variation of donor quenching Q depends on the oligomeric state of the complex, being proportional to $(1-P_D)^{n-1}$, where P_D is the relative fraction of donor-labeled protein, and n is the number of subunits in the complex (see eq. 4 in Methods). Due to the power law, no variation of donor quenching is expected for monomers as the donor fraction decreases, a linear increase of Q is expected for dimers, and a curved relationship is expected for trimers and higher oligomers. We performed two independent experiments, labeling only one of the two proteins with donor and acceptor fluorophores while leaving the other unlabeled. By labeling only either the FtsL or the FtsB moieties of the FtsLB



complex, the procedure allowed us to calculate the number of subunits of FtsL and of FtsB individually.

As illustrated in Fig. 2.3a, donor quenching increased linearly for FtsL-labeled samples when the acceptor fraction was increased. We used the sum of residuals between the experimental data and the models to compare the fits. The residual of the 2-subunits linear model (dashed line, residual $r = 0.001$) is 10-fold smaller than the

residuals of the 3-subunit model (continuous line, $r = 0.01$), indicating that two FtsL molecules are present in the FtsLB complex. The quenching data of FtsB (Fig. 2.3b) also display a progressive increase of donor quenching, establishing that at least two FtsB subunits are present in the FtsLB complex. However, the fit to two subunits ($r = 0.0055$) is only marginally better than the fit to three subunits ($r = 0.0064$), therefore, the data cannot differentiate between these two models, as in the case of FtsL. The fit, however, can reasonably rule out a 4-subunit model (dotted line, $r = 0.02$).

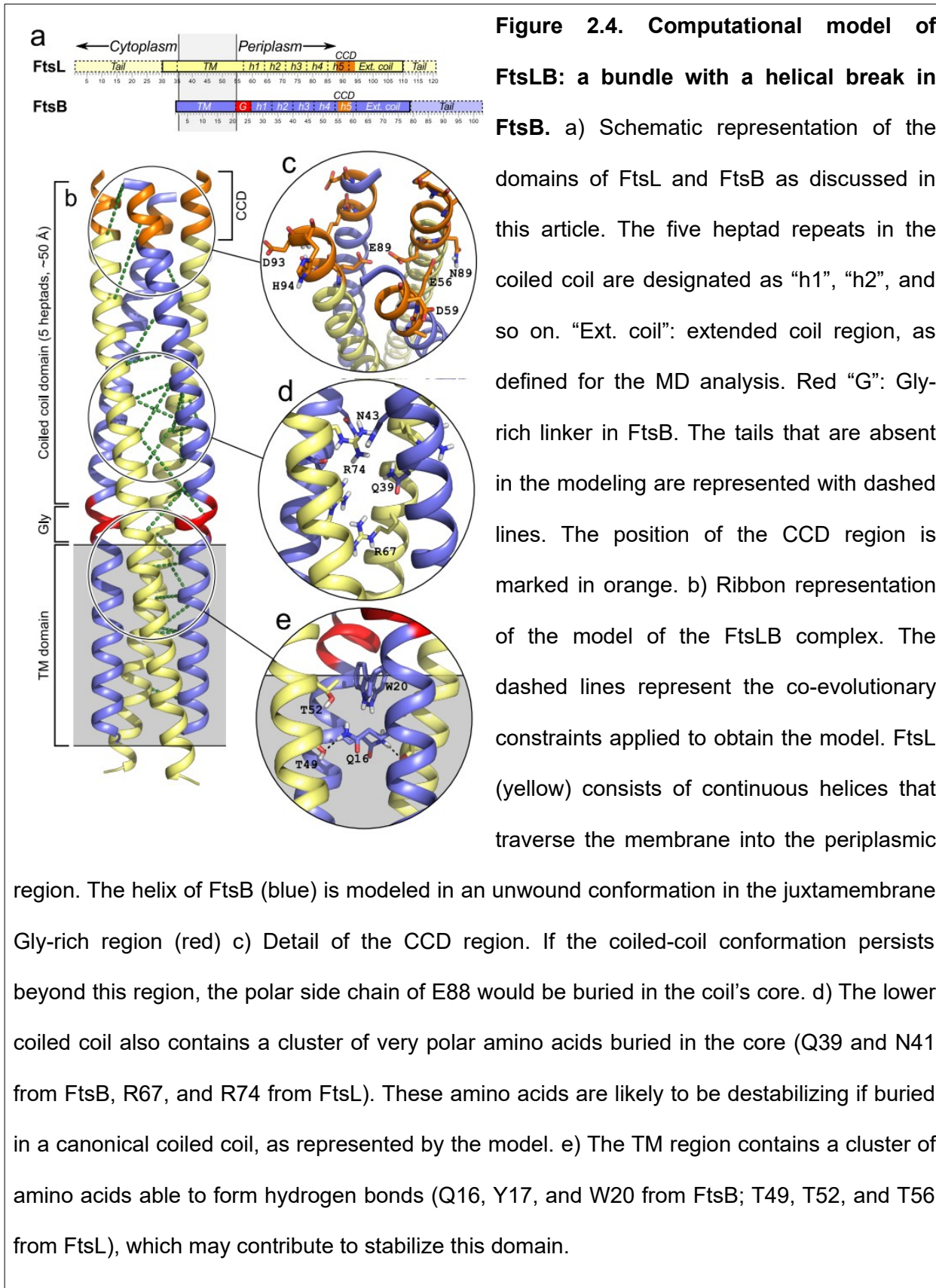
Overall, the analysis confirms that the FtsLB complex is a higher-order oligomer. Considering the entire body of available evidence, the most likely model is an L_2B_2 hetero-tetramer. Since FtsL fits well to a model containing two subunits, the possible states supported by the data are L_2B_2 or L_2B_3 stoichiometries. However, a 2:3 stoichiometry is in disagreement with previous FRET data that indicated that the FtsLB complex has an equivalent number of FtsL and FtsB subunits (43). A 2:3 pentamer is also a less common oligomeric form in nature than a 2:2 hetero-tetramer (69). In addition, a 2:3 pentamer would be necessarily asymmetrical, whereas the co-evolutionary contacts are strongly consistent with a standard symmetrical organization (Fig. 2.2b and c). Finally, 2:2 would also be consistent with a previous estimate of the stoichiometry of the divisome based on ribosome profiling data (70).

2.3.4 Molecular modeling of the FtsLB helical bundle

We used a Monte Carlo docking procedure guided by the evolutionary-based distance constraints to create an all-atom computational model of the structure of the TM and coiled-coil domains of the tetrameric complex (residues 1-61 of FtsB and 35-91 of FtsL). The model, which is illustrated in Fig. 2.4a, consists of a four-helix bundle that

spans the membrane and projects into the periplasmic region for approximately 55 Å. The structure is well packed, with the exception of a small void (approximately 12 Å³) present at the level of the juxtamembrane linker region. A majority of the co-evolutionary distance constraints used to derive the model (dashed lines in the figure, listed in supplementary Table S2.1) are satisfied: of the 27 side chain pairs involved, 22 are in contact (minimal distance between heavy atoms, d_{min} < 5 Å), four are in proximity (d_{min} < 10 Å) and only one pair is separated by over 10 Å (FtsL Q66 with FtsB I26). Because an L₃B₃ hexamer could not be entirely excluded, we modeled also this stoichiometry. The co-evolutionary restraints were well satisfied by the resulting model, but the model is significantly under-packed, with the presence of an incomplete pore spanning parts of the TM and coiled-coil domains (supplementary Fig. S2.3). For this reason, the L₃B₃ model was no longer pursued.

The TM region of the L₂B₂ model forms a helical bundle characterized by a left-handed crossing angle (7° for FtsB and 10° for FtsL, tilt angle of the helices with respect to the membrane normal). The two TM helices of FtsB are in closer proximity to each other compared to the two helices of FtsL (inter-helical distance of 13.6 Å and 15.2 Å respectively). Remarkably, the conformation of FtsB is similar to a model of a FtsB dimer that we obtained previously (RMSD 2.5 Å, supplementary Fig. S2.4). This previous model was obtained from the effect of point mutations on the homodimerization of the TM domain of FtsB in the absence of FtsL, as assayed with TOXCAT (38). The convergence of two completely independent sets of data – evolutionary information and experimental mutagenesis – to a similar model is a strong indication that the conformation and interface of the TM helices of FtsB are correctly predicted.



The C-terminal side of the TM region contains a number of side chains that can form hydrogen bonds, including the polar Q16. In the lowest-energy model, Q16 acts as a hydrogen bond donor to the side chain hydroxyl group of T49 of FtsL (Fig. 2.4b). Small changes in conformation would allow alternative interactions of Q16 with a number of other donor and acceptor groups. In particular, Q16 could form self-interactions with Q16 from the opposing chain, as well as potential hydrogen bonds with T52 of FtsL and W20 of FtsB.

As expected, FtsL was modeled as a continuous helix across the TM and coiled-coil domains. Also as expected, the change of orientation of the interface between the same two domains of FtsB required the introduction of a break in the α -helix in the juxtamembrane region (red). We opted to model the linker in the least perturbing conformation (an unwound helix), even though the Gly-rich linker is likely to adopt a more extended conformation. The relative flexibility of the linker regions of FtsL and FtsB will be addressed later using molecular dynamics.

The periplasmic region (residue 27-61 in FtsB and 58-91 in FtsL) produced a well packed canonical coiled coil. The coil is approximately five heptad-repeats long (~35 amino acids). Interestingly, the domain is unusually rich in polar amino acids occurring at *a* and *d* buried positions, with a total of twelve. These polar amino acids are equally contributed by both proteins (three per subunit), although FtsB contains only neutral side chains (Q39, N43, N50), whereas FtsL contains amino acids that are normally charged (R67, R74, E80). A region around the second and third heptad-repeats of the coiled coil is particularly polar, where R67 and R74 from FtsL and Q39 and N43 from FtsB occur in close proximity. The presence of so many buried hydrophilic side chains is

interesting because they are likely to destabilize the coiled coil. In particular, the four Arg residues contributed by FtsL would be charged even if buried inside the protein core, and thus very costly to desolvate (71). Another potentially charged side chain, E80 in FtsL, is in the core in the modeled complex, but it is placed toward the end of the predicted coiled coil, near the CCD region, and thus it may be solvent accessible.

2.3.5 Molecular dynamics suggest a stable TM region with an intricate network of hydrogen bonding

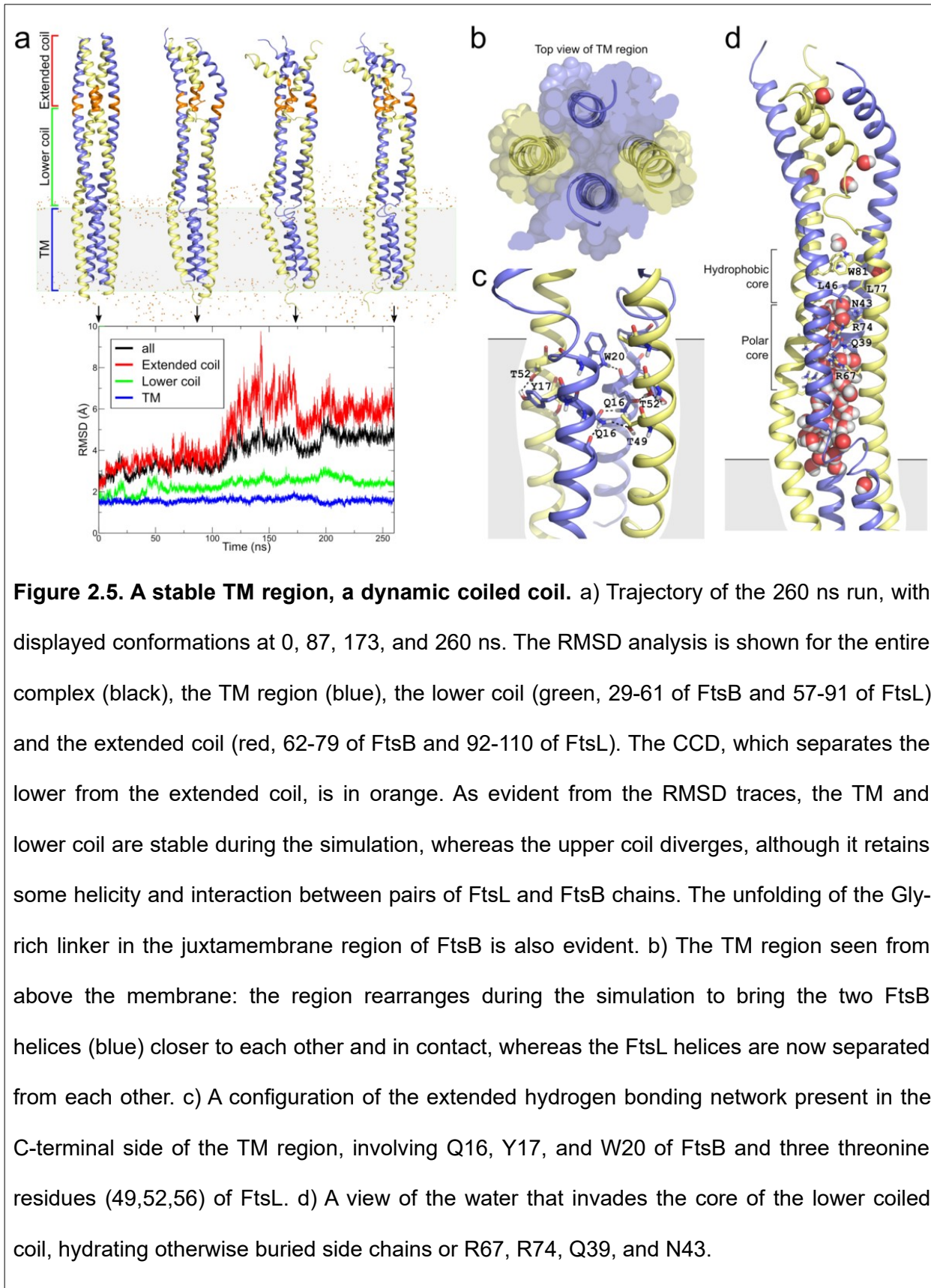
Two features – the presence of a flexible linker and a potentially destabilized coiled coil – raise questions about the dynamic properties of the FtsLB complex. To address them, we performed molecular dynamics (MD) simulations of the FtsLB model in explicit POPE bilayers. For this simulation, we extended the coiled-coil conformation by approximately 20 amino acids beyond the region predicted by the co-evolutionary contacts, to avoid end-effects and to test the coil boundaries. We will refer to this added region as the “extended coil” (92-110 for FtsL and 62-79 for FtsB) and to the section predicted by the co-evolutionary analysis as the “lower coil” (29-61 of FtsB and 57-91 of FtsL). Three replica MD simulations were run for 260 ns (run 1, Fig. 2.5) and for 200 ns (runs 2 and 3, supplementary Fig. S2.5).

During the simulation, the RMSD from the initial structure increases to approximately 4, 5, and 6 Å in the three replica runs (black traces in Fig. 2.5a and Fig. S2.5). The majority of these changes are localized to the “extended coil” section (red traces), which quickly separates and partially unfolds. The “lower coil” remains relatively stable during the run (final RMSD around 2.3, 3.4, and 2.9 Å, green traces). The most stable region is

the TM domain, which remains stable for the entire run across all three simulations, with average RMSDs around 1.6, 1.9, and 2.3 Å during the three runs (blue traces).

A slight rearrangement of the relative orientation of the TM helices is observed, which brings the two FtsB helices closer to each other by approximately 1-2 Å, and, consequently, further separates the FtsL helices by a similar distance. This rearrangement gives the bundle a less “square” and more “rhomboid” configuration, one in which extensive packing occurs not only between FtsL and FtsB, and also between the two FtsB helices, whereas the contacts between the two FtsL helices become reduced (Fig. 2.5b). With the two helices of FtsB in closer proximity, their conformation becomes even more similar to our previous model of a FtsB dimer (RMSD ~2 Å, supplementary Fig. S2.4b) (38).

A second important change that occurs in the TM region during the MD runs is a rearrangement and expansion of the hydrogen bonding network. In the C-terminal section of FtsLB there are 12 side chains in close proximity that are able to hydrogen bond (three from each helix: Q16, Y17, and W20 in FtsB, and three threonines, 49, 52, and 56, in FtsL). With the exception of W20, all these side chains have both donor and acceptor groups. In addition, Q16 is also very flexible. Therefore, the network can rearrange in multiple configurations. Fig. 2.5c illustrates one of the configurations observed, which displays a total of seven inter-helical hydrogen bonds. The configuration of the hydrogen bonding network varies over the simulations but some interactions are predominant during the runs (supplementary Table S2.2). The most persistent interaction is between Y17 of FtsB subunit A and the side chain of T52 of FtsL subunit C (Y17 of subunit B prefers to interact with the backbone carbonyl of L48). Q16



interacts primarily with the side chain hydroxyl groups of T49 and T52 from FtsL and with Q16 from the opposed FtsB helix. W20 primarily donates to the side chain hydroxyl group of FtsL T56, but it can also donate to the carbonyl group of Q16 side chain. This extended network of hydrogen bonds is likely to contribute significantly to the association of the TM region, which can form a stable oligomer in isolation *in vitro* (43).

As a control, we also performed a 160 ns simulation of a structural model that has comparably low energy but does not satisfy the evolutionary constraints in the TM region (“bad model”, Fig. S2.5d). The TM region rearranges away from the initial model relatively quickly, reaching an RMSD of over 3 Å in the first 60 ns. Its average (2.8 Å) and maximum (3.5 Å) are higher than the RMSD of the TM region in the three replica runs of the “good” model (1.6, 1.9, and 2.3 Å, with maxima of 2.1, 2.4, and 2.7 Å, respectively).

2.3.6 A continuous FtsL helix and a dynamic coiled coil

Different sections of the coiled coil behave differently during the MD runs. These are notable in the helicity analysis presented in supplementary Fig. S2.6. The “extended coil” – the region that extends beyond the pattern of co-evolutionary contacts consistent with a coiled coil (Fig. 2.2) – unfolds partially as a bundle during the runs, although the region retains substantial helicity and interactions still occur between pairs of FtsL and FtsB helices. The likely occurrence of a breakage of the helix between the “lower” and the “extended” coil regions was also hypothesized by a previous modeling analysis of the periplasmic region of the FtsQLB complex (55). Interestingly, the location of the transition between these two regions roughly corresponds to the CCD.

The “lower coil” remains more stable during the run (final RMSD around 2.3, 3.4, and 2.9 Å). However, notable changes occur even in this region, providing further indication that the FtsLB complex may not be built to form a rigid, canonical, tetrameric coiled coil. Partial unfolding of the FtsL helix is observed in subunit C, and occasional unfolding is also notable in both FtsL subunit in the third replica run.

In the transition between the TM and coiled-coil domains, the segment of 5-10 amino acids centered around the Gly-rich section of FtsB rapidly unfolds from the “unwound helix” conformation imposed by the modeling, unlinking the two domains and adopting a flexible and extended conformation (Fig. 2.5a). Conversely, the juxtamembrane region of FtsL remains stable as a continuous helix throughout the duration of all three replica runs. The unfolding of the Gly-rich linker of FtsB creates an opening that allows water to access the core of the four-helix bundle (Fig. 2.5d). Water molecules penetrate deeply up into the core of the coil, solvating the strongly polar side chains that would otherwise be buried in the structure (Arg 67 and Arg 74 from FtsL and Gln 39 and Asn 43 from FtsB, “polar core” in Fig. 2.5d). In this region near the membrane, the coil becomes essentially separated by the water into two two-helix bundles. Water is excluded from the above layer, where the four-helix bundle becomes compact again around a hydrophobic core consisting of Leu 46 from FtsB and Leu 77 and Trp 81 from FtsL (“hydrophobic core” in Fig. 2.5d).

With all caution in drawing conclusions from a theoretical model, it appears unlikely that a core so enriched in strongly polar amino acids would produce a very stable coiled coil. A possibility is that the stability of the coil is purposely “detuned” because the function of the FtsLB complex requires a weak coil, possibly to allow for a

conformational change. A second hypothesis is that the region is actually designed to split into two separate two-helix coils. This split is most evident as illustrated in the last frame of MD run number 3 (supplementary Fig. S2.5). A “split” coiled coil would be consistent with the observation that a solubilized version of the periplasmic region of FtsLB forced into a hetero-dimeric form binds to FtsQ with high affinity (49–51), suggesting that association with FtsQ may be mediated by two independent binding domains of FtsLB. Such an organization would designate the TM region as the major factor driving tetramerization.

2.3.7 Functional analysis: the effect of mutations in the TM region is consistent with the predicted interface

To investigate how the model’s structural features support the function of FtsLB, a series of rationally designed variants of the complex were tested *in vivo* for their ability to support cell division. Because FtsL and FtsB are essential proteins, the mutant proteins were introduced into strains in which a chromosomal copy of the wild-type protein is under the control of a repressible promoter (45, 47). This allows for the depletion of the wild-type copy and the induction of the mutant version to reveal its phenotype. The expectation is that the most severe mutations will produce cells that elongate but are unable to divide, resulting in the formation of very long filaments, whereas less severe mutations will allow the cells to divide but will produce sub-populations of elongated cells. To assess each mutant, we measured the distribution of cell lengths, as exemplified in Fig. 2.6a for the L15A mutant of FtsB. The data for each individual mutant are reported in supplementary Fig. S2.7.

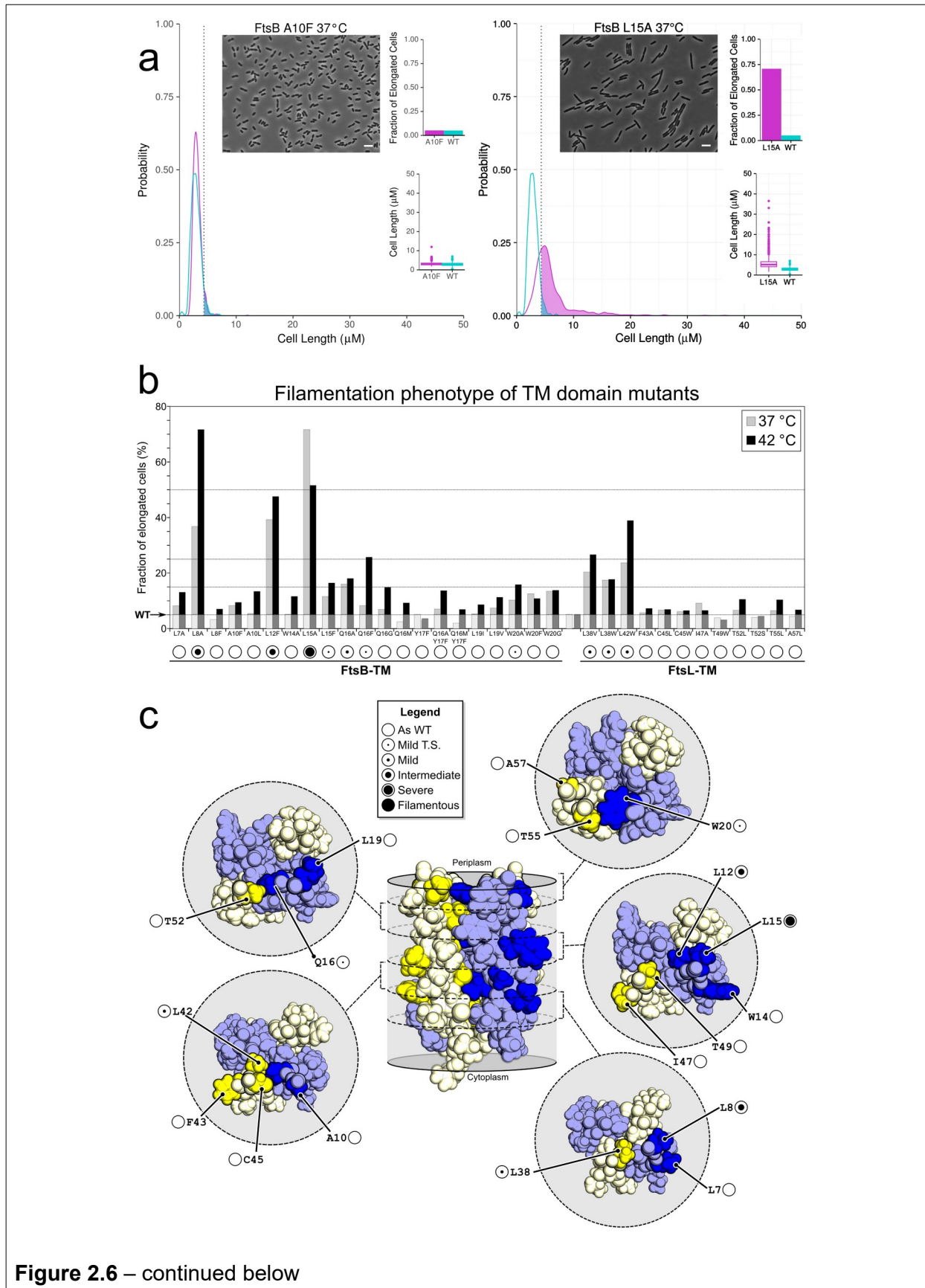
**Figure 2.6 – continued below**

Figure 2.6. Mutations at the interface of the TM domain cause mild phenotypes *in vivo*.

a) Examples of *in vivo* analysis of point mutants with wild-type-like (A10F) and defective (L15A) phenotypes. The distribution of cells lengths is compared between the wild type (aqua) and the mutant (magenta). L15A displays 72% of cells that are longer than the 95th percentile in the wild-type distribution (colored areas, past the dotted line). As such, it is classified as a “Severe” mutation. Graphs for each individual mutant are provided and explained in detail in supplementary Fig. S2.7. Scale bar: 5 μm. b) Phenotypes of TM domain mutants at 37 and 42 °C growth conditions. Classification is indicated using filled circles below: “Filamentous”: all cells are elongated at 37 °C; “Severe”: >50% of the cells elongated; “Intermediate”: >25%; “Mild”: >15%; and “Mild Temperature-Sensitive”: >15% of cells elongated at 42 °C. c) Location of the mutations within the structure of the TM domain. All mutations that display a cell division phenotype map within the interface of the helical bundle. All mutations on the outer surface of the bundle display “As WT” phenotypes.

Although none of the point mutations caused filamentous phenotypes, many produced elongated cells. To determine if the difference between each mutant’s and the wild type’s length distributions was significant, we used the Mann–Whitney *U* test (72). However, as a consequence of the very large sample size of each experiment (500 to >1,000 cells), minuscule differences can be statistically significant even if they are not biologically relevant. To overcome this issue, we adopted an operative classification based on the fraction of elongated cells observed for each variant. We defined as “elongated” those cells that are longer than the 95th percentile in the distribution of wild-type cell length (Fig. 2.6a). Based on this threshold, we defined phenotypes as “Mild Temperature-Sensitive” (“Mild T.S.”) when >15% (i.e. >3 fold compared to the wild type) of cells were elongated only at the less permissive temperature of 42 °C; as “Mild” when

>15% of cells were elongated at 37 °C; as “Intermediate” when >25% of cells were elongated (>5 fold); as “Severe” when over 50% of the cells were elongated (>10 fold); and, finally, as “Filamentous” when all cells were filamentous. The example of Fig. 2.6a, which has 72% elongated cells at 37 °C, is therefore classified as “Severe”.

The fractions of elongated cells for each variant in the TM region of FtsL and FtsB are reported in Fig. 2.6b, with the relative classification reported at the bottom. The variants include a variety of drastic small-to-large amino acid changes (such as A10F in FtsB and L38W in FtsL), large-to-small changes (such as W14A and L8A in FtsB), as well as some conservative mutations (such as L19I in FtsB). We expected to observe division phenotypes when mutations affected the packing or hydrogen bonding at positions that mediate interaction between the helices. The results are in good agreement with this prediction. First, all positions that displayed impaired cell division phenotypes (L8, L12, L15, Q16, and W20 in FtsB; L38 and L42 in FtsL, Fig. 2.6b) occur at the helix-helix interfaces, as illustrated schematically in Fig. 2.6c. In addition, all positions predicted to be away from the interface and exposed solely to lipids are classified as indistinguishable from wild type (L7, A10, and W14 in FtsB; F43, I47 in FtsL). However, some of the TM region mutations that were predicted to be detrimental displayed little or no effect (for example, Q16M, W20A, C45W, and T49W). This is particularly noticeable for the C-terminal side of the TM bundle, a section characterized by an extensive hydrogen bonding network (Fig. 2.5c). Mutations of T49, T52, and T55 of FtsL and Y17 of FtsB have no effect, and those of Q16 and W20 of FtsB have little or no phenotype. Even a double mutation (Q16M/Y17F or Q16A/Y17F) that removes two hydrogen bonding groups, is completely tolerated.

The finding is surprising because the C-terminal side of the TM bundle is the region with the highest number of co-evolutionary “connections”, suggesting that these positions would be structurally or functionally important. Moreover, Q16 and W20 of FtsB are nearly absolutely conserved in proteobacteria (38). A potential explanation is that the hydrogen bonding network may be sufficiently robust, extensive, and plastic to accommodate changes. Because of the large network, the removal of some donors and acceptors may not be sufficiently detrimental to destabilize the complex. Conversely, the N-terminal region – which is mediated exclusively by packing of hydrophobic residues – could be more sensitive to disruption of the complementary side chain packing. It is also possible that thermodynamic stability of the TM region is not strictly required for function, at least in the conditions tested.

To investigate whether there is an overall correspondence between the observed biological phenotypes and predictions based on the structural model, we calculated mutational energies *in silico* for all TM mutants and compared them with the fraction of elongated cells observed for each variant (using the 42 °C data to maximize the dynamic range of the experimental observations). We calculated the energies using either a rigid body model without backbone movement, and with FoldX, a method specifically calibrated to calculate the folding stability of protein mutants (73). The data is plotted in supplementary Fig. S2.8. The energies produced by FoldX statistically correlate with the severity of the phenotypes by Rank Order Spearman Correlation Coefficient analysis ($r = 0.4631$, $N = 29$, $p < 0.01$) (74). We conclude that perturbation of stability estimated on the basis of the structural model is a reasonably good predictor of the functional state of FtsLB.

2.3.8 The juxtamembrane and coiled coil of FtsB are tolerant to mutation

We applied a similar mutational approach to investigate the functional importance of the coiled coil and of the juxtamembrane region. The results are reported in Fig. 2.7 (and Fig. S2.7). We first tested if the evolutionarily conserved Gly-rich juxtamembrane linker of FtsB (22-GKNG-25) is essential. A potential role for Gly is to provide structural flexibility, as suggested by our MD simulations. Alternatively, because of Gly's less restrictive Ramachandran distribution, this amino acid can also be required in a rigid structure to enable conformations of the backbone that are forbidden to all other amino acids.

We tested individual and double Gly-to-Ala mutations at positions 22 and 25. They presented either no defects (G22A and G22A/G25A) or a mild TS phenotype (G25A) (Fig. 2.7a). A possible explanation is that the structure of the linker retains sufficient flexibility even when G22 and G25 are substituted by Ala. To further test the flexibility of the linker, we inserted a series of Ala residues (up to three) between the TM domain and the coiled-coil region (between positions F21 and G22), with the rationale that insertions should be better tolerated in a flexible region. The cells appear largely unaffected by the changes (only the two-Ala insertion mutation displays a mild TS phenotype, Fig. 2.7b). The outcome is therefore consistent with a flexible FtsB linker and confirms the presence of a helical break between the membrane and periplasmic domains of FtsB. These observations are not consistent with the alternative hypothesis that Gly is required to enable a rigid backbone conformation.

We also applied this Ala-insertion strategy to test the coiled-coil region of FtsB. A single additional Ala residue was inserted between the "b" and "c" positions (i.e. in a

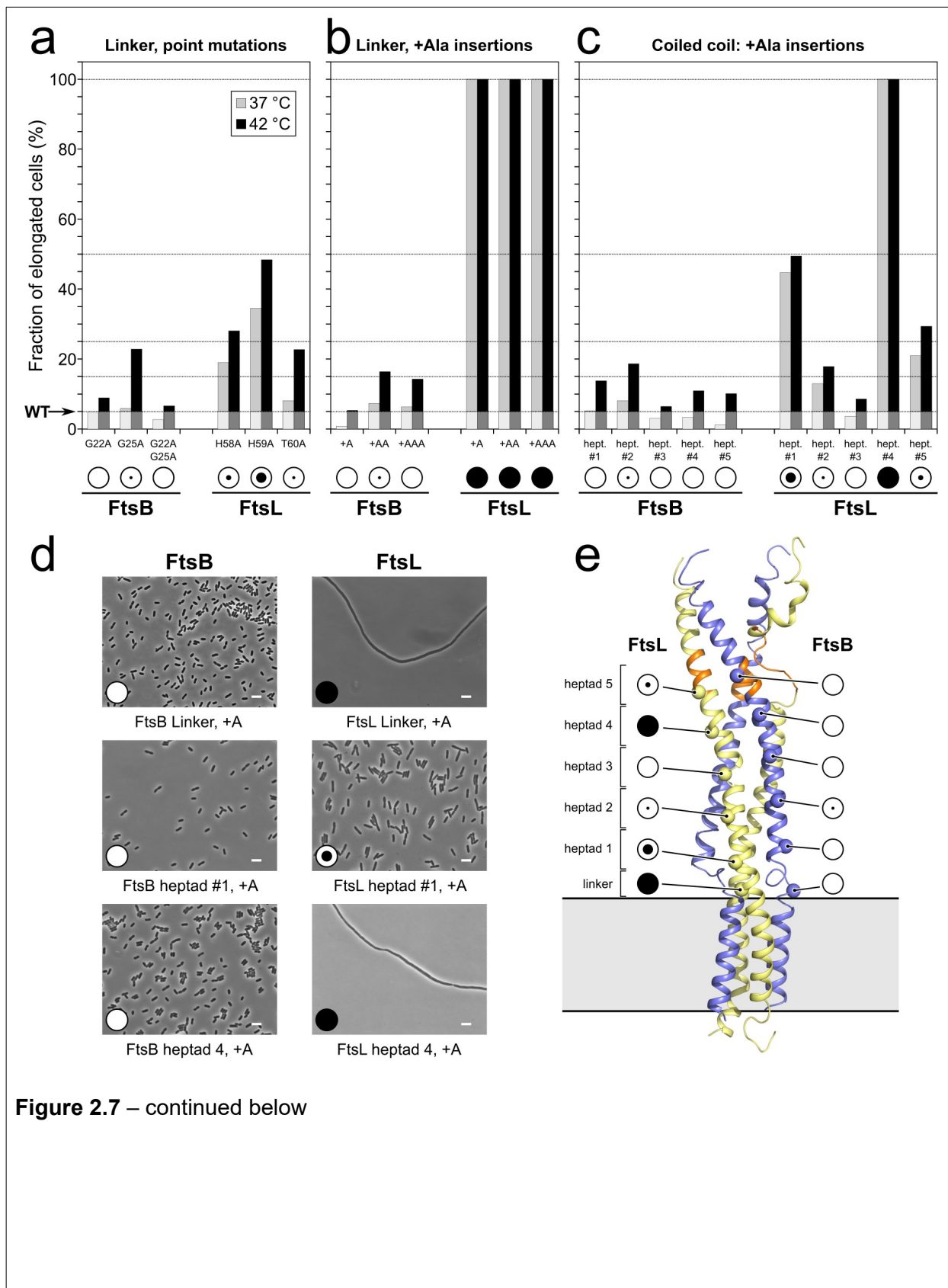


Figure 2.7 – continued below

Figure 2.7. The juxtamembrane and coiled-coil regions of FtsL are sensitive to mutation. a) Phenotypic analysis of juxtamembrane (“linker” region) point mutations of FtsL and FtsB, classified as detailed in Fig. 2.6. Graphs for each individual mutant are provided in supplementary Fig. S2.7. b) Alanine insertion mutation (1-3 extra residues) in the same region. c) Ala insertion mutations in the coiled-coil region (operated between positions “b” and “c” in the heptad repeats). d) Representative images of Ala insertion mutants in the linker and periplasmic coiled coil of FtsB and FtsL. Images for all mutants are provided in Fig. S2.7. e) Observed phenotype of the mutants mapped onto the molecular model. Constriction control domain is displayed in orange. The evidence is consistent with a flexible linker in FtsB, with the presence of a helical break, and with an uninterrupted helix that runs through the membrane and periplasmic regions for FtsL.

position that is solvent exposed) of each of the five heptad repeats. Most of these five insertion mutants did not display any impairment, with the exception of a mild TS phenotype for the second-heptad insertion after position A37 (Fig. 2.7c). Overall, the analysis suggests that the coiled coil of FtsB is likely to be quite plastic and able to tolerate insertion mutations all along its length.

2.3.9 Integrity of the juxtamembrane and coiled-coil regions of FtsL is essential for function

Whereas the juxtamembrane and coiled-coil domains of FtsB appeared tolerant to insertion, the opposite was observed for FtsL. We first introduced single, double, and triple Ala-insertion mutations in the juxtamembrane region of FtsL (between positions A57 and H58). If the helix of FtsL is uninterrupted, the insertions should introduce strain into the structure because they would either produce a 100° rotation of the helix for

each additional Ala or, more likely, introduce distortions into the helix. We observed that all insertion mutants – even the single Ala insertion – produced cells that were completely filamentous (Fig. 2.7b and cell images in panel Fig. 2.7c). These are the most dramatic phenotypes observed in the whole study. The results are consistent with the hypothesis that FtsL forms an uninterrupted helix that runs through the membrane and periplasmic regions.

We also tested the juxtamembrane linker of FtsL with a series of point substitutions (H58A, H59A, and T60A, Fig. 2.7a). Interestingly, we observed some degree of functional disruption, particularly with the H59A mutation, which displays a 7-fold increase in the number of elongated cells compared to wild type at 37 °C. In our model, H59 is solvent exposed and engaged only in minor interactions with the FtsB helix. It is possible that this position is important for interactions with other components of the divisome, possibly with the periplasmic domain of FtsQ, which was shown to crosslink with this region of FtsL (48).

Finally, we scanned the entire coiled-coil region of FtsL by Ala insertion (Fig. 2.7c), as we did with FtsB. We observed a severe phenotype for the first-heptad insertion, a mild phenotype for the second-heptad insertion, and a wild-type phenotype for the third-heptad insertion. A completely filamentous phenotype is then observed when Ala is inserted in the fourth-heptad repeat (after position R82). It is difficult to speculate what might cause such a dramatic defect, but we note that the mutation is in proximity to the CCD region of FtsL (88-94, highlighted in orange in Fig. 2.7e). Insertion at position 89 – which is within the CCD and which would correspond to the fifth-heptad, if the coiled coil persisted in this region – produced a mild phenotype (~4-fold increase in elongated

cells). Overall, the periplasmic coiled coil of FtsL is sensitive to mutation, whereas the same domain of FtsB is tolerant, as schematically illustrated in Fig. 2.7e. Interestingly, this outcome is the opposite of that observed for the mutagenesis of the TM region, where FtsB was the sensitive subunit compare to much milder phenotype displayed by FtsL (Fig. 2.6).

2.4 Conclusions

The topology of the FtsLB complex – a helical bundle spanning the membrane and periplasmic space, with terminal tails available for binding other components – is widely conserved evolutionarily (6, 50). The widespread occurrence of FtsLB across a broad variety of bacterial species with different cellular envelopes implies that this specific domain organization fulfills some important functional purpose, which is still unknown. To investigate this question, we have analyzed the structure-function relationship of the extended helical region of FtsLB, revealing a number of important features regarding the organization of the complex.

This study confirms that FtsLB is a higher-order oligomer and provides evidence that the complex consists of a hetero-tetramer. It identifies with a high degree of confidence the interface of the helical bundle region of the complex. It also produces a structural model of FtsLB validated experimentally through functional analysis. Further validation is also provided by a notable convergence of features in FtsB (the conformation of the TM helices and the presence of a flexible linker) that were also predicted in a prior model of FtsB based on a completely orthogonal set of experimental data (38).

The number of strongly polar, and even charged, amino acids that are predicted to be buried in the core of the coiled coil is a surprising and likely important finding, suggesting that the coil region may not be built for enhanced structural stability. A structural alternative to a monolithic four-helix coil could be the formation of two independent “dimeric” branches formed by one FtsL and one FtsB subunit. This possibility is consistent with previous observations that FtsLB fragments can bind to FtsQ with high-affinity even when forced in a hetero-dimeric state (49–51).

We found that the integrity of the extended helix of FtsL is essential for the complex. A continuous helix is likely important for structural stability: given that the juxtamembrane linker of FtsB is disordered, a stable FtsL helix is probably necessary for nucleating the coiled coil. This hypothesis is in good agreement with the observation that amino acid insertions are most detrimental at the base of this domain. The helix of FtsL is also an interesting candidate for acting as a mechanical connection that could propagate a postulated allosteric conformational change (41, 42) across the periplasmic, TM, and cytoplasmic regions. For example, the cytoplasmic region of FtsL is important for the recruitment of FtsW (47), therefore it is possible that FtsLB could control the activation of the FtsWI peptidoglycan synthase complex through direct interaction by coordinating a signal from the periplasm (i.e. interaction with FtsN). This study provides structural groundwork necessary for investigating this and other hypotheses with coordinated biophysical and functional studies, which are necessary to finally clarify the precise role and the molecular mechanisms of the FtsLB complex in bacterial cell division.

2.5 Experimental Procedures

2.5.1 Co-evolutionary analysis

Sequences of FtsL and FtsB homologues were collected using the DELTA-BLAST algorithm on the RefSeq database (75). These sequences were filtered to include only proteobacterial species and then concatenated by matching the organism name in each record. The paired sequences were then aligned using the Clustal-W algorithm with 5 guide tree and 5 Hidden Markov Model iterations (76). Columns in the alignment with a gap fraction higher than 0.3 were masked. This paired multi-sequence alignment (MSA) was analyzed with the EV-Couplings algorithm (56) using default parameters and ignoring membrane topology, which would otherwise assume that sequential TM domains are anti-parallel. The top 95 (the number of unmasked columns in the MSA divided by two) evolutionary constraints – i.e. the co-varying residues – predicted by EV-Fold between FtsL and FtsB were used for analysis and molecular modeling. The paired alignment is provided as a supplementary FASTA file. A total of 1291 sequences were used in the alignment. The number of effective sequences after reweighting for similarity is 883.1, corresponding approximately 4.6 sequences per residue. From this, approximately 40% of the top 95 contacts are estimated to be false positive pairs in the co-evolutionary analysis (77).

2.5.2 Modeling the TM region of FtsLB

All modeling was performed using programs written in the Molecular Software Library (MSL) (78). For the TM domain, ideal helices corresponding to residues 1-21 of FtsB and residues 35-58 of FtsL were generated. C_2 rotational symmetry (or C_3 , in the

case of the hexamer) was preserved around the Z-axis for FtsB helices and FtsL helices. The geometry of the FtsL and FtsB bundles was defined by the following parameters: inter-helical distance (d); rotation around the helical axis (ω); crossing-angle (θ) and position of the crossing point (s). Additionally, the orientation of the FtsL and FtsB bundles were changed by operating a rotation (Ω) and a translation (S) of each helix bundle about the Z-axis.

Starting from an initial random assignment of the parameters, the FtsLB TM helix complex was optimized using a Monte Carlo procedure that altered the inter-helical geometry. The conformation of the side chains was periodically optimized with a 5% probability after each move. Side chain optimization was performed with a greedy trials algorithm using the backbone-dependent Energy-Based Conformer Library (bEBL) applied at the SL80 level (79, 80). Energies were calculated using the CHARMM 22 van der Waals function (81) and the hydrogen bonding function of SCWRL 4 (82) as implemented in MSL. Additionally, sigmoidal distance restraints were placed between the $C\alpha$ atoms of each pair of top co-evolving positions (83), using the following form:

$$(1) \quad E_{sigmoid} = \frac{w}{1 + e^{-a(r - r_0)}} + C$$

where $E_{sigmoid}$ is the additional energy term, w is the weight, a is the slope, C is the intercept, r is the distance between the atoms, and r_0 is the distance cutoff. For these experiments, w was set to 10 kcal/mol, a was set to 0.5 \AA^{-1} , C was set to -2.5 kcal/mol, and r_0 was set to 10 Å.

For each pair of co-evolving residues, there are multiple pairs in the complex corresponding to the same residues on different chains. Only the restraints with the

lowest energies for each pair were added to the energy score while the remaining ones were masked. The evolutionary constraints are listed in supplementary Table S2.1. Models were sorted by energy and clustered using a greedy algorithm and a Ca root mean square deviation (RMSD) threshold of 2.5.

As a negative control for the molecular dynamics simulations, a second model of the TM domain was produced by identifying a conformation with comparable energy of the initial model but with poor agreement with the co-evolutionary data (“bad model”). In this model, only one pair of co-evolving positions had a minimum heavy atom distance below 5 Å, and only two pairs had Ca distances below 10 Å, whereas all pairs satisfy these conditions in the “good model”.

In silico mutational energies for the mutants in the transmembrane region were calculated in two ways. Rigid-backbone repacking was performed using MSL. Point mutations of interest were generated and neighboring side chains were repacked using 100 rounds of a greedy trials algorithm. Mutated residues were repacked at the SL99 conformer level of the bEBL library; residues within 8, 16, and 20 Å were repacked at the SL95, SL90, and SL80 levels respectively. Van der Waals radii were scaled by 0.8. Energies of the mutants were subtracted from that of the wild type to calculate their $\Delta\Delta E$. Mutations were also analyzed using the FoldX Suite (73). The models were first energy-minimized using the *RepairPDB* command with the membrane parameter set to true. Mutant $\Delta\Delta G$ calculations were performed using the *buildModel* command with the membrane parameter set to true.

2.5.3 Modeling the coiled-coil domains of FtsL and FtsB

Supercoiled helices corresponding to residues 52-94 of FtsL and 21-63 of FtsB were generated by using a coiled-coil generator based on a previously described coiled-coil parameterization (84). The super-helical radius (r_1), super-helical pitch (P), helical rotation (Φ_1), and Z-shift (s) of both FtsL and FtsB were freely altered, while the rise per residue (h) and helical radius (r_0) were kept constant. Additionally, the orientation of the FtsL and FtsB bundles were changed by operating a rotation (Ω) and a translation (S) of each helix bundle about the Z-axis. C_2 symmetry (C_3 for the hexamer) was preserved within the FtsL backbones and the FtsB backbones.

The coiled coils were optimized using a Monte Carlo procedure, changing their super-helical parameters starting from an initial assignment of random parameters. Side chain conformational sampling was performed with a variable number of conformers with the positions that participate at a canonical coiled-coil interface receiving higher sampling: the *a* and *d* positions were sampled at the SL80 conformer level of the bEBL library, *e* and *g* positions at the SL75 level, *b* and *c* at the SL70 level, and *f* at the SL60 level. Energies were calculated based on CHARMM 22 van der Waals and CHARMM 22 electrostatic terms. Additionally, sigmoidal restraints for each co-evolving pair in the coiled-coil region were added, as described above.

2.5.4 Modeling the juxtamembrane regions of FtsL and FtsB

Top models of the TM and coiled-coil domains were connected by aligning the helical residues 52-58 of FtsL, which were present in the models of both regions. The RMSD between the C α atoms of these residues was minimized while keeping the main axis of both domains parallel to and centered on the Z-axis. The juxtamembrane regions

of FtsL and FtsB were then replaced with loops corresponding to fragments from the PDB as described previously (38). For FtsB, six-residue loops, corresponding to positions 21-26, with four flanking helical residues on each side were used, with an additional sequence requirement that the fragment contain at least one glycine. For FtsL, fifteen-residue fragments with four flanking helical residues on each side were used with the requirement that the loop have helical secondary structure. Long helix fragments were used to better distribute minor deviation in alignment between the transmembrane and coiled-coil helices. The connecting regions were optimized based on a greedy trials algorithm to minimize steric clashing, and the final model was minimized using BFGS constrained optimization using CHARMM (85). Structural voids were analyzed using BetaCavityWeb (86). For the creation of the “bad model”, the TM model that did not satisfy the co-evolutionary constraints was aligned and connected to the same model of the coiled-coil domain using an identical procedure.

2.5.5 All-atom molecular dynamic simulations

For the molecular dynamics simulations, the model’s coiled-coil region was extended, to avoid edge effects, to residues 110 (FtsL) and 79 (FtsB). The cytoplasmic side of FtsL was also extended to include residues 30-34, modeled in ideal α -helix. Four all-atom MD simulations (a 260 ns run, two 200 ns replica runs, and a 160 ns control run on the control “bad model”) were performed using the CHARMM36 force field and NAMD 2.10 software (87, 88). CHARMM-GUI membrane builder (89) was used to prepare systems composed of a POPE bilayer consisting of 301 lipids, the FtsLB tetramer, an ionic concentration of 0.150 M NaCl, and 59034 TIP3P water molecules for hydration. The size of the boxes at the beginning of the simulation were approximately

$97 \times 97 \times 242 \text{ \AA}^3$ for runs 1, 2, and 3 and $97 \times 97 \times 245 \text{ \AA}^3$ for the control run. The simulations were initially minimized and equilibrated for 75 ps at an integration time of 1 fs/step and for 600 ps at an integration time of 2 fs/step. The integration time step for the production runs of each of the systems was 2.0 fs/step. The simulations were carried out in the NPT ensemble at a pressure of 1 atmosphere and a temperature of 310.15 K, using the Nose-Hoover Langevin piston and Langevin dynamics method. Particle Mesh Ewald was used for electrostatic interactions and a 12 Å cutoff was applied to Lennard-Jones interactions with a switching function from 10 to 12 Å. The RMSD analysis was performed using the RMSD trajectory tool in VMD (90). Hydrogen bonding analysis was performed with an in-house script.

Helicity analysis was performed by measuring the backbone dihedrals and the distance between O_i-N_{i+4} for each residue in each selected frame of the simulation. If the O_i-N_{i+4} distance was between 2.0-4.2 Å and the backbone dihedral angles within the favored alpha helical region as defined in PROCHECK (91), the residue was classified as helical. If the O_i-N_{i+4} distance was within 5 Å and the backbone dihedral angles within either the favored or allowed alpha helical region, the residue was classified as near-helical. Otherwise, the residue was classified as non-helical.

2.5.6 Cloning, expression, purification and labeling of FtsLB constructs for FRET measurements

The His-tagged FtsB and Strep-tagged Cys-less (C41A, C45A) FtsL₃₅₋₁₂₁ (supplementary Table S2.3) were introduced into a modified pETDuet-1 vector at restriction sites Ncol/HindIII and NdeI/Xhol respectively. For fluorophore labeling, cysteine mutations were either introduced to FtsB (S97C) or to Cys-less FtsL (I100C)

via Quikchange mutagenesis (Novagene). All constructs were confirmed by DNA sequencing (Quintarabio).

The plasmids were transformed into BL21 (DE3) cells. Individual colonies were picked and grown overnight in 3 mL of LB broth containing 100 µg/mL of ampicillin, before being diluted 1:500 in 1 L of ZYP-5052 auto-induction media as described (92), and grown at 37 °C until reaching an optical density at 600 nm (OD₆₀₀) of 0.8, after which it was incubated for an additional 20 hours at 25 °C. The cells were then lysed by sonication in 10mL/g lysis buffer (50 mM NaCl, 50 mM HEPES, 10 mM TCEP, brought to pH 7.0 with NaOH) supplemented with 0.25 mg/ml lysozyme, 5 mM β-mercaptoethanol and 1mM phenylmethylsulfonyl fluoride (PMSF). The inclusion body fraction was separated by centrifugation at 10,000 g for 20 minutes, followed by ultracentrifugation of the supernatant at 130,000 g for 30 minutes to isolate the cell membranes. The FtsLB complex was then extracted from the membrane fraction with lysis buffer supplemented with 18 mM *n*-decyl-β-D-maltopyranoside (DM; Anatrace) and 10mM TCEP, rocking at 4 °C overnight. Solubilized protein was added to 3 mL of Ni-NTA agarose resin (Qiagen) and rocked for 2 hours at 4 °C before the resin was washed and the complex was labeled on-column with either Cyanine3 (Cy3) or Cyanine5 (Cy5) maleimide (Lumiprobe) for FtsB or FtsL. On-column fluorophore labeling was performed by running 3 column volumes of Ni wash buffer (300 mM NaCl, 25 mM HEPES pH 8.0, 50 mM imidazole, 10 mM TCEP, brought to pH 7.0 with NaOH) supplemented with 5.4 mM DM, 3 column volumes Cy3 or Cy5 labeling buffer (100 µM Cy3 or Cy5 maleimide, 5.4 mM DM, 50 mM NaCl, 50 mM HEPES pH 8.0, brought to pH 7.0 with NaOH), 6 column volumes of Ni wash buffer supplemented with 450 µM *n*-

dodecyl- β -D-maltoside (DDM; Avanti Polar Lipids), and 2 column volumes elution buffer (300 mM NaCl, 25 mM HEPES pH 8.0, 450 μ M DDM, 300 mM imidazole, brought to pH 7.0 with NaOH). For quantification, the elution fractions were dialyzed overnight at 4 °C against FRET buffer (300 mM NaCl, 25 mM HEPES pH 8.0, 450 μ M DDM, brought to pH 7.0 with NaOH).

Labeling efficiency of each fraction was quantified by UV-VIS spectroscopy, using absorbance at 280 nm (protein), 550 nm (Cy3), and 650 nm (Cy5). First, the concentration of the protein was calculated, taking into account the absorbance of the fluorophore:

$$(2) \quad [Protein] = \frac{A_{280} - (A_{Cy} \times CF_{Cy})}{\varepsilon_{280}}$$

where A_{280} is the absorbance at 280 nm, A_{Cy} is the absorbance at 550 nm (Cy3 labeled samples) or 650 nm (Cy5 labeled samples), ε_{280} is the molar extinction coefficient of FtsLB at 280 nm ($32,430 \text{ M}^{-1} \text{ cm}^{-1}$), and CF_{Cy} is the appropriate correction factor ($CF_{Cy^3} = 0.11$ and $CF_{Cy^5} = 0.05$) to subtract the contribution of the fluorophore to absorbance at 280 nm. Then, the labeling efficiency P_{Cy} was calculated according to:

$$(3) \quad P_{Cy} = \frac{A_{Cy}}{[Protein] \times \varepsilon_{Cy}}$$

where ε_{Cy} is the molar extinction coefficient of the fluorophore ($\varepsilon_{Cy^3} = 150,000 \text{ M}^{-1} \text{ cm}^{-1}$ at 550 nm, $\varepsilon_{Cy^5} = 250,000 \text{ M}^{-1} \text{ cm}^{-1}$ at 650 nm). Cysteine-less versions of the FtsL and FtsB constructs were also purified and labeled three times with the same protocol to determine background labeling, which was negligible.

A second round of purification could be performed by loading the Ni-NTA purified FtsLB complex over a streptavidin column. The most concentrated Ni-NTA elution fractions were added to 3 mL streptavidin resin and rocked for 2 hours at 4 °C before being washed with 3 column volumes of streptavidin buffer (20 mM Tris, 300 mM NaCl, 0.1 mM EDTA, 0.5 mM TCEP, brought to pH 8.0 with NaOH) with 450 µM DDM, followed by elution with 3 column volumes of streptavidin buffer plus 2.5 mM desthiobiotin (initially dissolved in 1 mL of DMSO) and 450 µM DDM. Samples from each fraction of the Ni and strep column were boiled in 4× SDS-PAGE loading buffer, before being run on NuPage 4-12% Bis-Tris protein gels at 150 V for 1 hour (ThermoFisher Scientific). Because the FtsLB complex obtained after Ni-NTA had sufficient purity for FRET studies, this second chromatography was not routinely performed, but it was used initially to confirm the stability of the FtsLB complex.

2.5.7 FRET measurements

In all experiments, the FtsLB complex was diluted to 1.35 µM in FRET buffer, which contains 450 µM DDM, for a final protein: detergent molar ratio of 1:333. Experiments were performed by labeling either the FtsL moiety (FtsL-C41A/C45A/I100C + FtsB) or the FtsB moiety (FtsL-C41A/C45A + FtsB-S97C) in the protein complex. All FRET analysis was performed on an M1000 Tecan plate reader, with excitation set at 550 nm and emission recorded from 560 nm to 800 nm in 1 nm increments.

The formation of FtsL/FtsB oligomers *in vitro* was assessed by measuring FRET on a 50:50 mix FtsL_{Cy3}/FtsB_{unlabeled} and FtsL_{unlabeled}/FtsB_{Cy5} complexes, which were compared to a 50:50 mix of FtsL_{Cy3}/FtsB_{unlabeled} and FtsL_{unlabeled}/FtsB_{unlabeled} (donor only sample)

complexes and a 50:50 mix of FtsL_{unlabeled}/FtsB_{Cy5} and FtsL_{unlabeled}/FtsB_{unlabeled} (acceptor only sample) complexes.

The stoichiometric analysis of FtsL was performed by mixing FtsL_{Cy3}/FtsB_{unlabeled} (donor) and FtsL_{Cy5}/FtsB_{unlabeled} (acceptor) samples in different ratios, from 20:80 donor:acceptor, up to 90:10, in 10% increments. To determine donor fluorescence in the absence of the acceptor, equivalent samples were produced by mixing FtsL_{Cy3}/FtsB_{unlabeled} (donor) and FtsL_{unlabeled}/FtsB_{unlabeled} (unlabeled) in the same molar ratios. The stoichiometric analysis of FtsB was performed similarly. Donor (Cy3) fluorescence was recorded using its peak emission at 570nm. Quenching (Q) of the donor fluorophore was calculated, as explained below, according to equation 6, from donor/acceptor labeled protein sample mixes (F) and donor/unlabeled protein sample mixes (F_0). Each experiment was independently replicated at least 5 times.

2.5.8 Fitting of experimental FRET data to obtain the number of subunits

Fitting for different oligomeric states was performed as described by Adair and Engelman (68):

$$(4) \quad Q = \left(1 - \frac{f_Q}{f_D}\right) \left(1 - P_D^{n-1}\right)$$

where donor quenching Q is related to the molar fluorescence of the quenched donor f_Q in the presence of the acceptor, the molar fluorescence of the donor f_D in the absence of acceptor, the number of subunits in the oligomer n , and the molar fraction of donor-labeled protein P_D .

P_D was calculated as:

$$(5) \quad P_D = \frac{[D]}{[D] + [A]}$$

where $[D]$ is the molar concentration of donor-labeled protein and $[A]$ is the molar concentration of acceptor-labeled protein.

Relative quenching was calculated as:

$$(6) \quad Q = 1 - \frac{F}{F_0}$$

where F is the experimentally measured quenched fluorescence for a certain donor/acceptor molar fraction and F_0 is the experimentally measured unquenched fluorescence of the same amount of donor, obtained in the absence of acceptor and in the presence of an equivalent amount of unlabeled protein. In equation 4, the quantity related to the molar fluorescence can be treated as an overall unknown constant k :

$$(7) \quad \left(1 - \frac{f_Q}{f_D}\right) = k$$

The parameter k was thus fit using a least square procedure to the experimental data Q as a function of donor fraction P_D , according to:

$$(8) \quad Q(P_D) = k(1 - P_D^{n-1})$$

for the different oligomeric states n . The relative quality of the fits to different oligomeric states was assessed by comparing the sum of the squared residuals between the experimental data and the models.

2.5.9 Bacterial strains, plasmids, and media for *in vivo* experiments

The phenotypic analysis was performed using depletion strain NB946 for FtsB (7) and MDG277 for FtsL (45). For all experiments described, bacterial cells were grown in LB media supplemented with 100 µg/ml spectinomycin (Dot Scientific) and the appropriate carbon source. Medium was supplemented with 0.2% w/v L-arabinose (Sigma) or 0.2% w/v D-glucose (Sigma) to respectively induce or repress the expression of chromosomal copies of the wild-type genes regulated by the P_{BAD} promoter. 20 µM isopropyl-β-D-1-thiogalactoside (IPTG) was added to the media to induce the expression of mutant genes regulated by the pTrc promoter in the plasmid. Point mutants and insertion mutants of FtsL and FtsB were constructed in plasmid pNG162 (45) using either standard Quikchange mutagenesis or Inverse PCR mutagenesis.

2.5.10 Depletion strain experiments

The protocol for the depletion strain experiment was adapted from Gonzalez and Beckwith (45). In short, a mutated copy of FtsB or FtsL was transformed into their respective depletion strains. Strains were grown overnight at 37 °C on a LB plate supplemented with arabinose and spectinomycin. A single colony from the plate was grown overnight at 37 °C in 3 mL of LB medium supplemented with arabinose and spectinomycin. The overnight culture was then diluted 1:100 into fresh LB medium containing the same supplement and grown to an OD₆₀₀ of ~0.3. An aliquot of 1 mL of culture was washed twice with LB media lacking any sugar, then diluted 1:100 into 3 ml fresh LB media supplemented with glucose and IPTG to induce the expression of the mutated gene and the repression of the wild-type gene. The cells were then grown at 37 °C or at 42 °C for 3.5 hours prior to microscopy, the approximate time necessary to

deplete the cells of the wild-type chromosomal copy (45). Depletion strains provided with their respective wild-type copy of the protein in the plasmid were tested as positive controls, and, similarly, depletion strains with no protein in the plasmid (empty vector) were tested as negative controls.

2.5.11 Microscopy and cell length measurement

10 µL of cell samples were mounted on a No. 1.5, 24×50 mm (0.16 to 0.19 mm thickness) cover glass slide (Fisher scientific). Cells were cushioned with a 3% w/v agarose gel pad to restrict the movement of the live cells. Cells were optically imaged using a Nikon Eclipse Ti inverted microscope equipped with crossed polarizers and a photometrics CoolSNAP HQ2 CCD camera using a Nikon 100× oil objective lens. Phase-contrast images of bacterial cells were recorded with 70 ms exposure time using Nikon NIS Elements software. Multiple snapshots were collected for each experiment. All images were analyzed to measure the cell length in Oufti (93) using one single optimized parameter set.

2.5.12 Whole-cell lysate preparation and Western Blotting

Expression level across all variants was assessed by Western Blot analysis (supplementary Fig. S2.9). 3.0 mL of cells were pelleted and resuspended in 500 µL sonication buffer (25mM Tris-HCl, 2mM EDTA; pH 8.0). The cells were sonicated, and centrifuged at 16,000g for 5 min before collecting the supernatant. Total protein concentration was determined by BCA assay (Pierce). 150 µL of lysates were mixed with 50 µL 4× LDS sample buffer (Novex, Life technologies) and boiled at 95 °C for 5 min. For each sample, the equivalent of 10 µg of total protein was separated by SDS-

PAGE (Invitrogen) and transferred to PVDF membrane (VWR). HRP tagged anti-Flag (M2) antibodies (Sigma, 1:1,000) were used for immunoblotting analysis.

2.6 Supplemental information

Table S2.1. Top 95 predicted co-evolutionary contacts between FtsL and FtsB

FtsB		FtsL		Co-evo ranking		Structural model	
Position	Heptad ¹	Position	Heptad ¹	Rank ²	Score ³	Min distance (Å) ⁴	C _o distance (Å) ⁵
TM domain							
T 5	e	P 39	a	28	0.18971	4.76	6.43
L 12	e	C 45	g	8	0.23962	3.61	7.56
L 12	e	I 46	a	41	0.17785	3.71	5.86
L 15	a	I 46	a	5	0.27006	4.01	8.11
L 15	a	V 53	a	86	0.15394	4.61	8.40
Q 16	b	T 49	d	12	0.23363	3.08	6.86
L 19	e	T 52	g	78	0.15754	3.58	8.40
L 19	e	T 56	d	75	0.15967	3.49	7.66
Coiled coil							
I 26	e	Q 66	g	76	0.15946	11.22**	16.52
Y 29	a	T 56	d	15	0.21667	7.97*	10.12
Y 29	a	T 60	a	39	0.17999	5.91*	8.69
V 32	d	T 64	e	22	0.20568	4.54	7.28
D 35	g	R 67	a	23	0.20543	4.03	8.08
D 35	g	V 71	e	27	0.19052	4.46	7.78
V 36	a	L 63	d	10	0.23707	5.38*	9.22
V 36	a	L 70	d	11	0.23583	3.78	7.70
Q 39	d	T 64	e	59	0.16512	9.17*	14.52
Q 39	d	R 67	a	74	0.15968	3.37	10.34
Q 40	e	Q 66	g	16	0.21574	3.54	9.58
Q 40	e	L 70	d	25	0.19574	3.48	6.94
N 43	a	R 74	a	62	0.16375	3.33	7.96
K 47	e	E 73	g	3	0.3737	3.88	9.46
R 49	g	W 81	a	6	0.25888	2.78	8.18
L 53	d	W 81	a	49	0.1721	3.52	10.29
I 57	a	E 80	g	29	0.1897	8.62*	13.43
N 61	e	E 87	g	13	0.22554	3.78	9.25
N 61	e	L 91	d	2	0.41222	4.06	6.67
Other							
65		103		33	0.18404		
67		101		19	0.21003		
68		105		72	0.16013		
68		107		55	0.16661		
79		107		7	0.24894		
80		106		1	0.41824		
80		108		53	0.16726		
83		116		45	0.17608		
87		121		67	0.16224		
7		112		51	0.16889		
7		117		14	0.21928		
31		113		80	0.15693		

37	46	89	0.15313
37	54	77	0.1583
38	40	63	0.16335
48	111	48	0.17405
64	44	94	0.15196
70	88	32	0.18635
74	37	24	0.19954
88	52	84	0.15532
92	113	91	0.15285
94	48	42	0.17769
94	99	93	0.1522
95	29	66	0.16249
95	30	60	0.16504
95	33	79	0.15708

¹Residue assignment to a canonical coiled-coil heptad repeat, assuming a continuous transmembrane-coiled-coil helix.

²Pair ranking originated from the EV-Couplings algorithm.

³Pseudo-likelihood maximization (PLM) score computed for the pair of positions from the EV-Couplings algorithm.

⁴Minimum distance between heavy atoms of the residues in the computational model of the L₂B₂ tetramer. Asterisks denote outliers not well satisfied by the computational model. Single asterisk: distances above 5 Å; double asterisks: distances above 10 Å.

⁵Minimum distance between alpha carbons of the residues, which were used to compute sigmoidal distance restraints during the modeling procedure.

Table S2.2. Network of hydrogen bonds observed in TM domain of FtsLB during molecular dynamics simulation, run 1¹

Chain	Position	Chain	Position ²	Occupancy
A	Y17	C	T52	92%
A	W20	C	T56	81%
A	Q16	C	T49	81%
A	Q16	B	Q16	62%
B	Q16	B	W20	39%
B	Y17	D	L48b	31%
A	Q16	C	T52	26%
B	Q16	C	T49	18%
A	Y17	C	L48b	13%
A	Q16	A	Y17	11%
B	Y17	D	T52	10%
B	W20	A	Q16b	8%
B	Q16	D	T49	2%
A	Q16	A	V13b	1%

¹The most frequently observed side-chain to side-chain or side-chain to backbone hydrogen bonding interactions in the molecular dynamics simulations are listed. Chains A and B correspond to FtsB while chains C and D correspond to FtsL. The percentage is cumulative of all possible combinations of donor-acceptor interactions between the two residues. Co-occurring interactions between different donors and acceptors within the same pair of residues are not double-counted.

²The letter “b” indicates that the hydrogen bonding involves a backbone group.

Table S2.3. Sequences of FtsB and FtsL used for *in vitro* FRET experiments.

Name	Sequence ¹
His ₈ -FtsB	<i>MGS</i> HHHHHHHHDYDIP <u>TSENLYFQGGSGMGKLT</u> LLLAI <u>LVWLQYSLW FGKNGIHDYTRVNDVAQQATNAKLKARNDQLFAE<u>I</u>DDLN<u>GGQE</u>ALE ERARNELSMTRPGETFYRLVPDASKRAQSAGQNRR</u>
His ₈ -FtsB-S97C	<i>MGS</i> HHHHHHHHDYDIP <u>TSENLYFQGGSGMGKLT</u> LLLAI <u>LVWLQYSLW FGKNGIHDYTRVNDVAQQATNAKLKARNDQLFAE<u>I</u>DDLN<u>GGQE</u>ALE ERARNELSMTRPGETFYRLVPDASKRA<u>QCAG</u>QNRR</u>
Strep-FtsL ₃₅₋₁₂₁ -C41A-C45A (Cys-less FtsL)	<i>MSNW</i> SH <u>PQFEKDYD</u> IP <u>TSENLYFQGGSGFGKLP</u> A <u>LFIA</u> A <u>IILTAVTVV TTAHTRLLTAQREQLVLERDALDI<u>EWRNLILEENALGDHSRVERIAT</u> EKLQMHVDP<u>SQENIVVQK</u></u>
Strep-FtsL ₃₅₋₁₂₁ -C41A-C45A-I100C	<i>MSNW</i> SH <u>PQFEKDYD</u> IP <u>TSENLYFQGGSGFGKLP</u> A <u>LFIA</u> A <u>IILTAVTVV TTAHTRLLTAQREQLVLERDALDI<u>EWRNLILEENALGDHSRVER</u>C<u>AT</u> EKLQMHVDP<u>SQENIVVQK</u></u>

¹The sequences of the added purification tags (His₈ or Strep) are in italics. Mutations are

highlighted in bold and underlined.

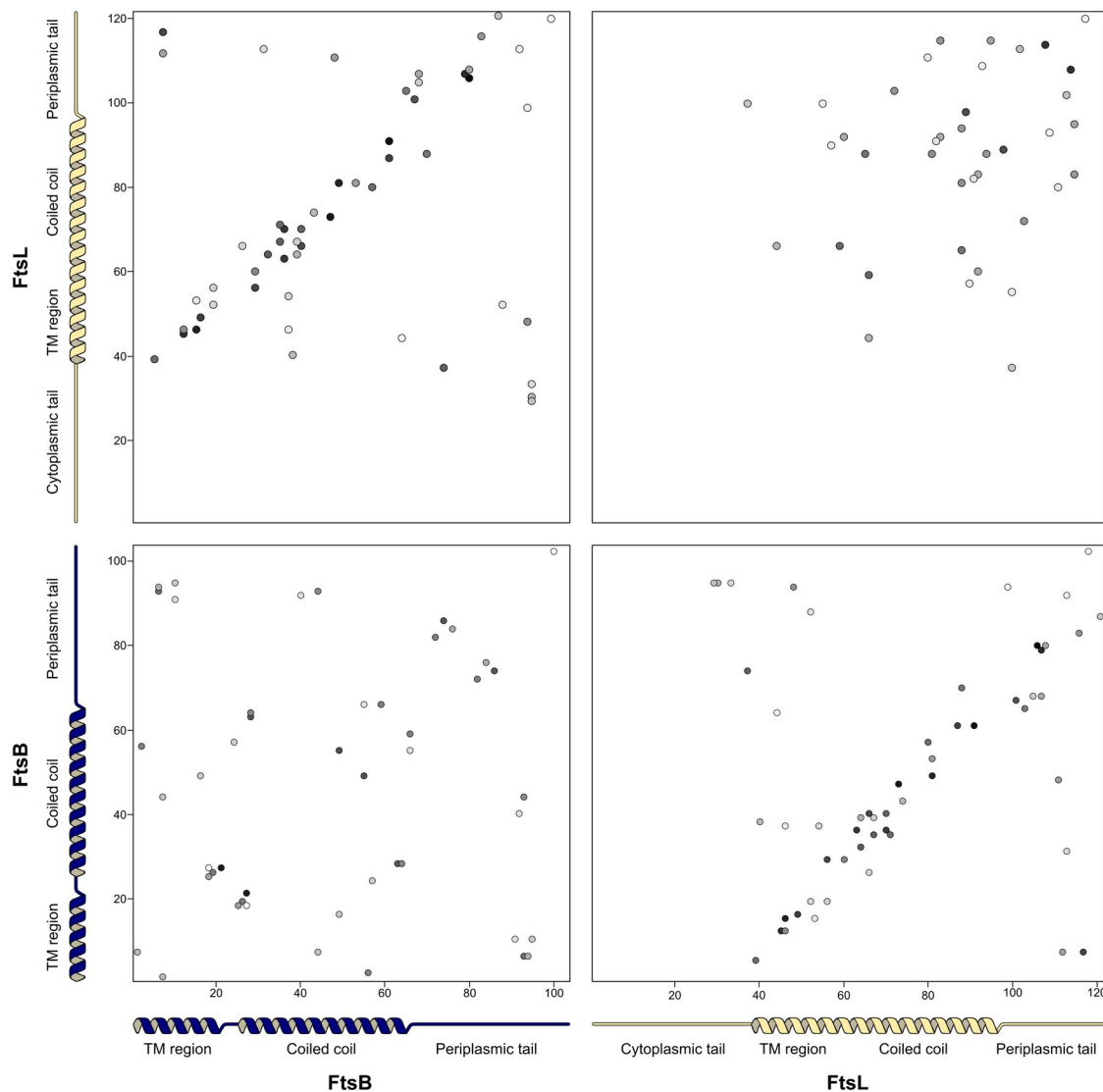


Figure S2.1. Co-evolutionary analysis of the paired alignment of FtsB and FtsL sequences. Map of potential contacts between positions in the sequence in FtsB and FtsL, inferred by co-evolutionary analysis. The top-left and bottom-right quadrants correspond to the FtsB-FtsL potential contacts reported in Fig. 2.2. In addition, this figure reports the potential intra-subunit contacts, within FtsB (bottom-left) and within FtsL (top-right).

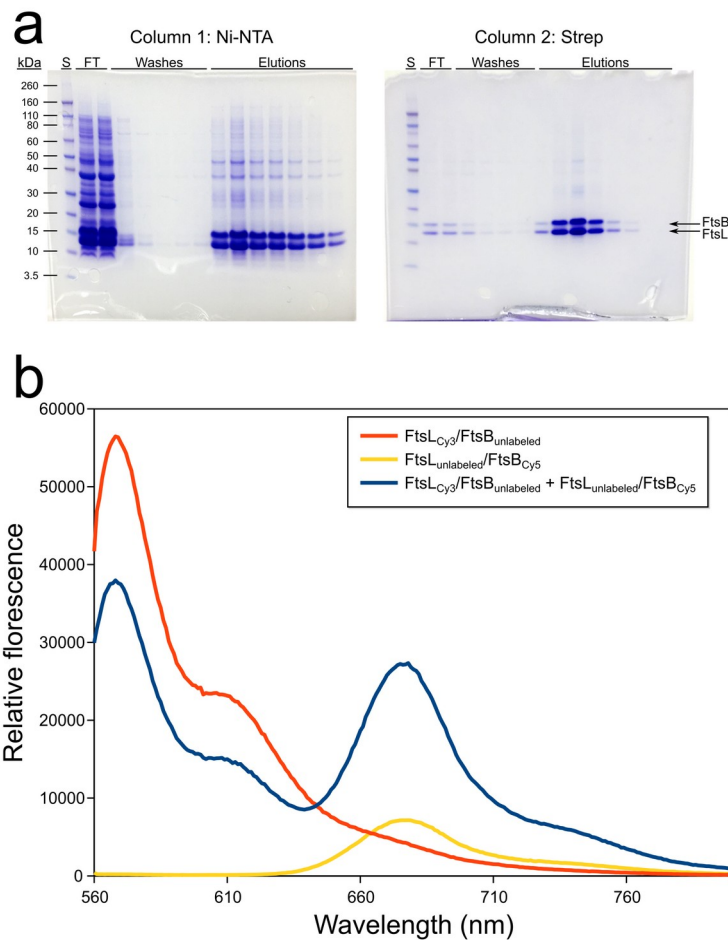


Figure S2.2. Determination of FtsL and FtsB association *in vitro*.

a) Co-expressed strep-tagged FtsL and His-tagged FtsB proteins co-elute when run over consecutive Ni-NTA and streptavidin columns, demonstrating that FtsLB a stable complex in detergent. The density of the bands is consistent with a 1:1 stoichiometric ratio. S: standard ladder; FT: flow-through fractions.

b) Acceptor-labeled FtsB (FtsL_{unlabeled}/FtsB_{Cy5}) and donor-labeled FtsL (FtsL_{Cy3}/FtsB_{unlabeled}) were mixed in a 50:50 ratio and equilibrated and

emission spectrum was recorded (blue line, excitation wavelength 550 nm). The mixed sample shows a substantial increase of acceptor emission around 680 nm, indicating proximity between FtsB_{Cy5} and FtsL_{Cy3}. The emission scan is compared to those of an acceptor-only sample (red, 50:50 mix of FtsL_{unlabeled}/FtsB_{Cy5} and FtsL_{unlabeled}/FtsB_{unlabeled}) and of a donor-only sample (yellow, 50:50 mix of FtsL_{Cy3}/FtsB_{unlabeled} and FtsL_{unlabeled}/FtsB_{unlabeled}). For these two control samples, mixing with FtsL_{unlabeled}/FtsB_{unlabeled} was performed to maintain identical total protein concentration and protein:detergent ratios. All other conditions are identical to the stoichiometric analysis of Fig. 2.3.

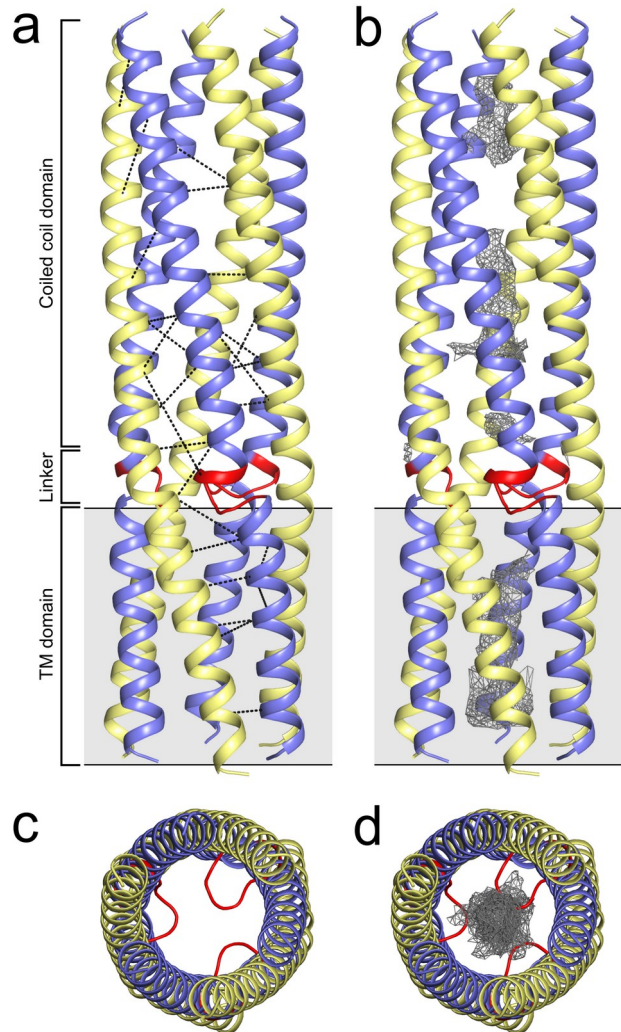
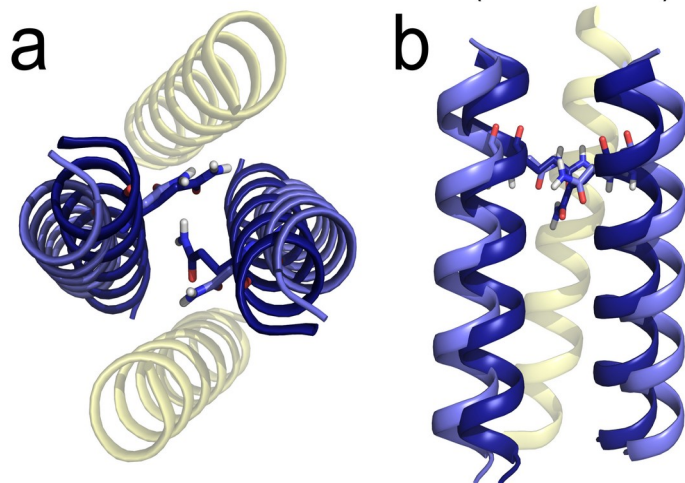
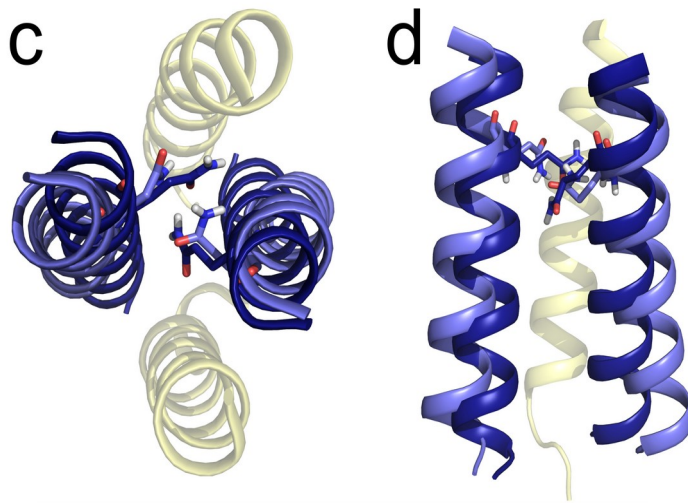


Figure S2.3. Hexameric model of the FtsLB complex. a) Model of the L₃B₃ hexamer with the co-evolutionary restraints (Table S2.1) shown as black dashes. Most of the evolutionary constraints are fit by this model. FtsB rendered in blue, FtsL rendered in yellow, and the juxtamembrane linker in FtsB highlighted in red. b) Solvent-accessible cavities rendered in gray wireframe. These cavities do not form a complete channel and are instead occluded by bulky side chains and the juxtamembrane linker of FtsB. c) and d) Top-down views of the hexameric model presented in a and b.

FtsB dimer vs FtsLB tetramer (initial model)



FtsB dimer vs FtsLB tetramer (MD model)



■ FtsB dimer – ■ FtsB and ■ FtsL in FtsLB

Figure S2.4. The configuration of the TM region of FtsB is similar to a previous model obtained in the absence of FtsL. Structural alignment of the L₂B₂ complex to a model of the FtsB homodimer. a) Top-down and b) side views of an alignment with the L₂B₂ model (blue, yellow) with the model of the homodimer (dark blue), which was previously generated using mutagenesis data based on a genetic reporter assay of self-association (38). Residue Q16 is shown in sticks. The interface of FtsB is the same in both models, but the helices are farther apart in the L₂B₂ tetramer. c) and d) Top-down and side views of the FtsB homodimer model aligned with the last

frame of the 260 ns MD simulation. The FtsB helices have moved closer together, improving the RMSD of the alignment from 2.5 Å to ~2 Å.

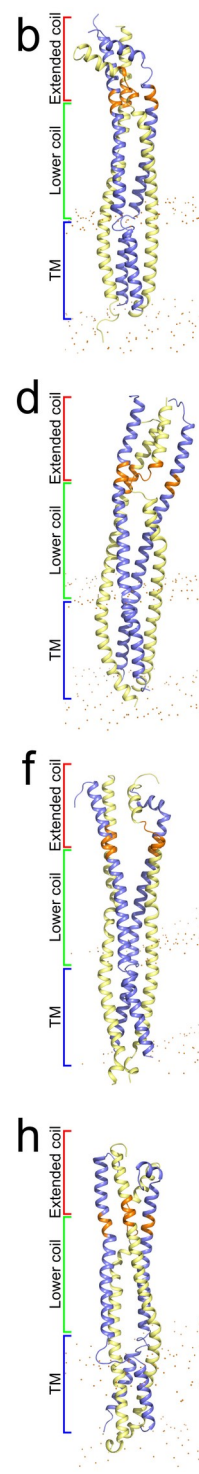
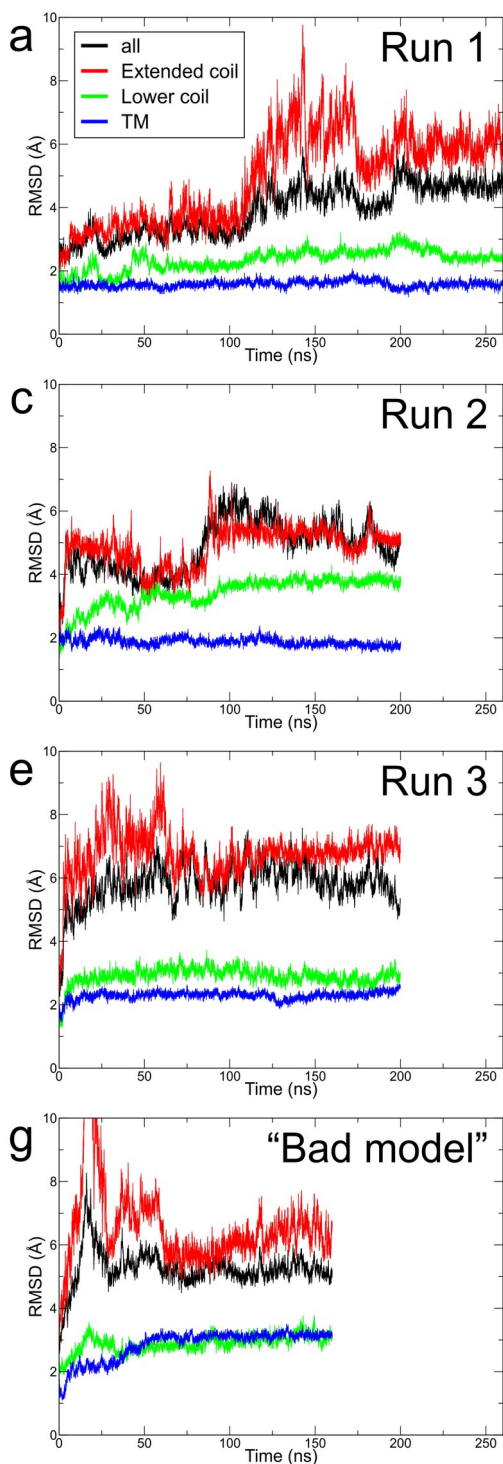


Figure S2.5. RMSD analysis of the three replica MD runs and of a “bad model”. The figure is similar to Fig. 2.5a (Run 1). The RMSD analysis is shown for the entire complex (black), the TM region (blue), the lower coil (green, 29-61 of FtsB and 57-91 of FtsL) and the extended coil (red, 62-79 of FtsB and 92-110 of FtsL). The CCD, which separates the lower from the extended coil is in orange.

a) Trajectory of the 260 ns Run 1.
 b) Conformation of the last step of the trajectory. c) and d) Trajectory of the 200 ns Run 2. e) and f) Trajectory of the 200 ns Run 3. g) and h) Trajectory of 160 ns run of a “bad model”, an alternate low energy model in which the conformation of the TM region does not satisfy most of the evolutionary constraints. It is notable how the RMSD of the TM

region quickly rises to a higher value (approximately 3 Å, compared to the same variable in Runs 1-3, which is around 2 Å).

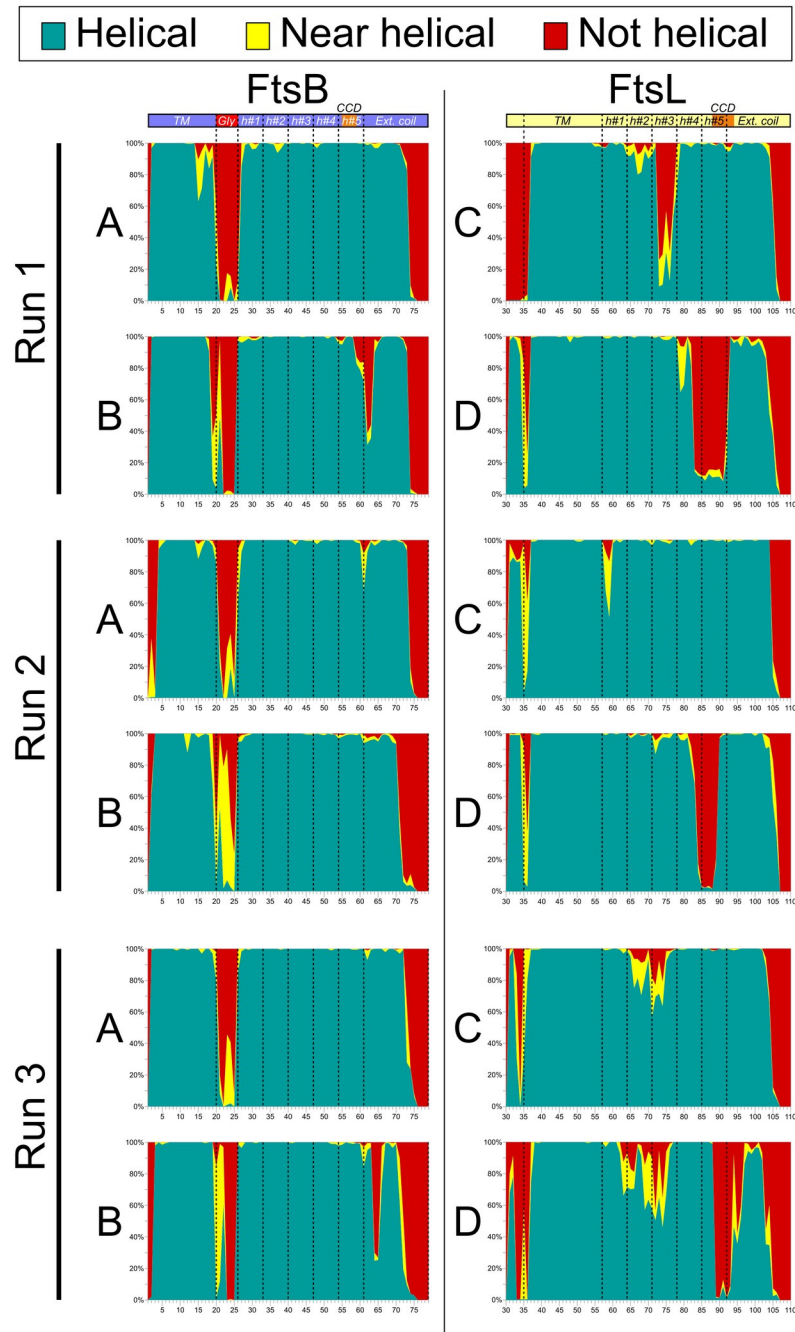


Figure S2.6. Analysis of helicity in the three replica MD runs. The graphs display the fraction of time each position adopted a helical conformation (green), nearly helical (yellow) or non-helical (red). A and B are the two individual FtsB chains (left panels) and C and D are the two individual FtsL chains (right panels).

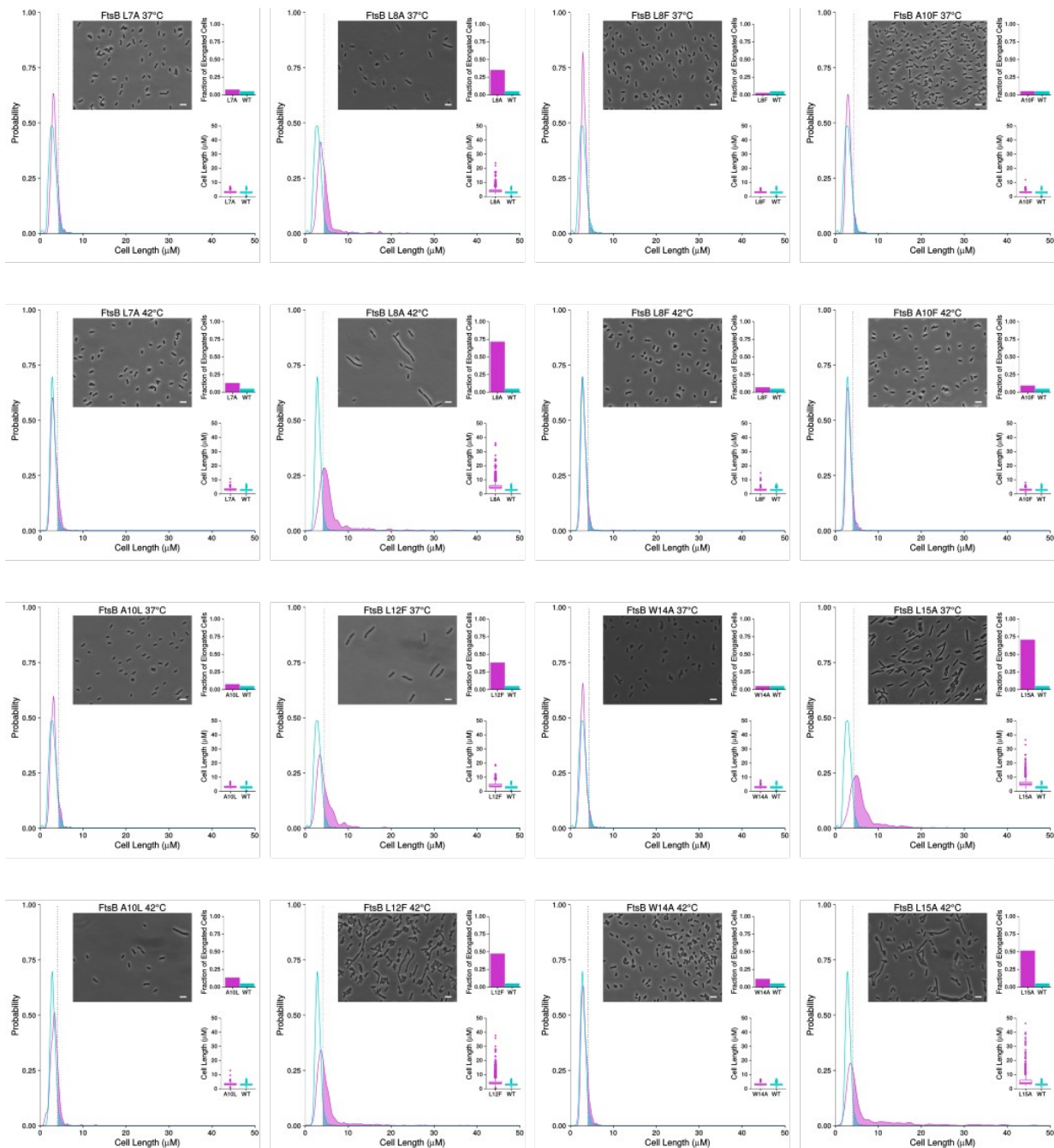


Figure S2.7 – continued below

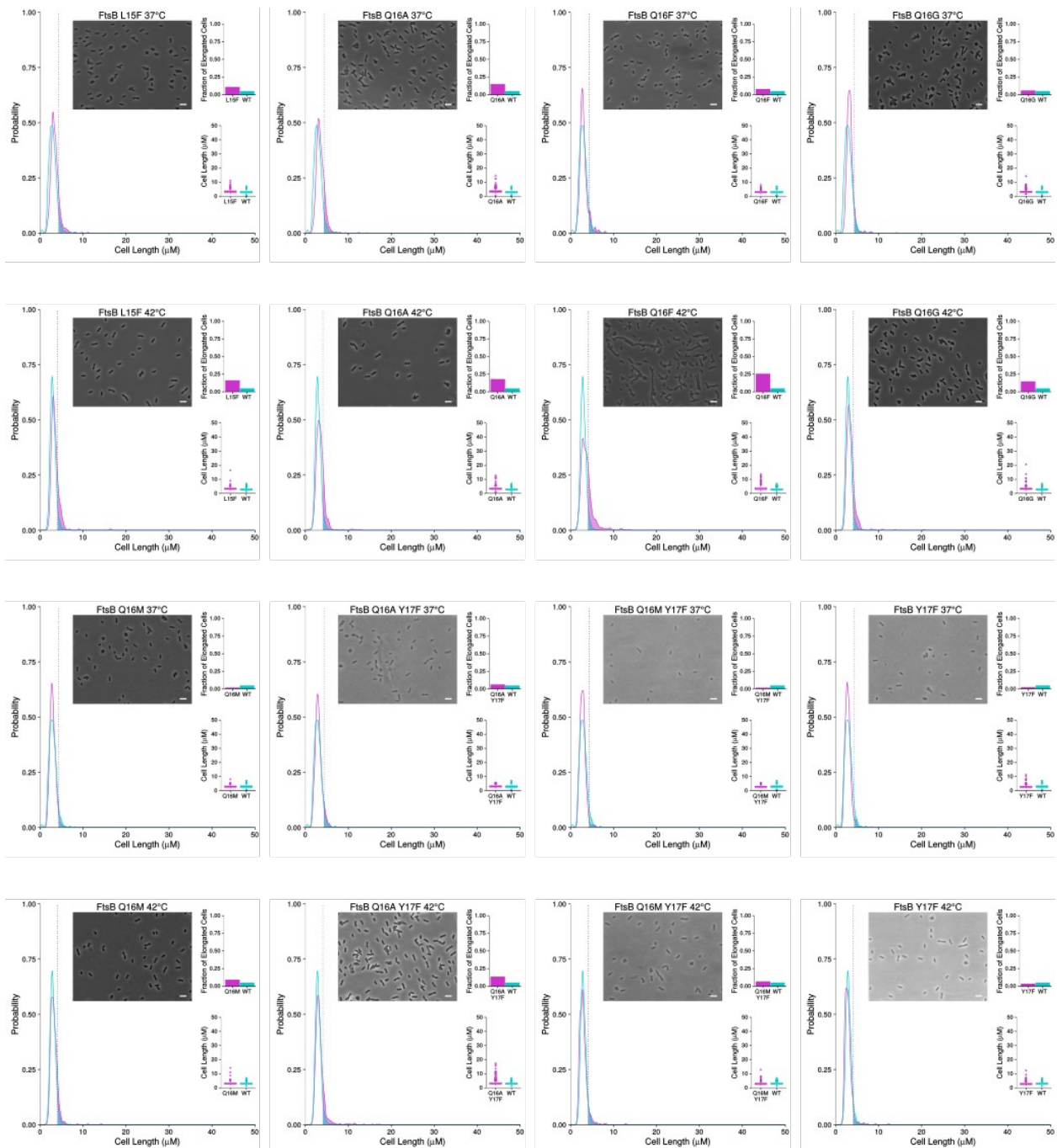


Figure S2.7 – continued below

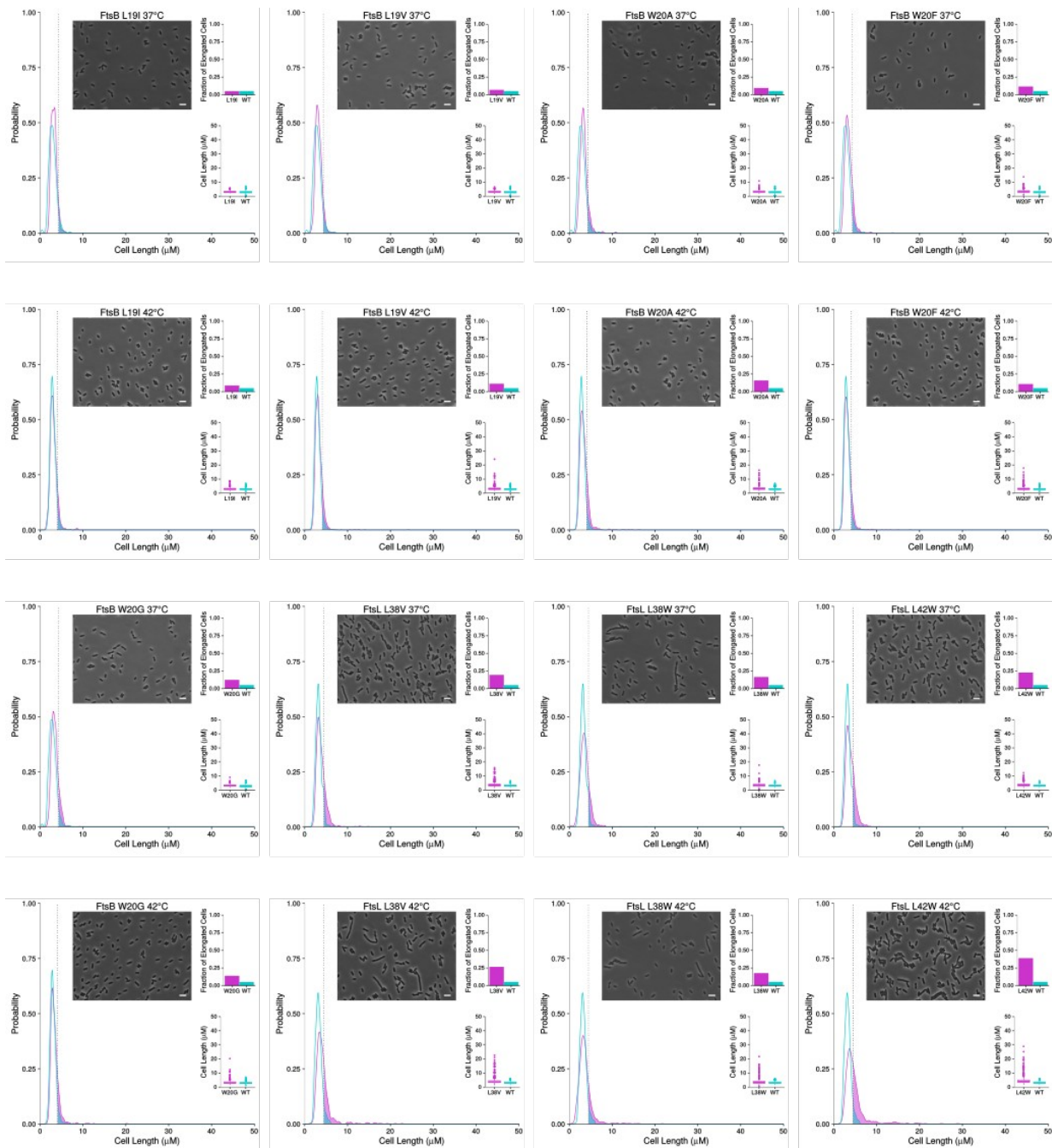


Figure S2.7 – continued below

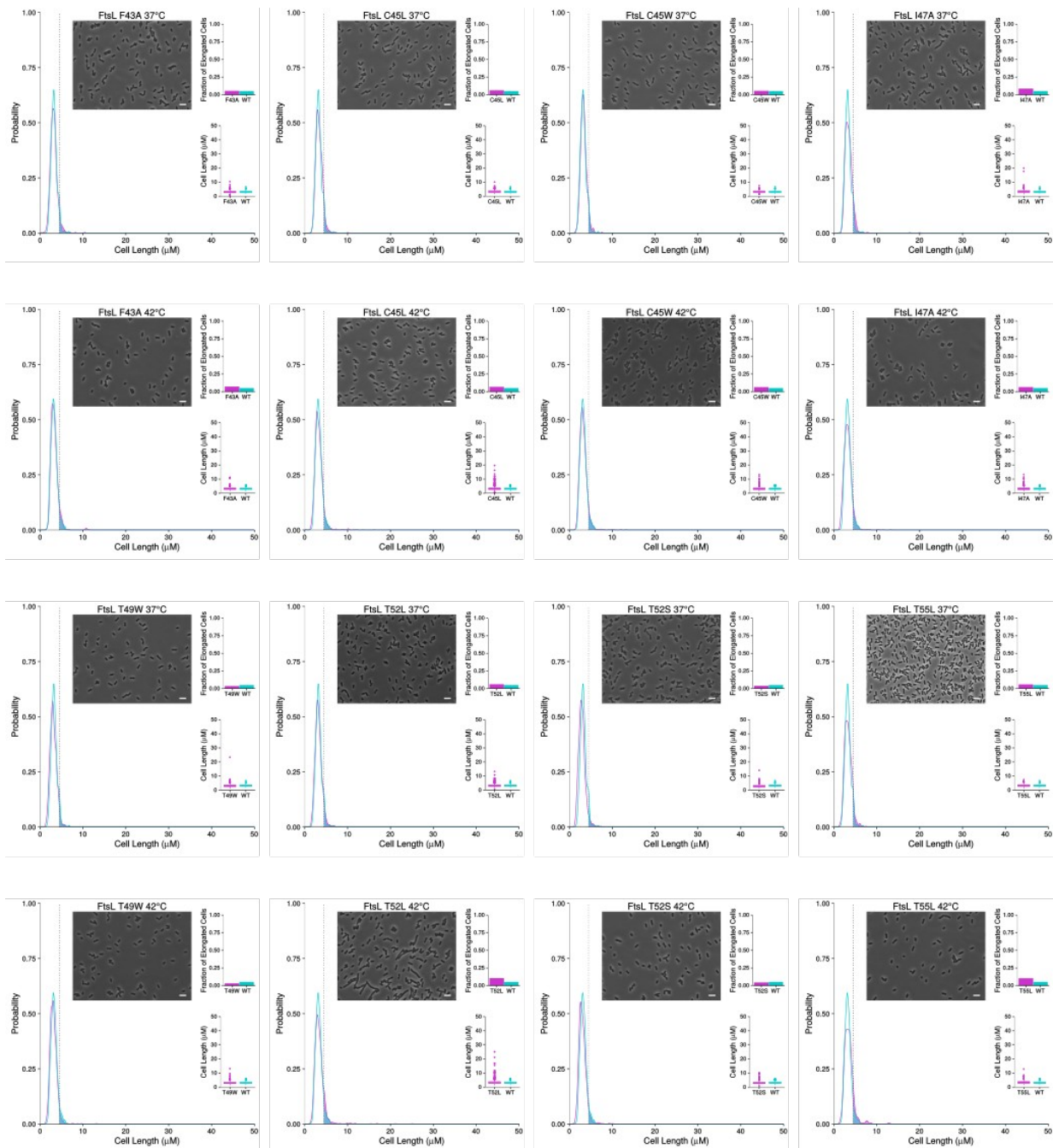


Figure S2.7 – continued below

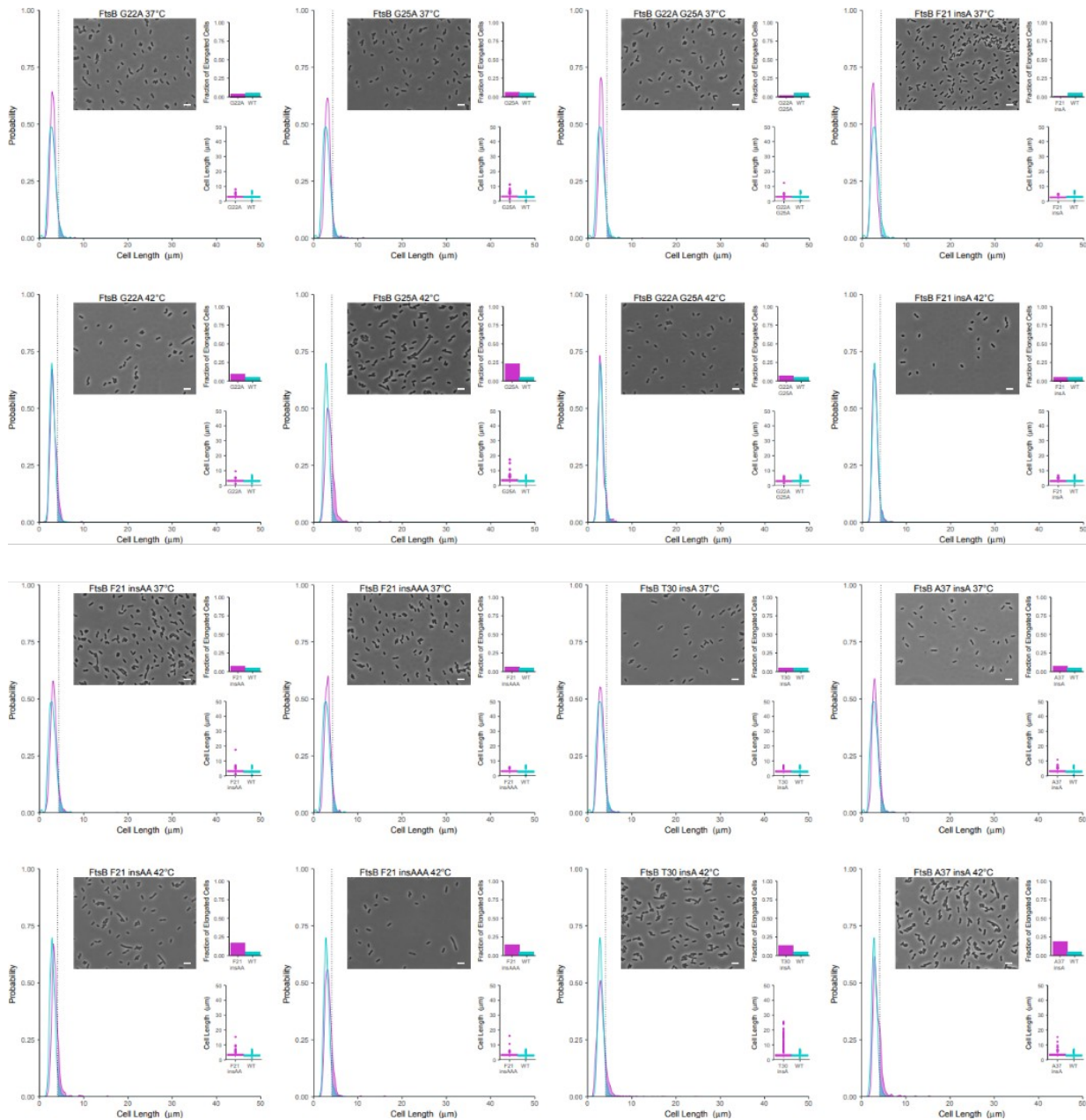


Figure S2.7 – continued below

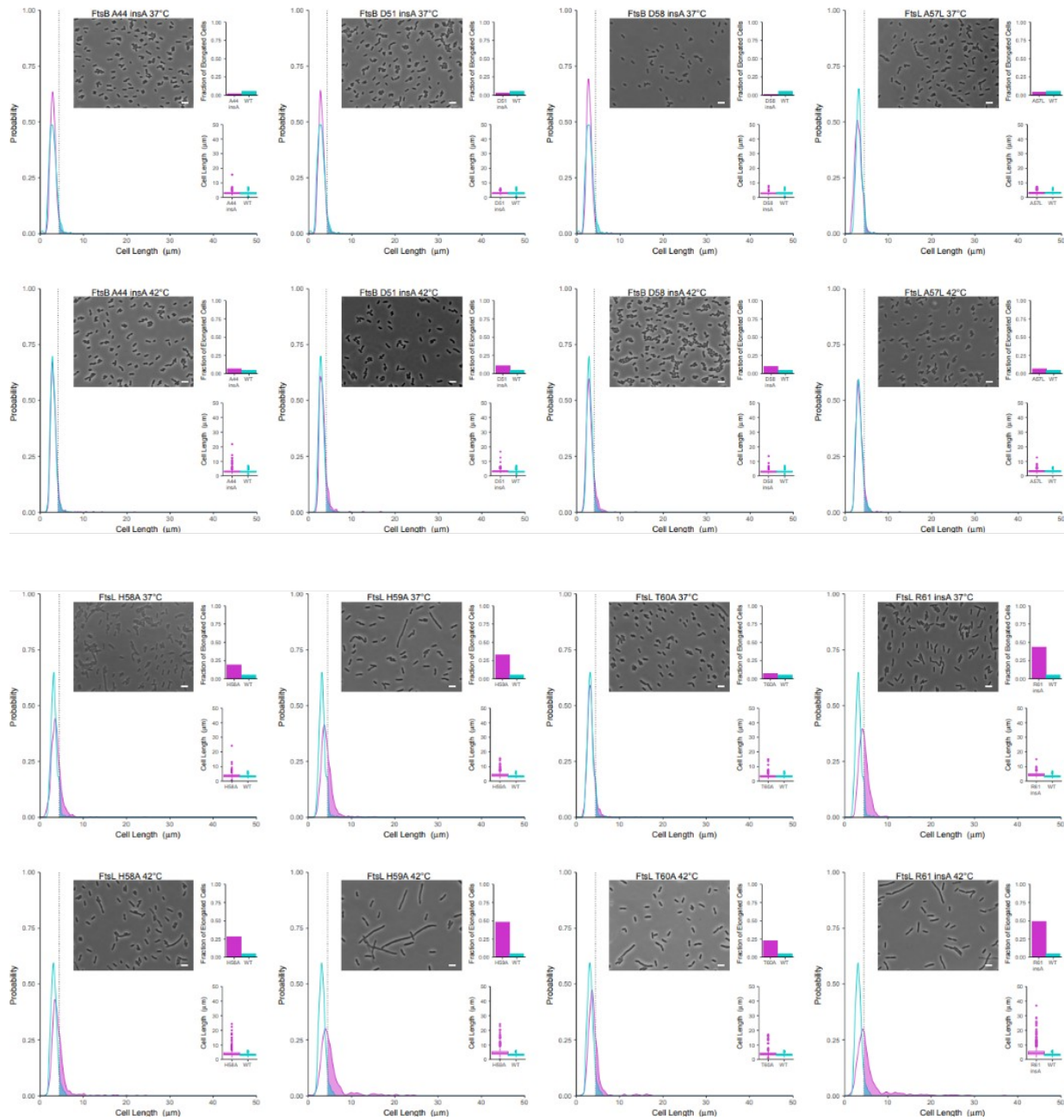


Figure S2.7 – continued below

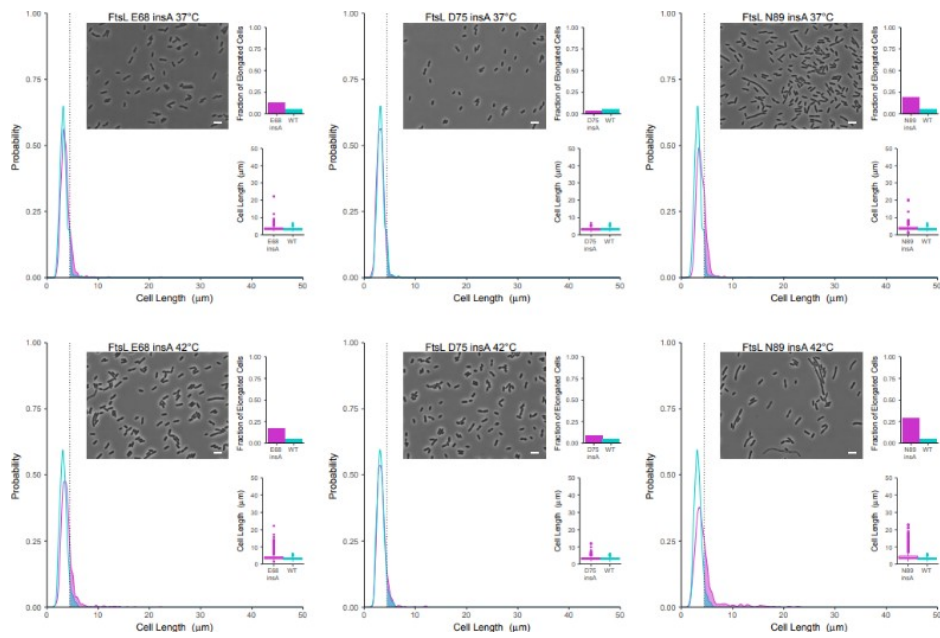


Figure S2.7. Full analysis of cell division phenotypes of point and alanine insertions mutants reported in Figure 2.6 and Figure 2.7. The distribution of cell lengths for each point substitution or insertion mutant was compared between wild type (aqua) and mutant (magenta) cell population. Center: kernel density functions of mutant and wild-type cell lengths. The area above the 95th percentile of the wild-type distribution (dotted line) is shaded. Insert: representative photo of mutation. Scale bar corresponds to 5 μm . Right, top: fraction of cells above the 95th percentile of wild-type cell length. Right, bottom: box and whisker plots of cell lengths for wild-type and mutant. Whiskers represent the interquartile range multiplied by 1.5.

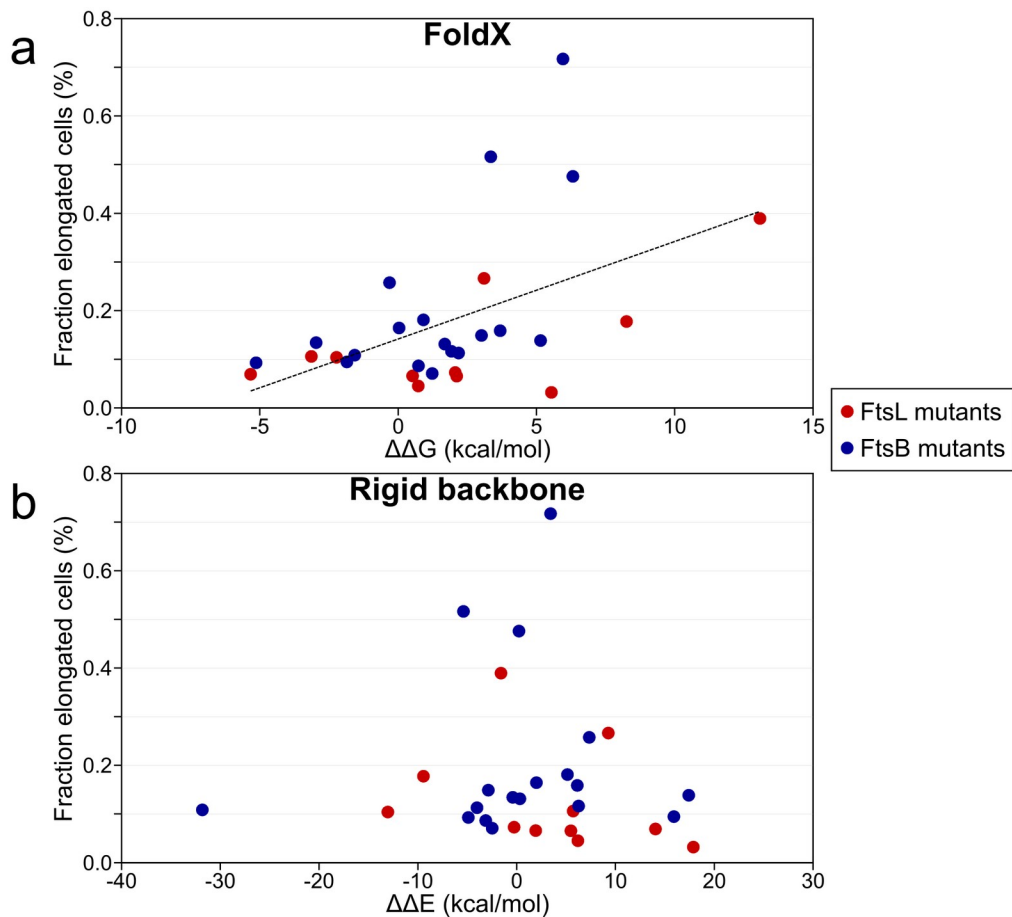


Figure S2.8. Comparison of the predicted mutational energy and the biological phenotypes of the mutants in the transmembrane region. Biological phenotype (expressed as the fraction of elongated cells, as defined in Fig. 2.6) compared with the energy of destabilization of each mutant calculated *in silico* using a) FoldX or b) rigid body repacking in which the mutation was modeled without relaxing the backbone. The energies predicted by FoldX correlate statistically with the severity of the phenotypes by Rank Order Spearman Correlation Coefficient analysis, which does not assume a linear model ($r = 0.4631$, $N = 29$, $p < 0.01$), and by linear regression ($R^2 = 0.25$, $p < 0.01$, dashed line). Correlation with rigid backbone energies is not statistically significant.

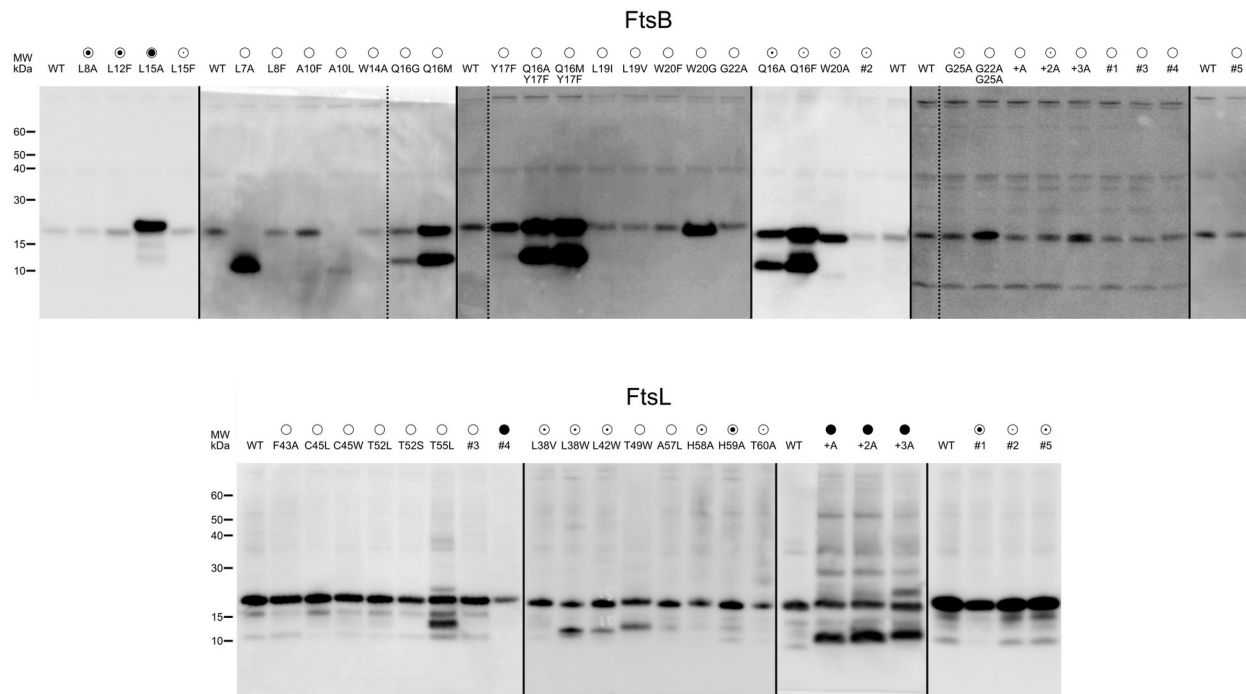


Figure S2.9. Expression level of FtsB and FtsL mutants assessed by Western Blot analysis. Image of all western blots of the FtsB and FtsL mutants tested in this work. The circles indicate the observed phenotypes, as defined in Fig. 2.6. The FtsB wild type and its mutants display a notably fainter band with respect to the FtsL variants. Protein expression level of the FtsB and FtsL mutants with defective phenotypes are generally comparable and to the respective wild type. There are cases of FtsB mutants with increased protein level. These correspond to mutations in a specific region of the TM domain of FtsB, involving L15, Q16, Y17 or W20. These mutants with increased protein level correspond to interfacial positions that have a wild-type-like (Q16M, Y17F, Q16M/Y17F, Q16A/Y17F, W20A), mild temperature-sensitive (Q16F), mild (Q16A) phenotypes, or, in one case, a severe phenotype (L15A). It is possible that these apparent increases in protein levels are due to reduced protein degradation, possibly because the mutations mask a site recognized by a membrane protease. Additionally, two FtsB mutants (L7A and A10L) present faint full-length bands and significant degradation. However, these mutants are viable and are classified as wild-type-like. Individual gels are separated by solid lines. Spliced lanes within the same gel are indicated by a dashed line.

2.7 Acknowledgments

We thank Drs. Jon Beckwith and Mark Gonzalez for kindly providing plasmids and strains relative to the *in vivo* analysis and for guidance in performing the experiments. The work was supported by National Institutes of Health Grant (NIH) R01-GM0997522, National Science Foundation (NSF) grant CHE-1415910 to A.S., and NSF grant DMS-1661900 to Q.C. DBW and JAC were supported by NSF grant DMR-1121288. J.L.R. and R.C were supported by NIH grant R01-GM120260. A.A.H. was supported by a Shaw Scientist Award, a Beckman Young Investigator Award, and startup funds from the University of Wisconsin-Madison. S.G.F.C. and G.D.V. acknowledge support by the NLM training grant 5T15LM007359 to the CIBM Training Program. G.D.V. was also supported by a SciMed GRS fellowship. S.G.F.C. was also supported by a William R. & Dorothy E. Sullivan Wisconsin Distinguished Graduate Fellowship. D.A.M. was supported by the Steenbock Predoctoral Fellowship. S.J.C. was supported by the Dr. James Chieh-Hsia Mao Wisconsin Distinguished Graduate Fellowship and by the William H. Peterson fellowship. Computational resources from the Extreme Science and Engineering Discovery Environment (XSEDE), supported by NSF grant number OCI-1053575, are greatly appreciated. We thank Dr. Kai Cai for assistance during the biophysical studies and Dr. Elizabeth Caselle for critical reading of the manuscript.

2.8 Author contributions

D.A.M., S.G.F.C., C.R.A., G.D.V., Q.C., and A.S. designed research; D.A.M., S.G.F.C., C.R.A., G.D.V., and A.S. analyzed data; S.G.F.C. performed the co-evolutionary analysis (Fig. 2.2) and molecular modeling (Fig. 2.4); C.R.A. and S.G.F.C.

performed the FRET analysis (Fig. 2.3); G.D.V. performed molecular dynamics (Fig. 2.5); D.A.M. performed the microscopic analysis (Fig. 2.6 and 2.7); S.J.C. contributed to protein purification; A.S.K., A.A.H., R.C., and J.L.R. contributed to the FRET analysis; L.M.L., S.J.C., J.A.C., N.R., and D.B.W. contributed to the microscopic analysis; Q.C. supervised the molecular dynamics; A.S. supervised the project; D.A.M., S.G.F.C., C.R.A., G.D.V., S.J.C., and A.S. wrote the manuscript.

2.9 References

1. Wang, L., Khattar, M. K., Donachie, W. D., and Lutkenhaus, J. (1998) FtsI and FtsW are localized to the septum in *Escherichia coli*. *J. Bacteriol.* **180**, 2810–2816
2. Hale, C. A., and de Boer, P. A. J. (2002) ZipA is required for recruitment of FtsK, FtsQ, FtsL, and FtsN to the septal ring in *Escherichia coli*. *J. Bacteriol.* **184**, 2552–2556
3. Hale, C. A., and de Boer, P. A. (1999) Recruitment of ZipA to the septal ring of *Escherichia coli* is dependent on FtsZ and independent of FtsA. *J. Bacteriol.* **181**, 167–176
4. Liu, Z., Mukherjee, A., and Lutkenhaus, J. (1999) Recruitment of ZipA to the division site by interaction with FtsZ. *Mol. Microbiol.* **31**, 1853–1861
5. Chen, J. C., and Beckwith, J. (2001) FtsQ, FtsL and FtsI require FtsK, but not FtsN, for co-localization with FtsZ during *Escherichia coli* cell division. *Mol. Microbiol.* **42**, 395–413
6. Buddelmeijer, N., and Beckwith, J. (2004) A complex of the *Escherichia coli* cell division proteins FtsL, FtsB and FtsQ forms independently of its localization to the septal region. *Mol Microbiol.* **52**, 1315–27
7. Buddelmeijer, N., Judson, N., Boyd, D., Mekalanos, J. J., and Beckwith, J. (2002) YgbQ, a cell division protein in *Escherichia coli* and *Vibrio cholerae*, localizes in codependent fashion with FtsL to the division site. *Proc. Natl. Acad. Sci. U.S.A.* **99**, 6316–6321
8. Mercer, K. L. N., and Weiss, D. S. (2002) The *Escherichia coli* cell division protein FtsW is required to recruit its cognate transpeptidase, FtsI (PBP3), to the division site. *J. Bacteriol.* **184**, 904–912

9. Schmidt, K. L., Peterson, N. D., Kustusch, R. J., Wissel, M. C., Graham, B., Phillips, G. J., and Weiss, D. S. (2004) A predicted ABC transporter, FtsEX, is needed for cell division in *Escherichia coli*. *J. Bacteriol.* **186**, 785–793
10. Goehring, N. W., Gueiros-Filho, F., and Beckwith, J. (2005) Premature targeting of a cell division protein to midcell allows dissection of divisome assembly in *Escherichia coli*. *Genes Dev.* **19**, 127–137
11. Goehring, N. W., Gonzalez, M. D., and Beckwith, J. (2006) Premature targeting of cell division proteins to midcell reveals hierarchies of protein interactions involved in divisome assembly. *Mol. Microbiol.* **61**, 33–45
12. Ghigo, J. M., Weiss, D. S., Chen, J. C., Yarrow, J. C., and Beckwith, J. (1999) Localization of FtsL to the *Escherichia coli* septal ring. *Mol. Microbiol.* **31**, 725–737
13. Lutkenhaus, J., Pichoff, S., and Du, S. (2012) Bacterial cytokinesis: From Z ring to divisome. *Cytoskeleton (Hoboken)*. **69**, 778–790
14. de Boer, P. A. J. (2010) Advances in understanding *E. coli* cell fission. *Curr. Opin. Microbiol.* **13**, 730–737
15. Erickson, H. P., Anderson, D. E., and Osawa, M. (2010) FtsZ in bacterial cytokinesis: cytoskeleton and force generator all in one. *Microbiol. Mol. Biol. Rev.* **74**, 504–528
16. Bisson-Filho, A. W., Hsu, Y.-P., Squyres, G. R., Kuru, E., Wu, F., Jukes, C., Sun, Y., Dekker, C., Holden, S., VanNieuwenhze, M. S., Brun, Y. V., and Garner, E. C. (2017) Treadmilling by FtsZ filaments drives peptidoglycan synthesis and bacterial cell division. *Science*. **355**, 739–743
17. Yang, X., Lyu, Z., Miguel, A., McQuillen, R., Huang, K. C., and Xiao, J. (2017) GTPase activity-coupled treadmilling of the bacterial tubulin FtsZ organizes septal cell wall synthesis. *Science*. **355**, 744–747
18. Ortiz, C., Natale, P., Cueto, L., and Vicente, M. (2016) The keepers of the ring: regulators of FtsZ assembly. *FEMS Microbiol. Rev.* **40**, 57–67
19. Haney, S. A., Glasfeld, E., Hale, C., Keeney, D., He, Z., and de Boer, P. (2001) Genetic analysis of the *Escherichia coli* FtsZ.ZipA interaction in the yeast two-hybrid system. Characterization of FtsZ residues essential for the interactions with ZipA and with FtsA. *J. Biol. Chem.* **276**, 11980–11987
20. Szwedziak, P., Wang, Q., Freund, S. M., and Löwe, J. (2012) FtsA forms actin-like protofilaments. *EMBO J.* **31**, 2249–2260
21. Du, S., Pichoff, S., and Lutkenhaus, J. (2016) FtsEX acts on FtsA to regulate divisome assembly and activity. *Proc. Natl. Acad. Sci. U.S.A.* **113**, E5052–5061

22. Yang, D. C., Peters, N. T., Parzych, K. R., Uehara, T., Markovski, M., and Bernhardt, T. G. (2011) An ATP-binding cassette transporter-like complex governs cell-wall hydrolysis at the bacterial cytokinetic ring. *Proc. Natl. Acad. Sci. U.S.A.* **108**, E1052–1060
23. Männik, J., Bailey, M. W., O'Neill, J. C., and Männik, J. (2017) Kinetics of large-scale chromosomal movement during asymmetric cell division in *Escherichia coli*. *PLoS Genet.* **13**, e1006638
24. Aarsman, M. E. G., Piette, A., Fraipont, C., Vinkenvleugel, T. M. F., Nguyen-Distèche, M., and den Blaauwen, T. (2005) Maturation of the *Escherichia coli* divisome occurs in two steps. *Mol. Microbiol.* **55**, 1631–1645
25. Vollmer, W., and Bertsche, U. (2008) Murein (peptidoglycan) structure, architecture and biosynthesis in *Escherichia coli*. *Biochim. Biophys. Acta.* **1778**, 1714–1734
26. Cho, H., Wivagg, C. N., Kapoor, M., Barry, Z., Rohs, P. D. A., Suh, H., Marto, J. A., Garner, E. C., and Bernhardt, T. G. (2016) Bacterial cell wall biogenesis is mediated by SEDS and PBP polymerase families functioning semi-autonomously. *Nat Microbiol.* 10.1038/nmicrobiol.2016.172
27. Meeske, A. J., Riley, E. P., Robins, W. P., Uehara, T., Mekalanos, J. J., Kahne, D., Walker, S., Kruse, A. C., Bernhardt, T. G., and Rudner, D. Z. (2016) SEDS proteins are a widespread family of bacterial cell wall polymerases. *Nature.* **537**, 634–638
28. Emami, K., Guyet, A., Kawai, Y., Devi, J., Wu, L. J., Allenby, N., Daniel, R. A., and Errington, J. (2017) RodA as the missing glycosyltransferase in *Bacillus subtilis* and antibiotic discovery for the peptidoglycan polymerase pathway. *Nat Microbiol.* **2**, 16253
29. Mohammadi, T., Sijbrandi, R., Lutters, M., Verheul, J., Martin, N. I., den Blaauwen, T., de Kruijff, B., and Breukink, E. (2014) Specificity of the transport of lipid II by FtsW in *Escherichia coli*. *J. Biol. Chem.* **289**, 14707–14718
30. Mohammadi, T., van Dam, V., Sijbrandi, R., Vernet, T., Zapun, A., Bouhss, A., Diepeveen-de Bruin, M., Nguyen-Distèche, M., de Kruijff, B., and Breukink, E. (2011) Identification of FtsW as a transporter of lipid-linked cell wall precursors across the membrane. *EMBO J.* **30**, 1425–1432
31. Yang, J.-C., Van Den Ent, F., Neuhaus, D., Brevier, J., and Löwe, J. (2004) Solution structure and domain architecture of the divisome protein FtsN. *Mol. Microbiol.* **52**, 651–660
32. Di Lallo, G., Fagioli, M., Barionovi, D., Ghelardini, P., and Paolozzi, L. (2003) Use of a two-hybrid assay to study the assembly of a complex multicomponent protein machinery: bacterial septosome differentiation. *Microbiology (Reading, Engl.)*. **149**, 3353–3359

33. Karimova, G., Dautin, N., and Ladant, D. (2005) Interaction network among *Escherichia coli* membrane proteins involved in cell division as revealed by bacterial two-hybrid analysis. *J. Bacteriol.* **187**, 2233–2243
34. Müller, P., Ewers, C., Bertsche, U., Anstett, M., Kallis, T., Breukink, E., Fraipont, C., Terrak, M., Nguyen-Distèche, M., and Vollmer, W. (2007) The essential cell division protein FtsN interacts with the murein (peptidoglycan) synthase PBP1B in *Escherichia coli*. *J. Biol. Chem.* **282**, 36394–36402
35. Alexeeva, S., Gadella, T. W. J., Jr, Verheul, J., Verhoeven, G. S., and den Blaauwen, T. (2010) Direct interactions of early and late assembling division proteins in *Escherichia coli* cells resolved by FRET. *Mol. Microbiol.* **77**, 384–398
36. Busiek, K. K., Eraso, J. M., Wang, Y., and Margolin, W. (2012) The early divisome protein FtsA interacts directly through its 1c subdomain with the cytoplasmic domain of the late divisome protein FtsN. *J. Bacteriol.* **194**, 1989–2000
37. Massey, T. H., Mercogliano, C. P., Yates, J., Sherratt, D. J., and Löwe, J. (2006) Double-stranded DNA translocation: structure and mechanism of hexameric FtsK. *Mol. Cell.* **23**, 457–469
38. LaPointe, L. M., Taylor, K. C., Subramaniam, S., Khadria, A., Rayment, I., and Senes, A. (2013) Structural organization of FtsB, a transmembrane protein of the bacterial divisome. *Biochemistry*. **52**, 2574–2585
39. van den Ent, F., Vinkenvleugel, T. M. F., Ind, A., West, P., Veprintsev, D., Nanninga, N., den Blaauwen, T., and Löwe, J. (2008) Structural and mutational analysis of the cell division protein FtsQ. *Mol. Microbiol.* **68**, 110–123
40. Mosyak, L., Zhang, Y., Glasfeld, E., Haney, S., Stahl, M., Seehra, J., and Somers, W. S. (2000) The bacterial cell-division protein ZipA and its interaction with an FtsZ fragment revealed by X-ray crystallography. *EMBO J.* **19**, 3179–3191
41. Tsang, M.-J., and Bernhardt, T. G. (2015) A role for the FtsQLB complex in cytokinetic ring activation revealed by an ftsL allele that accelerates division. *Mol. Microbiol.* **95**, 925–944
42. Liu, B., Persons, L., Lee, L., and de Boer, P. A. J. (2015) Roles for both FtsA and the FtsBLQ subcomplex in FtsN-stimulated cell constriction in *Escherichia coli*. *Mol. Microbiol.* **95**, 945–970
43. Khadria, A. S., and Senes, A. (2013) The Transmembrane Domains of the Bacterial Cell Division Proteins FtsB and FtsL Form a Stable High-Order Oligomer. *Biochemistry*. **52**, 7542–7550

44. Guzman, L. M., Weiss, D. S., and Beckwith, J. (1997) Domain-swapping analysis of FtsI, FtsL, and FtsQ, bitopic membrane proteins essential for cell division in *Escherichia coli*. *J. Bacteriol.* **179**, 5094–5103
45. Gonzalez, M. D., and Beckwith, J. (2009) Divisome under construction: distinct domains of the small membrane protein FtsB are necessary for interaction with multiple cell division proteins. *J. Bacteriol.* **191**, 2815–2825
46. Robichon, C., King, G. F., Goehring, N. W., and Beckwith, J. (2008) Artificial septal targeting of *Bacillus subtilis* cell division proteins in *Escherichia coli*: an interspecies approach to the study of protein-protein interactions in multiprotein complexes. *J. Bacteriol.* **190**, 6048–6059
47. Gonzalez, M. D., Akbay, E. A., Boyd, D., and Beckwith, J. (2010) Multiple interaction domains in FtsL, a protein component of the widely conserved bacterial FtsLBQ cell division complex. *J. Bacteriol.* **192**, 2757–2768
48. van den Berg van Saparoea, H. B., Glas, M., Vernooy, I. G. W. H., Bitter, W., den Blaauwen, T., and Luirink, J. (2013) Fine-mapping the Contact Sites of the *Escherichia coli* Cell Division Proteins FtsB and FtsL on the FtsQ Protein. *J. Biol. Chem.* **288**, 24340–24350
49. Glas, M., van den Berg van Saparoea, H. B., McLaughlin, S. H., Roseboom, W., Liu, F., Koningstein, G. M., Fish, A., den Blaauwen, T., Heck, A. J. R., de Jong, L., Bitter, W., de Esch, I. J. P., and Luirink, J. (2015) The Soluble Periplasmic Domains of *Escherichia coli* Cell Division Proteins FtsQ/FtsB/FtsL Form a Trimeric Complex with Submicromolar Affinity. *J. Biol. Chem.* **290**, 21498–21509
50. Masson, S., Kern, T., Le Gouëllec, A., Giustini, C., Simorre, J.-P., Callow, P., Vernet, T., Gabel, F., and Zapun, A. (2009) Central domain of DivIB caps the C-terminal regions of the FtsL/DivIC coiled-coil rod. *J. Biol. Chem.* **284**, 27687–27700
51. Noirclerc-Savoye, M., Le Gouëllec, A., Morlot, C., Dideberg, O., Vernet, T., and Zapun, A. (2005) In vitro reconstitution of a trimeric complex of DivIB, DivIC and FtsL, and their transient co-localization at the division site in *Streptococcus pneumoniae*. *Mol. Microbiol.* **55**, 413–424
52. Daniel, R. A., and Errington, J. (2000) Intrinsic instability of the essential cell division protein FtsL of *Bacillus subtilis* and a role for DivIB protein in FtsL turnover. *Mol. Microbiol.* **36**, 278–289
53. Daniel, R. A., Noirot-Gros, M.-F., Noirot, P., and Errington, J. (2006) Multiple interactions between the transmembrane division proteins of *Bacillus subtilis* and the role of FtsL instability in divisome assembly. *J Bacteriol.* **188**, 7396–404

54. Bramkamp, M., Weston, L., Daniel, R. A., and Errington, J. (2006) Regulated intramembrane proteolysis of FtsL protein and the control of cell division in *Bacillus subtilis*. *Mol. Microbiol.* **62**, 580–591
55. Villanelo, F., Ordenes, A., Brunet, J., Lagos, R., and Monasterio, O. (2011) A model for the *Escherichia coli* FtsB/FtsL/FtsQ cell division complex. *BMC Struct. Biol.* **11**, 28
56. Marks, D. S., Colwell, L. J., Sheridan, R., Hopf, T. A., Pagnani, A., Zecchina, R., and Sander, C. (2011) Protein 3D structure computed from evolutionary sequence variation. *PLoS ONE*. **6**, e28766
57. Hopf, T. A., Schärfe, C. P. I., Rodrigues, J. P. G. L. M., Green, A. G., Kohlbacher, O., Sander, C., Bonvin, A. M. J. J., and Marks, D. S. (2014) Sequence co-evolution gives 3D contacts and structures of protein complexes. *eLife*. 10.7554/eLife.03430
58. Ghigo, J.-M., and Beckwith, J. (2000) Cell Division in *Escherichia coli*: Role of FtsL Domains in Septal Localization, Function, and Oligomerization. *J. Bacteriol.* **182**, 116–129
59. McDonnell, A. V., Jiang, T., Keating, A. E., and Berger, B. (2006) Paircoil2: improved prediction of coiled coils from sequence. *Bioinformatics*. **22**, 356–358
60. Wolf, E., Kim, P. S., and Berger, B. (1997) MultiCoil: a program for predicting two- and three-stranded coiled coils. *Protein Sci.* **6**, 1179–1189
61. Delorenzi, M., and Speed, T. (2002) An HMM model for coiled-coil domains and a comparison with PSSM-based predictions. *Bioinformatics*. **18**, 617–625
62. Lupas, A., Van Dyke, M., and Stock, J. (1991) Predicting coiled coils from protein sequences. *Science*. **252**, 1162–1164
63. Alva, V., Nam, S.-Z., Söding, J., and Lupas, A. N. (2016) The MPI bioinformatics Toolkit as an integrative platform for advanced protein sequence and structure analysis. *Nucleic Acids Res.* **44**, W410-415
64. Brown, J. H., Cohen, C., and Parry, D. A. (1996) Heptad breaks in alpha-helical coiled coils: stutters and stammers. *Proteins*. **26**, 134–145
65. Hicks, M. R., Walshaw, J., and Woolfson, D. N. (2002) Investigating the tolerance of coiled-coil peptides to nonheptad sequence inserts. *J. Struct. Biol.* **137**, 73–81
66. Schmidt, N. W., Grigoryan, G., and DeGrado, W. F. (2017) The accommodation index measures the perturbation associated with insertions and deletions in coiled-coils: Application to understand signaling in histidine kinases. *Protein Sci.* **26**, 414–435

67. Strelkov, S. V., Schumacher, J., Burkhard, P., Aebi, U., and Herrmann, H. (2004) Crystal structure of the human lamin A coil 2B dimer: implications for the head-to-tail association of nuclear lamins. *J. Mol. Biol.* **343**, 1067–1080
68. Adair, B. D., and Engelman, D. M. (1994) Glycophorin A helical transmembrane domains dimerize in phospholipid bilayers: a resonance energy transfer study. *Biochemistry*. **33**, 5539–5544
69. Levy, E. D., Pereira-Leal, J. B., Chothia, C., and Teichmann, S. A. (2006) 3D complex: a structural classification of protein complexes. *PLoS Comput. Biol.* **2**, e155
70. Egan, A. J. F., and Vollmer, W. (2015) The stoichiometric divisome: a hypothesis. *Front Microbiol.* **6**, 455
71. Harms, M. J., Schlessman, J. L., Sue, G. R., and García-Moreno, B. (2011) Arginine residues at internal positions in a protein are always charged. *Proc. Natl. Acad. Sci. U.S.A.* **108**, 18954–18959
72. Mann, H. B., and Whitney, D. R. (1947) On a Test of Whether one of Two Random Variables is Stochastically Larger than the Other. *Ann. Math. Statist.* **18**, 50–60
73. Schymkowitz, J., Borg, J., Stricher, F., Nys, R., Rousseau, F., and Serrano, L. (2005) The FoldX web server: an online force field. *Nucleic Acids Res.* **33**, W382–388
74. Spearman, C. (1904) The Proof and Measurement of Association between Two Things. *The American Journal of Psychology*. **15**, 72–101
75. O'Leary, N. A., Wright, M. W., Brister, J. R., Ciufo, S., Haddad, D., McVeigh, R., Rajput, B., Robbertse, B., Smith-White, B., Ako-Adjei, D., Astashyn, A., Badretdin, A., Bao, Y., Blinkova, O., Brover, V., Chetvernin, V., Choi, J., Cox, E., Ermolaeva, O., Farrell, C. M., Goldfarb, T., Gupta, T., Haft, D., Hatcher, E., Hlavina, W., Joardar, V. S., Kodali, V. K., Li, W., Maglott, D., Masterson, P., McGarvey, K. M., Murphy, M. R., O'Neill, K., Pujar, S., Rangwala, S. H., Rausch, D., Riddick, L. D., Schoch, C., Shkeda, A., Storz, S. S., Sun, H., Thibaud-Nissen, F., Tolstoy, I., Tully, R. E., Vatsan, A. R., Wallin, C., Webb, D., Wu, W., Landrum, M. J., Kimchi, A., Tatusova, T., DiCuccio, M., Kitts, P., Murphy, T. D., and Pruitt, K. D. (2016) Reference sequence (RefSeq) database at NCBI: current status, taxonomic expansion, and functional annotation. *Nucleic Acids Res.* **44**, D733–745
76. Li, W., Cowley, A., Uludag, M., Gur, T., McWilliam, H., Squizzato, S., Park, Y. M., Buso, N., and Lopez, R. (2015) The EMBL-EBI bioinformatics web and programmatic tools framework. *Nucleic Acids Res.* **43**, W580–584
77. Kamisetty, H., Ovchinnikov, S., and Baker, D. (2013) Assessing the utility of coevolution-based residue-residue contact predictions in a sequence- and structure-rich era. *Proc. Natl. Acad. Sci. U.S.A.* **110**, 15674–15679

78. Kulp, D. W., Subramaniam, S., Donald, J. E., Hannigan, B. T., Mueller, B. K., Grigoryan, G., and Senes, A. (2012) Structural informatics, modeling, and design with an open-source Molecular Software Library (MSL). *J Comput Chem.* **33**, 1645–1661
79. Subramaniam, S., and Senes, A. (2012) An energy-based conformer library for side chain optimization: Improved prediction and adjustable sampling. *Proteins.* **80**, 2218–2234
80. Subramaniam, S., and Senes, A. (2014) Backbone dependency further improves side chain prediction efficiency in the Energy-based Conformer Library (bEBL). *Proteins.* **82**, 3177–3187
81. MacKerell, Bashford, D., Bellott, Dunbrack, Evanseck, J. D., Field, M. J., Fischer, S., Gao, J., Guo, H., Ha, S., Joseph-McCarthy, D., Kuchnir, L., Kuczera, K., Lau, F. T. K., Mattos, C., Michnick, S., Ngo, T., Nguyen, D. T., Prodhom, B., Reiher, W. E., Roux, B., Schlenkrich, M., Smith, J. C., Stote, R., Straub, J., Watanabe, M., Wiórkiewicz-Kuczera, J., Yin, D., and Karplus, M. (1998) All-Atom Empirical Potential for Molecular Modeling and Dynamics Studies of Proteins. *The Journal of Physical Chemistry B.* **102**, 3586–3616
82. Krivov, G. G., Shapovalov, M. V., and Dunbrack, R. L. (2009) Improved prediction of protein side-chain conformations with SCWRL4. *Proteins.* **77**, 778–795
83. Ovchinnikov, S., Kinch, L., Park, H., Liao, Y., Pei, J., Kim, D. E., Kamisetty, H., Grishin, N. V., and Baker, D. (2015) Large-scale determination of previously unsolved protein structures using evolutionary information. *Elife.* **4**, e09248
84. North, B., Summa, C. M., Ghirlanda, G., and DeGrado, W. F. (2001) D_n-symmetrical tertiary templates for the design of tubular proteins. *Journal of Molecular Biology.* **311**, 1081–1090
85. Brooks, B. R., Bruccoleri, R. E., Olafson, B. D., States, D. J., Swaminathan, S., and Karplus, M. (1983) CHARMM: A program for macromolecular energy, minimization, and dynamics calculations. *Journal of Computational Chemistry.* **4**, 187–217
86. Kim, J.-K., Cho, Y., Lee, M., Laskowski, R. A., Ryu, S. E., Sugihara, K., and Kim, D.-S. (2015) BetaCavityWeb: a webserver for molecular voids and channels. *Nucleic Acids Res.* **43**, W413-418
87. Klauda, J. B., Venable, R. M., Freites, J. A., O'Connor, J. W., Tobias, D. J., Mondragon-Ramirez, C., Vorobyov, I., MacKerell, A. D., and Pastor, R. W. (2010) Update of the CHARMM all-atom additive force field for lipids: validation on six lipid types. *J Phys Chem B.* **114**, 7830–7843
88. Phillips, J. C., Braun, R., Wang, W., Gumbart, J., Tajkhorshid, E., Villa, E., Chipot, C., Skeel, R. D., Kalé, L., and Schulter, K. (2005) Scalable molecular dynamics with NAMD. *J Comput Chem.* **26**, 1781–1802

89. Jo, S., Kim, T., Iyer, V. G., and Im, W. (2008) CHARMM-GUI: a web-based graphical user interface for CHARMM. *J Comput Chem.* **29**, 1859–1865
90. Humphrey, W., Dalke, A., and Schulten, K. (1996) VMD: visual molecular dynamics. *J Mol Graph.* **14**, 33–38, 27–28
91. Laskowski, R. A., Rullmann, J. A., MacArthur, M. W., Kaptein, R., and Thornton, J. M. (1996) AQUA and PROCHECK-NMR: programs for checking the quality of protein structures solved by NMR. *J. Biomol. NMR.* **8**, 477–486
92. Studier, F. W. (2005) Protein production by auto-induction in high density shaking cultures. *Protein Expr. Purif.* **41**, 207–234
93. Paintdakhi, A., Parry, B., Campos, M., Irnov, I., Elf, J., Surovtsev, I., and Jacobs-Wagner, C. (2016) Oufti: an integrated software package for high-accuracy, high-throughput quantitative microscopy analysis. *Mol. Microbiol.* **99**, 767–777

Chapter 3: Structural and functional analysis of the *E. coli* FtsLB periplasmic domain

This chapter was prepared to be submitted for future publication as:

Samuel J. Craven, Samson G. F. Condon, Gladys Diaz-Vazquez, and Alessandro Senes. Structural and functional analysis of the *E. coli* FtsLB periplasmic domain.

My contributions to this chapter are the production of constructs, data collection, and data analysis for *in vivo* mutations made throughout FtsLB; the expression and purification of protein as well as the data collection and analysis for circular dichroism experiments; and writing and editing the manuscript.

3.1 Abstract

Cell division in bacteria is mediated by a multiprotein machine called the divisome, which acts at the division site to direct constrictive force and remodel the cell wall into a septum. In *Escherichia coli*, an essential component of the divisome is the FtsLB complex, which is necessary for recruiting other proteins to the division site and is involved with triggering septum formation. However, the molecular mechanisms behind FtsLB function and the overall structure of the complex are not well understood. Here, we provide evidence to support functional relevance for distinct regions of the FtsLB complex – namely, a marginally stable FtsLB coiled coil and a constrained FtsB linker region. Sequence conservation and *in vivo* complementation experiments demonstrate that nonideal interfacial residues within the FtsLB coiled coil have functional importance, possibly to enable conformational flexibility within the complex and/or to promote a dual-heterodimeric arrangement for the periplasmic domain. We model such an arrangement *in silico* and present molecular dynamics simulations that contrast to our previous FtsLB model. We also provide *in vivo* evidence that the FtsB flexible, juxtamembrane linker region is constrained for length. Together, these results suggest that key regions throughout the FtsLB complex play an important role in cell division regulation by tuning FtsLB to the proper relative flexibility needed for signaling cell wall synthase activities.

3.2 Introduction

Cell division in gram-negative bacteria is a complex process involving intricate coordination between numerous cellular components. Central to this coordination is the divisome, a multiprotein complex consisting of around 12 essential proteins (FtsZ, FtsA, ZipA, FtsE, FtsX, FtsK, FtsQ, FtsL, FtsB, FtsW, FtsI, and FtsN, in *Escherichia coli*; Fig. 3.1a) and a suite of nonessential, conditionally essential, and redundant proteins (1, 2). These proteins mediate the various functions necessary for cell division to occur, including establishing the site of division, coordinating invagination of the inner and outer membranes during cytokinesis (the physical process of cell division), and remodeling the cell wall at midcell into a septum to compartmentalize the nascent daughter cells. If any of these functions is abrogated through deletion or mutation of essential proteins, the bacteria can continue to elongate and replicate their DNA, but they will be unable to divide and form distinct daughter cells, resulting in the formation of long filaments and eventual cell lysis and death.

The essential divisome proteins are recruited to the division site in a roughly hierarchical manner (Fig. 3.1b) (1) through interactions with a ring-like arrangement of FtsZ – a tubulin homologue that readily polymerizes in the presence of GTP (3–6). This Z-ring (or proto-ring) is not a continuous structure but instead consists of numerous laterally-overlapping FtsZ protofilaments (7) that are constantly being turned over due to FtsZ GTPase activity. Concomitant polymerization and depolymerization from opposite ends of FtsZ protofilaments results in directional movement of the entire protofilament without movement of the individual FtsZ monomers. This “treadmilling” activity somehow coordinates the spatiotemporal localization of other divisome components like

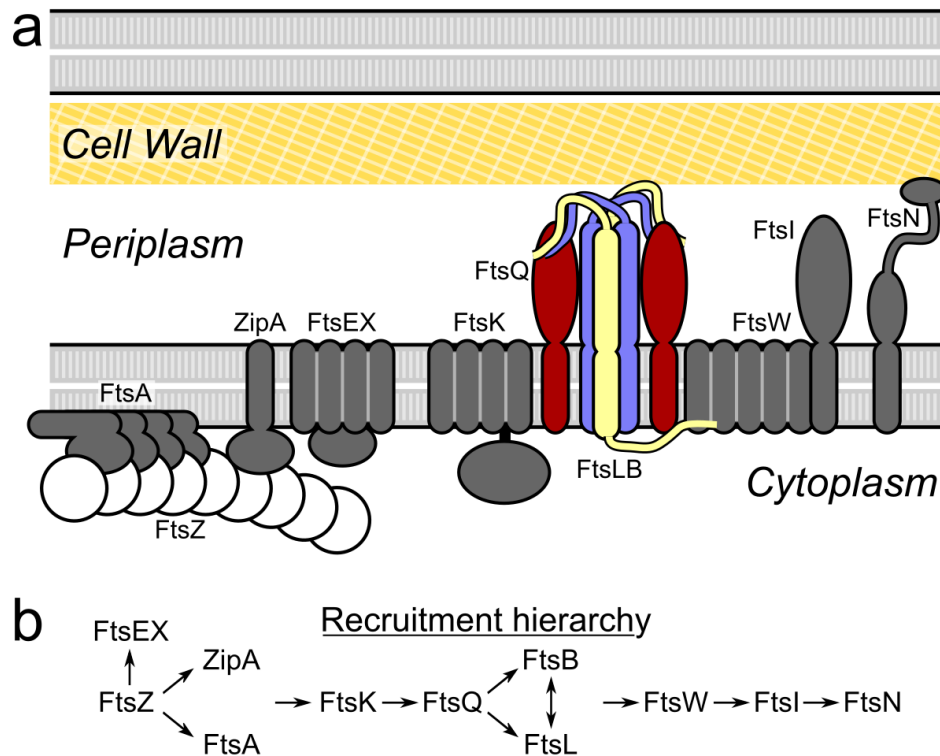


Figure 3.1. The *E. coli* divisome. a) Schematic representation of the essential components of the *E. coli* divisome. Special emphasis is placed on the FtsQLB subcomplex that bridges the functions in divisome assembly and regulation. The stoichiometries presented are not necessarily representative of the actual divisome. b) The divisome assembles in a roughly hierarchical manner, with arrows representing order of dependence for localization to the septum. This hierarchy generally corresponds to the timing of recruitment to the division site.

the machinery necessary for remodeling the cell wall (8–11). Various proteins are involved with stabilizing the Z-ring and modulating interactions between FtsZ protofilaments, including the essential proteins FtsA and ZipA, which also tether the Z-ring to the membrane (12–18). FtsA also plays a critical role in regulating divisome

assembly in a manner dependent on its oligomerization state, which is influenced by ZipA and other downstream divisome proteins like FtsEX (19–22). FtsEX also activates peptidoglycan (PG) hydrolases in the periplasm, which may enable coordination between divisome assembly and septal PG remodeling (22, 23).

PG remodeling is the final critical step of cytokinesis. It involves breakdown of old PG at the division site and the synthesis of new material to form first a septum and, eventually, the poles of the nascent daughter cells. Numerous nonessential enzymes are involved in this process (24, 25), but the essential synthesis of new material is performed by the FtsWI complex (26, 27). FtsW is a PG glycosyltransferase that polymerizes novel glycan strands from lipid II precursors (27, 28) (FtsW was also previously reported to have lipid II flippase activity (29–31)). FtsI is the cognate transpeptidase of FtsW (32–34) and is responsible for crosslinking the glycan polymers to form a network of PG strands (35). This process requires other PG synthases (e.g., the bifunctional glycosyltransferase/transpeptidase PBP1b (36, 37)) and various PG hydrolases, but extensive functional redundancy between these proteins means that no individual component is essential apart from FtsWI. However, the mere presence of the FtsWI complex at midcell is not sufficient for cytokinesis, as the divisome must first be activated.

Activation of PG reconstruction does not occur until the last essential divisome protein, FtsN, accumulates at midcell (38). FtsN is a bitopic membrane protein that topologically bridges the cell wall in the periplasm with the Z-ring in the cytoplasm (39). Its C-terminal, periplasmic SPOR domain binds to nascent PG produced at the forming septum (40, 41), whereas its N-terminal, cytoplasmic tail directly influences divisome assembly through interactions with FtsA (42–45). Another critical region of FtsN is a

short periplasmic domain that provides the minimal requirement to rescue a *ΔftsN* strain when overexpressed (41). Although the precise mechanism by which FtsN triggers PG reconstruction is not known, it is thought to occur through a positive-feedback loop. Interactions between the FtsN cytoplasmic tail and FtsA, along with interactions with other components in the periplasm, promote an “on” state for the divisome that activates septal PG remodeling (21, 46, 47). The nascent PG that is formed as a result serves to recruit more FtsN to midcell via its SPOR domain (41), and the increased FtsN localization further activates the divisome.

Evidence indicates that FtsN-mediated activation of FtsWI and other septal PG synthases depends on the FtsLB complex. In the first place, FtsLB is essential for recruitment of FtsWI to the division site (32, 48), and this likely occurs through a direct interaction between FtsW and the N-terminal, cytoplasmic tail of FtsL (49). Additionally, a series of *ΔftsN*-suppressing mutations were identified within a small region (referred to as the Constriction Control Domain, or CCD) of both the FtsL and FtsB periplasmic domains (21, 46), which further indicates a role for FtsLB in regulation of PG synthesis. These gain-of-function mutations enable PG remodeling to be triggered in the absence of FtsN, which suggests that FtsLB links FtsN to PG synthases. In the current model (39), some structural change (mediated by direct or indirect interactions with FtsN) causes a switch in FtsLB from an “off” to “on” state. This switch, in turn, would trigger the large-scale septal PG reconstruction that enables division to complete. The mechanistic details behind this FtsLB “off/on” switch are unclear, although one possibility is that FtsLB maintains inhibition of PG synthases until FtsN signals their release (50). Alternatively, FtsLB may physically sequester synthases away from sites of active PG synthesis. The spatiotemporal dynamics of different PG synthases have been

shown to depend on FtsZ treadmilling (8–10), and recent findings have suggested that this could result in separate populations of inactive synthases (those tracking the treadmilling FtsZ protofilaments) and active synthases (those released from FtsZ to instead localize to sites of active synthesis) (11). Presumably, FtsLB would be required to link the synthases to FtsZ protofilaments, and the “off/on” switch may therefore entail a physical release of the PG remodeling machinery.

To investigate the mechanisms behind the FtsLB “off/on” switch, a detailed understanding of the complex is required. FtsL and FtsB are both small (121 and 103 residues, respectively) but essential bitopic membrane proteins that share a similar topology, with a short (FtsL) or minimal (FtsB) N-terminal tail in the cytoplasm, a single transmembrane (TM) region spanning the inner membrane, and a larger, C-terminal periplasmic domain (Fig. 3.2). The periplasmic domains of both proteins comprise a juxtamembrane coiled coil, the CCD (in which the $\Delta ftsN$ -suppressing mutations were identified), and a C-terminal region that interacts with FtsQ for recruitment to midcell (49, 51–54). FtsB also contains a short, Gly-rich linker between the TM and coiled-coil regions, which may provide flexibility between these regions, enable proper interactions with FtsL, and potentially facilitate conformational changes during the “off/on” switch (55, 56). FtsLB likely exists as a 2:2 heterotetrameric complex (56), which is formed largely through interactions between the TM and coiled-coil regions of both proteins (51, 55, 57, 58). The TM domains seem to be especially important for FtsLB formation, however, as they can interact apart from the remainder of the complex (58), whereas the coiled-coil interactions are too weak to enable complex formation without the TM domains (59, 60).

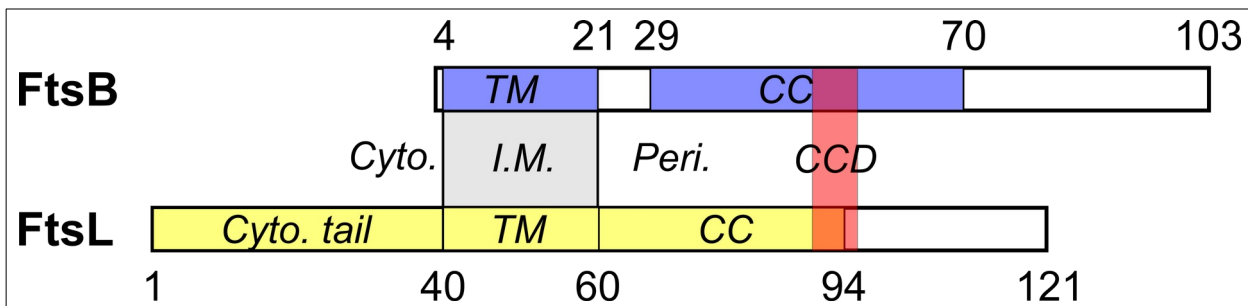


Figure 3.2. Topology diagram for FtsL and FtsB. Both proteins are single-pass transmembrane (TM) proteins located in the inner membrane (I.M.) in *E. coli*. Coiled-coil (CC) regions are involved with formation of the FtsLB complex and overlap with the constriction control domain (CCD; red region; approximately residues 88-94 in FtsL and 55-59 in FtsB), in which gain-of-function mutations have been identified that allow bypass of other divisome components, namely FtsN. Numbers listed represent approximate boundaries of the regions depicted, though the exact positions are not necessarily known.

As noted previously, coiled-coil predictions based on amino acid sequence are fairly weak for FtsB and, in particular, for FtsL (53, 60). The ideal coiled coil would be expected to contain primarily hydrophobic residues at the helix interface (represented by *a* and *d* positions in the *abcdefg* heptad repeat), and the presence of multiple charged and polar residues at its core would likely destabilize the coiled coil (56). In *E. coli*, FtsL contains a pair of arginine residues (R67 and R74) at *a* positions, whereas FtsB contains a *d* position glutamine (Q39) and two *a* position asparagines (N43 and N50). Despite these nonideal residues, co-evolutionary analyses and molecular modeling indicates that FtsLB still forms a canonical coiled-coil interface, but these experiments also suggest that the polar interfacial residues in FtsB do not fully

complement the charged interfacial residues of FtsL, likely leading to a destabilized complex (56). This raises the possibility that FtsLB evolved a marginally stable coiled coil, potentially to accommodate dynamics of the complex (e.g., during FtsN-mediated signaling of cytokinesis). Marginally stable coiled-coil domains have been shown to have functional roles in other proteins including sensor kinases (61–63) and pathogen virulence factors (64), and in a specific case, the degree of hydrophobicity of a coiled-coil interface was shown to impact the local rigidity of the protein and cause a shift in its enzymatic activity (65). The presence of these nonideal, interfacial residues in FtsL and FtsB raises the possibility that similar functional relevance may be associated with a marginally stable FtsLB coiled coil.

In this paper, we analyze the conservation of nonideal, interfacial residues in the FtsLB coiled coil across diverse species and demonstrate in *E. coli* that introducing hydrophobic mutations into these positions results in cell division defects *in vivo*. This may be due to over-rigidifying a region of the complex that normally requires a degree of plasticity. We also show that the charge identity of the interfacial residues in FtsL is important, indicating those residues may play a more nuanced role than simply destabilizing the hydrophobic coiled-coil interface. We incorporate the *in vivo* results into computational models and molecular dynamics (MD) simulations that propose a splitting of the periplasmic domain of FtsLB into a pair of two-helix coils instead of a single four-helix coil as originally proposed (56). We also present evidence that the flexible juxtamembrane linker region of FtsB is constrained for length instead of containing extra slack, which may present structural restrictions on the arrangement of FtsLB. Finally, we show that a predicted alanine interface in FtsB is not crucial for function of the complex.

3.3 Results

3.3.1 The periplasmic domains of FtsL and FtsB contain multiple conserved polar and charged residues

To determine if nonideal FtsLB coiled-coil residues are a common feature outside of *E. coli*, we investigated the overall conservation of polar and charged residues (Asp, Glu, His, Arg, Lys, Gln, and Asn, to be specific) within the complex core interface by aligning homologues from diverse bacterial taxa. There was substantial variation in the total number of nonideal amino acids at *a* and *d* positions in both FtsL and FtsB, but the most common count was three for each protein, matching the number observed in *E. coli* FtsL and FtsB (Fig. 3.3). Across Proteobacteria, approximately half of all FtsL homologues and two thirds of FtsB homologues had three nonideal residues within the coiled-coil domains. Firmicutes showed less consistent trends, and in total, around one third of all paired sequences for FtsL and FtsB had three nonideal residues. The distribution was largely unimodal with no strong correlation in one direction or another.

Additionally, the overall pattern of nonideal residues along the length of the coiled-coil domains in FtsLB is conserved throughout Proteobacteria. The vast majority of FtsL homologues have nonideal residues at the *3a* (heptad number, heptad position) and *5a* positions (typically with a third nonideal residue at a more variable position), while FtsB homologues tend to have nonideal residues at the *2d*, *3a*, and *4a* positions (Fig. 3.4). Thus, both the position and total number of nonideal residues is conserved in FtsB, while in FtsL the total number is more conserved than the position. Such a pattern suggests the possibility that the FtsL coiled coil is tuned for instability, consistent with its weaker coiled-coiled predictions (53, 56).

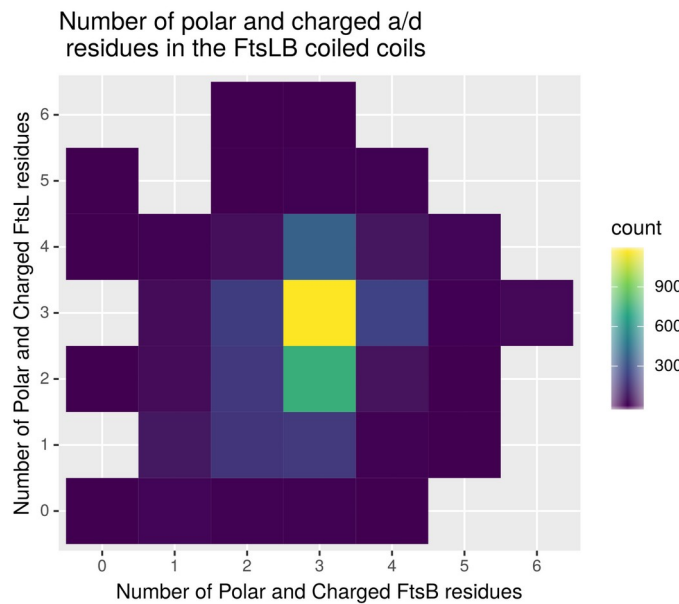
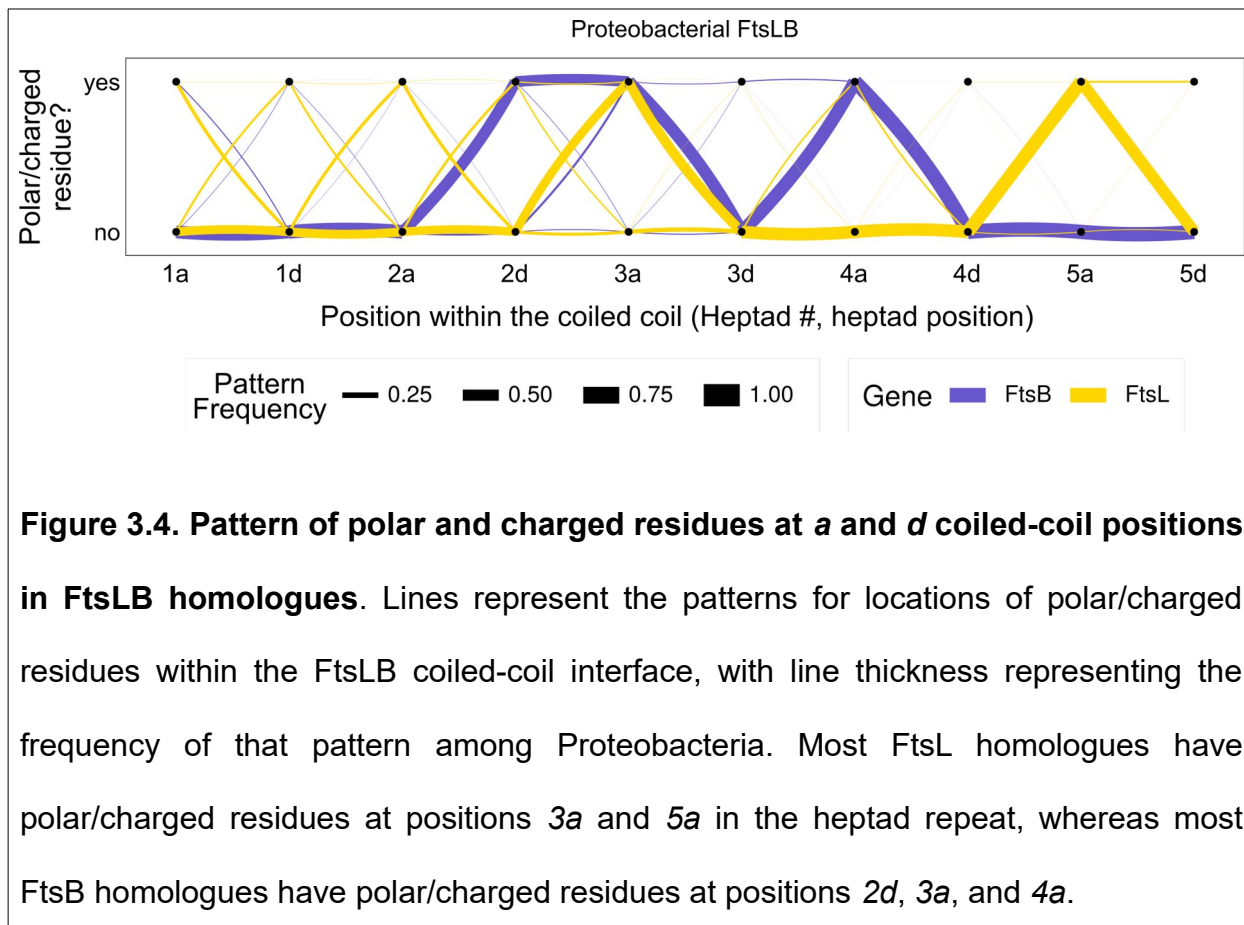


Figure 3.3. Number of nonideal residues in homologues of FtsL and FtsB. Heatmap demonstrating the number of nonideal residues within the coiled-coil interfaces of FtsL vs. FtsB from various bacterial species. Color indicates the count of species with that number of nonideal coiled-coil residues. Most frequently, FtsL and FtsB have three nonideal coiled-coil residues in their interfaces.

3.3.2 Nonideal amino acids at the coiled-coil interface are important for function

To determine if the nonideal residues within the *E. coli* FtsLB coiled-coil interface have functional relevance, we performed *in vivo* complementation experiments in which the nonideal residues in either protein were mutated to a hydrophobic identity (Ile for *a* positions and Leu for *d* positions, as is common in canonical coiled coils (66)) and introduced into depletion strains to test the functionality of the mutant protein. Along with the five nonideal interfacial residues discussed earlier (FtsL R67/R74 and FtsB Q39/N43/N50), we also mutated W81 of FtsL, since aromatic residues tend to be excluded from natural coiled-coil interfaces (66) and a previous paper had pointed out that a W81Y mutation in FtsL greatly increased the predicted coiled-coil propensity (53).



In these experiments, both wild-type (WT) and mutant FtsL and FtsB constructs were expressed with an N-terminal FLAG-tag (flag3) to aid in western blot analysis; prior work has indicated that these tags do not affect FtsL or FtsB function to a noticeable degree (49, 54). Nonfunctional mutations in either protein produced cells that were unable to divide but continued elongating to result in long filaments. Less disruptive mutations gave rise to cells that retained a reduced ability to divide, therefore resulting in an average increase in cell length or subpopulations of elongated or filamentous cells. We compared the cell length distributions of the mutant and WT cells to assess the severity of each mutation (Fig. 3.5). This was accomplished using the same classification scheme as previously described (56). In short, cells with lengths longer than the 95%

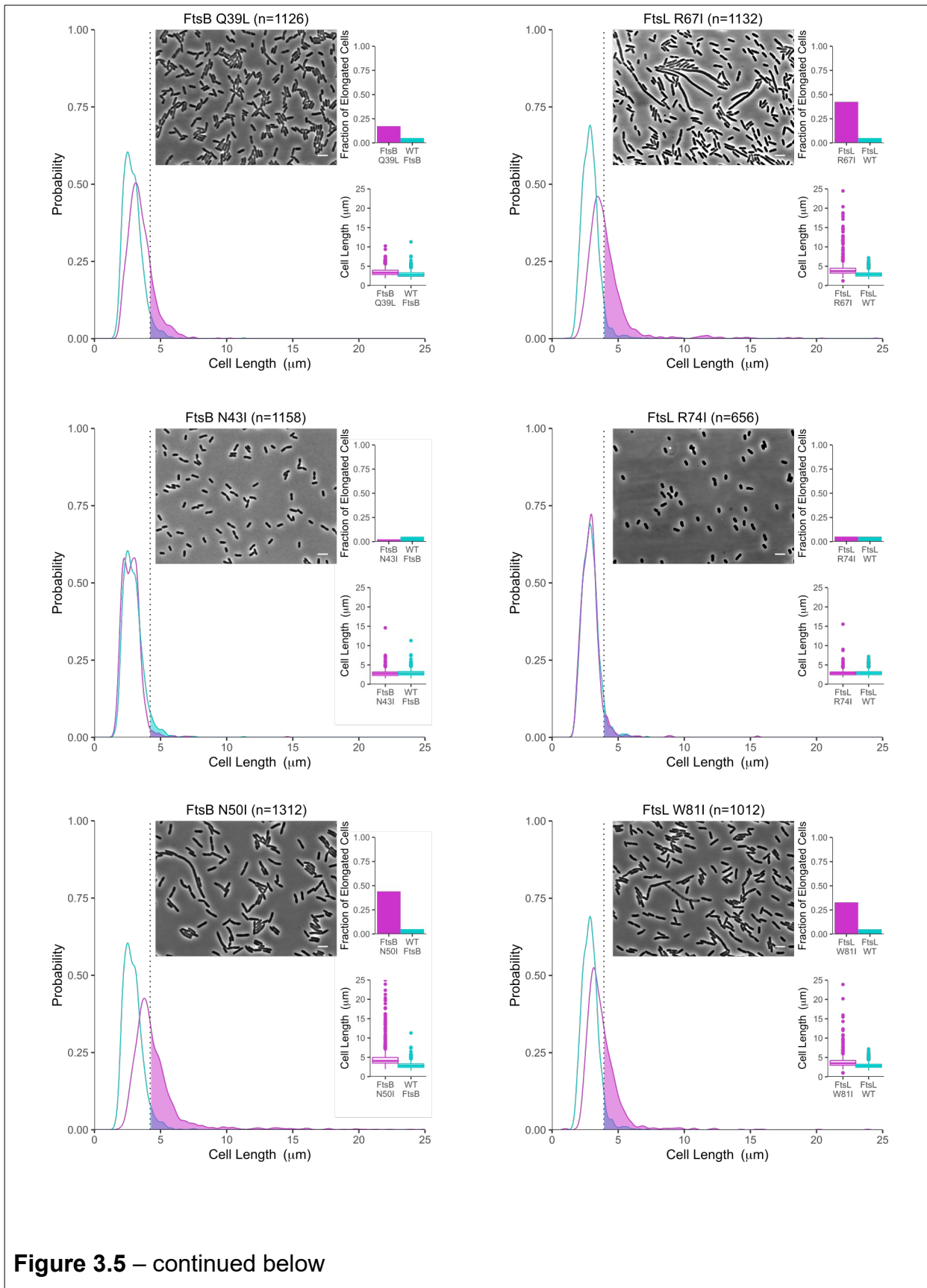
**Figure 3.5 – continued below**

Figure 3.5. Mutations in the nonideal coiled-coil residues cause defects *in vivo*.

Cell length distribution comparisons (represented by a kernel density estimation and a box plot) between wild-type (WT) cells (cyan; n=1296 for FtsB; n=1059 for FtsL) and those containing mutations (magenta) in FtsB or FtsL to convert nonideal *a* and *d* coiled-coil residues to a canonical hydrophobic identity (Ile or Leu, respectively). As an example, FtsB Q39L displays 17% of cells that are longer than the 95th percentile in the WT distribution (shaded areas to the right of the dotted line; quantified in the bar graph), which corresponds to a mild elongation phenotype. Representative phase-contrast images are included with 5 μm scale bar. Cells were grown at 37°C. Length distributions for the corresponding growths at 42°C are provided in Figure S3.2.

percentile in the WT length distribution were considered “elongated”. Length distributions for the various mutations were compared to this threshold, and phenotypes with <15% of total cells being elongated were classified as “WT-like,” >15% as “mild,” >25% as “moderate,” >50% as “severe,” and “filamentous” when complete filamentation occurred. As shown in Fig. 3.5, four of the six mutations tested (FtsL R67I and W81I; FtsB Q39L and N50I) resulted in mild to moderate phenotypes when mutated to the hydrophobic amino acids leucine or isoleucine, whereas the remaining two mutations (FtsL R74I and FtsB N43I) were WT-like. To exclude the possibility that the division defects were due to changes in protein expression, we performed western blot analyses, (Fig. S3.1), which indicated that each mutant was expressed similarly to WT (except for FtsB N43I, which showed increased expression). As these mutations are likely to increase coiled-coil stability, these results suggest that the FtsLB coiled coil has evolved to a marginal stability. These “idealized” mutations may therefore over-rigidify

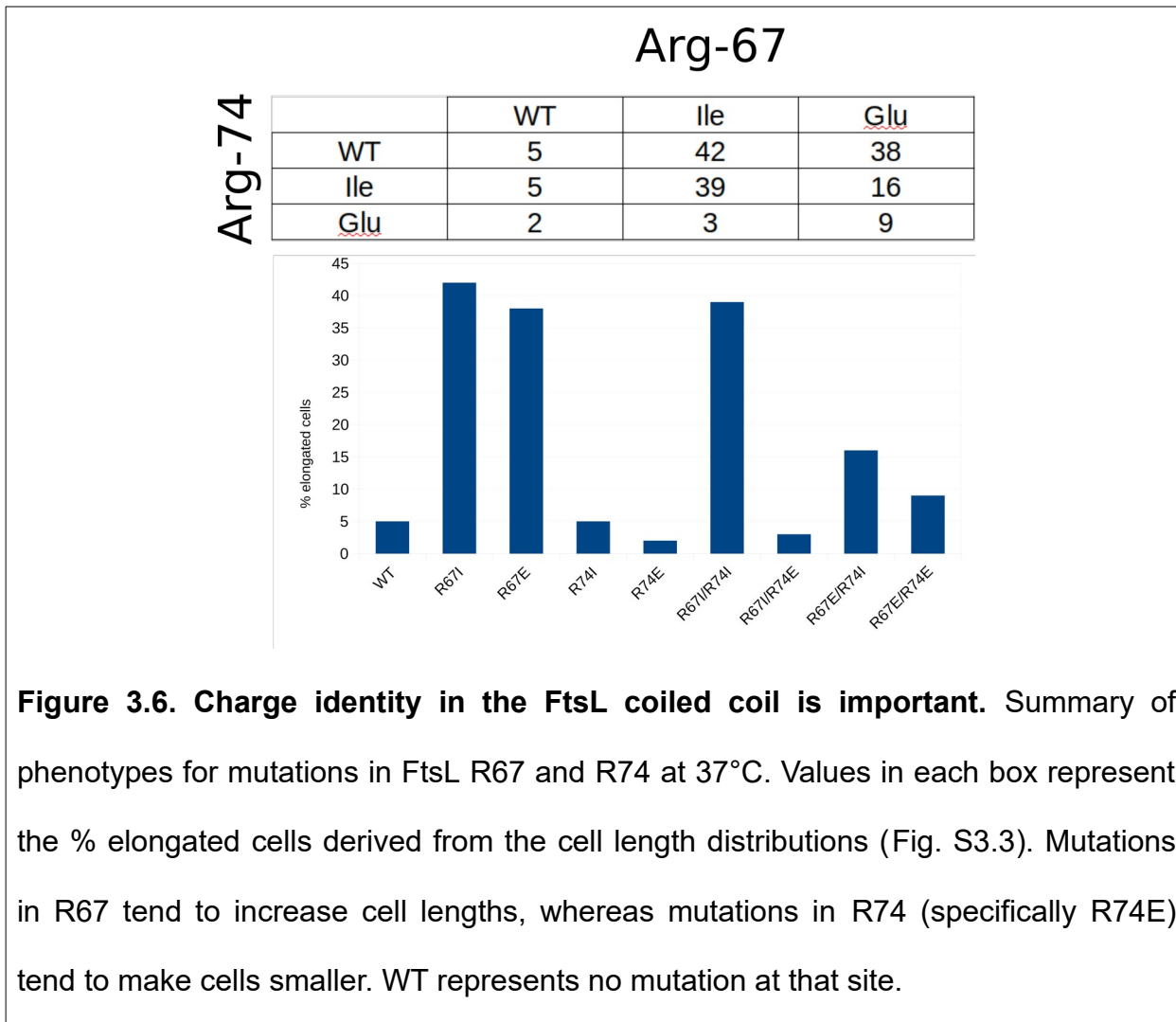
the coiled coil and disrupt some function of FtsLB like its role in FtsN-stimulated signaling of septal PG synthesis.

Considering the conservation of nonideal residues at specific positions within the FtsL coiled coil (Fig. 3.4), we were surprised to find that the FtsL R74I mutation produced WT-like cells whereas the R67I mutation gave a moderate elongation defect. In *E. coli*, R74 is a 3 α coiled-coil position, which is a highly conserved location for nonideal residues across FtsL sequences among Proteobacteria. FtsL R67, on the other hand, is a 2 α position, which typically contains a hydrophobic residue. It was unexpected that a poorly conserved nonideal position has a larger impact on FtsL function compared to a highly conserved position, and the underlying mechanism behind this is currently unclear.

3.3.3 The charge identity of nonideal FtsL residues has functional relevance

If the primary function of the FtsL residues R67 and R74 (R67, in particular, since it is sensitive to mutation) is to provide instability to the coiled coil, then it is possible that the identity of the charged amino acid (either positive or negative) may be unimportant. In order to test this, we performed a double charge reversal on these residues (R67E+R74E) and tested for cell division defects *in vivo* (summarized in Fig. 3.6; western blots in Fig. S3.1; cell length distributions in Fig. S3.3). We found that the double charge reversal resulted in WT-like cells, indeed suggesting that a charge at those positions is sufficient, regardless of identity. Similarly, both R67K and R74K mutations also resulted in WT-like cells (Fig. S3.3), which strengthens this hypothesis.

Interestingly, the individual charge reversals told a different story. The R74E mutation resulted in cells that appeared largely WT-like or even a bit small, which is



unsurprising considering the R74I mutation was also WT-like. The R67E mutation, on the other hand, produced a moderate phenotype, on par with the R67I mutation (38% and 42%, respectively). This finding is surprising, because it suggests that the R74E mutation somehow suppresses the R67E defect to reestablish WT-like cells in the double mutant.

We identified a few possible explanations for the defective R67E mutant compared to the WT-like R67E+R74E mutant. First, the R67E mutation could lead to the formation of a salt bridge between the negative E67 residue and the positive R74 residue, thereby

neutralizing the unfavorable burial of uncharged side chains in the hydrophobic coiled-coil interface. This is unlikely the reason, however, as positions 67 and 74 are separated by two helical turns and are too far apart to readily form a salt bridge. As an alternative explanation, the relative ease of protonating acidic glutamate residues compared to deprotonating basic arginine residues (67, 68) could provide a lower energetic barrier to burial of the mutated E67 residue within the hydrophobic coiled-coil interface. In other words, natural protonation of the mutated E67 residue could stabilize the coiled coil relative to the native R67 identity and therefore allow the R67E phenotype to mimic the R67I phenotype. This would not, however, explain why the R67E+R74E double mutation resulted in a WT-like phenotype.

How the FtsL R74E mutation suppresses R67E is still unclear, but as noted previously, the cells resulting from R74E alone appeared slightly smaller than WT, suggesting that the mutation may trigger early cell division. In this case, the suppression of R67E by R74E could be due to a simple competition between delayed cell division (R67E) and early cell division (R74E). Other such gain-of-function mutations in FtsLB have been identified before (21, 46), predominantly within the CCD, and a similar effect may be seen with R74E. To test this, we examined if R74E could also suppress the moderately elongated phenotype of R67I. Like was the case for R67E+R74E, the double R67I+R74E mutation resulted in WT-like cells, suggesting that R74E may indeed cause early cell division. Regardless of how FtsL positions 67 and 74 relate to each other though, the overall phenotypes observed in this analysis indicate that the charge identity of nonideal residues in the FtsLB coiled coil is important, and the mere presence of any charge at the interface is not sufficient for proper function.

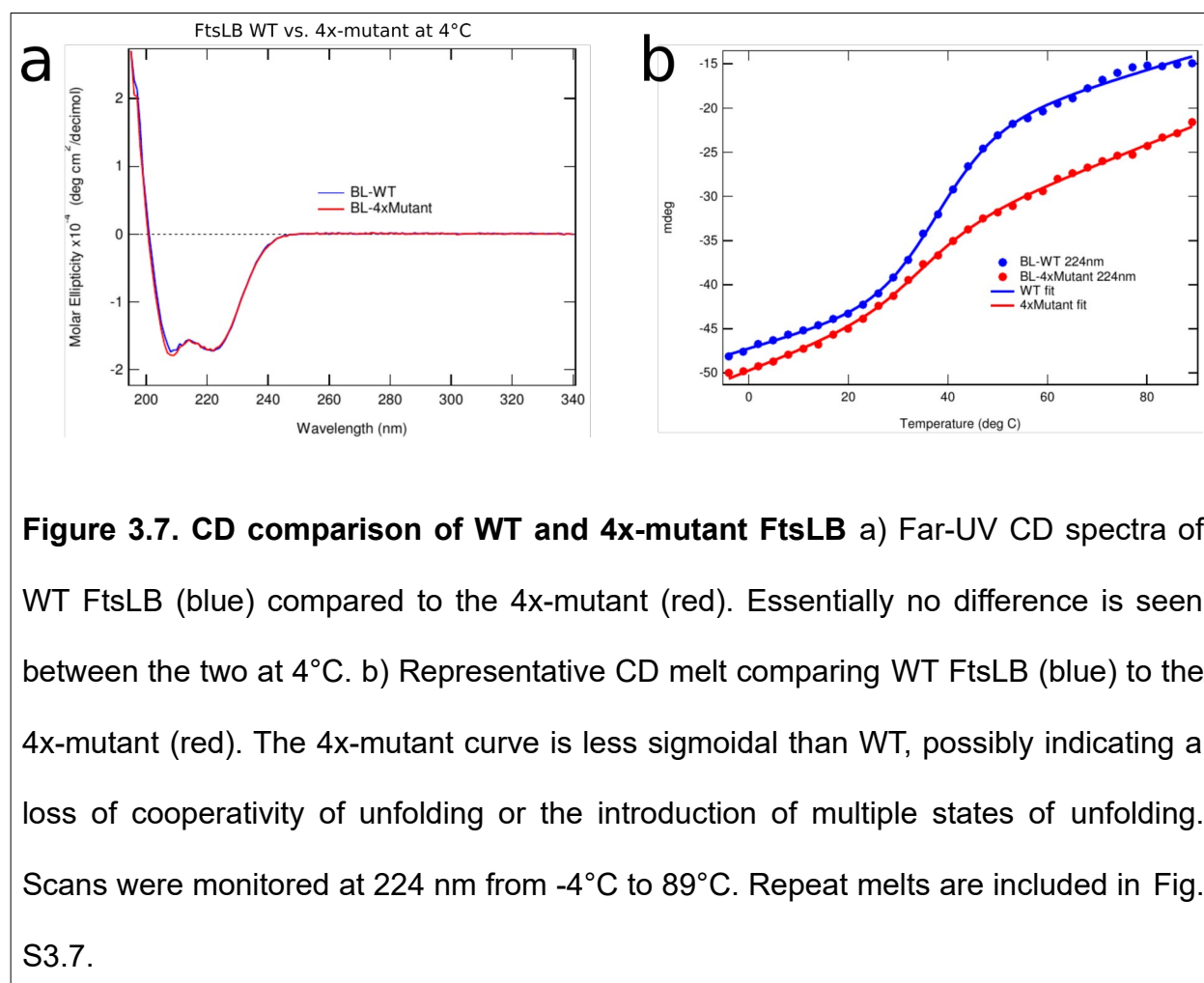
3.3.4 Circular dichroism spectra reveal structural effects of the nonideal coiled-coil interface

Based on the *in vivo* complementation experiments, we hypothesized that increasing the hydrophobicity of the FtsLB coiled-coil interface causes cell division defects by over-rigidifying the complex. To obtain direct structural evidence for this hypothesis, we analyzed the stability of purified FtsLB complex (Fig. S3.5) *in vitro* using circular dichroism (CD) experiments. For these experiments, we used a version of FtsL lacking both the N-terminal tail (FtsL₃₅₋₁₂₁) as well as both native cysteine residues (C41A+C45A). The N-terminal tail of FtsL is likely unstructured and would therefore reduce the average helical content of the complex. It is also unnecessary for the interaction between FtsL and FtsB (49), so we rationalized its removal would be unlikely to impact the structure of the TM and coiled-coil regions of the complex. The native cysteines of FtsL tended to cause crosslinking during purification, and we had previously shown that they are not required for function (56). Due to the strong absorbance of commonly used reducing agents in the UV region where CD experiments are performed, we elected to use a Cys-less version of FtsL so that reducing agents could be omitted from the buffer. That being said, initial CD experiments indicated no structural difference between FtsLB with and without cysteines in the absence of reducing agents (data not shown).

We obtained CD spectra comparing purified His-FtsB/Strep-FtsL₃₅₋₁₂₁-C41A-C45A (termed “WT” for these experiments) to His-FtsB-Q39L-N43I/Strep-FtsL₃₅₋₁₂₁-C41A-C45A-R67I-R74I (termed “4x-mutant”) at 4°C in detergent (Fig. 3.7a). The resulting spectra indicated little difference between the two samples, suggesting that either the mutations do not cause any structural effects or that these effects are minimal at low temperature. We then obtained spectra comparing the samples at increased

temperatures (Fig. S3.6). These data indicated that the 4x-mutant retains more helical content than WT at higher temperatures as well as after cooling back to the starting temperature, which suggested a higher melting temperature and increased stability for the 4x-mutant.

To better compare the WT to the 4x-mutant samples, we performed thermal melt CD, monitoring the signal at 224 nm (Fig. 3.7b). Unexpectedly, the resulting melts did not indicate an increased melting temperature for the 4x-mutant. Instead, the increased helicity of the 4x-mutant at higher temperatures seems to be due to a transition from the sigmoidal curve seen in the WT sample to a much more linear curve, which precluded confident melting temperature determination. This transition in the shape of the melting



curve could indicate a loss of cooperativity of unfolding for the 4x-mutant; however, it is also possible that multiple states of folding are involved. Further biophysical analyses would be needed to better explain what structural changes are caused by the mutations and whether the effects seen are due to the presence of detergent instead of the native lipid environment. Regardless, some sort of structural difference between the WT and 4x-mutant complex is evident, and in general, the 4x-mutant appears to retain more helicity than WT and may therefore be more stable.

3.3.5 Remodeling the FtsLB coiled coils to accommodate nonideal residues

We originally modeled the tetrameric FtsLB complex as a parallel four-helix bundle spanning the transmembrane and coiled-coil domains (referred to here as the I-model) (56). This arrangement oriented FtsB in a way that preserved the homodimeric interface seen in the crystal structure (55). However, this arrangement buries the arginine residues of FtsL (R67 and R74 at coiled-coil α positions) in a hydrophobic interface, potentially destabilizing the complex. Indeed, molecular dynamics simulations of this model showed that water infiltrated the core of the coiled-coil domain, whereas the membrane-embedded segment of the FtsLB complex remained relatively static throughout the simulations (56). We wondered whether an alternate arrangement of the coiled-coil domain could more favorably accommodate these nonideal residues. Polar and charged residues tend to occur more frequently in the interfaces of dimeric coiled coils (α positions, in particular) compared to those of higher-order coiled coils (66), and we therefore modeled the coiled-coil domains of FtsLB as two separate two-helix coils (referred to as Y-model) and reconnected them to the previously modeled heterotetrameric transmembrane domain (Fig. 3.8a). This periplasmic, paired two-helix

arrangement for FtsLB is consistent with *in vitro* evidence that the coiled-coil domains form heterodimers in the absence of their transmembrane domains (59, 69). Additionally, this rearrangement does not bury the FtsL arginine residues as severely, letting them escape and better access the bulk solvent (compared to the I-model).

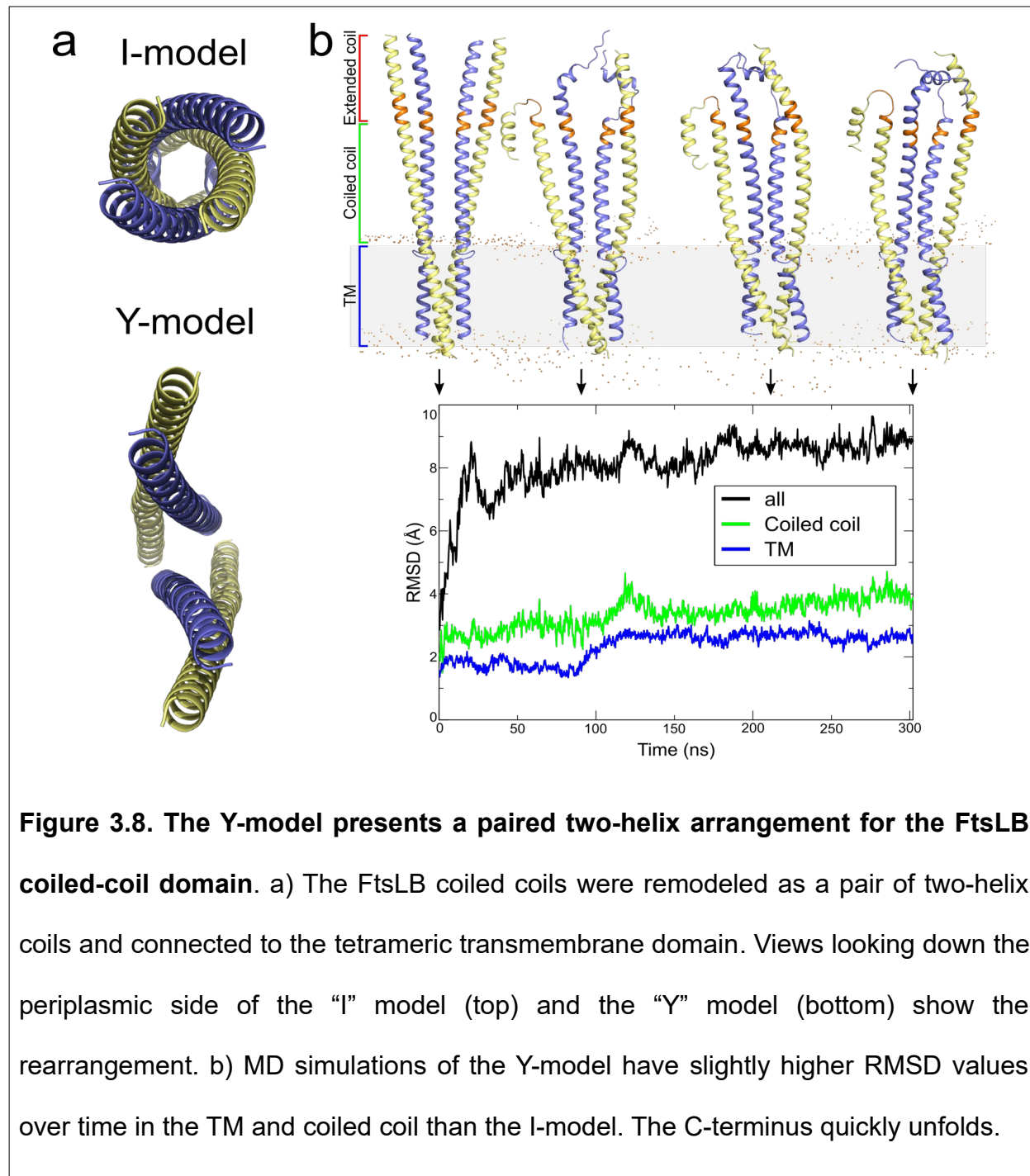


Figure 3.8. The Y-model presents a paired two-helix arrangement for the FtsLB coiled-coil domain. a) The FtsLB coiled coils were remodeled as a pair of two-helix coils and connected to the tetrameric transmembrane domain. Views looking down the periplasmic side of the “I” model (top) and the “Y” model (bottom) show the rearrangement. b) MD simulations of the Y-model have slightly higher RMSD values over time in the TM and coiled coil than the I-model. The C-terminus quickly unfolds.

Surprisingly, the Y-model did not lead to any clashes or distortions of the continuous FtsL helix when reattached to the transmembrane domain. Molecular dynamics simulations of the rearranged FtsLB complex (Fig. 3.8b) showed slightly higher divergence from the starting structure compared to the original model (56), but water molecules did not infiltrate the two-helix coiled-coil interfaces. Some of the increased divergence is attributable to the flexibility of the two-helix coiled coils, which are unconstrained from one another as compared to the four-helix coiled-coil arrangement. Currently, we do not have strong *in vivo* or *in vitro* evidence to support the Y-model over the I-model as the native structure, and it remains possible that interconversions between the two occur naturally or even as part of the FtsLB regulatory function.

3.3.6 The FtsB flexible juxtamembrane linker is constrained for length

In our previous work (55, 56), we concluded that a juxtamembrane linker region in FtsB containing a pair of highly conserved glycine residues (G22 and G25) is likely to adopt a flexible structure. This was demonstrated by inserting alanine residues into the FtsB linker and the corresponding region in FtsL (lacks such a glycine-rich region), which resulted in minor elongation phenotypes for FtsB and complete filamentation for FtsL. We rationalized that the flexible structure of the FtsB linker region provides tolerance to residue insertion, whereas FtsL is likely a continuous helix and is unable to tolerate residue insertion (a single residue would either cause a 100° rotation of the interface around the helical axis or introduce major distortions).

If the FtsB linker allows residue insertion, then a logical follow-up question is whether it can tolerate residue deletion or if it is already constrained for length. To test this, we individually deleted residues K23, N24, and I26 within the FtsB linker and

monitored cell division defects using the same *in vivo* complementation experiments as described earlier. As summarized in Fig. 3.9 (cell length distributions in Fig. S3.8), deletion of each of these residues caused moderate to severe elongation phenotypes without impacting protein expression levels, as analyzed via western blot (Fig. S3.1). The deletions were noticeably more severe than the corresponding alanine mutations (K23A, N24A, and I26A), which were each WT-like, suggesting that it is the loss of linker length and not the loss of the specific residue identity that caused the defect. Interestingly, we were able to completely complement the deletion of either K23 or N24 by combining the deletion with a single alanine insertion following F21 (same location as the alanine insertions in our prior work (56)), which again suggests that it is the loss of length and not the loss of the specific residue that caused the division defect. The single

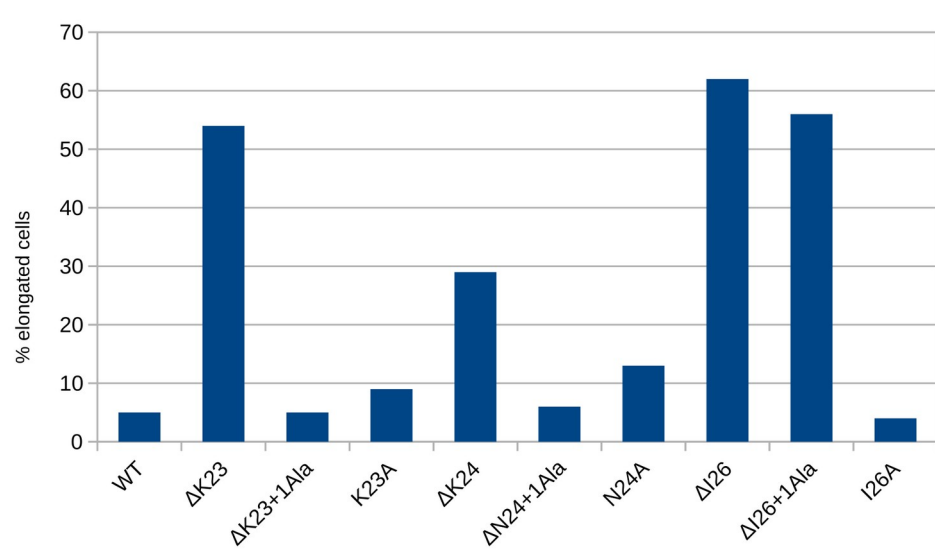


Figure 3.9. FtsB linker mutations. Summary of phenotypes for mutations in the FtsB flexible linker at 37°C. The Y-axis represents the % elongated cells derived from the cell length distributions (Fig. S3.8). Deletion of residues causes moderate to severe elongation defects, indicating the linker is constrained for length.

alanine insertion did not, however, complement the deletion of I26. For some reason, the residue at position 26 in FtsB is needed for function, though perhaps the insertion of a residue before the glycine pair (i.e., following position 21) is unable to complement the loss of a residue after the glycine pair (i.e., at position 26). Alternatively, the exact starting point of the FtsB coiled coil is unclear, and the I26 deletion could impact its structure. Regardless, the WT-like phenotype of the I26A mutation indicates that the specific identity of the residue is not very important. Together, these data indicate that the flexible linker region in FtsB is unlikely to be slack, as we have seen in some of our computational modeling. Instead, the length of the linker is likely limiting and an important structural constraint for the relative positioning of the TM and coiled-coil regions of FtsB within our models.

3.3.7 Snapshots of the FtsLB MD trajectories are tolerant of deletions

The juxtamembrane region of FtsB is enriched in glycine residues and forms a flexible, dynamic linker in the MD simulations, suggesting that the linker does not form a fixed conformation. The length of the linker may be limiting, however, which would explain why it is tolerant of insertions (56) but much less tolerant of deletions. To investigate whether the *in vivo* impact of loop deletions could be recapitulated in the computational models, we used the Rosetta remodel application to shorten the juxtamembrane linker of FtsB by individually deleting positions 23, 24, and 26. Since the linker deletions produce moderate to severe filamentation defects *in vivo*, we would expect the models to be destabilized or for the remodeling protocol to fail in reconnecting the two domains. However, reconstructing the shorter linker was achieved in all cases, and the Rosetta energy score did not strongly increase compared to

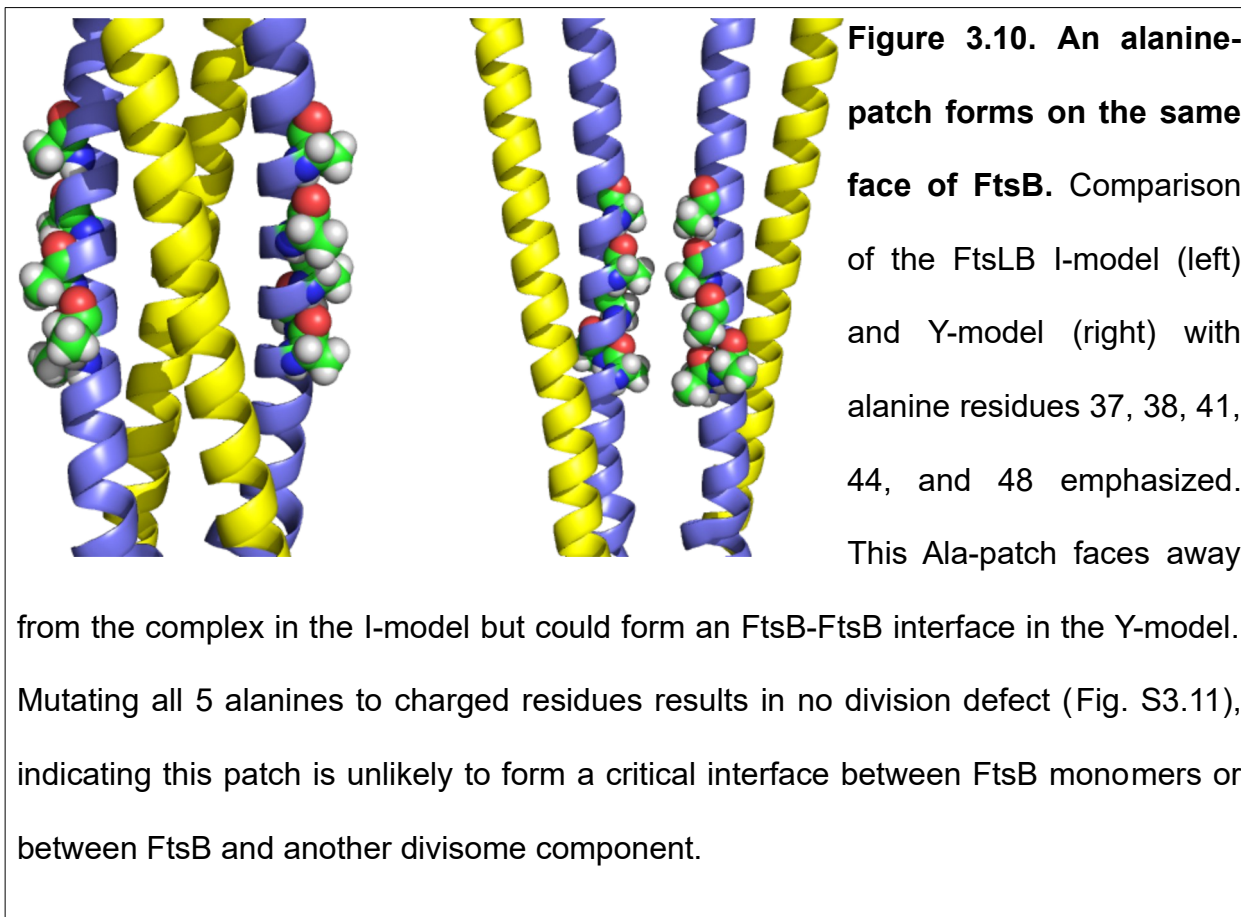
remodeling the WT loop (Fig. S3.10). To investigate this further, we performed the same remodeling on snapshots of the MD trajectories to investigate whether the FtsB linker explores a conformation that is sensitive to deletions. Some conformations were more destabilized upon deleting linker residues, such as chain B of MD run 3 of the FtsLB I-model, which produced consistently much worse models for FtsB Δ26 than WT across the snapshots. However, no conformation or set of conformations were identified that led to drastic changes in the deletions compared to WT, suggesting that these conformations are not extended enough to be sensitive to deletions and that any changes we did observe were stochastic in nature. As such, the deletions are either disrupting a conformation that has not been sampled, or the shortened linker alters the dynamics of the FtsLB complex in some way.

3.3.8 A potential FtsB alanine interface is not crucial for function

Over the course of the MD simulations, a stretch of alanine residues (positions 37, 38, 41, 44, and 48) on the solvent-exposed face of the FtsB coiled-coil domain began to interact with the same face of the opposing FtsB helix (Fig. 3.10). Though these residues are not highly conserved, alanine residues are somewhat common at these positions in FtsB, and we rationalized that the relatively small size and hydrophobic nature of the alanines could allow for the formation of a tightly packed FtsB-FtsB interface, specifically within the Y-model. Alternatively, these alanine residues face away from each other in our I-model and could therefore be involved with packing against another protein like FtsQ should the I-model be representative of the natural structure.

To test if these residues are important for function, we mutated all five alanine residues to either glutamate or aspartate, since the introduction of so many negative

charges so close together would likely disrupt any interface that formed around these positions. Unexpectedly, even with all five alanine residues mutated at once (AAAAA→DDDEE or AAAAA→EEEED), no effects were seen on cell length (Fig. S3.11; western blots in Fig. S3.1), indicating that these residues are not forming a major interface nor have any other essential function. These results still provide important information for our modeling, however, since they cast suspicion on any models that form an interface mediated by these alanine residues. Along with this, the ability to introduce so many negative charges into FtsB without greatly impacting function (and presumably structure) of the complex has implications for structural studies such as X-ray crystallography. Currently, no structures for the full periplasmic region of FtsLB have been produced, and dramatic changes to the surface of FtsLB (such as the introduction



of five negative charges) would likely modify crystal packing and potentially allow formation of better crystals for structure determination.

3.4 Conclusions

In this paper, we identify various mutations within the FtsLB periplasmic region that cause defects in cell division, and we produce a new computational model based on these data. We show that the coiled coils of FtsL and FtsB contain interfacial residues that are normally disfavored in canonical coiled-coil sequences but are nevertheless crucial for function in this complex. It is likely that these nonideal residues impart a marginal stability to the FtsLB coiled coil and may also drive the complex to form a pair of two-helix coils instead of a single four-helix coil. We also show that the flexible Gly-rich FtsB linker is constrained for length, indicating that this region may impose structural limitations on the arrangement of the FtsLB periplasmic domain. The functional implications of these structural aspects are largely hypothetical at the moment, but it is easy to speculate on what they could be. Perhaps a highly stable FtsLB coiled coil would be too rigid to allow proper signaling of septal PG synthesis upon accumulation of FtsN. Maybe a four-helix coiled coil would disfavor FtsQ binding, whereas the two-helix arrangement could more easily bind an FtsQ pair, as speculated for the 2:2:2 FtsQLB complex (70–72). It is even tempting to envision a scenario in which a switch between the two arrangements is crucial to FtsLB-mediated signaling – a conformational change that might not be possible were the coiled coil overly stable or the FtsB linker shortened. Whether any of these scenarios actually represent reality waits to be seen, but the work presented here lays a foundation for further analysis into this essential cell division complex. It is likely that a combination of biophysical,

biochemical, genetic, and computational experimentation will be required to directly address these questions, but the payoff will be worth the efforts. As essential components of a fundamental process within the bacterial life cycle, a better understanding of these proteins has important implications for any research involving bacterial growth and division. More specifically, as bacterial-specific proteins that lack clear human homologues, FtsL and FtsB represent excellent targets for drug design, and a better understanding of the structure of the FtsLB complex is clearly needed in this regard. Moreover, as the periplasmic region of proteins are generally more accessible to antibiotics than cytoplasmic regions (which are separated from the surrounding environment by an extra membrane barrier), a detailed understanding of the structural arrangement of the FtsLB coiled coil is especially applicable in regards to drug design.

3.5 Experimental Procedures

3.5.1 Plasmid cloning

For the *in vivo* complementation experiments, mutant variants of FtsB or FtsL were cloned via standard QuikChange mutagenesis or inverse PCR into pMDG7 (54) (flag3-FtsB) or pMDG29 (49) (flag3-FtsL), respectively. For the CD experiments, the His-tagged FtsB and Strep-tagged Cys-less (C41A and C45A) FtsL_{35–121} were ligated into a modified pETDuet-1 vector at restriction sites NcoI/HindIII and NdeI/Xhol, respectively. Point mutations were introduced using standard QuikChange mutagenesis. All constructs were confirmed by DNA sequencing (Quintarabio). A complete plasmid inventory is included in Table S3.1.

3.5.2 Bacterial strains, plasmids, and media for *in vivo* experiments

The *in vivo* phenotypic analyses were performed using depletion strains NB946 (73) for FtsB and MDG277 (54) for FtsL (both obtained from Jon Beckwith and associates) in which the WT copy of the protein of interest is under control of a repressible P_{BAD} promoter within the chromosome. These strains were transformed with plasmids containing either WT protein (positive control), empty vector (negative control), or a mutant version of the protein to test for defects in cell division as evidenced by an increase in cell length. For all experiments described, bacterial cells were grown in LB medium supplemented with 100 µg/mL spectinomycin (Dot Scientific) and the appropriate carbon source. Medium was supplemented with 0.2% (w/v) L-arabinose (Sigma) or 0.2% (w/v) D-glucose (Sigma) to induce or repress, respectively, the expression of chromosomal copies of the WT genes regulated by the P_{BAD} promoter. 20 µM isopropyl-β-D-1-thiogalactoside (IPTG) was added to the medium to induce the expression of mutant genes regulated by the P_{trc} promoter in the plasmid.

3.5.3 Depletion strain experiments

The protocol for the depletion strain experiments was adapted from Gonzalez and Beckwith (54). In short, a plasmid containing a mutant copy of FtsB or FtsL was transformed into its respective depletion strain. Strains were grown overnight at 37 °C on an LB plate supplemented with arabinose and spectinomycin. A single colony from the plate was grown overnight at 37°C in 3 mL of LB medium supplemented with arabinose and spectinomycin. The overnight culture was then diluted 1:100 into fresh LB medium containing the same supplement and grown to an OD₆₀₀ of ~0.3. An aliquot of 1 mL of culture was washed twice with LB medium lacking any sugar and then diluted

1:100 into 3 mL of fresh LB medium supplemented with glucose, IPTG, and spectinomycin to induce the expression of the mutant gene and to repress the WT gene. The cells were then grown at 37°C for 3.5 hr, the approximate time necessary to deplete the cells of the WT chromosomal copy. Cells were also grown at 42°C in order to stress the cells and potentially reveal thermosensitive mutations, and those cell length distributions are included in the supplemental information. The cells were then placed on ice to stop growth before imaging. Depletion strains provided with their respective WT copy of the protein in the plasmid were tested as positive controls, and, similarly, depletion strains with no protein in the plasmid (empty vector) were tested as negative controls.

3.5.4 Microscopy and cell length measurements

10 µl of cell samples were mounted on a number 1.5, 24 X 50 mm (0.16 – 0.19 mm thickness) cover glass slide (Fisher or VWR). Cells were cushioned with a 3% (w/v) agarose gel pad to restrict the movement of the live cells. Cells were optically imaged using a Nikon Eclipse Ti inverted microscope equipped with crossed polarizers and a Photometrics CoolSNAP HQ2 CCD camera using a Nikon X100 oil objective lens. Phase-contrast images of bacterial cells were recorded with a 50 ms exposure time using Nikon NIS Elements software. Multiple snapshots were collected for each experiment. All images were analyzed to measure the cell length in Oufit (74) using one single optimized parameter set and manual verification.

3.5.5 Western blots

Expression level across all mutant variants was assessed by Western blot analysis (Fig. S3.1). 3.0 mL of cells were pelleted and resuspended in 300 µl of lysis buffer (50

mM HEPES pH 8.0, 50 mM NaCl) with 5 mM β -mercaptoethanol (β ME). The cells were sonicated and centrifuged at 21,000 \times g for 10 min before collecting the supernatant. Total protein concentration was determined by BCA assay (Pierce). 120 μ l of lysates were mixed with 40 μ l of 4x LDS sample buffer (Novex, Life Technologies) with β ME and boiled at 98°C for 3 min. For each FtsL or FtsB sample, the equivalent of 7 μ g or 15 μ g, respectively, of total protein was separated by SDS-PAGE (Invitrogen) and transferred to polyvinylidene difluoride membrane (VWR). Horseradish peroxidase-tagged anti-FLAG (M2) antibodies (Sigma; 1:1000) were used for immunoblotting analysis.

3.5.6 Protein expression and purification for CD

Plasmids were transformed into BL21(DE3) cells (NEB) and plated overnight at 37°C on LB agar with 100 μ g/mL ampicillin. Cells were washed off the plates with 1mL LB broth and inoculated into 1 L of ZYP-5052 autoinduction medium as described (75) and grown at 37°C until reaching an OD₆₀₀ of ~0.8, after which they were incubated overnight at 22°C. Following expression, cells were pelleted, resuspended in cell wash buffer (100 mM NaCl + 10 mM HEPES pH 8.0), pelleted again, flash frozen, and stored at -80°C for future use. The cells were then lysed by sonication in 10 mL/g lysis buffer (50 mM NaCl, 50 mM HEPES pH 8.0) supplemented with 0.5 mg/mL lysozyme, 5 mM β ME, 1 mM phenylmethylsulfonyl fluoride, 1 mM EDTA, and a protease inhibitor cocktail providing (final concentrations) 8 μ M leupeptin (Peptides International), 11.2 μ M E-64 (Peptides International), 0.32 μ M aprotinin (ProSpec), and 0.32 mM 4-(2-aminoethyl)benzenesulfonyl fluoride (Gold BioTechnology). The inclusion body fraction was separated by centrifugation at 10,000 \times g for 20 min, followed by ultracentrifugation

of the supernatant at 180,000 x g for 30 min to isolate the cell membranes. The FtsLB complex was then extracted from the membrane fraction with lysis buffer supplemented with 18 mM n-decyl- β -D-maltopyranoside (DM; Anatrace) and 5 mM β ME, rocking at room temperature overnight. Non-resuspended debris was separated from the solubilized protein via centrifugation at 10,000 x g for 20 min. The supernatant was added to ~3 mL of Ni-NTA-agarose resin (Qiagen) and rocked for 2 h at 4°C before performing gravity-flow purification. Purification was performed by running 10 column volumes of Ni wash buffer (300 mM NaCl, 25 mM HEPES pH 8.0, 50 mM imidazole, 1 mM β ME) supplemented with 510 μ M n-dodecyl- β -D-maltopyranoside (DDM; Avanti Polar Lipids) and 10 column volumes of elution buffer (300 mM NaCl, 25 mM HEPES pH 8.0, 300 mM imidazole, 1 mM β ME) also supplemented with 510 μ M DDM. Protein purity was assessed via SDS-PAGE (Invitrogen).

3.5.7 CD experiments

Purified FtsLB protein was dialyzed twice at room temperature for at least 2 h into 1 L CD buffer (10 mM phosphate buffer pH 7.4, 100 mM NaF) supplemented with 170 mM DDM (1x critical micelle concentration to prevent detergent exchange), then overnight at 4°C in 1 L CD buffer supplemented with 510 mM DDM. Samples were kept at 4°C or on ice from this point forward. Protein concentration was determined against the final dialysis buffer using A_{280} and an extinction coefficient of 32,430 M⁻¹cm⁻¹ for the FtsLB complex (calculated via ExPASy). Protein was diluted to 140 μ M, then filtered with 0.22 μ m (13 mm diameter) PVDF syringe filters (CELLTREAT) before redetermining the final protein concentration. Samples were degassed in a vacuum chamber for at least 30 min, then centrifuged for 20 min at 21,000 x g. The final dialysis

buffer was also filtered and degassed in the same manner to use as a blank in the CD experiments. CD spectra were obtained using an Aviv model 420 CD spectrometer and quartz cuvettes with a 0.1 cm pathlength. All spectra were recorded in 1 nm increments, with either a 10 s or 20 s averaging time, and after a 5 min equilibration time upon reaching a 0.3°C deadband. The spectra were baseline corrected by buffer subtraction. For the CD-monitored thermal melting experiments, the samples were heated at 3°C intervals with a 10 min equilibration time and 20 s averaging time. Because the transitions were not reversible, detailed thermodynamic analyses were not carried out, and the curves were only fitted to sigmoidal transitions to calculate their temperature midpoints (T_m).

3.5.8 Bioinformatic analyses

Homologues of FtsB and FtsL were collected using the DELTA-BLAST algorithm (76) on the RefSeq database (77). FtsB-FtsL pairs were concatenated by taxonomic identifier. In the case of multiple sequences per taxa, the one with the lowest E-value to the query FtsB or FtsL sequence was selected. Sequences were aligned using the MAFFT algorithm (78). Coiled-coil domains were predicted using Paircoil2 (79), COILS (80), and DeepCoil (81). Statistical analyses were performed in R (82) with the aid of the following packages: tidyverse (83), Biostrings (84), zoo (85), taxize (86), rentrez (87), and tidygraph (88).

3.5.9 Modeling the FtsLB complex

Modeling of the FtsLB complex was performed as described previously (56). Briefly, the transmembrane and coiled-coiled domains of the FtsLB complex were each modeled separately using software written in MSL (89). Modeling was guided by

physical force fields as well as sigmoidal distance restraints connecting strongly coupled pairs of FtsB-FtsL residues from a co-evolutionary analysis (90). C2 symmetry was enforced between the FtsB chains and the FtsL chains. The transmembrane and coiled-coiled domains were then aligned via the FtsL juxtamembrane helices and connected using a PDB fragment assembly strategy (89). For the Y-model of the FtsLB complex, a FtsLB two-helix coiled coil was generated using the strategy outlined above. This was aligned and fused to the previously modeled FtsLB transmembrane domain and made C2-symmetric in order to generate the full complex.

3.5.10 Modeling the effect of loop deletions in FtsB

Modeling the effect of deletions within the FtsB juxtamembrane linker was done using the remodel application in ROSETTA (91). To determine if there was a particular conformation of the linker region that was sensitive to deletions, template structures corresponding to 50 ns snapshots of the MD trajectories for the I-model and Y-model were used. Each model was relaxed using the ROSETTA relax protocol with the relax:thorough flag set to true and with constraints to the starting backbone and side chain coordinates (92). One hundred structures were attempted for each deletion on each chain of FtsB. Two flanking residues on either side of the deletion were allowed to be flexible during the remodeling procedure. For comparison, this process was repeated for a “wild-type” remodel, where no residue was deleted and residues 22-25 of FtsB were allowed to be flexible.

3.6 Supplemental information

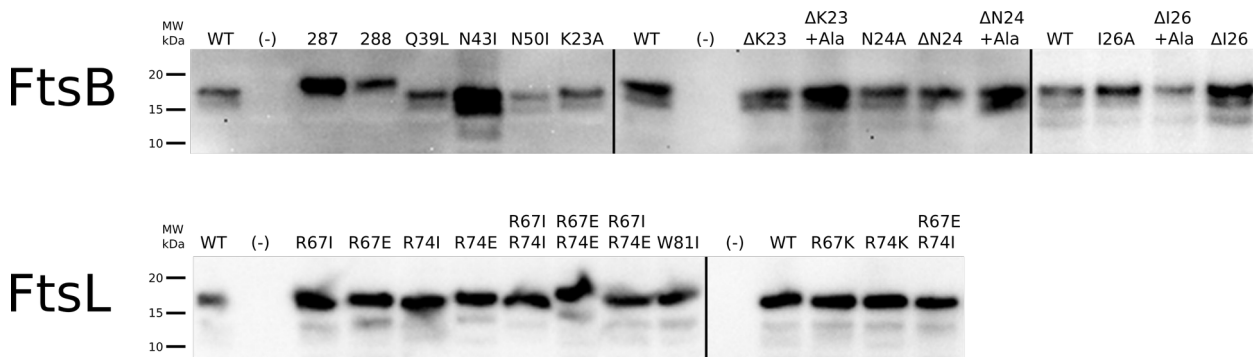


Figure S3.1. Expression level of all FtsB and FtsL mutants used in this work as assessed by Western Blot analysis. Around twice as much whole cell lysate (normalized to total protein) was loaded for FtsB samples as for FtsL samples. Protein expression level of the FtsB and FtsL mutants with defective phenotypes are generally comparable to the respective wild type (WT). Negative controls (-) show no detectable signal for either protein. 287 is FtsB A37D/A38D/A41D/A44E/A48E, and 288 is FtsB A37E/A38E/A41E/A44D/A48D. Both 287 and 288 show a band with slightly increased molecular weight, which may be due to the increased number of negatively charged residues in these mutants. There are cases of FtsB mutants with increased protein level (N43I, in particular), though it is unclear why. Individual gels are separated by solid lines.

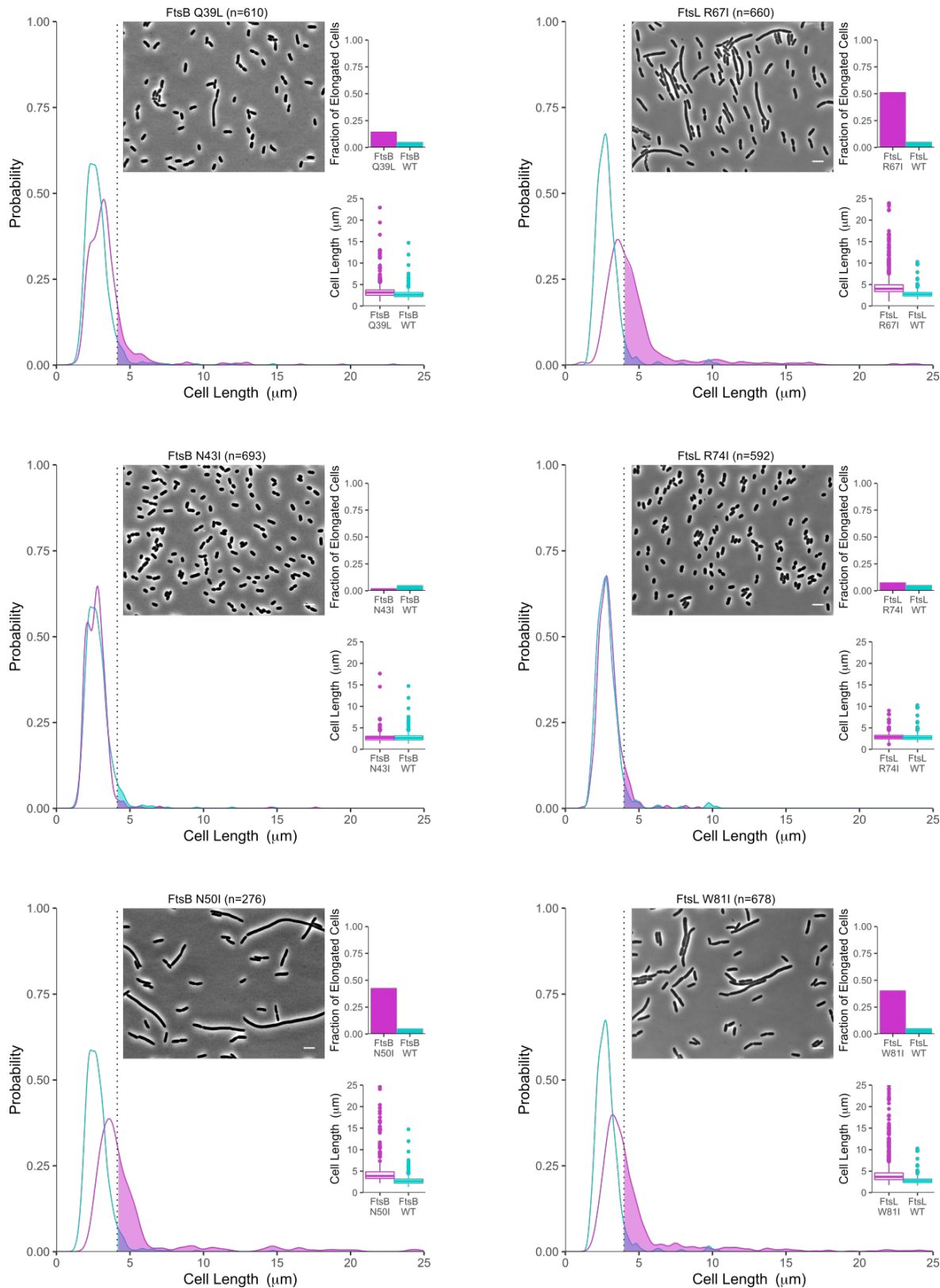


Figure S3.2 – continued below

Figure S3.2. Mutations in the nonideal coiled-coil residues at 42°C. Length distribution comparisons between wild-type cells (cyan; n=651 for FtsB; n=404 for FtsL) and those containing mutations (magenta) in FtsB or FtsL to convert nonideal *a* and *d* coiled-coil residues to a canonical hydrophobic identity (Ile or Leu, respectively). As an example, FtsB Q39L displays 15% of cells that are longer than the 95th percentile in the wild-type distribution (shaded areas to the right of the dotted line), which corresponds to a mild elongation phenotype. Representative phase-contrast images are included with 5 μm scale bar. Cells were grown at 42°C. Length distributions for the corresponding growths at 37°C are provided in Fig. 3.5.

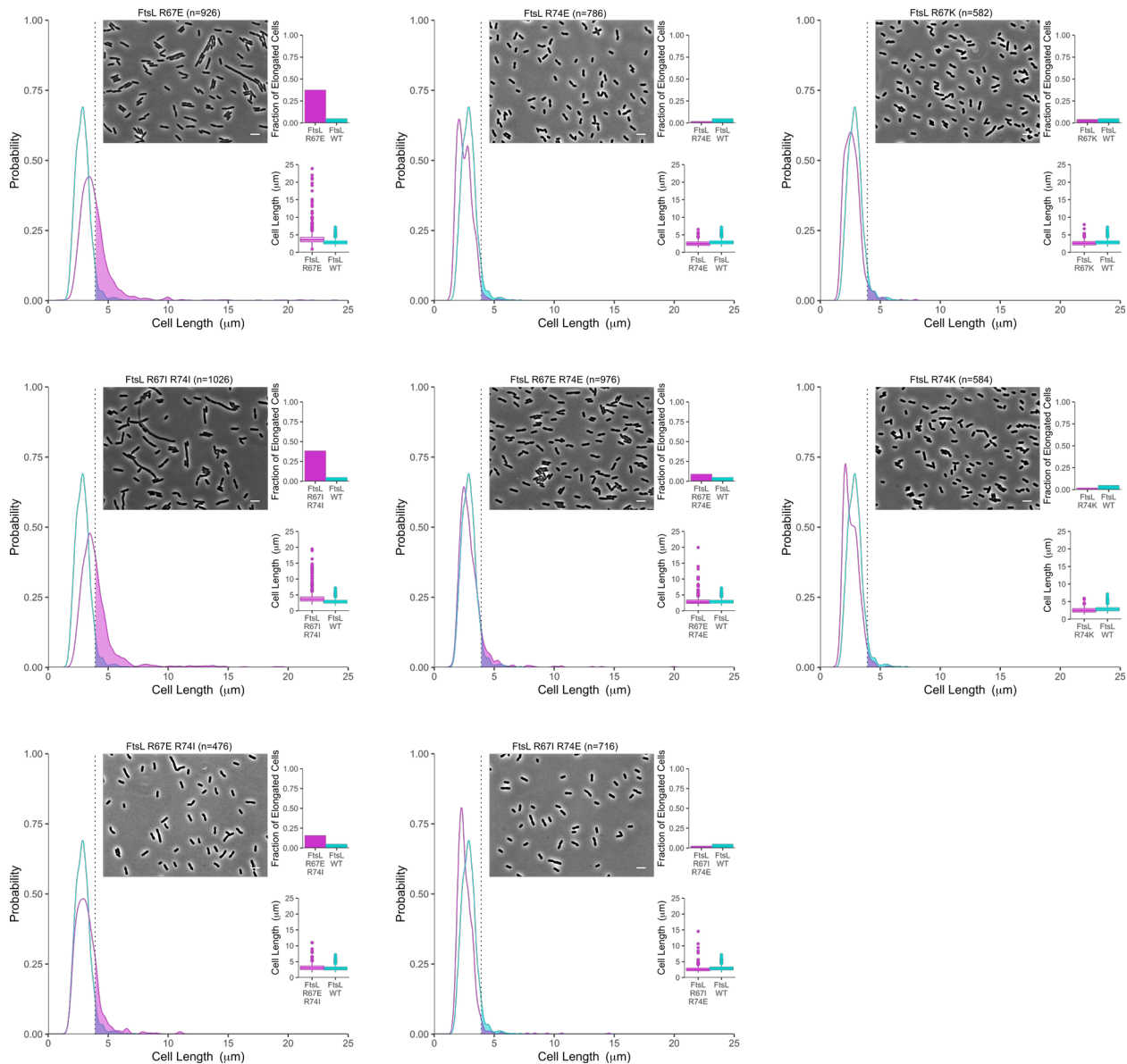


Figure S3.3. Mutations in FtsL R67 and R74 at 37°C. Length distribution comparisons between wild-type cells (cyan; n=1059) and those containing mutations (magenta) in FtsL. As an example, FtsL R67E displays 38% of cells that are longer than the 95th percentile in the wild-type distribution (shaded areas to the right of the dotted line), which corresponds to a "moderate" elongation phenotype. Representative phase-contrast images are included with 5 μm scale bar. Cells were grown at 37°C. Length distributions for the corresponding growths at 42°C are provided in Fig. S3.4.

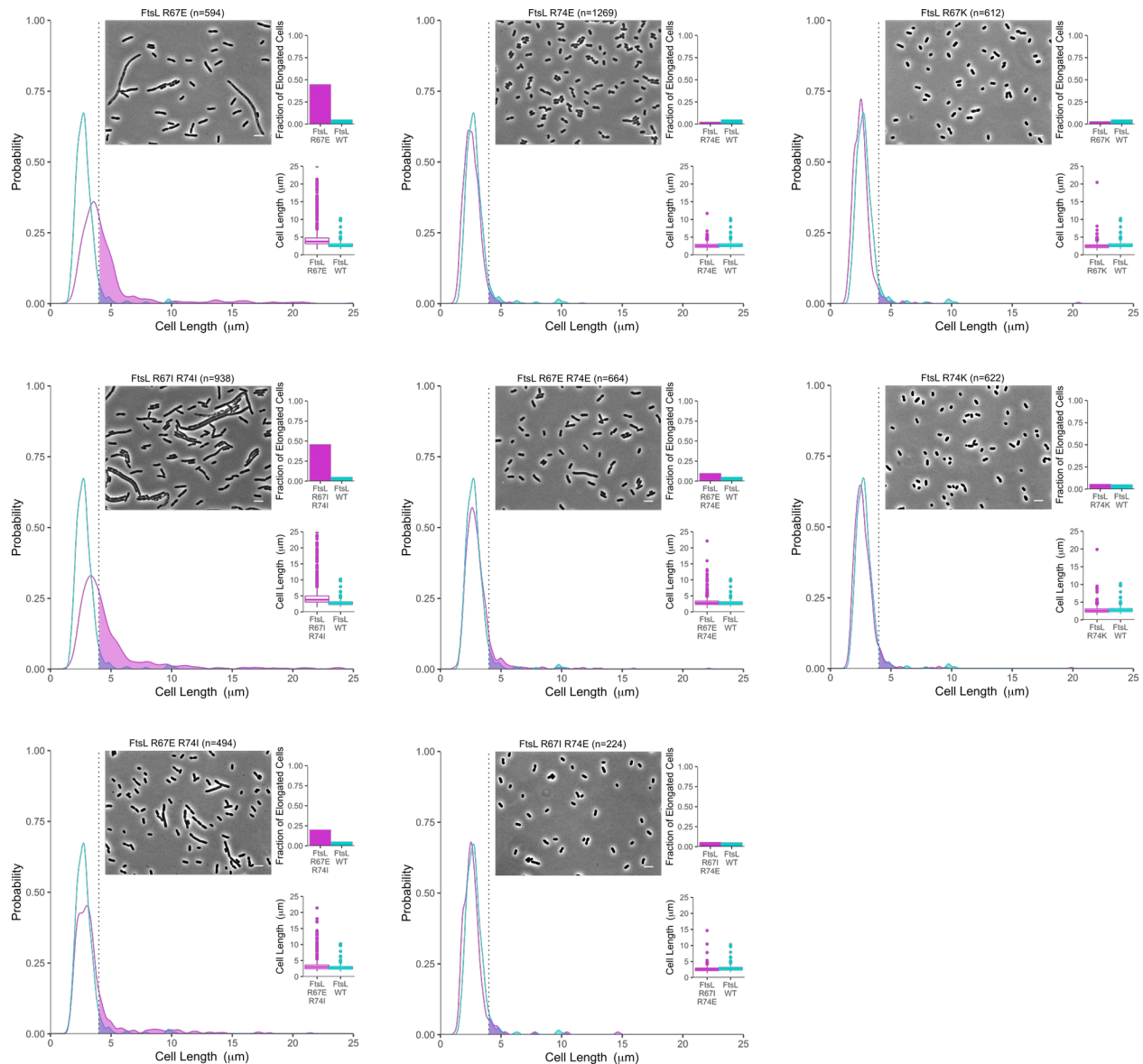


Figure S3.4. Mutations in FtsL R67 and R74 at 42°C. Length distribution comparisons between wild-type cells (cyan; n=404) and those containing mutations (magenta) in FtsL. As an example, FtsL R67E displays 45% of cells that are longer than the 95th percentile in the wild-type distribution (shaded areas to the right of the dotted line), which corresponds to a moderate elongation phenotype. Representative phase-contrast images are included with 5 μm scale bar. Cells were grown at 42°C. Length distributions for the corresponding growths at 37°C are provided in Fig. S3.3.

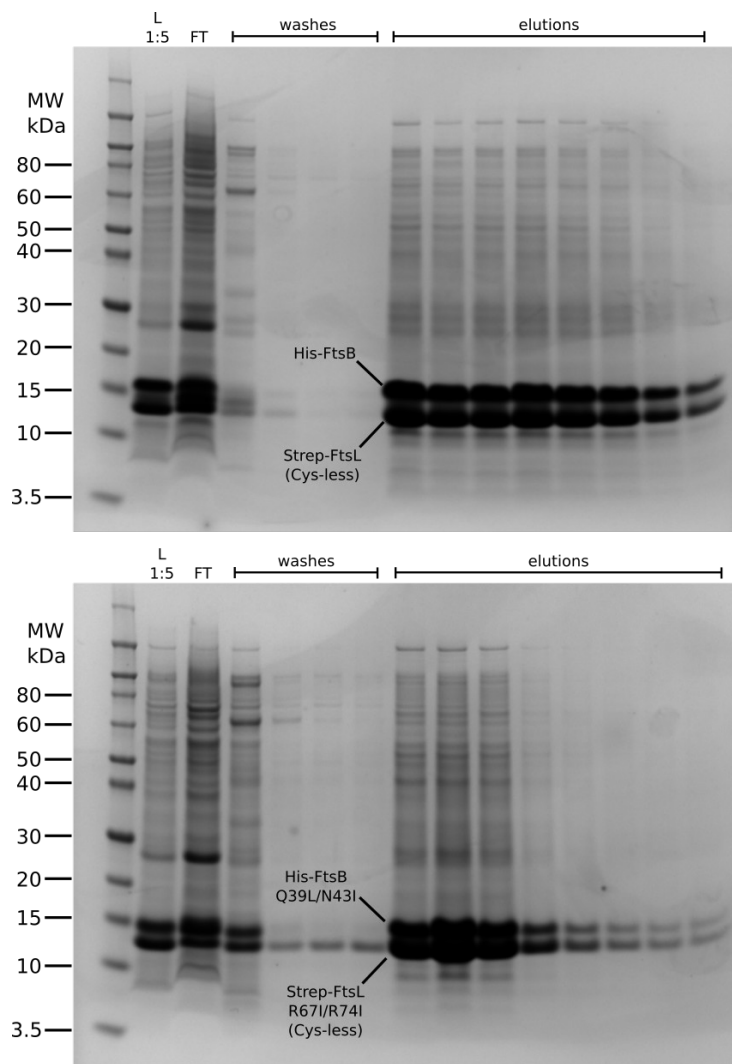


Figure S3.5. Purification of samples for CD experiments. SDS-PAGE gels of representative Ni-NTA purifications for both WT (top) and mutant (bottom) samples used in the CD experiments. "L" represents the column load (sample diluted 1:5 from actual load) obtained from detergent extraction of the membrane fraction following cell lysis. "FT" is the flowthrough fraction. Molecular weight (MW) markers are listed to the left.

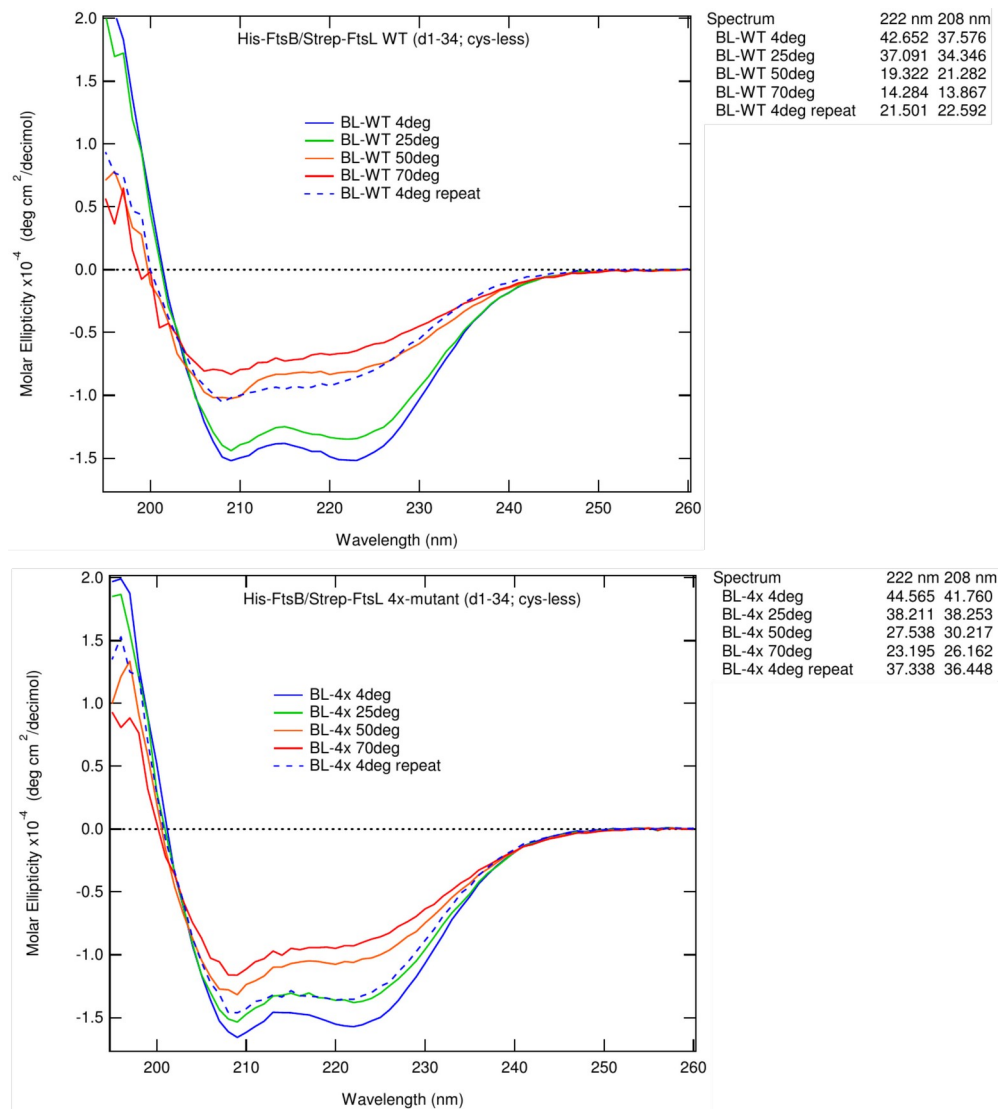


Figure S3.6. CD comparison of WT and 4x-mutant FtsLB at different temperatures.

Far-UV CD spectra of WT FtsLB (top) compared to the 4x-mutant (bottom) at a variety of temperatures. In general, the 4x-mutant is more helical than WT at higher temperatures. The blue dashed line (4deg repeat) represents a final run at 4°C after the sample had already been heated for the 70°C run. The 4x-mutant regains more helical signal for the “4deg repeat” run compared to WT, which may indicate an increased stability. Helicity predictions (% helicity) based on 222 nm and 208 nm signals are included to the right of each graph.

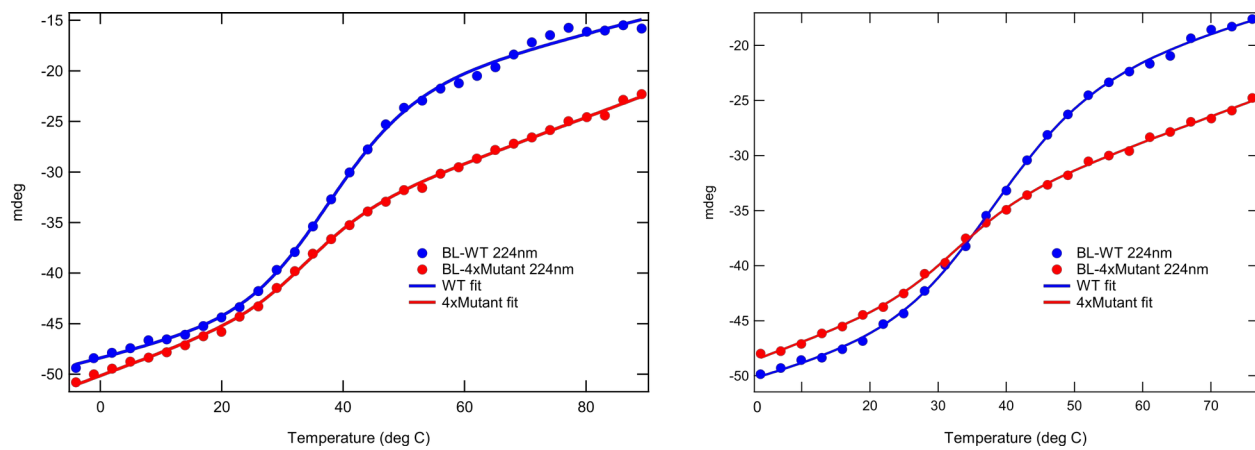


Figure S3.7. Independent CD-monitored thermal melt repeats. Repeat CD melt runs comparing WT FtsLB (blue) to the 4x-mutant (red). Separate protein preparations were used for each run. In each case, the 4x-mutant curve is less sigmoidal than WT, possibly indicating a loss of cooperativity of unfolding or the introduction of multiple states of unfolding. Scans were monitored at 224 nm.

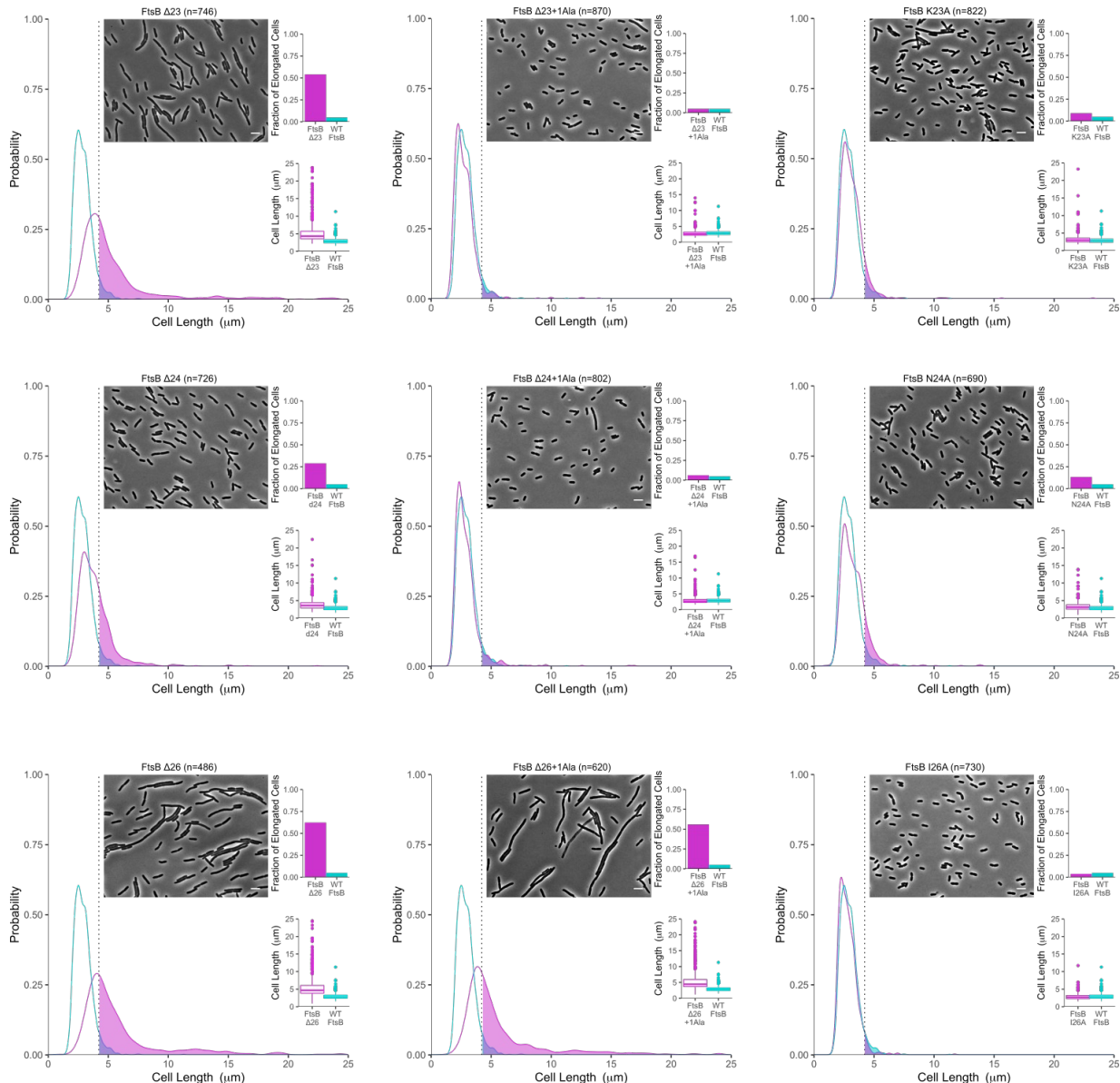


Figure S3.8. Mutations in the FtsB flexible linker at 37°C. Length distribution comparisons between wild-type cells (cyan; n=1296) and those containing mutations (magenta) in FtsB. As an example, FtsB Δ23 displays 54% of cells that are longer than the 95th percentile in the wild-type distribution (shaded areas to the right of the dotted line), which corresponds to a severe elongation phenotype. Representative phase-contrast images are included with 5 μm scale bar. Cells were grown at 37°C. Length distributions for the corresponding growths at 42°C are provided in Fig. S3.9.

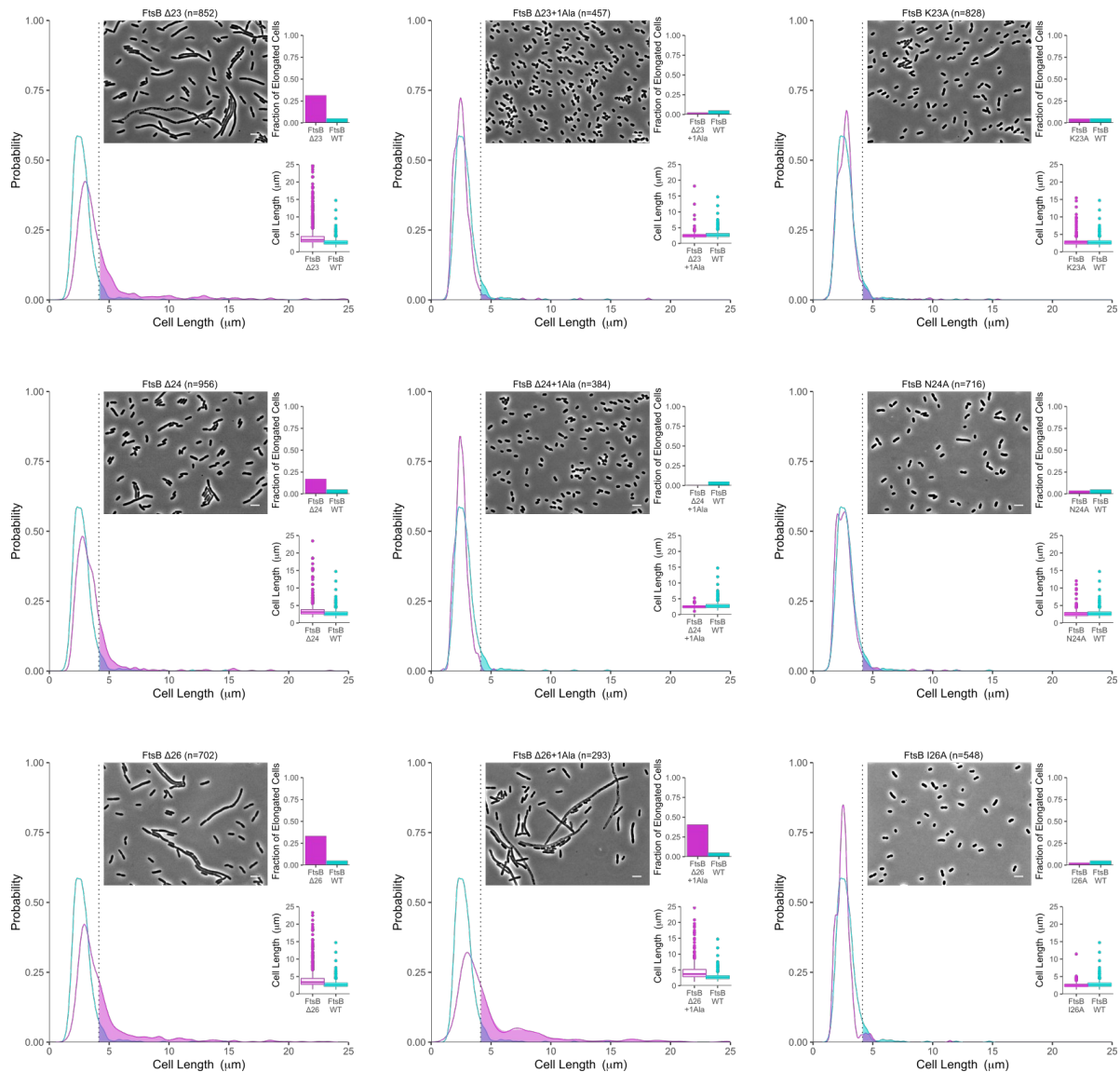


Figure S3.9. Mutations in the FtsB flexible linker at 42°C. Length distribution comparisons between wild-type cells (cyan; n=651) and those containing mutations (magenta) in FtsB. As an example, FtsB Δ23 displays 32% of cells that are longer than the 95th percentile in the wild-type distribution (shaded areas to the right of the dotted line), which corresponds to a moderate elongation phenotype. Representative phase-contrast images are included with 5 μm scale bar. Cells were grown at 42°C. Length distributions for the corresponding growths at 37°C are provided in Fig. S3.8.

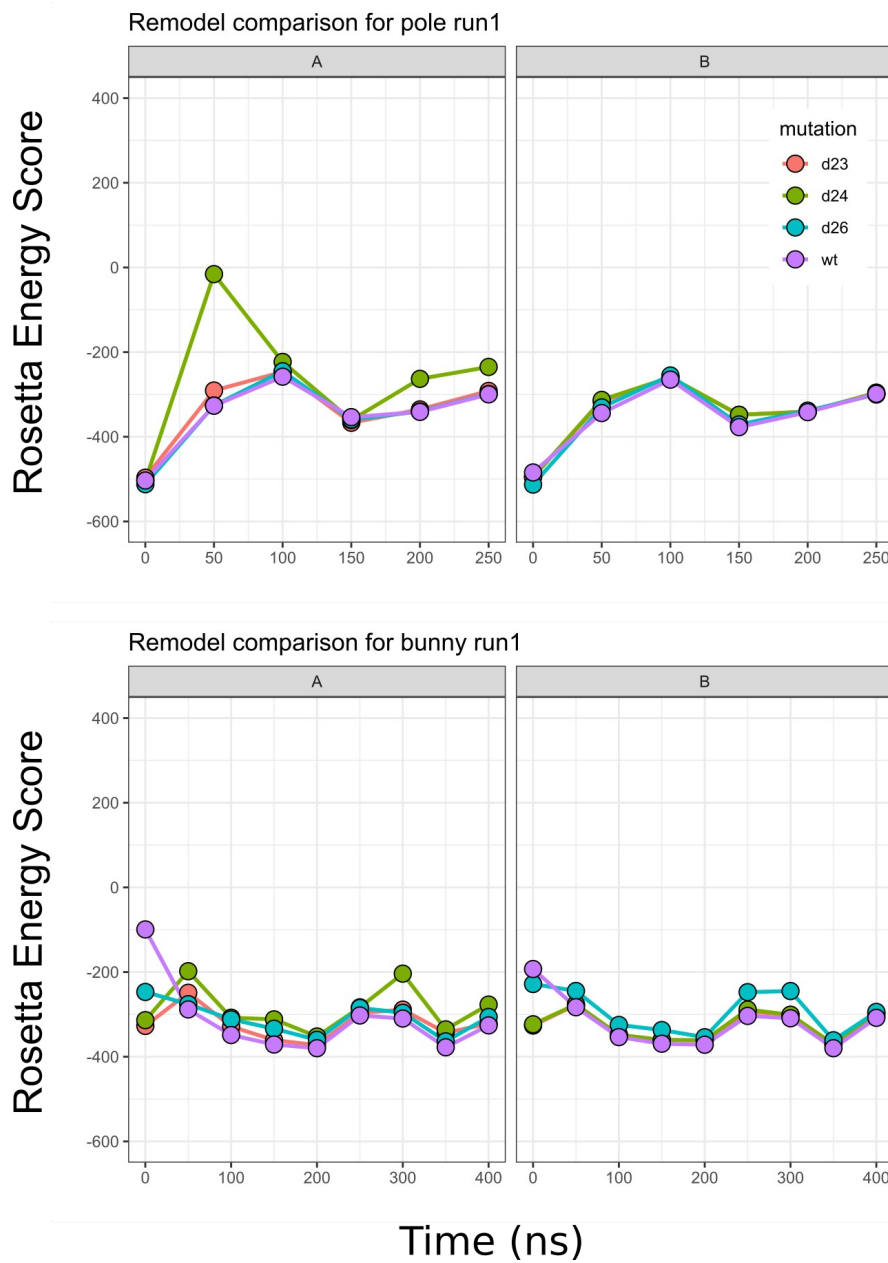


Figure S3.10. Deletions within the juxtamembrane linker of FtsB do not lead to strong destabilization *in silico*. Snapshots of the all-atom molecular dynamics trajectories for both the Y-model (top) and I-model (bottom) were relaxed and subjected to a loop remodeling procedure to shorten the juxtamembrane linker of FtsB. Energy scores for the deletions are generally similar to when the full-length loop is remodeled (purple).

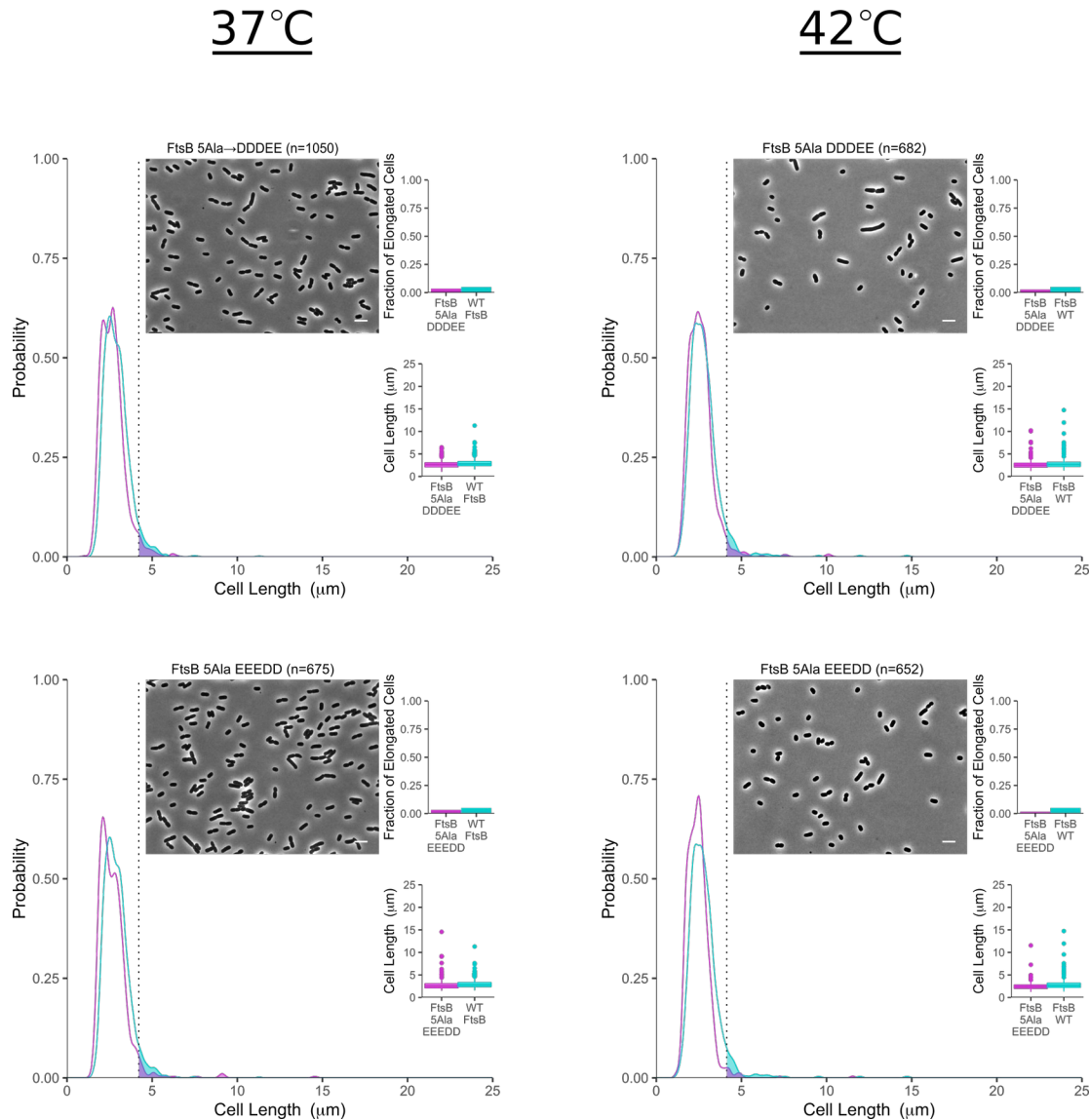


Figure S3.11. Mutations in the FtsB alanine patch. Length distribution comparisons between wild-type cells (cyan; n=1296 at 37°C; n=651 at 42°C) and those containing mutations (magenta) in FtsB at 37°C (left) or 42°C (right). As an example, FtsB 5Ala→DDDEE (A37D/A38D/A41D/A44E/A48E) displays 4% of cells that are longer than the 95th percentile in the wild-type distribution (shaded areas to the right of the dotted line) at 37°C, which corresponds to a WT-like elongation phenotype. FtsB 5Ala→EEEEDD is A37E/A38E/A41E/A44D/A48D. Representative phase-contrast images are included with 5 μm scale bar.

Strain/plasmid	Description	Parent vector	Source
BL21(DE3)	chemically competent <i>E. coli</i> for protein overexpression	-	New England BioLabs (C2527)
NB946	FtsB depletion strain	-	Buddelmeijer et al., 2002
MDG277	FtsL depletion strain	-	Gonzalez & Beckwith, 2009
pSJC020	His-FtsB Strep-FtsL ₃₅₋₁₂₁ C41A/C45A (Cys-less FtsL)	pETDuet-1	Condon et al., 2018
pSJC309	His-FtsB Q39L/N43I Strep-FtsL ₃₅₋₁₂₁ C41A/C45A/R67I/R74I	pETDuet-1	This paper
pNG162	IPTG-inducible, low-copy-number vector (empty)	pAM238	Goehring et al., 2006
pMDG7	flag3-FtsB	pNG162	Gonzalez & Beckwith, 2009
pSJC187	flag3-FtsB Q39L	pMDG7	This paper
pSJC188	flag3-FtsB N43I	pMDG7	This paper
pSJC208	flag3-FtsL N50I	pMDG7	This paper
pSJC248	flag3-FtsB ΔK23	pMDG7	This paper
pSJC249	flag3-FtsB ΔN24	pMDG7	This paper
pSJC251	flag3-FtsB ΔI26	pMDG7	This paper
pSJC287	flag3-FtsB A37D/A38D/A41D/A44E/A48E	pMDG7	This paper
pSJC288	flag3-FtsB A37E/A38E/A41E/A44D/A48D	pMDG7	This paper
pSJC306	flag3-FtsB ΔK23+1Ala(before G22)	pMDG7	This paper
pSJC307	flag3-FtsB ΔN24+1Ala(before G22)	pMDG7	This paper
pSJC308	flag3-FtsB ΔI26+1Ala(before G22)	pMDG7	This paper
pSJC321	flag3-FtsB K23A	pMDG7	This paper
pSJC322	flag3-FtsB N24A	pMDG7	This paper
pSJC323	flag3-FtsB I26A	pMDG7	This paper
pMDG29	flag3-FtsL	pNG162	González et al., 2010
pSJC183	flag3-FtsL R67I	pMDG29	This paper
pSJC185	flag3-FtsL R74I	pMDG29	This paper
pSJC190	flag3-FtsL R67I/R74I	pMDG29	This paper
pSJC194	flag3-FtsL R67E	pMDG29	This paper
pSJC201	flag3-FtsL R74E	pMDG29	This paper
pSJC220	flag3-FtsL W81I	pMDG29	This paper
pSJC254	flag3-FtsL R67E/R74E	pMDG29	This paper
pSJC304	flag3-FtsL R67I/R74E	pMDG29	This paper
pSJC324	flag3-FtsL R67K	pMDG29	This paper
pSJC325	flag3-FtsL R74K	pMDG29	This paper
pSJC326	flag3-FtsL R67E/R74I	pMDG29	This paper

Table S3.1. Strains and plasmids used in this chapter.

3.7 References

1. Du S, Lutkenhaus J. Assembly and activation of the *Escherichia coli* divisome. *Mol Microbiol*. 2017 Jul;105(2):177–87.
2. den Blaauwen T, Hamoen LW, Levin PA. The divisome at 25: the road ahead. *Curr Opin Microbiol*. 2017 Apr;36:85–94.
3. Bi EF, Lutkenhaus J. FtsZ ring structure associated with division in *Escherichia coli*. *Nature*. 1991 Nov 14;354(6349):161–4.
4. Mukherjee A, Lutkenhaus J. Guanine nucleotide-dependent assembly of FtsZ into filaments. *J Bacteriol*. 1994 May;176(9):2754–8.
5. Bramhill D, Thompson CM. GTP-dependent polymerization of *Escherichia coli* FtsZ protein to form tubules. *Proc Natl Acad Sci U S A*. 1994 Jun 21;91(13):5813–7.
6. Löwe J, Amos LA. Crystal structure of the bacterial cell-division protein FtsZ. *Nature*. 1998 Jan 8;391(6663):203–6.
7. Fu G, Huang T, Buss J, Coltharp C, Hensel Z, Xiao J. In vivo structure of the *E. coli* FtsZ-ring revealed by photoactivated localization microscopy (PALM). *PLoS One*. 2010 Sep 13;5(9):e12682.
8. Yang X, Lyu Z, Miguel A, McQuillen R, Huang KC, Xiao J. GTPase activity-coupled treadmilling of the bacterial tubulin FtsZ organizes septal cell wall synthesis. *Science*. 2017 17;355(6326):744–7.
9. Bisson-Filho AW, Hsu Y-P, Squyres GR, Kuru E, Wu F, Jukes C, et al. Treadmilling by FtsZ filaments drives peptidoglycan synthesis and bacterial cell division. *Science*. 2017 17;355(6326):739–43.
10. McCausland JW, Yang X, Lyu Z, Söderström B, Xiao J, Liu J. Treadmilling FtsZ polymers drive the directional movement of sPG-synthesis enzymes via a Brownian ratchet mechanism. *bioRxiv*. 2019 Nov 28;857813.
11. Yang X, McQuillen R, Lyu Z, Phillips-Mason P, Cruz ADL, McCausland JW, et al. FtsW exhibits distinct processive movements driven by either septal cell wall synthesis or FtsZ treadmilling in *E. coli*. *bioRxiv*. 2019 Nov 21;850073.
12. Hale CA, de Boer PA. Direct binding of FtsZ to ZipA, an essential component of the septal ring structure that mediates cell division in *E. coli*. *Cell*. 1997 Jan 24;88(2):175–85.
13. Hale CA, de Boer PA. Recruitment of ZipA to the septal ring of *Escherichia coli* is dependent on FtsZ and independent of FtsA. *J Bacteriol*. 1999 Jan;181(1):167–76.

14. RayChaudhuri D. ZipA is a MAP-Tau homolog and is essential for structural integrity of the cytokinetic FtsZ ring during bacterial cell division. *EMBO J.* 1999 May 4;18(9):2372–83.
15. Pichoff S, Lutkenhaus J. Unique and overlapping roles for ZipA and FtsA in septal ring assembly in *Escherichia coli*. *EMBO J.* 2002 Feb 15;21(4):685–93.
16. Pichoff S, Lutkenhaus J. Tethering the Z ring to the membrane through a conserved membrane targeting sequence in FtsA. *Mol Microbiol.* 2005 Mar;55(6):1722–34.
17. Pazos M, Natale P, Vicente M. A specific role for the ZipA protein in cell division: stabilization of the FtsZ protein. *J Biol Chem.* 2013 Feb 1;288(5):3219–26.
18. Krupka M, Rowlett VW, Morado D, Vitrac H, Schoenemann K, Liu J, et al. *Escherichia coli* FtsA forms lipid-bound minirings that antagonize lateral interactions between FtsZ protofilaments. *Nat Commun.* 2017 11;8:15957.
19. Shiomi D, Margolin W. Dimerization or oligomerization of the actin-like FtsA protein enhances the integrity of the cytokinetic Z ring. *Mol Microbiol.* 2007 Dec;66(6):1396–415.
20. Pichoff S, Shen B, Sullivan B, Lutkenhaus J. FtsA mutants impaired for self-interaction bypass ZipA suggesting a model in which FtsA's self-interaction competes with its ability to recruit downstream division proteins. *Mol Microbiol.* 2012 Jan;83(1):151–67.
21. Liu B, Persons L, Lee L, de Boer PAJ. Roles for both FtsA and the FtsBLQ subcomplex in FtsN-stimulated cell constriction in *Escherichia coli*. *Mol Microbiol.* 2015 Mar;95(6):945–70.
22. Du S, Pichoff S, Lutkenhaus J. FtsEX acts on FtsA to regulate divisome assembly and activity. *Proc Natl Acad Sci U S A.* 2016 23;113(34):E5052-5061.
23. Yang DC, Peters NT, Parzych KR, Uehara T, Markovski M, Bernhardt TG. An ATP-binding cassette transporter-like complex governs cell-wall hydrolysis at the bacterial cytokinetic ring. *Proc Natl Acad Sci U S A.* 2011 Nov 8;108(45):E1052-1060.
24. Egan AJF, Vollmer W. The physiology of bacterial cell division. *Ann N Y Acad Sci.* 2013 Jan;1277:8–28.
25. Booth S, Lewis RJ. Structural basis for the coordination of cell division with the synthesis of the bacterial cell envelope. *Protein Sci Publ Protein Soc.* 2019 Dec;28(12):2042–54.
26. Cho H, Wivagg CN, Kapoor M, Barry Z, Rohs PDA, Suh H, et al. Bacterial cell wall biogenesis is mediated by SEDS and PBP polymerase families functioning semi-autonomously. *Nat Microbiol.* 2016 Sep 19;1:16172.

27. Taguchi A, Welsh MA, Marmont LS, Lee W, Sjodt M, Kruse AC, et al. FtsW is a peptidoglycan polymerase that is functional only in complex with its cognate penicillin-binding protein. *Nat Microbiol.* 2019;4(4):587–94.
28. Meeske AJ, Riley EP, Robins WP, Uehara T, Mekalanos JJ, Kahne D, et al. SEDS proteins are a widespread family of bacterial cell wall polymerases. *Nature.* 2016 29;537(7622):634–8.
29. Mohammadi T, van Dam V, Sijbrandi R, Vernet T, Zapun A, Bouhss A, et al. Identification of FtsW as a transporter of lipid-linked cell wall precursors across the membrane. *EMBO J.* 2011 Apr 20;30(8):1425–32.
30. Mohammadi T, Sijbrandi R, Lutters M, Verheul J, Martin NI, den Blaauwen T, et al. Specificity of the transport of lipid II by FtsW in *Escherichia coli*. *J Biol Chem.* 2014 May 23;289(21):14707–18.
31. Leclercq S, Derouaux A, Olatunji S, Fraipont C, Egan AJF, Vollmer W, et al. Interplay between Penicillin-binding proteins and SEDS proteins promotes bacterial cell wall synthesis. *Sci Rep.* 2017 24;7:43306.
32. Mercer KLN, Weiss DS. The *Escherichia coli* cell division protein FtsW is required to recruit its cognate transpeptidase, FtsI (PBP3), to the division site. *J Bacteriol.* 2002 Feb;184(4):904–12.
33. Fraipont C, Alexeeva S, Wolf B, van der Ploeg R, Schloesser M, den Blaauwen T, et al. The integral membrane FtsW protein and peptidoglycan synthase PBP3 form a subcomplex in *Escherichia coli*. *Microbiol Read Engl.* 2011 Jan;157(Pt 1):251–9.
34. Sauvage E, Derouaux A, Fraipont C, Joris M, Herman R, Rocaboy M, et al. Crystal structure of penicillin-binding protein 3 (PBP3) from *Escherichia coli*. *PloS One.* 2014;9(5):e98042.
35. Botta GA, Park JT. Evidence for involvement of penicillin-binding protein 3 in murein synthesis during septation but not during cell elongation. *J Bacteriol.* 1981 Jan;145(1):333–40.
36. Nakagawa J, Tamaki S, Matsuhashi M. Purified Penicillin Binding Proteins 1Bs from *Escherichia coli* Membrane Showing Activities of Both Peptidoglycan Polymerase and Peptidoglycan Crosslinking Enzyme. *Agric Biol Chem.* 1979 Jun;43(6):1379–80.
37. Sung M-T, Lai Y-T, Huang C-Y, Chou L-Y, Shih H-W, Cheng W-C, et al. Crystal structure of the membrane-bound bifunctional transglycosylase PBP1b from *Escherichia coli*. *Proc Natl Acad Sci U S A.* 2009 Jun 2;106(22):8824–9.
38. Addinall SG, Cao C, Lutkenhaus J. FtsN, a late recruit to the septum in *Escherichia coli*. *Mol Microbiol.* 1997 Jul;25(2):303–9.

39. Weiss DS. Last but not least: new insights into how FtsN triggers constriction during *Escherichia coli* cell division. *Mol Microbiol*. 2015 Mar;95(6):903–9.
40. Ursinus A, van den Ent F, Brechtel S, de Pedro M, Höltje J-V, Löwe J, et al. Murein (peptidoglycan) binding property of the essential cell division protein FtsN from *Escherichia coli*. *J Bacteriol*. 2004 Oct;186(20):6728–37.
41. Gerding MA, Liu B, Bendezú FO, Hale CA, Bernhardt TG, de Boer PAJ. Self-enhanced accumulation of FtsN at Division Sites and Roles for Other Proteins with a SPOR domain (DamX, DedD, and RlpA) in *Escherichia coli* cell constriction. *J Bacteriol*. 2009 Dec;191(24):7383–401.
42. Rico AI, García-Ovalle M, Mingorance J, Vicente M. Role of two essential domains of *Escherichia coli* FtsA in localization and progression of the division ring. *Mol Microbiol*. 2004 Sep;53(5):1359–71.
43. Corbin BD, Geissler B, Sadasiyam M, Margolin W. Z-ring-independent interaction between a subdomain of FtsA and late septation proteins as revealed by a polar recruitment assay. *J Bacteriol*. 2004 Nov;186(22):7736–44.
44. Busiek KK, Eraso JM, Wang Y, Margolin W. The early divisome protein FtsA interacts directly through its 1c subdomain with the cytoplasmic domain of the late divisome protein FtsN. *J Bacteriol*. 2012 Apr;194(8):1989–2000.
45. Busiek KK, Margolin W. A role for FtsA in SPOR-independent localization of the essential *Escherichia coli* cell division protein FtsN. *Mol Microbiol*. 2014 Jun;92(6):1212–26.
46. Tsang M-J, Bernhardt TG. A role for the FtsQLB complex in cytokinetic ring activation revealed by an ftsL allele that accelerates division. *Mol Microbiol*. 2015 Mar;95(6):925–44.
47. Pichoff S, Du S, Lutkenhaus J. The bypass of ZipA by overexpression of FtsN requires a previously unknown conserved FtsN motif essential for FtsA-FtsN interaction supporting a model in which FtsA monomers recruit late cell division proteins to the Z ring. *Mol Microbiol*. 2015 Mar;95(6):971–87.
48. Weiss DS, Chen JC, Ghigo JM, Boyd D, Beckwith J. Localization of FtsI (PBP3) to the septal ring requires its membrane anchor, the Z ring, FtsA, FtsQ, and FtsL. *J Bacteriol*. 1999 Jan;181(2):508–20.
49. Gonzalez MD, Akbay EA, Boyd D, Beckwith J. Multiple interaction domains in FtsL, a protein component of the widely conserved bacterial FtsLBQ cell division complex. *J Bacteriol*. 2010 Jun;192(11):2757–68.
50. Boes A, Olatunji S, Breukink E, Terrak M. Regulation of the Peptidoglycan Polymerase Activity of PBP1b by Antagonist Actions of the Core Divisome Proteins FtsBLQ and FtsN. *mBio*. 2019 08;10(1).

51. Buddelmeijer N, Beckwith J. A complex of the *Escherichia coli* cell division proteins FtsL, FtsB and FtsQ forms independently of its localization to the septal region. *Mol Microbiol*. 2004 Jun;52(5):1315–27.
52. Goehring NW, Gonzalez MD, Beckwith J. Premature targeting of cell division proteins to midcell reveals hierarchies of protein interactions involved in divisome assembly. *Mol Microbiol*. 2006 Jul;61(1):33–45.
53. Ghigo JM, Beckwith J. Cell division in *Escherichia coli*: role of FtsL domains in septal localization, function, and oligomerization. *J Bacteriol*. 2000 Jan;182(1):116–29.
54. Gonzalez MD, Beckwith J. Divisome under construction: distinct domains of the small membrane protein FtsB are necessary for interaction with multiple cell division proteins. *J Bacteriol*. 2009 Apr;191(8):2815–25.
55. LaPointe LM, Taylor KC, Subramaniam S, Khadria A, Rayment I, Senes A. Structural organization of FtsB, a transmembrane protein of the bacterial divisome. *Biochemistry*. 2013 Apr 16;52(15):2574–85.
56. Condon SGF, Mahbuba D-A, Armstrong CR, Diaz-Vazquez G, Craven SJ, LaPointe LM, et al. The FtsLB subcomplex of the bacterial divisome is a tetramer with an uninterrupted FtsL helix linking the transmembrane and periplasmic regions. *J Biol Chem*. 2018 02;293(5):1623–41.
57. Robichon C, Karimova G, Beckwith J, Ladant D. Role of leucine zipper motifs in association of the *Escherichia coli* cell division proteins FtsL and FtsB. *J Bacteriol*. 2011 Sep;193(18):4988–92.
58. Khadria AS, Senes A. The transmembrane domains of the bacterial cell division proteins FtsB and FtsL form a stable high-order oligomer. *Biochemistry*. 2013 Oct 29;52(43):7542–50.
59. Glas M, van den Berg van Saparoea HB, McLaughlin SH, Roseboom W, Liu F, Koningstein GM, et al. The Soluble Periplasmic Domains of *Escherichia coli* Cell Division Proteins FtsQ/FtsB/FtsL Form a Trimeric Complex with Submicromolar Affinity. *J Biol Chem*. 2015 Aug 28;290(35):21498–509.
60. Kureisaite-Ciziene D, Varadajan A, McLaughlin SH, Glas M, Montón Silva A, Luirink R, et al. Structural Analysis of the Interaction between the Bacterial Cell Division Proteins FtsQ and FtsB. *mBio*. 2018 11;9(5).
61. Schmidt NW, Grigoryan G, DeGrado WF. The accommodation index measures the perturbation associated with insertions and deletions in coiled-coils: Application to understand signaling in histidine kinases. *Protein Sci Publ Protein Soc*. 2017;26(3):414–35.

62. Bhate MP, Lemmin T, Kuenze G, Mensa B, Ganguly S, Peters JM, et al. Structure and Function of the Transmembrane Domain of NsaS, an Antibiotic Sensing Histidine Kinase in *Staphylococcus aureus*. *J Am Chem Soc.* 2018;20;140(24):7471–85.
63. Albanesi D, Martín M, Trajtenberg F, Mansilla MC, Haouz A, Alzari PM, et al. Structural plasticity and catalysis regulation of a thermosensor histidine kinase. *Proc Natl Acad Sci U S A.* 2009 Sep 22;106(38):16185–90.
64. Stewart CM, Buffalo CZ, Valderrama JA, Henningham A, Cole JN, Nizet V, et al. Coiled-coil destabilizing residues in the group A *Streptococcus* M1 protein are required for functional interaction. *Proc Natl Acad Sci U S A.* 2016 23;113(34):9515–20.
65. Lesne E, Krammer E-M, Dupré E, Locht C, Lensink MF, Antoine R, et al. Balance between Coiled-Coil Stability and Dynamics Regulates Activity of BvgS Sensor Kinase in *Bordetella*. *mBio.* 2016 Mar 1;7(2):e02089.
66. Woolfson DN. The design of coiled-coil structures and assemblies. *Adv Protein Chem.* 2005;70:79–112.
67. Isom DG, Castañeda CA, Cannon BR, Velu PD, García-Moreno E B. Charges in the hydrophobic interior of proteins. *Proc Natl Acad Sci U S A.* 2010 Sep 14;107(37):16096–100.
68. Harms MJ, Schlessman JL, Sue GR, García-Moreno B. Arginine residues at internal positions in a protein are always charged. *Proc Natl Acad Sci U S A.* 2011 Nov 22;108(47):18954–9.
69. Noirclerc-Savoye M, Le Gouëllc A, Morlot C, Dideberg O, Vernet T, Zapun A. In vitro reconstitution of a trimeric complex of DivIB, DivIC and FtsL, and their transient co-localization at the division site in *Streptococcus pneumoniae*. *Mol Microbiol.* 2005 Jan;55(2):413–24.
70. Villanelo F, Ordenes A, Brunet J, Lagos R, Monasterio O. A model for the *Escherichia coli* FtsB/FtsL/FtsQ cell division complex. *BMC Struct Biol.* 2011 Jun 14;11:28.
71. van den Berg van Saparoea HB, Glas M, Vernooij IGWH, Bitter W, den Blaauwen T, Luijink J. Fine-mapping the contact sites of the *Escherichia coli* cell division proteins FtsB and FtsL on the FtsQ protein. *J Biol Chem.* 2013 Aug 23;288(34):24340–50.
72. Choi Y, Kim J, Yoon H-J, Jin KS, Ryu S, Lee HH. Structural Insights into the FtsQ/FtsB/FtsL Complex, a Key Component of the Divisome. *Sci Rep.* 2018 24;8(1):18061.

73. Buddelmeijer N, Judson N, Boyd D, Mekalanos JJ, Beckwith J. YgbQ, a cell division protein in *Escherichia coli* and *Vibrio cholerae*, localizes in codependent fashion with FtsL to the division site. *Proc Natl Acad Sci U S A.* 2002 Apr 30;99(9):6316–21.
74. Paintdakhi A, Parry B, Campos M, Irnov I, Elf J, Surovtsev I, et al. Oufti: an integrated software package for high-accuracy, high-throughput quantitative microscopy analysis. *Mol Microbiol.* 2016 Feb;99(4):767–77.
75. Studier FW. Protein production by auto-induction in high density shaking cultures. *Protein Expr Purif.* 2005 May;41(1):207–34.
76. Boratyn GM, Schäffer AA, Agarwala R, Altschul SF, Lipman DJ, Madden TL. Domain enhanced lookup time accelerated BLAST. *Biol Direct.* 2012 Apr 17;7:12.
77. O’Leary NA, Wright MW, Brister JR, Ciufo S, Haddad D, McVeigh R, et al. Reference sequence (RefSeq) database at NCBI: current status, taxonomic expansion, and functional annotation. *Nucleic Acids Res.* 2016 Jan 4;44(D1):D733–745.
78. Katoh K, Standley DM. MAFFT multiple sequence alignment software version 7: improvements in performance and usability. *Mol Biol Evol.* 2013 Apr;30(4):772–80.
79. McDonnell AV, Jiang T, Keating AE, Berger B. Paircoil2: improved prediction of coiled coils from sequence. *Bioinforma Oxf Engl.* 2006 Feb 1;22(3):356–8.
80. Lupas A, Van Dyke M, Stock J. Predicting coiled coils from protein sequences. *Science.* 1991 May 24;252(5009):1162–4.
81. Ludwiczak J, Winski A, Szczepaniak K, Alva V, Dunin-Horkawicz S. DeepCoil-a fast and accurate prediction of coiled-coil domains in protein sequences. *Bioinforma Oxf Engl.* 2019 Aug 15;35(16):2790–5.
82. R Core Team. R: A Language and Environment for Statistical Computing [Internet]. Vienna, Austria: R Foundation for Statistical Computing; 2019. Available from: <https://www.R-project.org/>
83. Wickham H. tidyverse: Easily Install and Load the “Tidyverse” [Internet]. 2017. Available from: <https://CRAN.R-project.org/package=tidyverse>
84. Pagès H, Aboyoun P, Gentleman R, DebRoy S. Biostrings: Efficient manipulation of biological strings. 2019.
85. Zeileis A, Grothendieck G. zoo: S3 Infrastructure for Regular and Irregular Time Series. *J Stat Softw.* 2005;14(6):1–27.

86. Chamberlain S, Szoecs E, Foster Z, Arendsee Z, Boettiger C, Ram K, et al. taxize: Taxonomic information from around the web [Internet]. 2019. Available from: <https://github.com/ropensci/taxize>
87. Winter DJ. rentrez: an R package for the NCBI eUtils API. *R J.* 2017;9(2):520–526.
88. Pedersen TL. tidygraph: A Tidy API for Graph Manipulation [Internet]. 2019. Available from: <https://CRAN.R-project.org/package=tidygraph>
89. Kulp DW, Subramaniam S, Donald JE, Hannigan BT, Mueller BK, Grigoryan G, et al. Structural informatics, modeling, and design with an open-source Molecular Software Library (MSL). *J Comput Chem.* 2012 Jul 30;33(20):1645–61.
90. Hopf TA, Schärfe CPI, Rodrigues JPGLM, Green AG, Kohlbacher O, Sander C, et al. Sequence co-evolution gives 3D contacts and structures of protein complexes. *eLife* [Internet]. 2014 Sep 25 [cited 2016 Jul 13];3. Available from: <http://elifesciences.org/lookup/doi/10.7554/eLife.03430>
91. Huang P-S, Ban Y-EA, Richter F, Andre I, Vernon R, Schief WR, et al. RosettaRemodel: A Generalized Framework for Flexible Backbone Protein Design. Uversky VN, editor. *PLoS ONE.* 2011 Aug 31;6(8):e24109.
92. Nivón LG, Moretti R, Baker D. A Pareto-Optimal Refinement Method for Protein Design Scaffolds. Zhang Y, editor. *PLoS ONE.* 2013 Apr 2;8(4):e59004.

Chapter 4: Identification of interaction sites between the essential cell division proteins FtsL and FtsW

This chapter was prepared to be submitted for future publication as:

Samuel J. Craven, & Alessandro Senes. Identification of the interaction sites between
the essential cell division proteins FtsL and FtsW.

My contributions to this chapter are the production of constructs, data collection, and
data analysis for *in vivo* mutations made throughout FtsL and FtsW; the expression and
purification of protein as well as the testing for the *in vitro* binding experiments; and
writing and editing the manuscript.

4.1 Abstract

In order for bacterial cell division to occur, various proteins must localize to midcell and assemble into the multiprotein divisome complex. In *Escherichia coli*, an important step in the divisome assembly pathway is recruitment of the essential cell wall synthase FtsW to the site of division through interaction with FtsL. Without the FtsL-FtsW interaction, cell division cannot occur, but despite the importance of this interaction to the bacterial life cycle, little is known of the specific binding sites in either FtsL or FtsW. In this chapter, I apply both *in vivo* complementation experiments and *in vitro* binding assays to identify residues in both proteins that are involved with this essential interaction. I pinpoint a clear FtsW-binding site within FtsL centered on residue Asp31, and I locate potential residues within FtsW that may compose the corresponding FtsL-binding site. I also identify mutations in FtsW that disrupt cell division without impacting binding to FtsL, suggesting some other critical function for the FtsW 4/5 cytoplasmic loop. Finally, I provide *in vivo* evidence that the length and flexibility of an FtsL linker region may play a role in regulating FtsW activity. Together, these results provide a clearer picture of how FtsL recruits FtsW to midcell during cell division, and they shed light on potential regulatory mechanisms for cell wall synthases. Though a small piece in the complex divisome puzzle, this chapter represents another step forward towards our understanding of the fundamental bacterial process that is cell division.

4.2 Introduction

The bacterial growth cycle in Gram-negative bacteria culminates in the splitting of the mother cell to form two identical daughter cells, a process referred to as cell division or cytokinesis. Though cell division may appear relatively simple at first glance, multiple events must be properly coordinated in order to avoid potentially catastrophic mishaps like chromosomal damage or cell lysis. Some of these events include establishment of the proper site of division, segregation of the newly replicated daughter chromosomes into separate daughter cells, and reorganization of the cell wall at the division site into a septum that will form the new poles of the daughter cells. These various aspects of cell division are coordinated through the activities of a multiprotein complex, referred to as the divisome, which assembles into a ring-like structure around the circumference of the cell at the site of division (1, 2).

Although over 30 proteins participate in divisome function, the most central of these is the tubulin homologue FtsZ (3). As the first essential divisome protein to localize to the division site (4), FtsZ establishes where the septum will form by polymerizing into protofilaments (5, 6) that provide a scaffold for recruitment of the rest of the divisome (1). FtsZ protofilaments also regulate divisome dynamics through their treadmilling activity (7, 8), in which concomitant growth and shrinkage from opposing ends of a filament results in unidirectional movement of the entire filament without movement of the individual FtsZ monomers. The spatiotemporal dynamics of various cell wall synthesis enzymes have been shown to correlate with FtsZ treadmilling (7–10), which indicates that a dynamic divisome is central to remodeling the cell wall at the division site into a septum during the late stages of cell division.

The *E. coli* cell wall, or peptidoglycan (PG) layer, consists of a meshwork of polysaccharide chains crosslinked by short peptides. Reorganization of the PG layer into a septum requires the coordination of numerous essential and nonessential enzymes that break down the PG at the division site and synthesize new material perpendicular to the long axis of the cell (11–13). To construct the polysaccharide chains, lipid II molecules bearing a disaccharide of an *N*-acetylmuramic acid (MurNAc) pentapeptide linked to *N*-acetylglucosamine (GlcNAc) are polymerized via the action of glycosyltransferase (GTase) enzymes (14). During division, the primary GTase enzymes include the essential multi-pass transmembrane (TM) protein FtsW (15, 16) and the bitopic, nonessential class A penicillin-binding protein (aPBP) PBP1b (17, 18). Following polymerization by GTases, PG polymers are then crosslinked together via their pentapeptides by the activity of transpeptidase (TPase) enzymes. As a bifunctional enzyme, PBP1b can catalyze both TPase and GTase reactions, but the essential division TPase activity is provided by the monofunctional class B penicillin-binding protein (bPBP) FtsI, also known as PBP3 (19–21).

FtsW is an integral membrane protein with approximately half of its 414 residues contributing to its ten TM regions (22). It is a member of the recently described SEDS (shape, elongation, division, and sporulation) family of proteins, to which the elongasome-specific RodA GTase also belongs (15, 23, 24). FtsW is known to be essential for cell division (25), but its specific role within the divisome has been a matter of some contention. Initially, FtsW was proposed to provide the lipid II flippase activity that moves the PG precursor from the inner to outer leaflet of the inner membrane (26–28). More recently, this activity has come into question, with FtsW's primary role now

generally considered to be that of the division-specific GTase (15, 16) and with MurJ as the primary lipid II flippase (29–31). This paradigm shift is at least partly due to the well-recognized interaction between FtsW and the single-pass membrane protein FtsI (32, 33), which together form the cognate FtsWI GTase-TPase pair responsible for the essential PG synthesis at the septum.

Localization of FtsW and FtsI to midcell requires prior localization of FtsQ, FtsL, and FtsB (32, 34–36), which are each single-pass TM proteins essential for the assembly and regulation of the divisome. FtsL and FtsB assemble to form a distinct FtsLB subcomplex (35, 37, 38), which recruits FtsWI to midcell primarily through an interaction between FtsW and the N-terminal, cytoplasmic tail of FtsL (39). For its own localization to the division site, FtsLB must interact with FtsQ, forming the FtsQLB subcomplex (36–38). Originally, the major function for FtsQLB within the divisome was thought to be simple recruitment of downstream components to midcell (40), but recent advances in our understanding of cell division regulation have indicated that FtsQLB plays a more complex role in signaling the final constriction event that completes cell division (41, 42). This signal is initiated by the last divisome protein to assemble at the division site, FtsN (43), which interacts either directly or indirectly with FtsQLB to switch it from an “off” to “on” state. This switch is somehow transmitted to the PG synthesis machinery to activate PG remodeling at the septum (41, 42), though what constitutes the difference between the FtsQLB “off” and “on” states is currently unclear. Recent research has indicated that FtsLB directly inhibits the GTase activity of PBP1b whereas FtsQ inhibits FtsI TPase activity *in vitro* (44), so the FtsQLB “off/on” switch may involve a release of PG synthase inhibition. This raises the possibility that FtsW GTase activity is also

regulated in a similar manner through its interaction with FtsL, though there is currently no direct evidence for this. An alternative explanation for FtsQLB-mediated regulation of PG synthases can be supported based on a recent model that proposed two distinct populations for FtsW at midcell: an inactive population that is spatially tethered to treadmilling FtsZ filaments and an active population that instead localizes to sites of active PG synthesis (10). Presumably, FtsQLB would be needed to recruit FtsW to the treadmilling FtsZ filaments, so the FtsQLB “off/on” switch may involve initial sequestration of FtsW (and potentially other synthases, as well) followed by FtsN-stimulated release of FtsW when the septum is ready to be formed. This would likely involve breaking the interaction between FtsL and FtsW, so detailed insights into how these proteins interact are important for understanding the role that FtsQLB plays in cell division regulation.

In this chapter, I present *in vivo* mutational experiments that point to a likely FtsW-binding site within the cytoplasmic tail of FtsL. I also identify a set of mutations in FtsW that disrupt localization and may correspond to the FtsL-binding site. Furthermore, I show that mutations within multiple residues of the 4/5 cytoplasmic loop of FtsW disrupt some essential function without affecting localization to midcell. I then discuss on-going work to demonstrate *in vitro* binding between FtsL and FtsW in order to validate the identified interacting residues. Finally, I provide evidence that the length and flexibility of a short linker region connecting the TM and FtsW-binding regions of FtsL are important for proper cell division to occur, possibly by positioning the binding site relative to the membrane and modulating the signal transduction involved with activation of FtsW during the final stages of cell division.

4.3 Results and discussion

4.3.1 Identification of the FtsW-interaction site in FtsL

In order to identify residues within the N-terminal, cytoplasmic tail of FtsL that are involved with the interaction with FtsW, I performed *in vivo* complementation experiments using an alanine-scanning approach. Because FtsL is an essential cell division protein, I employed *E. coli* depletion strains MDG277 (38) and MDG254 (39) (obtained from Mark Gonzalez and Jon Beckwith) for these experiments. Strain MDG277 contains wild-type (WT) FtsL under P_{BAD} (arabinose-inducible, glucose-repressible) control on the chromosome. Strain MDG254 is similar to MDG277 except that WT FtsL is under P_{BAD} control on a plasmid, and an extra copy of FtsW is present within the chromosome as a GFP fusion (GFP-FtsW) under isopropyl β -D-1-thiogalactoside (IPTG) control by a P_{trc} promoter. I transformed these strains with either a plasmid containing WT FtsL (positive control), an empty gene site (negative control), or an FtsL mutant derivative (Table S4.1), each under P_{trc} control. These depletion strains enabled me to test if mutant variants of FtsL could properly support cell division in the absence of WT FtsL. Phase-contrast imaging of the resulting cells provided cell length distributions, which I used to classify each mutation based on extent of cell division defect as explained in the materials and methods section of this chapter. I also introduced select FtsL mutants into MDG254 to test if GFP-FtsW could localize to the septum in the presence of such mutations. Experiments were performed both at 37°C to mimic natural conditions as well as 42°C to stress cells and potentially reveal thermosensitive mutations. Classification of mutants was performed as described previously (45) (see materials and methods section for more details).

Previous research had shown that an FtsL truncation produced from its second methionine residue (Met16) could complement depletion of WT FtsL (39), so the first third of the cytoplasmic tail is unlikely to be important for FtsW binding (see Fig. 4.1a). Instead, I decided to focus on residues 15-38, which lead up to the approximate start of the FtsL TM region. Initially, I split this region into four blocks of six residues each

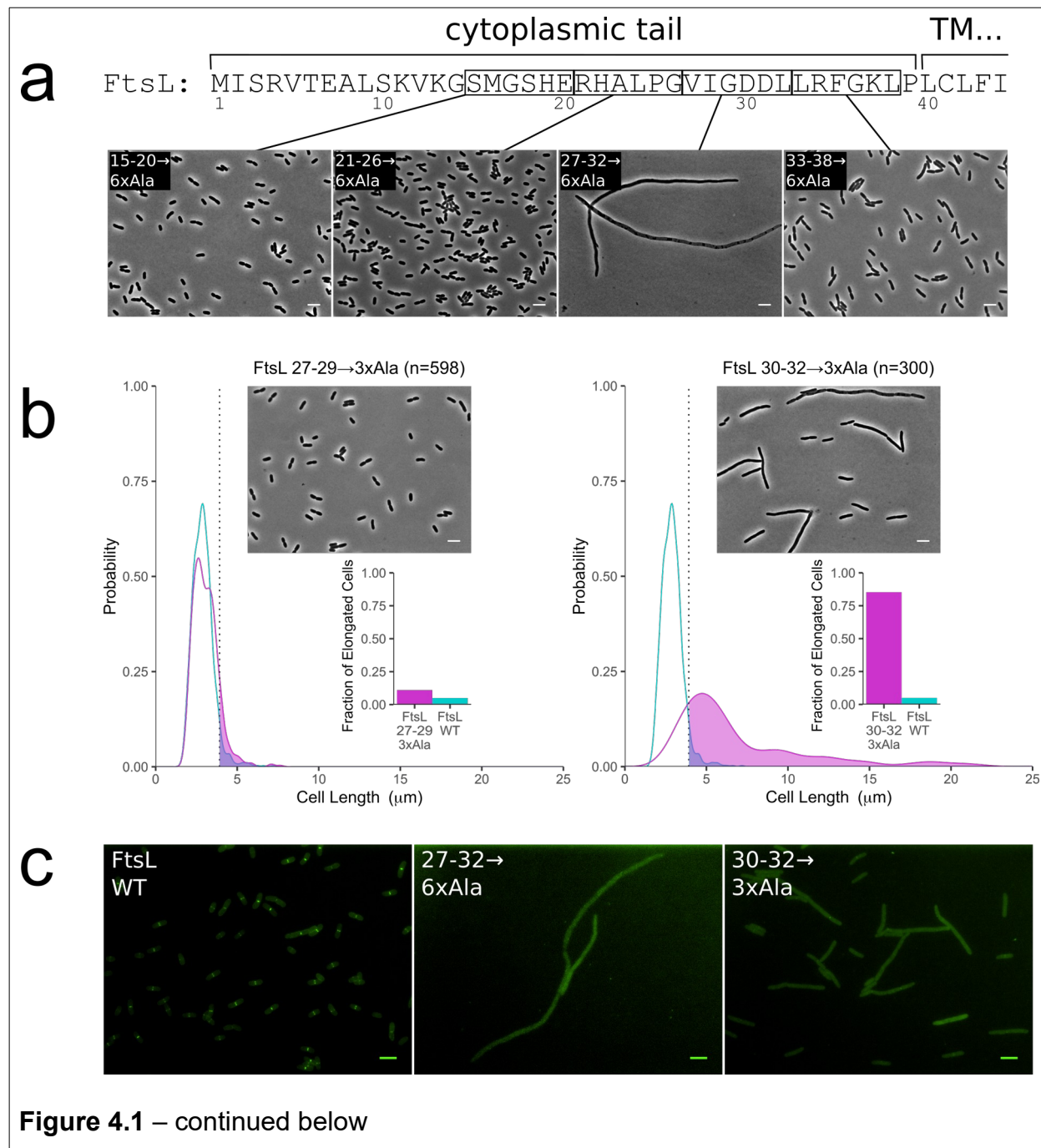


Figure 4.1. Mutations in the FtsL cytoplasmic tail disrupt cell division and FtsW localization. a) The essential region of the FtsL cytoplasmic tail was divided into six-residue blocks, which were mutated to alanine (6xAla) and tested for division defects at 37°C. b) Cell length distribution comparisons between WT cells (cyan; n=1059) and mutant cells (magenta). As an example, FtsL 30-32→3xAla displays 85% of cells that are longer than the 95th percentile in the WT distribution (shaded areas to the right of the dotted line; quantified in the bar graph), which corresponds to a "severe" elongation phenotype. c) Certain mutations affect localization of GFP-FtsW to the septum at 37°C. Representative GFP fluorescence images are included with a 5 μm scale bar.

(residues 15-20, 21-26, 27-32, and 33-38; Fig. 4.1a) and mutated the residues in each block to alanine (6xAla) in order to test for cell division defects in MDG277. The 6xAla mutations in the 15-20, 21-26, and 33-38 blocks in the FtsL cytoplasmic tail resulted in WT-like cells when grown at 37°C (Fig. 4.1a) and produced no defect to mild defects when grown at 42°C (cell length distributions included in Fig. S4.1 and S4.2; summarized in Table 4.1). Mutating residues 27-32 to 6xAla, however, resulted in completely filamentous cells even at 37°C, suggesting that this region is essential to cell division. Introduction of the 27-32→6xAla mutation into MDG254 cells resulted in a slightly less severe filamentation phenotype (potentially due to overall increased FtsW expression from the extra chromosomal copy of GFP-FtsW) but indicated a loss of GFP-FtsW localization to division sites (Fig. 4.1c). This supports this region as the potential FtsW-binding site in FtsL.

FtsL mutation	% of elongated cells at 37°C	% of elongated cells at 42°C
WT	5	5
15-20→6xAla	6	9
21-26→6xAla	8	16
27-32→6xAla	100	100
27-29→3xAla	11	18
30-32→3xAla	85	100
D30A	3	3
D30K	3	7
D31A	13	23
D31K	81	100
L32A	5	8
D30A/D31A	16	34
D30A/L32A	3	10
D31A/L32A	76	100
33-38→6xAla	13	22

Table 4.1. FtsL tail mutations. Summary of elongation defects for mutations within the potential FtsW-binding region of FtsL. Numbers correspond to bar graph values in Fig. S4.1 and S4.2.

To further narrow down which residues within the 27-32 region are important for division, I tested 3xAla mutations in residues 27-29 and 30-32. As shown in Fig. 4.1b and Table 4.1, the 27-29→3xAla mutation produced no division defect at 37°C and a mild defect at 42°C, whereas the 30-32→3xAla mutation resulted in a severe defect at 37°C and complete filamentation at 42°C. When tested in strain MDG254, the 30-32→3xAla mutation reproduced a similar elongation defect, but more importantly, GFP-FtsW foci were noticeably less frequent and less intense than the positive control containing WT FtsL (Fig. 4.1c). These data indicate that residues 30-32 are important in cell division, presumably participating in the interaction with FtsW; however, the somewhat milder phenotype of the 30-32→3xAla mutation compared to the 27-32→6xAla mutation (severe elongation vs. complete filamentation, respectively, at 37°C) suggests that residues 27-29 are somewhat involved in cell division as well, possibly via forming a portion of the FtsL-FtsW binding site.

I next performed individual alanine mutations within residues 30-32 to see if one or more specific residues are responsible for the division defect seen in the 3xAla mutation.

Initially, when I tested single alanine mutations (D30A, D31A, and L32A), the resulting phenotypes were generally WT-like, though a mild defect was seen for D31A at 42°C (summarized in Table 4.1; distributions in Fig. S4.1 and S4.2). This suggests that the FtsL-FtsW interaction is not primarily mediated by a single residue but instead by multiple individual interactions, as common in protein-protein binding. Still, in order to get as narrow of an interaction region as possible, I tested each possible pairwise mutation within the three residues. The D30A/D31A mutation resulted in mild (37°C) or moderate (42°C) defects, and the D30A/L32A mutation resulted in WT-like cells at both temperatures. The D31A/L32A mutation, on the other hand, resulted in severe elongation at 37°C and complete filamentation at 42°C. These data implicate Asp31 as the most important residue in this potential FtsW-binding region, though other residues (particularly Leu32) also play a role in this interaction.

Due to the presence of a pair of aspartate residues at positions 30 and 31 in FtsL, I rationalized that a salt bridge might be involved in the interaction between FtsL and FtsW. Mutation of these aspartate residues to alanine would break such a salt bridge, but the loss of that single interaction might not be enough to cause division defects, as suggested by the individual alanine mutations within residues 30-32. A charge-reversal mutation in Asp30 or Asp31, on the other hand, could potentially repel the corresponding positively charged region in FtsW, actively breaking the FtsL-FtsW interaction instead of just weakening it. A D30K mutation resulted in no discernible division defect at 37°C or 42°C, which supports the lack of defect seen by the D30A mutation. The D31K mutation, however, produced a severe elongation defect at 37°C and complete filamentation at 42°C (Table 4.1; distributions in Fig. S4.1 and S4.2). This is in line with the previous

finding that the D31A/L32A mutation disrupted division and the idea that the FtsL-FtsW interaction involves formation of a salt bridge, presumably between FtsL Asp31 and some positively charged residue in FtsW.

4.3.2 Identification of the FtsL-interaction site in FtsW

The likely site of interaction between FtsL and FtsW was limited to relatively few residues in FtsL (initially assumed to be between residues 15-38), but the same is not the case for FtsW. Presumably, the FtsL-FtsW interaction involves residues within the cytoplasm (though interactions between the TM regions could play a role), and FtsW has over 100 residues on the cytoplasmic side of the membrane (Fig. 4.2). Based on my identification of FtsL Asp31 as an important residue for the FtsL-FtsW interaction, I rationalized that one or more positively charged residues in FtsW are likely to play a role in this interaction; however, FtsW has over 20 arginine and lysine residues on the cytoplasmic face. Though FtsL could potentially bind to any of the cytoplasmic loops connecting TM domains, the N-terminal and C-terminal tails presented likely targets, so I started my search there.

Previous work had shown that FtsW could be expressed from residue Met31 and still support cell division (25), which indicates that residues 1-30 are not essential for function. In order to test if further truncations of both the N- and C-terminal tails of FtsW are also functional, I employed strain EC912 (32) (obtained from David Weiss), which has the WT copy of FtsW under P_{BAD} control on a plasmid. I transformed EC912 with either a plasmid containing GFP-FtsW (positive control), an empty gene site (negative control), or a GFP-FtsW mutant derivative. The use of a GFP fusion to FtsW enabled simultaneous testing for defects in cell division and FtsW localization due to specific

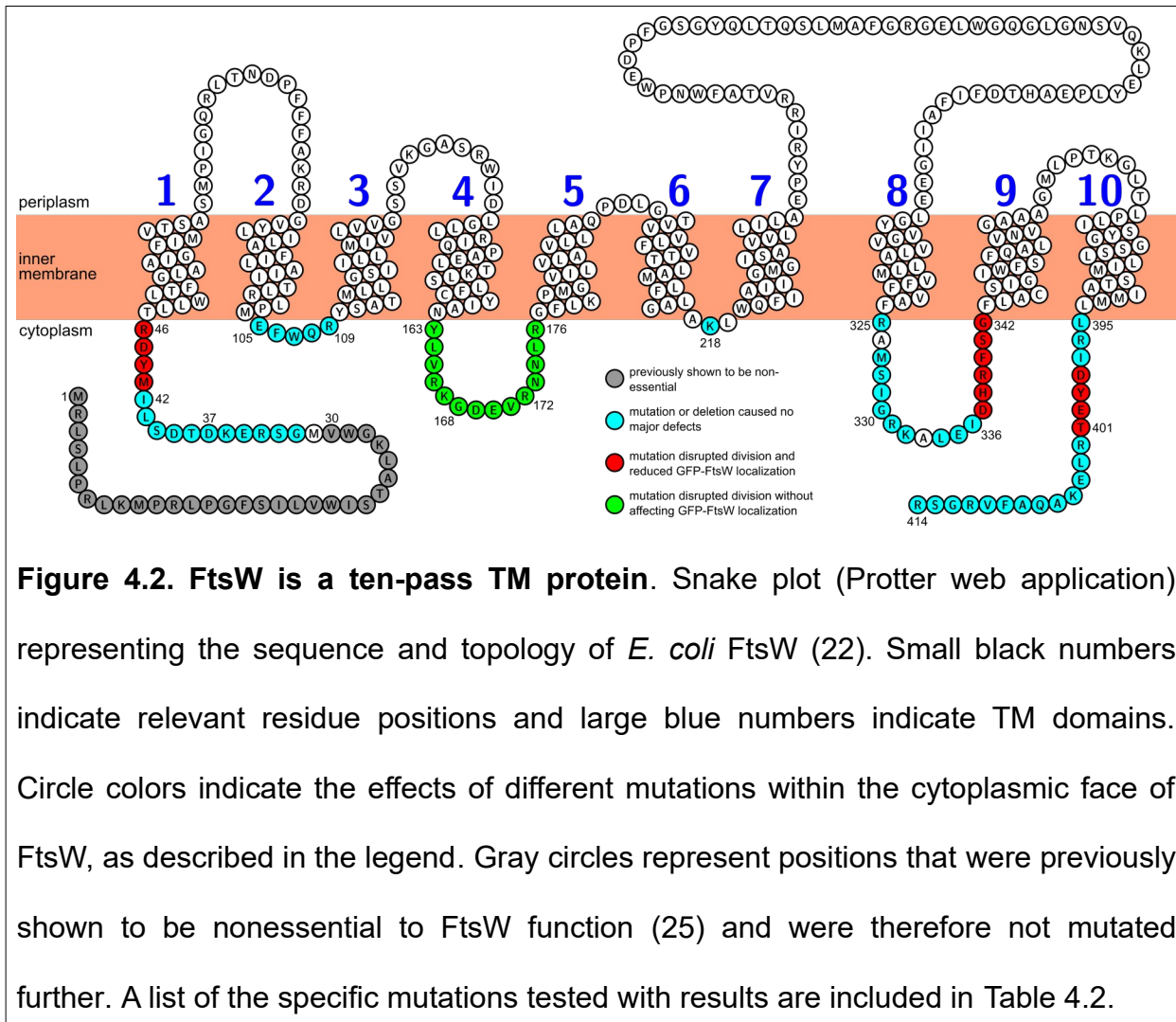


Figure 4.2. FtsW is a ten-pass TM protein. Snake plot (Protter web application) representing the sequence and topology of *E. coli* FtsW (22). Small black numbers indicate relevant residue positions and large blue numbers indicate TM domains. Circle colors indicate the effects of different mutations within the cytoplasmic face of FtsW, as described in the legend. Gray circles represent positions that were previously shown to be nonessential to FtsW function (25) and were therefore not mutated further. A list of the specific mutations tested with results are included in Table 4.2.

mutations in FtsW. For the following experiments, cells were grown at both 37°C and 42°C, but only results for the 37°C cells are reported since the phenotypes were generally indistinguishable between the two temperatures. Cell division and FtsW localization defects were categorized by eye since cell length distributions have not yet been determined nor localization frequencies calculated. Representative images for the mutant cells are included in Fig. S4.3.

Initially, I tested complete truncations of either tail of FtsW (Δ 1-46 and Δ 396-414), but, as summarized in Fig. 4.2 and Table 4.2, these mutations resulted in severe to

filamentous elongation defects as well as markedly reduced (though still occasional) GFP-FtsW localization at midcell. I then tested less severe truncations ($\Delta 1\text{-}42$ and $\Delta 402\text{-}414$), which both resulted in no noticeable defect in cell division and proper localization of GFP-FtsW at midcell. This suggested that loss of residues within the 43-46 or 396-401 regions caused the division defects seen in the full truncations of the

FtsW mutation	Division defect	FtsW localization
+ control	++	++
- control	--	--
$\Delta 1\text{-}42$	++	++
$\Delta 1\text{-}46$	--	-
32-37 \rightarrow 6xAla	++	++
38-42 \rightarrow 5xAla	++	++
43-44 \rightarrow 2xAla	++	++
45-46 \rightarrow 2xAla	+	+
43-46 \rightarrow 4xAla	--	-
R46E	++	++
105-109 \rightarrow 5xAla	+	++
R109E	++	+
163-165 \rightarrow 3xAla	-	++
166-167 \rightarrow 2xAla	--	++
163-168 \rightarrow 6xAla	--	++
R166E/K167E	-	++
169-171 \rightarrow 3xAla	--	++
172-176 \rightarrow 5xAla	-	++
R172E/R176E	+	++
K218E	++	++
325-330 \rightarrow 6xAla	+	++
R325E/R331E/K332E	++	+
331-336 \rightarrow 6xAla	++	++
337-339 \rightarrow 3xAla	++	++
R339E	++	++
340-342 \rightarrow 3xAla	++	+
337-342 \rightarrow 6xAla	--	-
395-397 \rightarrow 3xAla	++	+
R396E	++	++
398-399 \rightarrow 2xAla	++	++
400-401 \rightarrow 2xAla	++	++
396-401 \rightarrow 6xAla	--	-
398-401 \rightarrow 4xAla	--	-
$\Delta 396\text{-}414$	--	-
$\Delta 402\text{-}414$	++	++

Table 4.2. Summary of mutations made within the cytoplasmic face of FtsW.

“++” refers to no discernible defect. “+” refers to a small elongation defect or reduction in GFP foci frequency. “-” refers to a noteworthy elongation defect or the presence of only occasional GFP foci. “--” refers to a severe/filamentous elongation defect or the absence of GFP foci at division sites. Cells were grown at 37°C, and representative images are included in Fig. S4.3. Categorization was performed by eye since cell length distributions and foci frequencies have not yet been obtained. FtsW mutations are also summarized in Fig. 4.2.

tails, whereas the remainder of the tails are nonessential for cell division. I also tested various alanine substitutions in the 43-46 and 396-401 regions of full-length GFP-FtsW to see if they could replicate the defects seen in the complete tail truncations. The 4xAla mutations in residues 43-46 and 398-401 resulted in the formation of filamentous cells lacking GFP-FtsW foci (though occasional WT-like cells with GFP-FtsW foci could be seen in the 398-401→4xAla mutation). Interestingly, separate 2xAla substitutions in these regions resulted in WT-like cells with frequent GFP-FtsW foci, indicating that mutation of these smaller regions is not disruptive enough to cause division defects. Overall, these results suggest that large portions of both the N-terminal and C-terminal tails of FtsW are not important for FtsW localization or cell division in general. The juxtamembrane residues on both termini do seem to have some importance, though this could have more to do with proper membrane insertion or folding of FtsW instead of specifically localization to midcell by interaction with FtsL.

To identify potential FtsL-binding sites within the cytoplasmic inter-TM loops of FtsW, I took a brute-force approach and tested alanine mutations in each residue (either individually or in groups) for cell division defects *in vivo*. As summarized in Fig. 4.2 and Table 4.2, many of these mutations resulted in no discernible defect in cell division or GFP-FtsW localization. A 6xAla mutation in residues 337-342 of the 8/9 loop (the loop connecting TMDs 8 and 9), however, resulted in a mix of filamentous cells lacking GFP-FtsW foci and WT-like cells with occasional foci, similar to the 4xAla mutation in residues 398-401 of the C-terminal tail. 3xAla mutations in regions 337-339 and 340-342 resulted in WT-like cells with regular GFP-FtsW foci, suggesting multiple residues were involved in the defect caused by the 337-342→6xAla mutation.

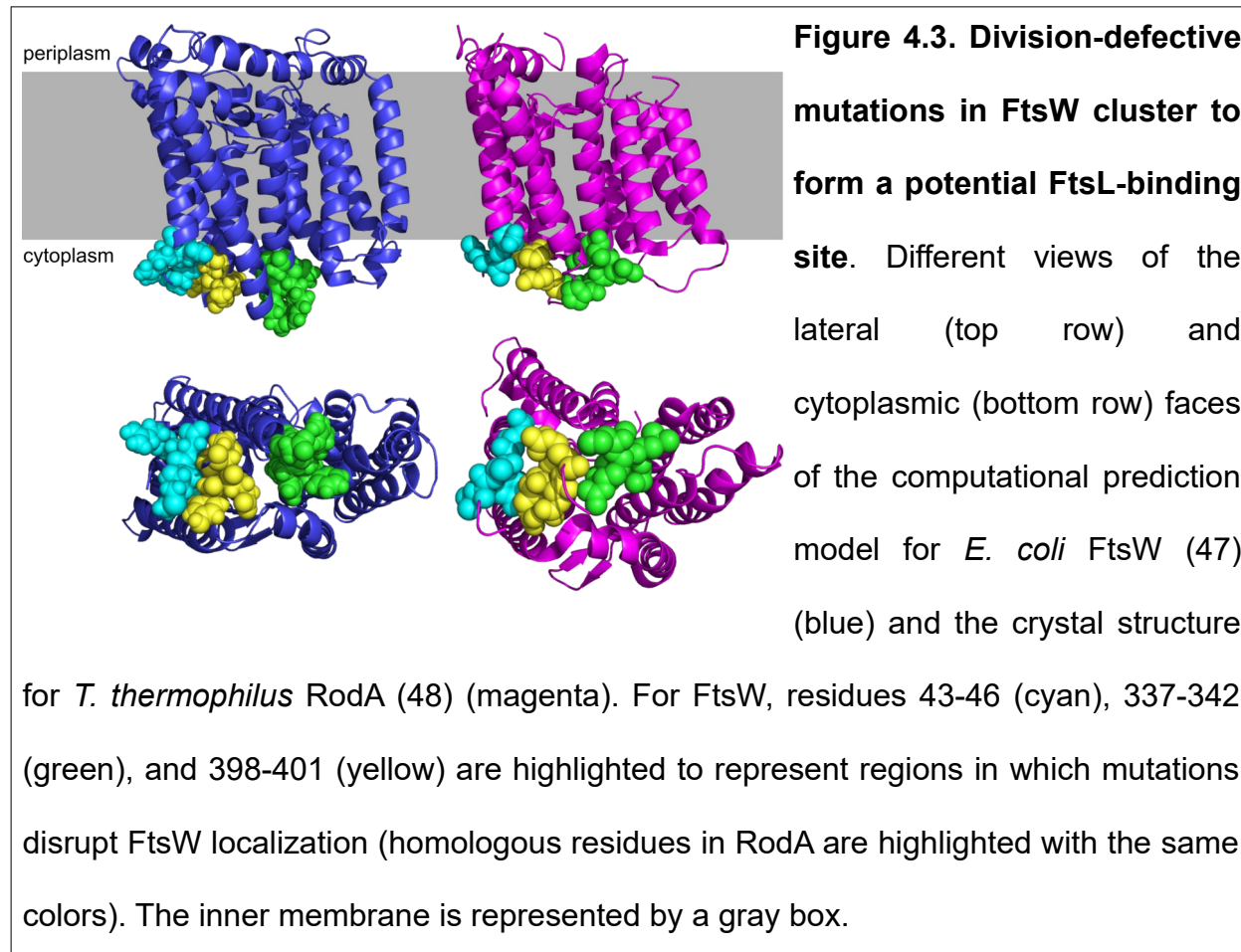
Interestingly, multiple alanine mutations throughout the 4/5 loop resulted in cell division defects (Fig. 4.2 and Table 4.2); however, in each case frequent GFP-FtsW foci could be seen throughout the elongated cells (Fig. S4.3). These results indicate that the 4/5 loop is essential for some function of FtsW (or possibly just proper folding of the protein), but this function does not impact localization of FtsW to midcell. One of these 4/5 loop mutations (169-171→3xAla) overlaps with a previously identified mutation (E170K) that was shown to disrupt cell division (46), though a clear mechanism was not proposed for the defect. Some potential functions for the 4/5 loop include interaction with other divisome components like FtsI, glycosyltransferase activity (would likely be indirect, since PG polymerization occurs in the periplasm), or possibly lipid II binding/flipping (though whether FtsW has lipid II flippase activity and if said activity is actually essential are controversial topics (15, 16, 26–28)). Further localization experiments and functional assays would be required to clarify a role for the 4/5 loop in FtsW function.

Since a charge reversal in Asp31 of the FtsL cytoplasmic tail produced a stronger elongation defect than the D31A mutation, I rationalized that charge-reversal mutations in FtsW may also produce more pronounced defects. To this end, I mutated each cytoplasmic arginine and lysine residue within positions 43-401 of FtsW to a glutamate residue (either individually or in groups of two or three). I assumed that positively charged residues within positions 1-42 and 402-414 were unlikely to be involved with FtsL binding since deletion of those regions produced no cell division defects, so no charge-reversal mutations were made within those regions. As summarized in Table 4.2, only the R166E/K167E double mutation produced a cell division defect, though GFP-

FtsW still localized to potential division sites. These residues are within the 4/5 loop, so the division defect is likely due to similar reasons as the alanine mutations throughout that loop.

Although no structures have been solved yet for FtsW, both a computational model for *E. coli* FtsW (in complex with the TM domain of FtsI) derived from co-evolutionary analysis and structure prediction (47) as well as a crystal structure for *Thermus thermophilus* RodA (48) (a homologue of FtsW) exist. To see if the FtsW-mislocalizing mutations from the complementation experiments (specifically, the alanine mutations in residues 43-46, 337-342, and 398-401) correspond to a potential FtsL-binding pocket, I plotted the residues on both the *E. coli* FtsW computational model and the *T. thermophilus* RodA crystal structure (using the homologous residues to the *E. coli* mutation sites). As shown in Fig. 4.3, the three identified regions cluster on the same half of the protein in both models. The two tail regions (positions 43-46 and 396-401) form a particularly close cluster that could represent an FtsL-binding region, whereas residues 337-342 in the 8/9 loop could support the structure of the binding site. Further experiments are needed to confirm these sites and to better narrow down which residues are most important, and I am working with other lab members on several different approaches to this end. First, computational modeling of the interaction between the FtsL cytoplasmic tail and FtsW should indicate if binding within the identified potential binding pocket (or elsewhere on the cytoplasmic face) is energetically favorable. Also, further analysis of *in vivo* mutations will potentially identify better combinations of residues that disrupt FtsW localization and support the computational modeling. Finally, identification of mutations in FtsW that suppress the

division-impairing mutations within the putative FtsW-binding site of FtsL (residues 27–32, in particular) could identify important residues for the FtsL-FtsW interaction, though my initial attempts to identify suppressors of FtsL D31K and 30–32→3xAla have not yet produced results.



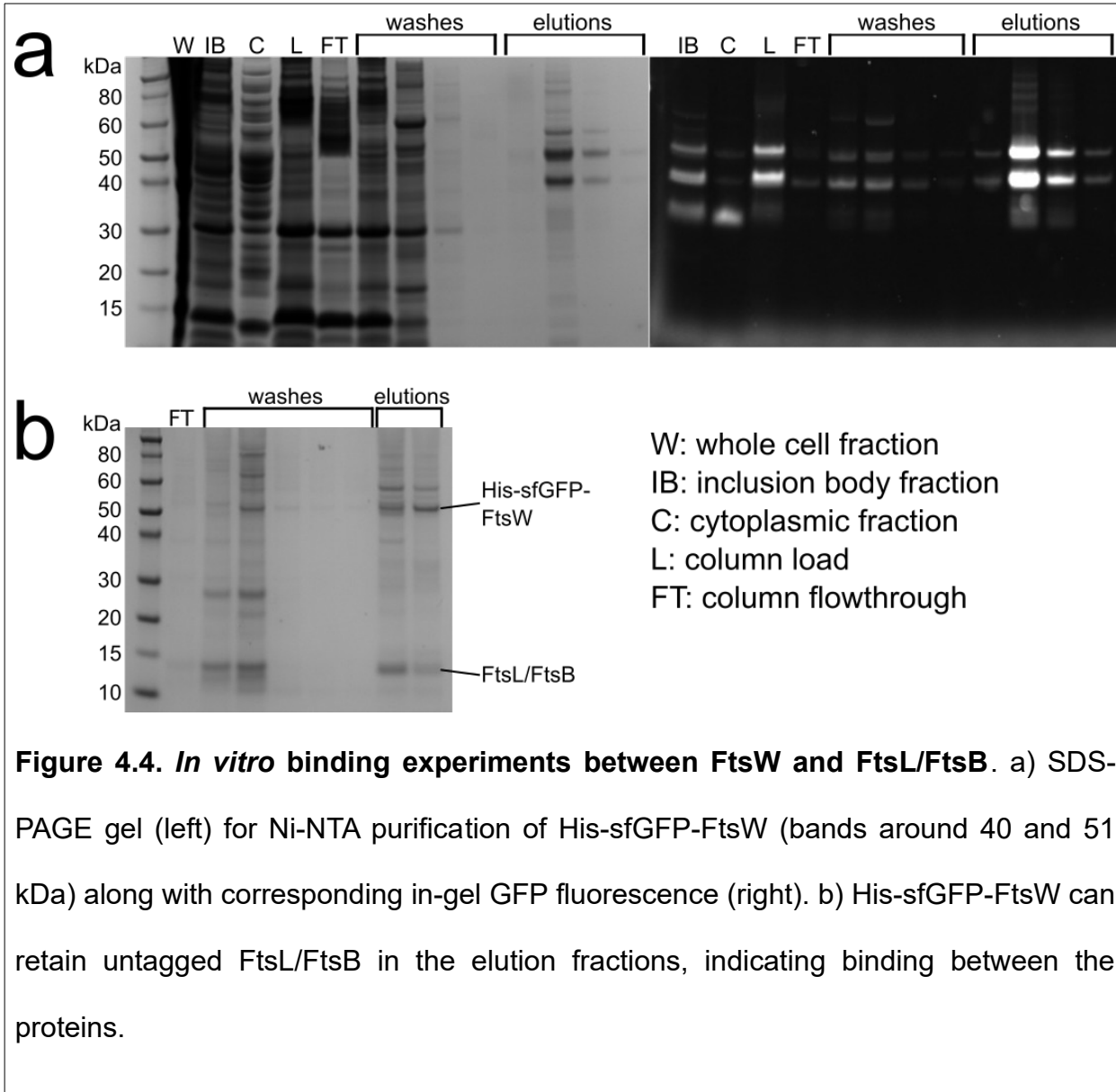
4.3.3 In vitro binding between FtsLB and FtsW

In order to confirm the identified binding sites for both FtsL and FtsW, I am currently developing experiments to demonstrate *in vitro* binding between purified FtsLB and FtsW. FtsW is notoriously difficult to handle *in vitro*, but some success has been achieved for experiments that require relatively small quantities of the protein (26–28, 31, 33, 44). For my research, I decided to optimize my own protocol and improve upon

prior methods to obtain larger quantities of FtsW. Currently I have established various expression and purification conditions for FtsW, which along with my methods for FtsLB production (covered in detail in Appendix 1), have enabled initial binding experiments between purified protein. These experiments are still ongoing and are likely the largest set of unfinished work that needs to be completed before I can submit this chapter for publication.

In order to express FtsW at levels appropriate for visualization on SDS-PAGE, I tested various constructs and expression conditions. In short, I tested FtsW with or without co-expression of FtsI, alone or with N- or C-terminal fusions to different GFP variants, as the WT sequence or as a codon-optimized sequence, via normal IPTG induction or autoinduction, and in various *E. coli* expression strains at various temperatures. The final expression conditions I settled on were co-expression of FtsI and His-sfGFP-FtsW (codon-optimized) in C43 cells via normal induction (1mM IPTG) overnight at 37°C, as explained in more detail in the materials and methods section. Isolation of the membrane fraction resulted in the identification of two prominent bands (as seen by in-gel GFP fluorescence) around 40 and 51 kDa, which I have been able to purify (Fig. 4.4). The predicted molecular weight of the His-sfGFP-FtsW construct is closer to 76 kDa; however, FtsW is known to run abnormally low on SDS-PAGE (46), so the upper band may correspond to the full-length construct, whereas the lower band may be a truncated product.

For the *in vitro* binding experiments, I purified His-sfGFP-FtsW and His-FtsL/FtsB separately via Ni-NTA resin. I then removed the His-tag from either sfGFP-FtsW or FtsL via TEV cleavage, combined the proteins in a 1:1 molar ratio, and reran the mixture



over Ni-NTA to determine retention of the untagged protein in the elution fractions (presumably due to interaction with the tagged protein). The relatively low levels of FtsW obtained from the purification have precluded a clear demonstration of FtsL-FtsW binding on Ni-NTA; however, initial results suggest that untagged WT-FtsL is retained in the elution fraction when mixed with His-sfGFP-FtsW (Fig. 4.4). Further experiments are

needed to demonstrate a clear binding as well as a lack of binding for different mutant versions of FtsL (namely, D31K and 27-32→6xAla).

An alternative approach to demonstrating on-column binding between FtsL and FtsW is to co-express FtsW with FtsLB and then purify all three proteins together. In this case, only one component would be His-tagged, and the other would contain a FLAG3-tag to enable identification via western blot. I have been favoring this approach as of late because it removes the need for initial purification of the separate proteins and the cleavage of the His tag, which greatly reduces the overall time for the procedure. The FtsL-FtsW interaction is also more likely to form in the native membrane environment compared to within detergent micelles, so this method may also give better results than the separate purification method. To this end, I have constructed a Duet vector (pSJC297) containing a polycistronic FtsB/FLAG3-FtsL in one multiple cloning site (MCS1) and His-sfGFP-FtsW in MCS2. Currently, I am in the process of optimizing expression and purification conditions for pSJC297, but initial expression tests (data not shown) have indicated that expression of FtsL and FtsB is much lower from this vector when compared to the normal method of expression (presented in Appendix 1). His-sfGFP-FtsW is still expressed to roughly similar levels, so the current method may be sufficient to detect protein in the Ni-NTA elution fractions via western blot or in-gel fluorescence for FLAG3-FtsL or His-sfGFP-FtsW, respectively. Conditions for maximum interaction between FtsB/FLAG3-FtsL and His-sfGFP-FtsW also need to be optimized, and specifically I plan to test different NaCl levels during purification, as the FtsL-FtsW interaction may involve formation of a salt bridge that could be disrupted by the high NaCl levels used in standard purification procedures (300mM).

4.3.4 The length and flexibility of an FtsL linker region may impact the interaction with FtsW

As shown earlier, the 33-38→6xAla mutation in the N-terminal, cytoplasmic tail of FtsL resulted in a mild elongation defect at 42°C (Table 4.1). Since these residues directly follow the presumed FtsW-binding site around residues 27-32, it is possible they also form a portion of this binding site and the mutation therefore could partially disrupt the FtsW interaction. Another potential role for these residues, however, could be in the proper positioning of the FtsW-binding site relative to the membrane. Presumably, if the binding site were too close to the membrane, then it would be unable to reach the appropriate site in FtsW, which would result in loss of FtsW localization and disruption of cell division. Therefore, some minimum number of residues between the TM and FtsW-binding regions of FtsL is likely needed, and deletions in this region would be expected to cause cell division defects.

To test if the length of this potential FtsL cytoplasmic linker region is important for cell division, I deleted residues 33-38 as well as 33-35 and 36-38 separately and compared the resulting *in vivo* phenotypes to alanine substitutions at those positions. A summary of the mutation phenotypes is included in Table 4.3, and the corresponding cell length distribution analyses are in Fig. S4.1 and S4.2. Deletion of all six residues resulted in a severe elongation phenotype at 37°C and complete filamentation at 42°C. Deletion of the smaller regions resulted in less severe phenotypes, with the Δ33-35 mutant cells showing mild to moderate elongation defects (at 37°C and 42°C, respectively) and the Δ36-38 cells showing moderate to severe elongation defects. These division defects are likely due more to the loss of length in the region than the loss of the specific residue

FtsL mutation	% of elongated cells – 37°C	% of elongated cells – 42°C
WT	5	5
33-35→3xAla	9	9
Δ33-35	19	27
36-38→3xAla	19	24
Δ36-38	33	51
33-38→6xAla	13	22
Δ33-38	90	100
33-38→GGSGGS	28	45
33-38→6xPro	100	100
P39A	37	24
P39N	11	13
L38-GGSGGS-P39	42	68
L38-6xPro-P39	81	100

Table 4.3. FtsL linker mutations.

Summary of elongation defects for mutations within the linker region of the FtsL cytoplasmic tail. Numbers correspond to bar graph values in Fig. S4.1 and S4.2.

identities, seeing as the corresponding alanine substitutions resulted in mild elongation defects at worst (even at 42°C). To perform the reverse experiment, I increased the length of the FtsL linker by introducing either a flexible six-residue sequence (GGSGGS) or a rigid six-residue sequence (6xPro) between residues L38 and P39. The L38-GGSGGS-P39 mutation resulted in moderate to severe elongation defects (at 37°C and 42°C, respectively), whereas the L38-6xPro-P39 mutation resulted in severe to completely filamentous elongation defects. This could be due to the length increase of the linker region, but an alternative explanation is that the insertions disrupted division by affecting the overall flexibility of the region, as discussed more in the next paragraphs. These results, however, overall indicate that the length of this linker region is important, likely due (at least in part) to proper positioning of the FtsW-binding site relative to the TM domain.

Aside from positioning the FtsW-binding site, another potential role for this FtsL linker region is to modulate FtsLB-mediated signal transduction during division. If the FtsN-initiated signal that triggers the final events of cell division involves cross-talk between FtsLB and FtsW, then the signal would likely need to travel from the

periplasmic region of FtsLB (the essential domain of FtsN is located in the periplasm, so the signal likely originates there (42, 49)), through the TM region, and finally to the FtsL-FtsW interaction site in the cytoplasm. In this scenario, the relative flexibility of the intervening residues (positions 33-39) between the TM domain and FtsW-binding site of FtsL could be an important factor for effective signal transduction. This mechanism is reminiscent of those seen in other transmembrane signal transducers, and in particular, it has been shown that the relative flexibility/helicity of the N-terminal juxtamembrane regions of various human integrin receptors correlates to their activation (50, 51). This modulation of activity was accomplished either by mutation of a conserved proline residue (51) or by introduction of a flexible sequence (50) preceding the TM regions of specific integrins. The mutation in the proline residue was suggested to result in increased local helicity (proline is a helix breaker), which lead to increased coupling between the N-terminal domain and the TM region. Flexibility may play a similar role in the juxtamembrane linker region of FtsL, seeing as an N-terminal proline cap is also present at position 39 and insertion of the GGSGGS flexible sequence impaired division.

To further investigate the role of flexibility in this FtsL linker region, I designed mutations to modulate the relatively helicity there (Table 4.3). Although, residue P39 is not highly conserved within proteobacteria, I tested mutations at that site due to the potential similarity to the conserved proline TM cap seen in certain integrins (51). An FtsL P39N mutation resulted in largely WT-like cells, whereas a P39A mutation gave a mix of mostly WT-like cells with subpopulations of elongated cells (Fig. S4.1 and S4.2). Like proline, asparagine is a common N-terminal cap or initiating residue for TM helices

(52), so either residue could potentially support a helical breakage between the linker and TM regions. Alanine, on the other hand, is a typical helix-forming residue, so the P39A mutation could increase the helical propensity of that region and disrupt proper signal transduction during division. Why the P39A mutation manifested as a mixed population of WT-like and elongated cells is unclear, though it could have something to do with a sort of all-or-none stimulation of cell division. In other words, cells that fail to divide at the proper time get locked into a division-impaired state which leads to subpopulations of elongated cells. The mechanisms behind such an effect are guesswork at this point, though they could involve locking FtsQLB and therefore FtsWI into the “off” state.

To further modify flexibility of the FtsL linker region, I tested more mutations within residues 33-38 for *in vivo* effects. Along with the 33-38→6xAla mutation described earlier (resulted in a mild elongation defect only at 42°C), I also made mutations to either increase flexibility (GGSGGS) or decrease flexibility (6xPro) within that region. The 33-38→GGSGGS mutation resulted in a mild elongation defect at 37°C and a moderate elongation defect at 42°C, whereas the 33-38→6xPro mutation resulted in complete filamentation at both temperatures (see Table 4.3 and Fig. S4.1 and S4.2). Along with the P39A, L38-GGSGGS-P39, and L38-6xPro-P39 mutations described earlier, these results suggest that a proper level of flexibility is needed within this FtsL linker connecting the FtsW-binding site to the TM region. Exactly how this relates to the function of FtsL mechanistically is unclear, but it may be due to a defect in signal transduction from the periplasmic domain, through the TM region, and on to the FtsW-binding site in the cytoplasm.

4.4 Conclusions

Proper assembly of the *E. coli* divisome requires an essential interaction between the N-terminal, cytoplasmic tail of FtsL and the cytoplasmic face of FtsW (39). Without this interaction, FtsW and FtsL are unable to localize to the division site and synthesis of the PG septum cannot occur. Despite the importance of this interaction, little work had been previously devoted to better understanding the specific residues involved in both FtsL and FtsW.

In this chapter, I explained my research to better map out potential interaction sites between FtsL and FtsW. I performed mutagenesis on the essential portion of the cytoplasmic FtsL tail to identify residues necessary for cell division and, in particular, for localization of GFP-FtsW to the division site. I identified a six-residue region (positions 27-32) in which mutations reduced FtsW localization, resulting in elongated cells. Individual mutations were performed in this region, and Asp31 was identified as a particularly important residue for this interaction, as a D31K charge-reversal mutation was capable of disrupting cell division by itself. I identified several potential regions on the cytoplasmic face of FtsW that resulted in cell division defects corresponding to reduced GFP-FtsW localization to midcell. These regions contain positively charged residues that have the potential to interact with Asp31 in FtsL; however, I was unable to identify specific charge-reversal mutations in FtsW that disrupted its localization to midcell. The identified regions roughly cluster to the same half of the FtsW cytoplasmic face (based on a computational prediction model for the *E. coli* FtsW structure as well as the crystal structure of the homologous RodA from *T. thermophilus*), and the regions located within the N- and C-terminal tails, in particular, form a cluster that could

correspond to the FtsL-binding site. Whether these regions actually interact with FtsL remains to be seen, and *in vitro* binding experiments to address this question are still underway.

Finally, I also provided evidence that the flexibility and length of the linker region between the putative FtsW-binding site and the TM region of FtsL are important for proper cell division. This raises the interesting question of what role such properties play within the FtsL cytoplasmic tail. Assuming the only function for the tail is to recruit FtsW to the division site, mutations outside the binding site would not be expected to interfere with cell division unless they impact the structure of the binding site or position it in such a way that it is unable to reach FtsW (as could be the case for the deletion mutations in the linker). Although mutations within this linker region could indeed have indirect effects on FtsW recruitment, another possibility is that they impact some other function of the FtsL cytoplasmic tail. Recent developments in our understanding of FtsLB function within the divisome have led to models in which FtsQLB is involved in the FtsN-stimulated signal transduction that triggers the completion of cell division. Although the mechanisms behind this signaling are still unclear, these models propose that FtsQLB plays a role either in inhibition of PG synthases or in their sequestration from sites of active PG synthesis. FtsLB and FtsQ have already been demonstrated to inhibit PBP1b GTase activity and FtsI TPase activity *in vitro* (44), and the direct interaction between FtsL and FtsW suggests that FtsLB may also regulate FtsW in a similar manner. Similarly, the FtsL-FtsW interaction may prevent FtsW from reaching sites of active PG synthesis by spatially tethering it to treadmilling FtsZ filaments until cell division is ready to be completed (10). In either case, FtsN would trigger the FtsQLB “off” to “on” switch

in the periplasm, and this signal would need to be sent through the TM and linker regions of FtsL and to the FtsL-FtsW interaction site in the cytoplasm. For such signal transduction to occur, an appropriate level of flexibility throughout the FtsLB complex (including the FtsL cytoplasmic linker region) would be required, which is a concept we addressed in our previous work relating to a flexible glycine-rich linker in FtsB (45) as well as a marginally stable coiled-coil domain in FtsLB (Chapter 3). Theoretically, any mutation affecting the relative flexibility of FtsLB could offset the fine tuning required for proper signal transduction and therefore disrupt cell division.

4.5 Materials and methods

4.5.1 Plasmid cloning

For the *in vivo* complementation experiments, mutant variants of FtsL or FtsW were cloned via standard QuikChange mutagenesis or inverse PCR into pMDG29 (39) (FLAG3-FtsL) or pSJC214 (GFP-FtsW), respectively. For the *in vitro* binding experiments, constructs were ligated into two multiple cloning sites (MCS) of a modified pETDuet-1 vector at restriction sites Ncol/HindIII (MCS1) and Ndel/Xhol (MCS2). Codon-optimized FtsW was amplified from a gene fragment (Twist Bioscience). All other constructs were amplified from various lab plasmids. Further plasmid editing was performed via standard Gibson assembly (53) and QuikChange mutagenesis.

4.5.2 Bacterial strains, plasmids, and media for *in vivo* experiments

The phenotypic analyses were performed using depletion strains MDG277 (38) or MDG254 (39) for FtsL and EC912 (32) for FtsW. For all experiments described,

bacterial cells were grown in LB medium supplemented with 100 µg/mL spectinomycin (Dot Scientific) or 100 µg/mL ampicillin and the appropriate carbon source. Medium was supplemented with 0.2% (w/v) L-arabinose (Sigma) or 0.2% (w/v) D-glucose (Sigma) to induce or repress, respectively, the expression of chromosomal copies of the WT genes regulated by the P_{BAD} promoter. 20 µM IPTG was added to the media to induce the expression of mutant genes regulated by the P_{trc} promoter in the plasmid.

4.5.3 Depletion strain experiments

The protocol for the depletion strain experiments was adapted from prior work (32, 38). In short, a mutated copy of FtsL or FtsW was transformed into its respective depletion strain. Strains were grown overnight at 37°C on an LB plate supplemented with arabinose and appropriate antibiotics. A single colony from the plate was grown overnight at 37°C in 3 mL of LB medium supplemented with arabinose and antibiotic. The overnight culture was then diluted 1:100 into fresh LB medium containing the same supplements and grown to an OD₆₀₀ of ~0.3. An aliquot of 1 mL of culture was washed twice with LB medium lacking any sugar and then diluted 1:100 into 3 mL of fresh LB medium supplemented with glucose, IPTG, and antibiotic to induce expression of the mutated gene and to repress the WT gene. The cells were then grown at 37 or 42°C for 3.5 h (MDG277 and MDG254) or 4.5 h (EC912), which is the approximate time necessary to deplete the cells of the WT protein. The cells were then placed on ice to stop growth before imaging. Depletion strains were provided with a copy of their respective WT protein in the plasmid for a positive control. Similarly, depletion strains with no protein in the plasmid (empty vector) were tested as negative controls.

4.5.4 Microscopy and cell length measurements

10 µl of cell samples were mounted on a number 1.5, 24 X 50 mm (0.16 – 0.19 mm thickness) cover glass slide (Fisher or VWR). Cells were cushioned with a 3% (w/v) agarose gel pad to restrict the movement of the live cells. Cells were optically imaged using a Nikon Eclipse Ti inverted microscope equipped with crossed polarizers and a Photometrics CoolSNAP HQ2 CCD camera using a Nikon X100 oil objective lens. Phase-contrast images of bacterial cells were recorded with a 50 ms exposure time using Nikon NIS Elements software. GFP images were recorded with a 3-5 s exposure time. Multiple snapshots were collected for each experiment. All images were analyzed to measure the cell length in Oufti (54) using one single optimized parameter set and manual verification. Comparison of cell length distributions was accomplished using the same classification scheme as previously described (45). Cells with lengths longer than the 95% percentile in the WT length distribution were considered “elongated”. Length distributions for the various mutations were compared to this threshold, and phenotypes with <15% of total cells being elongated were classified as “WT-like” or “no defect,” >15% as “mild,” >25% as “intermediate,” >50% as “severe,” and “filamentous” when complete filamentation occurred. Completely filamentous mutations resulted in a low cell count which precluded cell length distribution analysis.

4.5.5 Protein expression and purification for on-column binding

For FtsLB expression, plasmids were transformed into BL21(DE3) cells (NEB) and plated overnight at 37°C on LB agar with appropriate antibiotics. Cells were washed off the plates with 1-2 mL LB broth and inoculated into 1 L of ZYP-5052 autoinduction medium as described (55) and grown at 37°C until reaching an OD₆₀₀ of ~0.8, after

which they were incubated overnight at 25°C. For FtsW expression, plasmids were transformed into C43(DE3) cells (Lucigen) and plated overnight at 37°C on LB agar with appropriate antibiotics. Cells were washed off the plates with 1-2 mL LB broth and inoculated into 400 mL of LB media plus appropriate antibiotics and grown at 37°C until reaching an OD₆₀₀ of ~0.8, after which they were induced with 1 mM IPTG overnight at 37°C. Following expression, cells were pelleted, resuspended in cell wash buffer (100 mM NaCl + 10 mM HEPES pH 8.0), pelleted again, flash frozen, and stored at -80°C for future use. The cells were then lysed by sonication in 10 mL/g lysis buffer (50 mM NaCl, 50 mM HEPES pH 8.0) supplemented with 0.5 mg/mL lysozyme, 5 mM β-mercaptoethanol (βME), 1 mM phenylmethylsulfonyl fluoride, 1 mM EDTA, and a protease inhibitor cocktail providing (final concentrations) 8 μM leupeptin (Peptides International), 11.2 μM E-64 (Peptides International), 0.32 μM aprotinin (ProSpec), and 0.32 mM 4-(2-aminoethyl)benzenesulfonyl fluoride (Gold BioTechnology). The inclusion body fraction was separated by centrifugation at 10,000 x g for 20 min, followed by ultracentrifugation of the supernatant at 180,000 x g for 30 min to isolate the cell membranes. For FtsLB constructs, the protein was then extracted from the membrane fraction with lysis buffer supplemented with 18 mM n-decyl-β-D-maltopyranoside (DM; Anatrace) and 5 mM βME, rocking at room temperature overnight. For FtsW constructs, the protein was extracted from the membrane fraction with 20 mM HEPES pH 8.0, 500 mM NaCl, 20% glycerol, 5 mM βME, and 36 mM DM, rocking at room temperature overnight. Non-resuspended debris was separated from the solubilized protein via centrifugation at 10,000 x g for 20 min. The supernatant was added to Ni-NTA-agarose resin (Qiagen) and rocked for 2 h at 4°C before performing gravity-flow purification.

Purification was performed by running ten column volumes of Ni wash buffer (300 mM NaCl, 25 mM HEPES pH 8.0, 50 mM imidazole, 1 mM βME) supplemented with 0.51 mM n-dodecyl-β-D-maltopyranoside (DDM; Avanti Polar Lipids) (1 mM for FtsW constructs) and ten column volumes of elution buffer (300 mM NaCl, 25 mM HEPES pH 8.0, 300 mM imidazole, 1 mM βME) also supplemented with 0.51 mM DDM (1 mM for FtsW). Wash and elution buffers for FtsW constructs also contained 10% glycerol. Protein purity was assessed via SDS-PAGE (Invitrogen). To remove His-tags from FtsLB, elution fractions were combined with approximately 1:50 recombinant (His-tagged) tobacco etch virus (rTEV) protease and dialyzed overnight at room temperature in TEV dialysis buffer (25 mM Tris-HCl pH 7.5, 0.5 mM EDTA, 100 mM NaCl) supplemented with 0.5 mM tris(2-carboxyethyl)phosphine (TCEP) and 0.17 mM DDM (approximately the critical micelle concentration to prevent detergent loss during dialysis). Another Ni-NTA column was used as described above to remove rTEV and non-cleaved protein.

4.5.6 On-column binding experiments

Purified, His-tagged sfGFP-FtsW and untagged FtsL/FtsB were combined in ~1:1 molar ratios and dialyzed overnight at room temperature into 50 mM HEPES pH 8.0, 100 mM NaCl, 10% glycerol, 1 mM βME, and 0.17 mM DDM (to prevent detergent loss). The dialyzed protein was added to Ni-NTA resin equilibrated in the dialysis buffer (with 1 mM DDM) and left rocking at 4°C to batch bind for >2 h. The column was washed and eluted similar to explained above, and the resulting fractions were analyzed via SDS-PAGE for presence of FtsL/FtsB.

4.6 Supplemental information

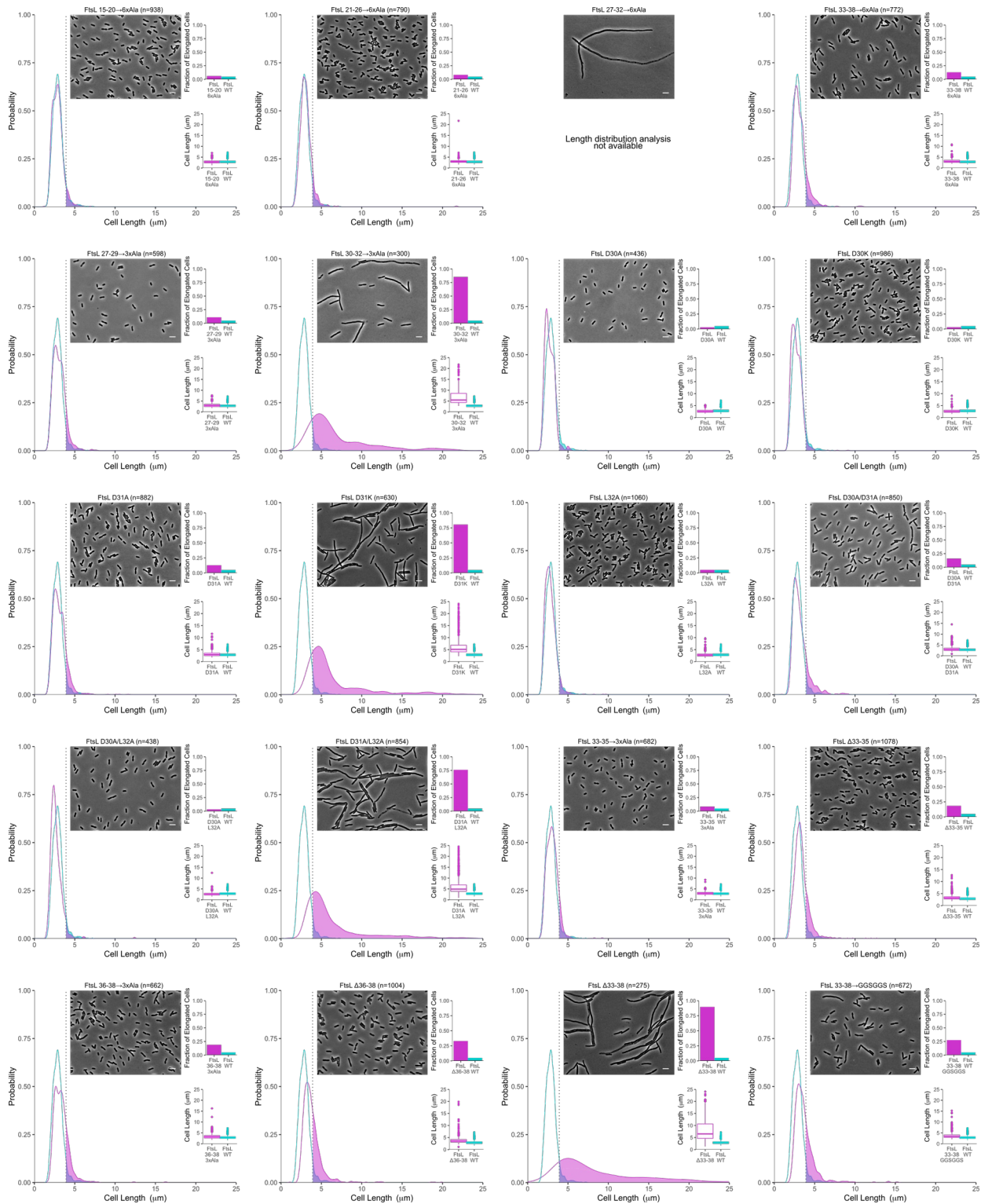


Figure S4.1 – continued below

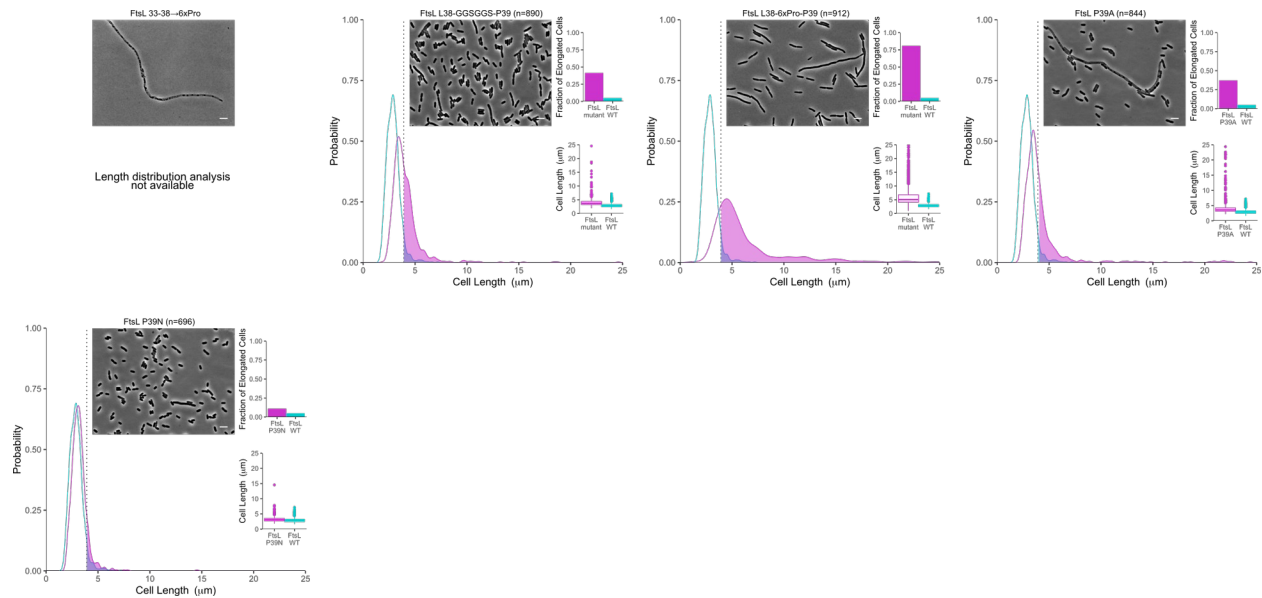


Figure S4.1. FtsL cytoplasmic mutations at 37°C. Cell length distribution comparisons (represented by a kernel density estimation and a box plot) between WT cells (cyan; n=1059) and those containing mutations (magenta) in the N-terminal, cytoplasmic tail of FtsL. As an example, FtsL D31K displays 81% of cells that are longer than the 95th percentile in the WT distribution (shaded areas to the right of the dotted line; quantified in the bar graph), which corresponds to a "severe" elongation phenotype. Mutations causing complete filamentation also resulted in low cell density, which precluded quantification of cell length distributions (fraction of elongated cells considered to be 100%). Representative phase-contrast images are included with 5 μm scale bar.

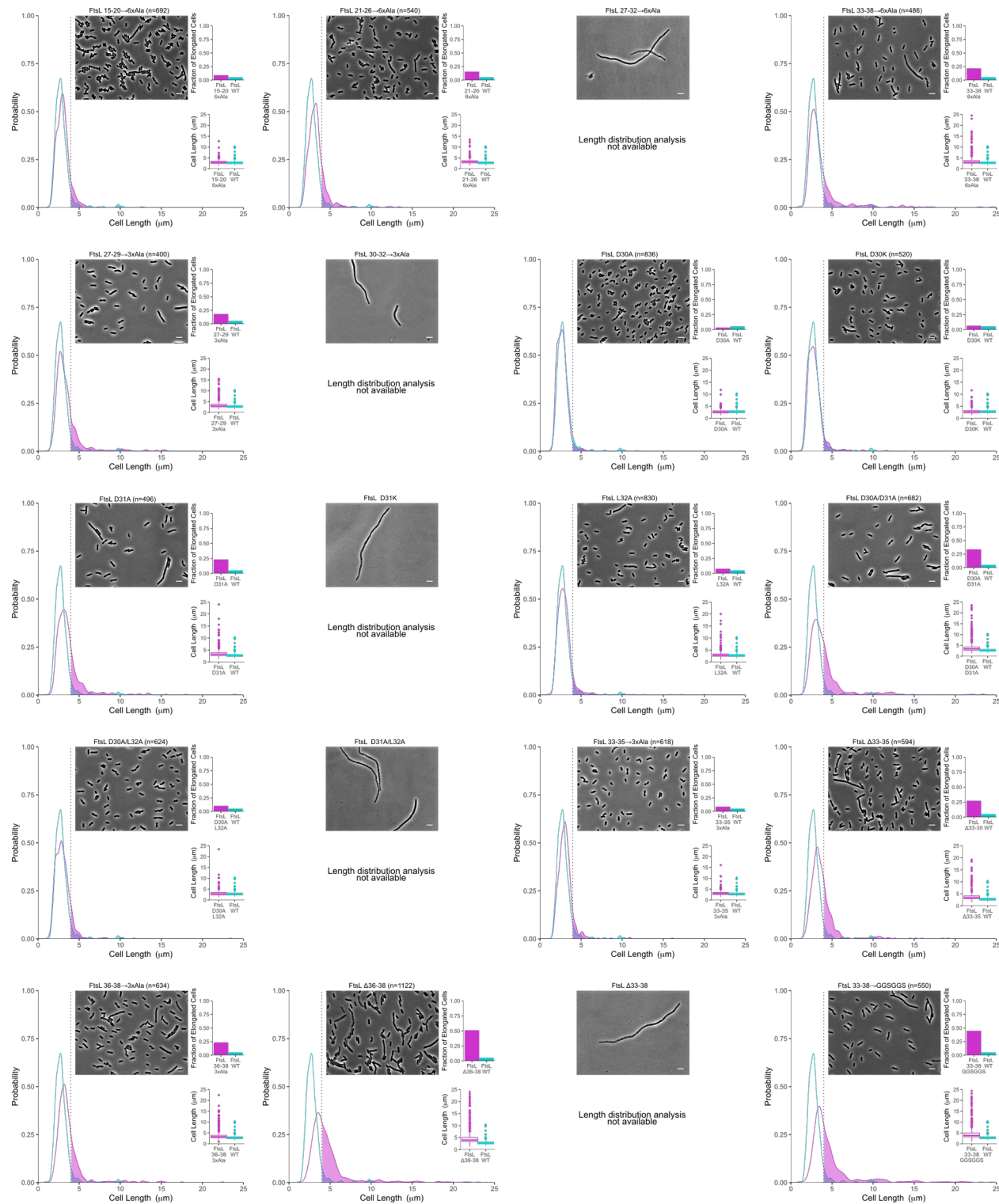


Figure S4.2 – continued below

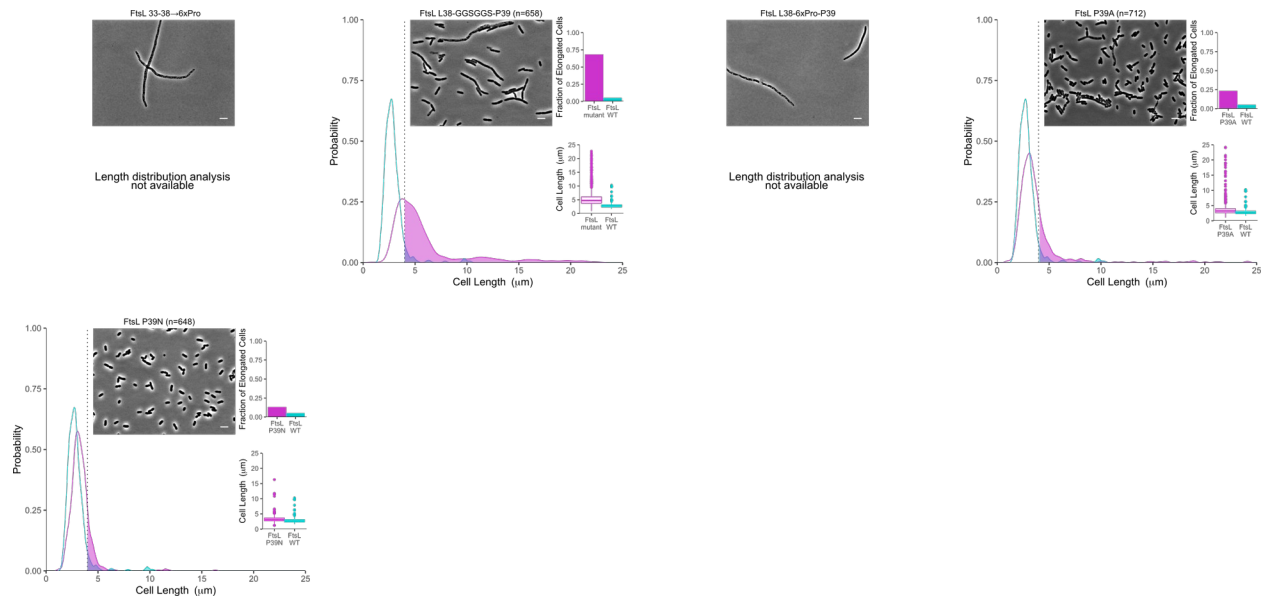


Figure S4.2. FtsL cytoplasmic mutations at 42°C. Cell length distribution comparisons (represented by a kernel density estimation and a box plot) between WT cells (cyan; n=404) and those containing mutations (magenta) in the N-terminal, cytoplasmic tail of FtsL. As an example, FtsL D31A displays 23% of cells that are longer than the 95th percentile in the WT distribution (shaded areas to the right of the dotted line; quantified in the bar graph), which corresponds to a "mild" elongation phenotype. Mutations causing complete filamentation also resulted in low cell density, which precluded quantification of cell length distributions (fraction of elongated cells considered to be 100%). Representative phase-contrast images are included with 5 μm scale bar.

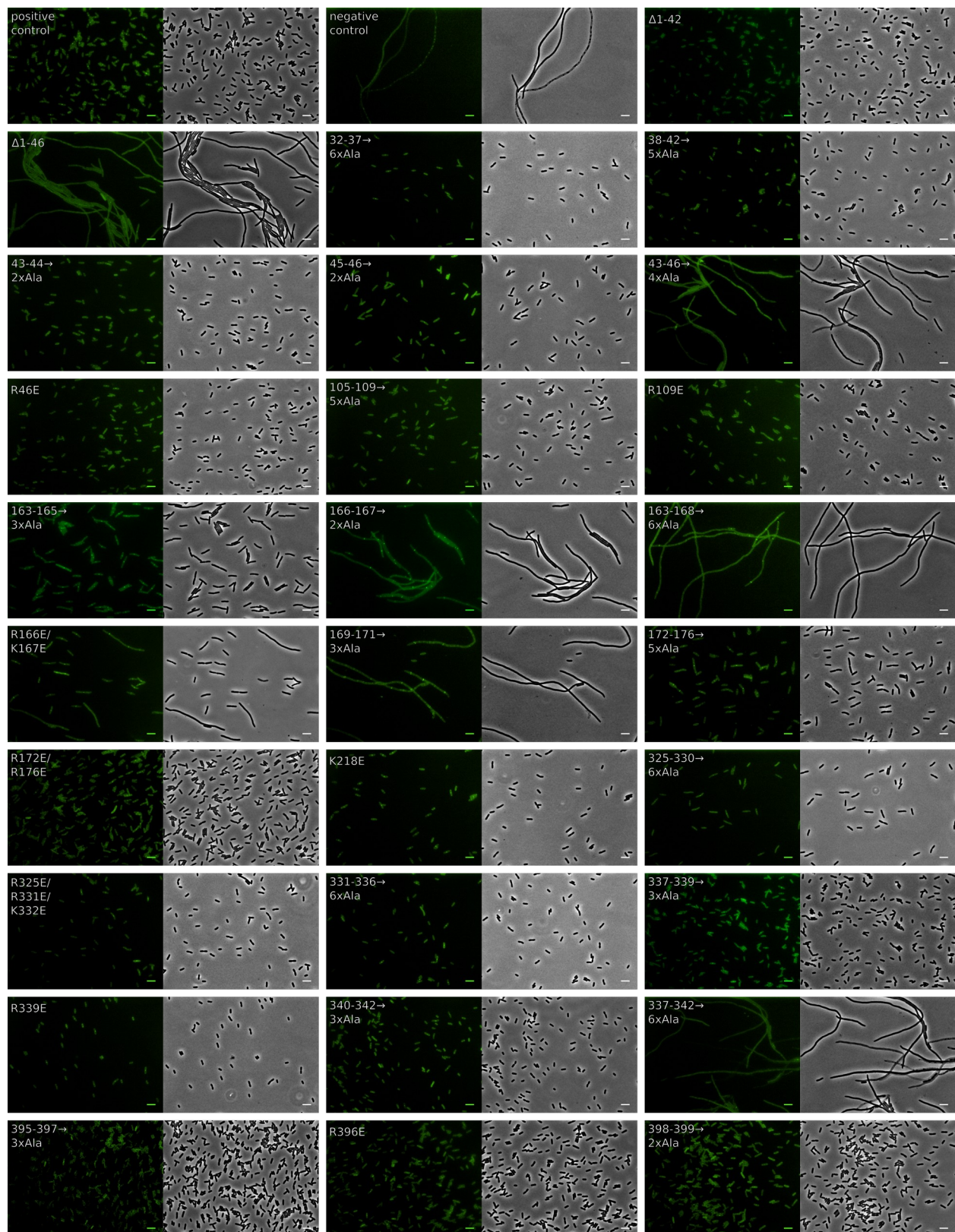


Figure S4.3 – continued below

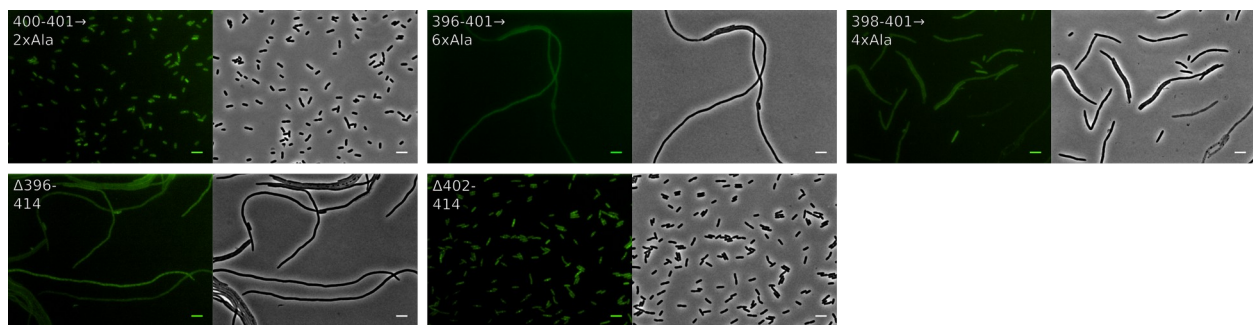


Figure S4.3. FtsW cytoplasmic mutations at 37°C. Representative GFP fluorescence and phase-contrast images with 5 μm scale bar for FtsW control and mutant cells. Phenotype summaries are presented in Fig. 4.2 and Table 4.2. Results for cells grown at 42°C are not reported since the phenotypes were generally indistinguishable from those grown at 37°C.

Strain/plasmid	Description	Resistance	Parent vector	Source
BL21(DE3)	chemically competent <i>E. coli</i> for protein overexpression	-	-	New England BioLabs (C2527)
C43(DE3)	chemically competent <i>E. coli</i> for toxic protein overexpression	-	-	Lucigen (60446)
MDG277	FtsL depletion strain	Kan	-	Gonzalez & Beckwith, 2009
MDG254	FtsL depletion strain with GFP-FtsW	Kan/Cam/Amp	-	Gonzalez & Beckwith, 2010
EC912	FtsW depletion strain	Kan/Cam	-	Mercer & Weiss, 2002
pSJC270	FtsB His-Tev-FLAG3-FtsL	Amp	pETDuet-1	This chapter
pSJC271	FtsI His-Tev-sfGFP-FtsW(codon opt) R2H	Amp	pETDuet-1	This chapter
pSJC281	FtsB His-Tev-FLAG3-FtsL 27–32→6xAla	Amp	pETDuet-1	This chapter
pSJC282	FtsB His-Tev-FLAG3-FtsL D31K	Amp	pETDuet-1	This chapter
pSJC297	FtsB FLAG3-FtsL His-Tev-sfGFP-FtsW(codon opt) R2H	Amp	pETDuet-1	This chapter
pNG162	IPTG-inducible, low-copy-number vector (empty)	Spec	pAM238	Goehring et al., 2006
pMDG29	FLAG3-FtsL	Spec	png162	Gonzalez et al., 2010
pSJC191	FLAG3-FtsL P39A	Spec	pMDG29	This chapter
pSJC193	FLAG3-FtsL P39N	Spec	pMDG29	This chapter
pSJC195	FLAG3-FtsL L38-GGSGGS-P39	Spec	pMDG29	This chapter
pSJC196	FLAG3-FtsL Δ36-38	Spec	pMDG29	This chapter
pSJC197	FLAG3-FtsL Δ33-38	Spec	pMDG29	This chapter
pSJC209	FLAG3-FtsL 36-38→3xAla	Spec	pMDG29	This chapter
pSJC210	FLAG3-FtsL Δ33-35	Spec	pMDG29	This chapter
pSJC211	FLAG3-FtsL 33-35→3xAla	Spec	pMDG29	This chapter
pSJC215	FLAG3-FtsL 15-20→6xAla	Spec	pMDG29	This chapter
pSJC216	FLAG3-FtsL 27-32→6xAla	Spec	pMDG29	This chapter
pSJC217	FLAG3-FtsL 33-38→GGSGGS	Spec	pMDG29	This chapter
pSJC218	FLAG3-FtsL 33-38→6xPro	Spec	pMDG29	This chapter
pSJC219	FLAG3-FtsL 21-26→6xAla	Spec	pMDG29	This chapter
pSJC221	FLAG3-FtsL 27-29→3xAla	Spec	pMDG29	This chapter
pSJC222	FLAG3-FtsL 30-32→3xAla	Spec	pMDG29	This chapter
pSJC224	FLAG3-FtsL 33-38→6xAla	Spec	pMDG29	This chapter
pSJC225	FLAG3-FtsL D30A	Spec	pMDG29	This chapter
pSJC228	FLAG3-FtsL D31A	Spec	pMDG29	This chapter
pSJC231	FLAG3-FtsL L32A	Spec	pMDG29	This chapter
pSJC232	FLAG3-FtsL L38-6xPro-P39	Spec	pMDG29	This chapter
pSJC235	FLAG3-FtsL D30A/D31A	Spec	pMDG29	This chapter
pSJC236	FLAG3-FtsL D30A/L32A	Spec	pMDG29	This chapter
pSJC238	FLAG3-FtsL D30K	Spec	pMDG29	This chapter
pSJC240	FLAG3-FtsL D31A/L32A	Spec	pMDG29	This chapter
pSJC241	FLAG3-FtsL D31K	Spec	pMDG29	This chapter
pDSW360	GFP-FtsW	Kan	pDSW311	Mercer & Weiss, 2002
pSJC214	GFP-FtsW	Amp	pDSW360	This chapter
pSJC257	GFP-FtsW 325-330→6xAla	Amp	pSJC214	This chapter
pSJC258	GFP-FtsW 337-342→6xAla	Amp	pSJC214	This chapter
pSJC259	GFP-FtsW Δ396-414	Amp	pSJC214	This chapter
pSJC260	GFP-FtsW Δ1-46	Amp	pSJC214	This chapter
pSJC261	GFP-FtsW 163-168→6xAla	Amp	pSJC214	This chapter
pSJC262	GFP-FtsW 331-336→6xAla	Amp	pSJC214	This chapter
pSJC263	GFP-FtsW 32-37→6xAla	Amp	pSJC214	This chapter
pSJC264	GFP-FtsW 38-42→5xAla	Amp	pSJC214	This chapter
pSJC265	GFP-FtsW 43-46→4xAla	Amp	pSJC214	This chapter
pSJC266	GFP-FtsW Δ402-414	Amp	pSJC214	This chapter
pSJC267	GFP-FtsW Δ408-414	Amp	pSJC214	This chapter
pSJC272	GFP-FtsW 163-165→3xAla	Amp	pSJC214	This chapter
pSJC273	GFP-FtsW 166-167→2xAla	Amp	pSJC214	This chapter
pSJC274	GFP-FtsW 169-171→3xAla	Amp	pSJC214	This chapter
pSJC275	GFP-FtsW Δ1-42	Amp	pSJC214	This chapter
pSJC276	GFP-FtsW 337-339→3xAla	Amp	pSJC214	This chapter
pSJC277	GFP-FtsW 396-401→6xAla	Amp	pSJC214	This chapter
pSJC283	GFP-FtsW K218E	Amp	pSJC214	This chapter
pSJC284	GFP-FtsW 105-109→6xAla	Amp	pSJC214	This chapter
pSJC285	GFP-FtsW 172-176→6xAla	Amp	pSJC214	This chapter
pSJC289	GFP-FtsW 340-342→3xAla	Amp	pSJC214	This chapter
pSJC290	GFP-FtsW 395-397→3xAla	Amp	pSJC214	This chapter
pSJC291	GFP-FtsW 398-401→4xAla	Amp	pSJC214	This chapter
pSJC296	GFP-FtsW 43-44→2xAla	Amp	pSJC214	This chapter
pSJC300	GFP-FtsW 45-46→2xAla	Amp	pSJC214	This chapter
pSJC312	GFP-FtsW 398-399→2xAla	Amp	pSJC214	This chapter
pSJC313	GFP-FtsW 400-401→2xAla	Amp	pSJC214	This chapter
pSJC314	GFP-FtsW R46E	Amp	pSJC214	This chapter
pSJC315	GFP-FtsW R109E	Amp	pSJC214	This chapter
pSJC316	GFP-FtsW R166E/K167E	Amp	pSJC214	This chapter
pSJC317	GFP-FtsW R172E/R176E	Amp	pSJC214	This chapter
pSJC318	GFP-FtsW R325E/R331E/K332E	Amp	pSJC214	This chapter
pSJC319	GFP-FtsW R339E	Amp	pSJC214	This chapter
pSJC320	GFP-FtsW R396E	Amp	pSJC214	This chapter

Table S4.1. Strains and plasmids used in this chapter.

4.7 References

1. Du S, Lutkenhaus J. Assembly and activation of the *Escherichia coli* divisome. *Mol Microbiol*. 2017 Jul;105(2):177–87.
2. den Blaauwen T, Hamoen LW, Levin PA. The divisome at 25: the road ahead. *Curr Opin Microbiol*. 2017 Apr;36:85–94.
3. Löwe J, Amos LA. Crystal structure of the bacterial cell-division protein FtsZ. *Nature*. 1998 Jan 8;391(6663):203–6.
4. Bi EF, Lutkenhaus J. FtsZ ring structure associated with division in *Escherichia coli*. *Nature*. 1991 Nov 14;354(6349):161–4.
5. Mukherjee A, Lutkenhaus J. Guanine nucleotide-dependent assembly of FtsZ into filaments. *J Bacteriol*. 1994 May;176(9):2754–8.
6. Bramhill D, Thompson CM. GTP-dependent polymerization of *Escherichia coli* FtsZ protein to form tubules. *Proc Natl Acad Sci U S A*. 1994 Jun 21;91(13):5813–7.
7. Yang X, Lyu Z, Miguel A, McQuillen R, Huang KC, Xiao J. GTPase activity-coupled treadmilling of the bacterial tubulin FtsZ organizes septal cell wall synthesis. *Science*. 2017 17;355(6326):744–7.
8. Bisson-Filho AW, Hsu Y-P, Squyres GR, Kuru E, Wu F, Jukes C, et al. Treadmilling by FtsZ filaments drives peptidoglycan synthesis and bacterial cell division. *Science*. 2017 17;355(6326):739–43.
9. McCausland JW, Yang X, Lyu Z, Söderström B, Xiao J, Liu J. Treadmilling FtsZ polymers drive the directional movement of sPG-synthesis enzymes via a Brownian ratchet mechanism. *bioRxiv*. 2019 Nov 28;857813.
10. Yang X, McQuillen R, Lyu Z, Phillips-Mason P, Cruz ADL, McCausland JW, et al. FtsW exhibits distinct processive movements driven by either septal cell wall synthesis or FtsZ treadmilling in *E. coli*. *bioRxiv*. 2019 Nov 21;850073.
11. Sauvage E, Kerff F, Terrak M, Ayala JA, Charlier P. The penicillin-binding proteins: structure and role in peptidoglycan biosynthesis. *FEMS Microbiol Rev*. 2008 Mar;32(2):234–58.
12. Egan AJF, Vollmer W. The physiology of bacterial cell division. *Ann N Y Acad Sci*. 2013 Jan;1277:8–28.
13. Booth S, Lewis RJ. Structural basis for the coordination of cell division with the synthesis of the bacterial cell envelope. *Protein Sci Publ Protein Soc*. 2019 Dec;28(12):2042–54.

14. Barrett D, Wang T-SA, Yuan Y, Zhang Y, Kahne D, Walker S. Analysis of glycan polymers produced by peptidoglycan glycosyltransferases. *J Biol Chem.* 2007 Nov 2;282(44):31964–71.
15. Meeske AJ, Riley EP, Robins WP, Uehara T, Mekalanos JJ, Kahne D, et al. SEDS proteins are a widespread family of bacterial cell wall polymerases. *Nature.* 2016 29;537(7622):634–8.
16. Taguchi A, Welsh MA, Marmont LS, Lee W, Sjödt M, Kruse AC, et al. FtsW is a peptidoglycan polymerase that is functional only in complex with its cognate penicillin-binding protein. *Nat Microbiol.* 2019;4(4):587–94.
17. Bertsche U, Breukink E, Kast T, Vollmer W. In vitro murein peptidoglycan synthesis by dimers of the bifunctional transglycosylase-transpeptidase PBP1B from *Escherichia coli*. *J Biol Chem.* 2005 Nov 11;280(45):38096–101.
18. Bertsche U, Kast T, Wolf B, Fraipont C, Aarsman MEG, Kannenberg K, et al. Interaction between two murein (peptidoglycan) synthases, PBP3 and PBP1B, in *Escherichia coli*. *Mol Microbiol.* 2006 Aug;61(3):675–90.
19. Botta GA, Park JT. Evidence for involvement of penicillin-binding protein 3 in murein synthesis during septation but not during cell elongation. *J Bacteriol.* 1981 Jan;145(1):333–40.
20. Weiss DS, Pogliano K, Carson M, Guzman LM, Fraipont C, Nguyen-Distèche M, et al. Localization of the *Escherichia coli* cell division protein FtsI (PBP3) to the division site and cell pole. *Mol Microbiol.* 1997 Aug;25(4):671–81.
21. Sauvage E, Derouaux A, Fraipont C, Joris M, Herman R, Rocaboy M, et al. Crystal structure of penicillin-binding protein 3 (PBP3) from *Escherichia coli*. *PloS One.* 2014;9(5):e98042.
22. Lara B, Ayala JA. Topological characterization of the essential *Escherichia coli* cell division protein FtsW. *FEMS Microbiol Lett.* 2002 Oct 29;216(1):23–32.
23. Cho H, Wivagg CN, Kapoor M, Barry Z, Rohs PDA, Suh H, et al. Bacterial cell wall biogenesis is mediated by SEDS and PBP polymerase families functioning semi-autonomously. *Nat Microbiol.* 2016 Sep 19;1:16172.
24. Emami K, Guyet A, Kawai Y, Devi J, Wu LJ, Allenby N, et al. RodA as the missing glycosyltransferase in *Bacillus subtilis* and antibiotic discovery for the peptidoglycan polymerase pathway. *Nat Microbiol.* 2017 Jan 13;2:16253.
25. Boyle DS, Khattar MM, Addinall SG, Lutkenhaus J, Donachie WD. ftsW is an essential cell-division gene in *Escherichia coli*. *Mol Microbiol.* 1997 Jun;24(6):1263–73.

26. Mohammadi T, van Dam V, Sijbrandi R, Vernet T, Zapun A, Bouhss A, et al. Identification of FtsW as a transporter of lipid-linked cell wall precursors across the membrane. *EMBO J.* 2011 Apr;30(8):1425–32.
27. Mohammadi T, Sijbrandi R, Lutters M, Verheul J, Martin NI, den Blaauwen T, et al. Specificity of the transport of lipid II by FtsW in *Escherichia coli*. *J Biol Chem.* 2014 May 23;289(21):14707–18.
28. Leclercq S, Derouaux A, Olatunji S, Fraipont C, Egan AJF, Vollmer W, et al. Interplay between Penicillin-binding proteins and SEDS proteins promotes bacterial cell wall synthesis. *Sci Rep.* 2017 24;7:43306.
29. Ruiz N. Bioinformatics identification of MurJ (MviN) as the peptidoglycan lipid II flippase in *Escherichia coli*. *Proc Natl Acad Sci U S A.* 2008 Oct 7;105(40):15553–7.
30. Sham L-T, Butler EK, Lebar MD, Kahne D, Bernhardt TG, Ruiz N. Bacterial cell wall. MurJ is the flippase of lipid-linked precursors for peptidoglycan biogenesis. *Science.* 2014 Jul 11;345(6193):220–2.
31. Bolla JR, Sauer JB, Wu D, Mehmood S, Allison TM, Robinson CV. Direct observation of the influence of cardiolipin and antibiotics on lipid II binding to MurJ. *Nat Chem.* 2018;10(3):363–71.
32. Mercer KLN, Weiss DS. The *Escherichia coli* cell division protein FtsW is required to recruit its cognate transpeptidase, FtsI (PBP3), to the division site. *J Bacteriol.* 2002 Feb;184(4):904–12.
33. Fraipont C, Alexeeva S, Wolf B, van der Ploeg R, Schloesser M, den Blaauwen T, et al. The integral membrane FtsW protein and peptidoglycan synthase PBP3 form a subcomplex in *Escherichia coli*. *Microbiol Read Engl.* 2011 Jan;157(Pt 1):251–9.
34. Weiss DS, Chen JC, Ghigo JM, Boyd D, Beckwith J. Localization of FtsI (PBP3) to the septal ring requires its membrane anchor, the Z ring, FtsA, FtsQ, and FtsL. *J Bacteriol.* 1999 Jan;181(2):508–20.
35. Buddelmeijer N, Judson N, Boyd D, Mekalanos JJ, Beckwith J. YgbQ, a cell division protein in *Escherichia coli* and *Vibrio cholerae*, localizes in codependent fashion with FtsL to the division site. *Proc Natl Acad Sci U S A.* 2002 Apr 30;99(9):6316–21.
36. Goehring NW, Gonzalez MD, Beckwith J. Premature targeting of cell division proteins to midcell reveals hierarchies of protein interactions involved in divisome assembly. *Mol Microbiol.* 2006 Jul;61(1):33–45.
37. Buddelmeijer N, Beckwith J. A complex of the *Escherichia coli* cell division proteins FtsL, FtsB and FtsQ forms independently of its localization to the septal region. *Mol Microbiol.* 2004 Jun;52(5):1315–27.

38. Gonzalez MD, Beckwith J. Divisome under construction: distinct domains of the small membrane protein FtsB are necessary for interaction with multiple cell division proteins. *J Bacteriol.* 2009 Apr;191(8):2815–25.
39. Gonzalez MD, Akbay EA, Boyd D, Beckwith J. Multiple interaction domains in FtsL, a protein component of the widely conserved bacterial FtsLBQ cell division complex. *J Bacteriol.* 2010 Jun;192(11):2757–68.
40. Natale P, Pazos M, Vicente M. The *Escherichia coli* divisome: born to divide. *Environ Microbiol.* 2013 Dec;15(12):3169–82.
41. Tsang M-J, Bernhardt TG. A role for the FtsQLB complex in cytokinetic ring activation revealed by an ftsL allele that accelerates division. *Mol Microbiol.* 2015 Mar;95(6):925–44.
42. Liu B, Persons L, Lee L, de Boer PAJ. Roles for both FtsA and the FtsBLQ subcomplex in FtsN-stimulated cell constriction in *Escherichia coli*. *Mol Microbiol.* 2015 Mar;95(6):945–70.
43. Addinall SG, Cao C, Lutkenhaus J. FtsN, a late recruit to the septum in *Escherichia coli*. *Mol Microbiol.* 1997 Jul;25(2):303–9.
44. Boes A, Olatunji S, Breukink E, Terrak M. Regulation of the Peptidoglycan Polymerase Activity of PBP1b by Antagonist Actions of the Core Divisome Proteins FtsBLQ and FtsN. *mBio.* 2019 08;10(1).
45. Condon SGF, Mahbuba D-A, Armstrong CR, Diaz-Vazquez G, Craven SJ, LaPointe LM, et al. The FtsLB subcomplex of the bacterial divisome is a tetramer with an uninterrupted FtsL helix linking the transmembrane and periplasmic regions. *J Biol Chem.* 2018 02;293(5):1623–41.
46. Khattar MM, Begg KJ, Donachie WD. Identification of FtsW and characterization of a new ftsW division mutant of *Escherichia coli*. *J Bacteriol.* 1994 Dec;176(23):7140–7.
47. Ovchinnikov S, Kinch L, Park H, Liao Y, Pei J, Kim DE, et al. Large-scale determination of previously unsolved protein structures using evolutionary information. *eLife.* 2015 Sep 3;4:e09248.
48. Sjödt M, Brock K, Dobihal G, Rohs PDA, Green AG, Hopf TA, et al. Structure of the peptidoglycan polymerase RodA resolved by evolutionary coupling analysis. *Nature.* 2018 05;556(7699):118–21.
49. Gerding MA, Liu B, Bendezú FO, Hale CA, Bernhardt TG, de Boer PAJ. Self-enhanced accumulation of FtsN at Division Sites and Roles for Other Proteins with a SPOR domain (DamX, DedD, and RlpA) in *Escherichia coli* cell constriction. *J Bacteriol.* 2009 Dec;191(24):7383–401.

50. Xiong Y-M, Chen J, Zhang L. Modulation of CD11b/CD18 adhesive activity by its extracellular, membrane-proximal regions. *J Immunol Baltim Md 1950.* 2003 Jul 15;171(2):1042–50.
51. Schmidt T, Ye F, Situ AJ, An W, Ginsberg MH, Ulmer TS. A Conserved Ectodomain-Transmembrane Domain Linker Motif Tunes the Allosteric Regulation of Cell Surface Receptors. *J Biol Chem.* 2016 19;291(34):17536–46.
52. Shelar A, Bansal M. Sequence and conformational preferences at termini of α -helices in membrane proteins: role of the helix environment. *Proteins.* 2014 Dec;82(12):3420–36.
53. Gibson DG, Young L, Chuang R-Y, Venter JC, Hutchison CA, Smith HO. Enzymatic assembly of DNA molecules up to several hundred kilobases. *Nat Methods.* 2009 May;6(5):343–5.
54. Paintdakhi A, Parry B, Campos M, Irnov I, Elf J, Surovtsev I, et al. Oufti: an integrated software package for high-accuracy, high-throughput quantitative microscopy analysis. *Mol Microbiol.* 2016 Feb;99(4):767–77.
55. Studier FW. Protein production by auto-induction in high density shaking cultures. *Protein Expr Purif.* 2005 May;41(1):207–34.

Chapter 5: Future directions and continuing work

5.1 Summary of dissertation: What have we learned?

In the preceding chapters, I described some of the research that I and various other members of the Senes lab performed in recent years. This work has largely focused on obtaining a more detailed understanding of the structure and function of the FtsLB complex in order to better explain its role within the divisome as a whole. Such work is especially important considering the centrality of FtsLB to divisome assembly/regulation and the general lack of information regarding this complex. From our work, we have made significant advances within the cell division field, and I firmly believe that the hypotheses we developed will form a basis for many future experiments within our research group and others as well.

In our 2018 JBC paper (1) (Chapter 2), we proposed the first-ever FtsLB model containing both soluble and transmembrane (TM) regions of the complex. Our computational predictions are based on FRET experiments that establish a likely 2:2 heterotetrameric arrangement for the complex as well as co-evolutionary data that provides a strong interface prediction throughout the complex. I further expand on this model in Chapter 3 by incorporating work with the FtsLB coiled coil to propose an alternative model with a paired, two-helix coiled-coil arrangement compared to the four-helix arrangement originally proposed. These data also suggest that the coiled coil of FtsLB has likely evolved to be marginally stable, which has important implications for the signaling role FtsLB is thought to play in triggering cytokinesis. However, these models still require *in vitro* validation, as discussed further in Section 5.2. I have also provided evidence that the Gly-rich linker region in FtsB is important for the function of the FtsLB complex (Chapter 2 and Chapter 3). Specifically, I showed that this linker can

tolerate residue insertion and likely provides flexibility between the coiled-coil and TM regions of FtsB. Such flexibility may be essential to the signal transduction mechanism of FtsLB, as it may enable conformational changes that convert FtsLB between the proposed “off” and “on” states (2, 3). This is complemented by FtsL, which lacks such a linker region and presumably provides a rigid backbone to support the complex. The FtsB linker also maintains a non-helical structure that enables the TM and coiled-coil regions to adopt the appropriate orientation for interaction with FtsL. A detailed understanding of what this non-helical arrangement entails will likely require more concrete structural data, but it is unlikely to be completely unfolded and floppy. This is evidenced by the fact that deletions within the region cause severe division defects, which indicates that the linker is constrained for length.

Finally, I have identified specific residues involved in the essential interaction between the FtsL cytoplasmic tail and FtsW (Chapter 4). This interaction has long been assumed, but this represents the first work (to my knowledge) that addresses specifically where binding occurs. Further work is required to determine whether the FtsL-FtsW interaction simply recruits FtsW to the division site or if it also plays a more nuanced role in regulating FtsW activity, but this research provides important initial steps towards understanding this essential aspect of divisome function.

5.2 What comes next?

The work presented in this dissertation is far from finished, and new research opportunities for our group have been realized as well. I will be personally addressing some of these projects during my postdoctoral training in the Senes lab, but a few of our

new graduate students will likely take over much of the work. Below, I will outline some of these potential projects and discuss what I think is most pressing as well as what is most exciting. I have already discussed in the previous chapters some work that is currently underway (e.g., further FtsW mutations to narrow down the FtsL-binding site and *in vitro* binding experiments to validate the FtsL-FtsW interaction), so here I will focus on other research avenues that could be developed into individual projects.

5.2.1 Construction of dual-depletion strains

Throughout my graduate school career, one specific limitation has constantly prevented me from testing various hypotheses: we do not have any *E. coli* strains that enable depletion of two divisome genes at the same time. We have obtained depletion strains for various individual divisome genes like FtsB, FtsL, and FtsW (4–6) (special thanks to Jon Beckwith, Mark Gonzalez, and David Weiss for providing these), but to my knowledge, dual-depletion strains for these genes do not exist. For this reason, we will need to construct our own strains if we wish to address certain hypotheses, as discussed below.

The most relevant of these strains would be a FtsLB dual-depletion strain, and one option to construct this would be to apply the same methods used to construct the FtsL depletion strain to the FtsB depletion strain (or vice versa). Originally, the two single-depletion strains were constructed by replacing the native gene locus with an antibiotic resistance gene and then reinserting a copy of the original gene back into the chromosome under control of a regulatable P_{BAD} promoter (5, 6). Presumably, both genes could be placed under P_{BAD} control within the same strain, which would enable simultaneous expression or repression depending on the sugars added to the growth

medium. This would produce a convenient strain containing the relevant components all within the chromosome, but this process is labor-intensive and requires techniques with which we are not very experienced. As a potentially simpler alternative, repression of either gene could be achieved by applying CRISPR interference (CRISPRi) to our depletion strains. CRISPRi would enable regulation of either FtsL or FtsB without the need for chromosome modifications, which would likely shorten the time required to set up the system for actual experimentation. I have briefly discussed this possibility with Jason Peters (a CRISPRi expert at UW-Madison), so there is potential for a collaboration with his group should this direction be taken. In either case, the resulting strain could then be transformed with separate plasmids containing FtsL and FtsB or a single vector containing both genes, which would enable complementation experiments with simultaneous expression of FtsL and FtsB mutants.

Currently, there are three main hypotheses I would like to test with such an FtsLB depletion strain. The first addresses the function of the FtsL cytoplasmic tail. As shown in Chapter 4, certain residues within this tail are needed to recruit FtsW to midcell; however, it remains unanswered if this interaction is also involved with regulating FtsW activity. A simple way to test the importance of this tail would be to move it from FtsL to FtsB. If the tail is involved with FtsW regulation, then moving it to FtsB would likely disrupt communication between FtsLB and FtsW. On the other hand, if the tail merely recruits FtsW to midcell, then it might not matter whether it is attached to FtsL or FtsB. The second question I would like to address is if the hydrophobic mutations introduced into the coiled-coil regions of FtsL and FtsB can be compensated by polar/charged mutations in the partner protein. This would further clarify if the overall function of the

nonideal interfacial residues is merely to destabilize the coiled coil or if they have a more complicated role. Finally, I would also like to test how gain-of-function mutations in one protein compete with loss-of-function mutations in the partner protein. This would lead to better insights into the individual roles of FtsL and FtsB in the FtsLB-mediated triggering of cytokinesis and cell division in general.

5.2.2 Obtaining better FtsLB thermodynamic data

In Chapter 3, I presented thermal melt circular dichroism (CD) spectra comparing wild-type FtsLB to a mutant containing four hydrophobic mutations in the nonideal coiled-coil residues (4x-mutant). These experiments were performed using purified protein in detergent, and the resulting data potentially reflect the fact that detergent is an imperfect membrane mimetic (7, 8). Specifically, I was unable to obtain a clear melting temperature shift between the constructs as was expected, and instead, the mutant spectrum lost the signature sigmoidal curve normally seen in thermal melt experiments. As discussed in Chapter 3, the mutations could produce this effect by introducing multiple FtsLB conformations, but another possibility is that the added hydrophobic residues caused increased interactions with the surrounding detergent, which interfered with the normal FtsLB unfolding pathway. To address this issue, a wider range of membrane mimetics needs to be tested, and I will likely need to move into lipid systems. CD can be performed using lipid bicelles (9), and I plan to initially focus in that direction, though the possibility of bilayer phase transitions occurring within the thermal melt temperature range may potentially complicate the use of bicelles. Regardless, one of our new students is excited to start working with me on this project, so I am hopeful that it will progress in a positive direction.

5.2.3 Further characterization of FtsW interactions and function

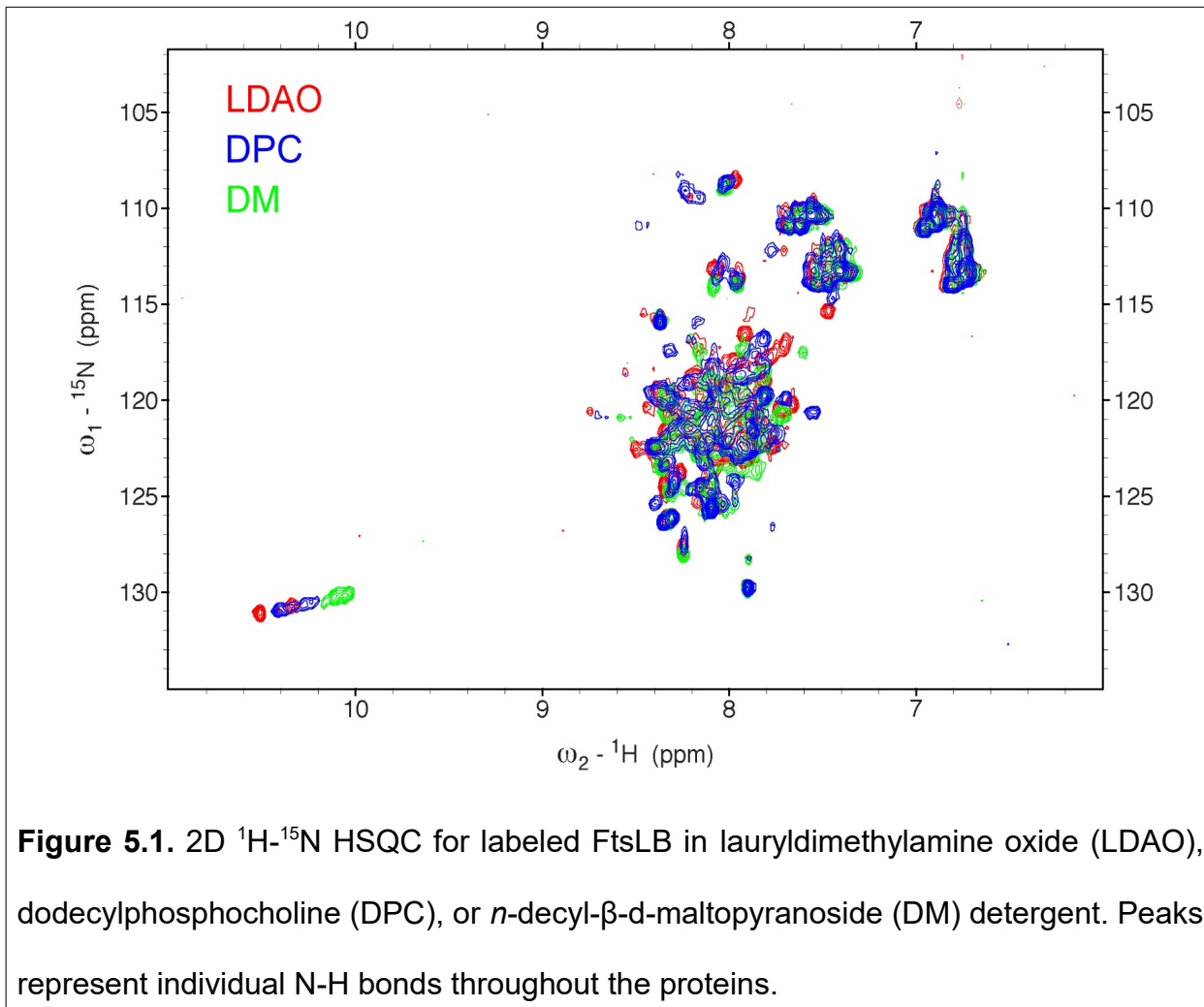
Throughout my graduate school career, most of my FtsW-related research has focused simply on the interaction with FtsL, but I plan to expand on this. As the recently identified central glycosyltransferase (GTase) for cell division (10, 11), FtsW presents multiple promising avenues of research, and we already have a system in place to test FtsW mutations *in vivo*. To keep in line with the FtsLB-centric focus of the Senes lab, one potential project would be to test if FtsLB has a regulatory effect on FtsW *in vitro*. This could be performed with either full-length FtsLB or just the FtsL cytoplasmic tail and should address our long-standing hypothesis that FtsL does more than just recruit FtsW. Alternatively, I have already shown in Chapter 4 that the 4/5 cytoplasmic loop of FtsW is critical for some function other than septal localization, and understanding the details of this loop will likely require both *in vitro* activity assays and *in vivo* complementation experiments. Finally, I plan on collaborating with other members of the Senes lab to produce computational models for the FtsL-FtsW interaction, which should help validate my *in vivo* results and provide support for future projects. Similar to the FtsLB CD work, I have already discussed continuing my FtsW research with help from another graduate student in the lab.

5.2.4 X-ray crystallography and NMR spectroscopy studies of FtsLB structure

During graduate school, I had two major projects that I suspended in favor of the work presented in Chapter 3 and Chapter 4. The first is an X-ray crystallography project in which I attempted to obtain a structure for the periplasmic region of FtsLB and FtsQLB in collaboration with the Ivan Rayment lab at UW-Madison. To date, a crystal structure for the periplasmic region of FtsQ has already been solved (12), and partial

structures for FtsB alone (13) or in complex with FtsQ (14, 15) exist, but no structures containing even a portion of FtsL have been solved. Most importantly for my research, no concrete structure for the FtsLB coiled-coil interaction exists. A complete structure of the periplasmic region of FtsLB (especially in complex with FtsQ) would greatly aid FtsLB research and also confirm if our computational models are correct (1). To this end, I spent a few years attempting to crystallize various FtsLB fusion constructs, but I was never able to obtain usable crystals. More details are presented in Appendix 2, but in summary, I was only able to produce small, flat crystals and long, thin needles that were difficult to reproduce. A postdoctoral researcher in the Senes lab continued work with related soluble constructs and managed to produce larger, reproducible crystals, but these did not diffract well and were not usable for structure determination. Multiple directions still remain to be explored, however, and one particularly promising (but challenging) option would be to crystallize full-length constructs containing the TM domains of FtsLB. This would remove the worry that the soluble fusions are altering the structure of the complex, but it would also likely increase the difficulty of obtaining usable crystals due to the requirement for membrane mimetics in the crystallization conditions. This project is definitely a high-risk/high-reward undertaking, but I think its potential warrants the effort, especially for anyone with structural inclinations.

My other structural project was put on hold largely due to the loss of a dedicated postdoctoral researcher and my need to graduate in a reasonable timeline. This project is a collaboration with the Katherine Henzler-Wildman lab at UW-Madison, and the goal is to obtain nuclear magnetic resonance (NMR) data to provide structural information for the full-length FtsLB complex. Though this project largely progressed into an



investigation of the FtsQ-FtsLB interaction (paper in preparation), the original direction is still viable and some foundational work has already been completed. Currently, we have initial heteronuclear single quantum coherence (HSQC) spectra for FtsLB in different detergents (Fig. 5.1), and the results are noisy but promising. Significant effort is still required to complete this project, but the potential for crucial information on the structural arrangement of FtsLB demands that this work is resumed. Specifically, we still need to optimize the membrane mimetic, so more detergents along with various forms of liposomes, bicelles, and nanodiscs should all be tested to improve our HSQC

spectra. From there, various labeling strategies such as general deuteration or ¹⁹F-labeling of tryptophan residues can be employed to compare structural changes between WT and mutant FtsLB constructs.

5.2.5 Cryo-EM on a subset of divisome proteins

With how rapidly cryogenic electron microscopy (cryo-EM) technology has improved in recent years (16), we have considered branching out from our crystallography and NMR collaborations to attack the FtsLB structural question from this additional angle. Currently, obtaining high-resolution structures for proteins as small as the FtsLB complex (the tetramer is ~50 kDa) is difficult using this technique (17), but a promising alternative would be to perform cryo-EM on larger complexes such as FtsQLB or even FtsQLBWI. I have already developed purification protocols for most of these proteins, so a significant portion of the preparatory work has already been completed. Conveniently, the Elizabeth Wright lab has recently moved to UW-Madison and is currently setting up a cryo-EM facility here, so we already have a potential collaborator nearby. Success with this project would likely address many of our current structural hypotheses and pave the way for new projects as well, so I am excited by the prospect of pursuing this option.

5.3 Conclusion

Overall, the focus of my graduate school research has been understanding the structure and function of the essential FtsLB divisome complex. In particular, I took an interdisciplinary approach by combining *in vivo* mutational analyses, diverse *in vitro* assays, and *in silico* modeling and simulations to elucidate various details of FtsLB. Not

only do the various data I provided have special relevance for the field of antibiotic drug design, but this work in general applies widely to studies of bacterial growth, seeing as FtsLB function is essential to cell survival. So much still remains to be discovered about FtsLB and the larger divisome as a whole, and most likely, continued research in this field will require further drawing on the strengths of different disciplines to provide novel insights into the fundamental bacterial process of cell division.

5.4 References

1. Condon SGF, Mahbuba D-A, Armstrong CR, Diaz-Vazquez G, Craven SJ, LaPointe LM, et al. The FtsLB subcomplex of the bacterial divisome is a tetramer with an uninterrupted FtsL helix linking the transmembrane and periplasmic regions. *J Biol Chem.* 2018 02;293(5):1623–41.
2. Liu B, Persons L, Lee L, de Boer PAJ. Roles for both FtsA and the FtsBLQ subcomplex in FtsN-stimulated cell constriction in *Escherichia coli*. *Mol Microbiol.* 2015 Mar;95(6):945–70.
3. Tsang M-J, Bernhardt TG. A role for the FtsQLB complex in cytokinetic ring activation revealed by an ftsL allele that accelerates division. *Mol Microbiol.* 2015 Mar;95(6):925–44.
4. Mercer KLN, Weiss DS. The *Escherichia coli* cell division protein FtsW is required to recruit its cognate transpeptidase, FtsI (PBP3), to the division site. *J Bacteriol.* 2002 Feb;184(4):904–12.
5. Buddelmeijer N, Judson N, Boyd D, Mekalanos JJ, Beckwith J. YgbQ, a cell division protein in *Escherichia coli* and *Vibrio cholerae*, localizes in codependent fashion with FtsL to the division site. *Proc Natl Acad Sci U S A.* 2002 Apr 30;99(9):6316–21.
6. Gonzalez MD, Beckwith J. Divisome under construction: distinct domains of the small membrane protein FtsB are necessary for interaction with multiple cell division proteins. *J Bacteriol.* 2009 Apr;191(8):2815–25.
7. Seddon AM, Curnow P, Booth PJ. Membrane proteins, lipids and detergents: not just a soap opera. *Biochim Biophys Acta.* 2004 Nov 3;1666(1–2):105–17.
8. Miles AJ, Wallace BA. Circular dichroism spectroscopy of membrane proteins. *Chem Soc Rev.* 2016 21;45(18):4859–72.

9. Loudet C, Khemtémourian L, Aussénac F, Gineste S, Achard M-F, Dufourc EJ. Bicelle membranes and their use for hydrophobic peptide studies by circular dichroism and solid state NMR. *Biochim Biophys Acta*. 2005 Aug 5;1724(3):315–23.
10. Meeske AJ, Riley EP, Robins WP, Uehara T, Mekalanos JJ, Kahne D, et al. SEDS proteins are a widespread family of bacterial cell wall polymerases. *Nature*. 2016 29;537(7622):634–8.
11. Taguchi A, Welsh MA, Marmont LS, Lee W, Sjödt M, Kruse AC, et al. FtsW is a peptidoglycan polymerase that is functional only in complex with its cognate penicillin-binding protein. *Nat Microbiol*. 2019;4(4):587–94.
12. van den Ent F, Vinkenvleugel TMF, Ind A, West P, Veprintsev D, Nanninga N, et al. Structural and mutational analysis of the cell division protein FtsQ. *Mol Microbiol*. 2008 Apr;68(1):110–23.
13. LaPointe LM, Taylor KC, Subramaniam S, Khadria A, Rayment I, Senes A. Structural organization of FtsB, a transmembrane protein of the bacterial divisome. *Biochemistry*. 2013 Apr 16;52(15):2574–85.
14. Kureisaite-Ciziene D, Varadajan A, McLaughlin SH, Glas M, Montón Silva A, Luirink R, et al. Structural Analysis of the Interaction between the Bacterial Cell Division Proteins FtsQ and FtsB. *mBio*. 2018 11;9(5).
15. Choi Y, Kim J, Yoon H-J, Jin KS, Ryu S, Lee HH. Structural Insights into the FtsQ/FtsB/FtsL Complex, a Key Component of the Divisome. *Sci Rep*. 2018 24;8(1):18061.
16. Nogales E. The development of cryo-EM into a mainstream structural biology technique. *Nat Methods*. 2016 Jan;13(1):24–7.
17. Herzik MA, Wu M, Lander GC. High-resolution structure determination of sub-100 kDa complexes using conventional cryo-EM. *Nat Commun*. 2019 04;10(1):1032.

Appendix 1 – FtsLB expression and purification

In this appendix, I present the protocol I developed for overexpression and purification of the FtsLB complex. This is intended to serve as a starting point for future Senes lab members to optimize their own protocols. In general, either protein can be His-tagged or Strep-tagged, and in fact, the proteins tend to express better when tagged (on the N-terminus). FtsL naturally contains two cysteine residues (C41 and C45), which tend to form FtsL dimers (even in the presence of reducing agents), so using Cys-less FtsL may be preferred. Implementing the high performance liquid chromatography (HPLC) purification results in higher purity and separation of FtsL from FtsB, but there is some concern that the process may damage the protein or cause folding issues. For this reason, it is acceptable (and possibly preferable) to skip this section depending on the sample required. If HPLC separation is included, resuspension of lyophilized samples should be performed using the dried film method to maximize incorporation into detergent micelles.

Buffers and other solutions

- **cell wash buffer:** 100 mM NaCl + 10 mM HEPES pH 8.0
- **HPLC buffer A:** 99.9% H₂O + 0.1% trifluoroacetic acid (TFA)
- **HPLC buffer B:** 99.9% acetonitrile (ACN) + 0.1% TFA
- **lysis buffer:** 50 mM NaCl + 50 mM HEPES pH 8.0
- **Ni-NTA wash buffer:** 300 mM NaCl + 25 mM HEPES pH 8.0 + 50 mM imidazole
- **Ni-NTA elution buffer:** 300 mM NaCl + 25 mM HEPES pH 8.0 + 300 mM imidazole
- **protease inhibitor cocktail (250x):** 2 mM leupeptin + 2.8 mM E-64 + 80 µM aprotinin + 80 mM 4-(2-aminoethyl)benzenesulfonyl fluoride

- **Strep-Tactin XT wash buffer:** 100 mM Tris-HCl pH 8.0 + 150 mM NaCl + 1 mM EDTA
- **Strep-Tactin XT elution buffer (IBA buffer BXT):** 100 mM Tris-HCl pH 8.0 + 150 mM NaCl + 1 mM EDTA + 50 mM biotin

Overexpression of FtsLB

- Transform BL21(DE3) cells with a pET-Duet vector containing the appropriate FtsL and FtsB constructs
- Plate onto LB agar with the appropriate antibiotics overnight @ 37°C
- Wash the plate(s) with ~1 mL of LB media and inoculate this wash into one or more 4 L flasks containing 1 L of autoinduction media (see Studier, 2005 for recipe) with appropriate antibiotics
- Grow shaking (~ 225 rpm) @ 37°C until O.D.₆₀₀ reaches ~0.8-1.0
- Take pre-induction samples for SDS-PAGE
- Move to 22°C for overnight expression (~16 hr)
- Take post-induction samples for SDS-PAGE
- Run SDS-PAGE to check for expression levels
- Pellet cells on JLA-8.1000 rotor at 2000 x g for 20 min at 4°C
- Resuspend cells in cell wash buffer and combine into a single flask
- Re-pellet cells again
- Scoop into liquid N₂ and store at -80°C

Lysis via sonication

- Put ~10 g of cells in 100 mL (1 g per 10 mL) lysis buffer + 5 mM β-Me
- Add 50 mg of lysozyme (1 mL of 50 mg/mL stock; final = 0.5 mg/mL)

- Add 1 mM EDTA pH = 8.0 (optional; only if performing M fraction prep)
- Add 400 uL protease inhibitor cocktail
- Chill on ice at least 30 min
- Add 1 mM PMSF immediately before sonication (1 mL of 100 mM stock)
- Set up large sonicator head with airflow
- Set sonicator to 5 sec “on” : 15 sec “off” for 4 min “on” total at 30-35% amp
- Monitor temperature; should remain <10°C
- Take fraction samples for SDS-PAGE

Cell fraction separation

- Pellet inclusion bodies with JLA-16.250 rotor at 10,000 x g for 20 min at 4°C
- Decant supernatant into Ti45 tubes and balance to within 0.03 g
- Pellet membrane fraction on Ti45 rotor at 180,000 x g for 30 min at 4°C
- Take fraction samples for SDS-PAGE
- Run SDS-PAGE gel on all fractions

FtsLB extraction from membrane (or inclusion body) fraction

- Resuspend membrane fraction at room temperature overnight in ~20 mL lysis buffer + 5 mM β-Me + 18 mM DM (10x critical micelle concentration)
- Pellet non-resuspended material with JLA16.250 rotor at 10,000 x g for 20 min at 4°C
- Alternatively, the majority of protein ends up in the inclusion body fraction, and the same extraction conditions can yield a large quantity for further use (there is some concern that the protein may not be folded correctly, but I have yet to see a difference in downstream applications)

Ni-NTA column

- Add membrane extraction to Ni-NTA resin (~0.5 mL resin per 1 g of cell lysed) pre-equilibrated with lysis buffer
- Batch bind at 4°C rocking for at least 2 h
- Pour resin/protein mix into column and let settle before collecting flowthrough fraction
- Run the column using 10 column volumes (CV) of wash buffer + 0.51 mM DDM + 1 mM β-Me followed by 10 CV of elution buffer + 0.51 mM DDM + 1 mM β-Me
(Column can be run at room temperature without any noticeable issues)
- Run SDS-PAGE on fractions to assess purity

Streptactin column (optional; improves purity and FtsL:FtsB ratio; skip if doing**HPLC)**

- Combine the Ni-NTA elution fractions with the most protein and add to Strep-Tactin XT (IBA) resin (>0.5 mL resin per 1 mL load) pre-equilibrated with Strep-TXT wash buffer + 0.51 mM DDM + 1 mM β-Me
- Batch bind at 4°C rocking for at least 2 h (overnight may be preferable)
- Pour resin/protein mix into column and let settle before collecting flowthrough fraction
- Run the column using >5 CV of Strep-Tactin XT wash buffer + 0.51 mM DDM + 1 mM β-Me followed by >5 CV Strep-Tactin XT elution buffer + 0.51 mM DDM + 1 mM β-Me
(Column can be run at room temperature without any noticeable issues)
- Run SDS-PAGE on fractions to assess purity

Reverse-phase HPLC column (optional; improves purity and separates FtsL from FtsB)

- Combine Ni-NTA elution fractions with the most protein and add 2,2,2-trifluoroethanol (TFE) to 60% with thorough mixing
- Filter samples through a 0.2 µm regenerated cellulose membrane to remove precipitated detergent (can also centrifuge first to separate the bulk of precipitate)
- Load sample onto a C3 reverse phase HPLC column (Agilent ZORBAX 300SB-C3) pre-equilibrated with 25% HPLC buffer B
- Standard HPLC method is 25% buffer B for 5 min, ramp to 40% buffer B over 5 min, ramp to 60% buffer B over 30 min, ramp to 98% buffer B over 10 min, hold at 98% buffer B for 5 min
- FtsB elutes ~24-26 min, FtsB breakdown product elutes ~1-2 min later, and FtsL elutes ~3 min after that
- Collect fractions and immediately freeze with liquid N₂ to minimize potentially damaging interactions between the protein and TFA
- Lyophilize fractions for solvent removal and storage

Resuspension into detergent via dried film method (only needed following HPLC)

- Add 1 mL TFE to lyophilized FtsL or FtsB (in glass vial) with gentle mixing to resuspend
- Dilute a small fraction at least 1:10 into lysis buffer + >0.51 mM DDM to determine protein concentration
- Make stocks of desired detergent dissolved in TFE (in glass vial)
- Thoroughly mix FtsB TFE stock into detergent TFE stock in the desired ratio and

with the amount needed to give the desired concentration following resuspension

- Thoroughly mix in FtsL TFE stock in the desired ratio
- Evaporate TFE from mixtures under N₂ gas (or Ar gas) until a dried film is formed
(try to spread out the film as much as possible in the glass vial)
- Leave overnight in a vacuum chamber to fully remove TFE
- Resuspend film in the desired buffer with the volume needed to give the desired concentration
- Re-determine concentration of sample

Appendix 2 – X-ray crystallography trials

As discussed in Chapter 5, I invested a significant portion of my graduate school career into an X-ray crystallography project to obtain structures for the periplasmic region of FtsLB and/or FtsQLB. This project was a continuation of work performed by a previous Senes lab graduate student, Loren LaPointe, and was in collaboration with the Ivan Rayment lab (specifically, the graduate students Becky Phillips and Michael Andreas). Although the various screens I performed did not result in any usable crystals, I really only scratched the surface of potential directions to take this project. A variety of other protein constructs and crystallization conditions remain to be tested, and the potential for obtaining sorely-needed FtsLB structural information provides (in my opinion) sufficient rationale for continuing this project. Below, I present the various constructs originally designed by Loren and myself for crystallization trials (Table A2.1) and discuss the different approaches I took with some of these. NEMO/IKK fusions to FtsB and FtsL, respectively, forced a 2:2 heterotetrameric arrangement, whereas E5/K5 fusions resulted

Plasmid name	Plasmid description
SNB (NB after Tev)	Strep-Tev-NEMO-FtsB(22-103)
HNB	His-Tev-NEMO-FtsB(22-103)
SNB-GS	Strep-Tev-NEMO-GS-FtsB(22-103)
HNB-GS	His-Tev-NEMO-GS-FtsB(22-103)
SN(C54L)B	Strep-Tev-NEMO(C54L)-FtsB(22-103)
SN(C54L)B-GS	Strep-Tev-NEMO(C54L)-GS-FtsB(22-103)
HN(C54L)B-GS	His-Tev-NEMO(C54L)-GS-FtsB(22-103)
HIL51 (IL51 after Tev)	His-Tev-IKK-FtsL(51-121)
HIL55	His-Tev-IKK-FtsL(55-121)
SIL55	Strep-Tev-IKK-FtsL(55-121)
HIL58-1A	His-Tev-IKK-Ala-FtsL(58-121)
HIL58-3A	His-Tev-IKK-AAA-FtsL(58-121)
SIL58-3A	Strep-Tev-IKK-AAA-FtsL(58-121)
HIL58-GS	His-Tev-IKK-GS-FtsL(58-121)
SIL58-GS	Strep-Tev-IKK-GS-FtsL(58-121)
HIL58-4fl	His-Tev-IKK-GSGA-FtsL(58-121)
SIL58-4fl	Strep-Tev-IKK-GSGA-FtsL(58-121)
pSJC070	Strep-Tev-NEMO-FtsB A91stop
pSJC071	Strep-Tev-NEMO-FtsB Y85stop
pSJC072	Strep-Tev-NEMO-FtsB A71stop
pSJC073	His-Tev-IKK-FtsL N116stop
pSJC074	His-Tev-IKK-FtsL H109stop
pSJC075	His-Tev-IKK-FtsL T102stop
pSJC076	His-Tev-IKK-FtsL S95stop
pSJC077	His-Tev-IKK-FtsL E88stop
pSJC078	His-Tev-IKK-FtsL E88K
pSJC081	Duet_Strep-Tev-E5-FtsB_His-Tev-K5-FtsL
FtsQ-long	His-Tev-FtsQ(49-276)
FtsQ-med (pSJC128)	His-Tev-FtsQ(58-276)
FtsQ-short	His-Tev-FtsQ(58-260)

Table A2.1. FtsB, FtsL, and FtsQ constructs used for X-ray crystallography and on-column binding experiments.

in a 1:1 heterodimeric arrangement. My intention is that this may serve as a guide so that anyone who continues this project will have some idea of how to proceed and know what not to repeat.

Expression and purification of FtsLB and FtsQ constructs

Below, I have included general protocols for the expression/purification of soluble FtsLB and FtsQ. These have not been intensively optimized, so changes can be made.

Expression

- Transform BL21(DE3) cells with FtsLB constructs or C41(DE3) cells with FtsQ constructs and plate overnight at 37°C on LB agar with appropriate antibiotics
- Scrape/wash colonies off plate into one or more 4 L flasks containing 1 L of LB plus 1 mM MgSO₄ and appropriate antibiotics
- Grow at 37°C until O.D.₆₀₀ reaches ~0.8-1.0, then induce expression with 1 mM IPTG at 18°C overnight (FtsLB) or 25°C for 6 hrs (FtsQ)
- Pellet cells on JLA-8.1000 rotor at 2000 x g for 20 min at 4°C
- Resuspend cells in 100 mM NaCl + 10 mM HEPES pH 8.0 (cell wash buffer) and combine into a single flask
- Re-pellet cells again
- Scoop into liquid N₂ and store at -80°C

Lysis via sonication and cell fraction separation

- Follow the same general protocols as provided in Appendix 1
- Include 150 mM NaCl in the lysis buffer for FtsQ constructs since it helps prevent the protein from crashing out
- Since these are soluble constructs, the initial spin at 10,000 x g is not needed

Purification via Ni-NTA and Strep-Tactin XT resin

- Again, follow the same general protocols as provided in Appendix 1
- Everything should be kept at 4°C at all times
- Batch binding is less necessary since soluble proteins tend to bind columns better
- Detergent is obviously not needed for soluble proteins
- Collect large elution fractions for FtsQ to reduce concentration and minimize precipitation
- Protein should be dialyzed into desired buffers and then concentrated
 - FtsLB constructs can generally be concentrated >10 mg/mL without any noticeable precipitation
 - FtsQ constructs tend to start precipitating >8 mg/mL, though inclusion of 150 mM NaCl in dialysis buffer can help minimize this
- Filter with 0.2 µm membrane then drop into liquid N₂ as ~30 uL beebees before storing at -80°C
- After thawing, filter and confirm concentration again before setting crystallization trays

General screens

Using the Rayment lab 144-condition screening collection at both room temperature and 4°C, I performed general crystallization screens (hanging drop method) on the following construct mixtures: NB + IL58-GS, NB + IL58-4fl, NB + IL58-4fl + FtsQ-short with and without 0.5 M trimethylamine oxide cryoprotectant, SNB + HIL58-4fl, and SNB + HIL58-4fl + FtsQ-short. I also modified the surface lysines of NB + IL58-4fl + FtsQ-

short using reductive methylation. I obtained crystals (Fig. A2.1) for NB + IL58-4fl + FtsQ-short in 100 mM Tris EDTA buffer pH 8.0 + 10.4% polyethylene glycol (PEG) 8K + 224 mM MgSO₄ (small plates) at both room temperature and 4°C (extracted, solubilized, and ran on SDS-PAGE to confirm presence of all three proteins; data not shown) as well as in 100 mM Hepps buffer pH 8.0 + 2.4 M AmPO₄(8) (long needles) at room temperature. I set up refinement screens and different additive screens for these conditions and managed to reproduce crystals in some conditions, but the size/shape of the crystals never improved and the overall reproducibility was very inconsistent. Ultimately, I decided to move on to different constructs, but the small success when FtsQ was present indicates that it may be needed to help organize the C-terminus of FtsLB and enable crystallization. After the limited success with the NEMO/IKK fusions, I

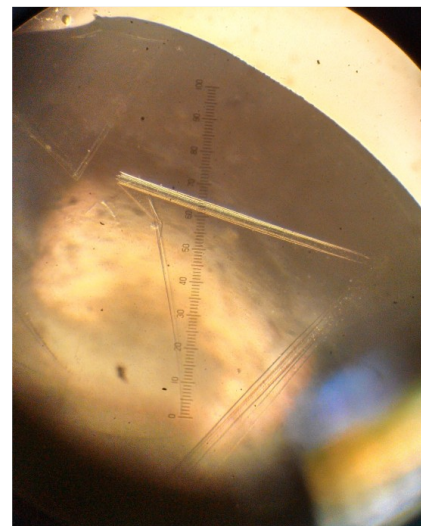
a**b**

Figure A2.1. Examples of NB + IL58-4fl + FtsQ-short crystals resulting from the 144-condition general screen. a) Small plates obtained in 100 mM Tris EDTA buffer pH 8.0 + 10.4% PEG 8K + 224 mM MgSO₄. b) Long needles obtained in 100 mM Hepps buffer pH 8.0 + 2.4 M AmPO₄(8).

realized that a dimeric arrangement for FtsLB may improve crystal formation by reducing the size of the complex and potentially minimizing conformational flexibility. A postdoctoral researcher in the lab, Elizabeth Caselle, was working on such a construct pair (E5/K5 fusions based on constructs previously described (1)), and at this point, she took charge of the crystallization efforts. The details are provided in her notebook and in her lab server folder (/data06/bcaselle/, at the time of writing), but in short, she was able to produce larger FtsQLB crystals that, unfortunately, did not diffract to a usable resolution.

I have a sneaking suspicion that the lack of success that Beth and I faced stems in part from FtsQ-FtsLB binding at a single location (the C-terminus), so FtsQ is likely to not be well packed against FtsLB throughout the complex. This is supported by small-angle X-ray scattering data from our lab (data not shown) and others (2) that indicates that soluble FtsQ binds soluble FtsLB in an apparent antiparallel manner, likely due to the absence of transmembrane regions that would normally enforce a parallel arrangement. Introduction of cysteine residues near the N-termini of FtsQ and FtsLB could result in formation of disulfide bridges that force those ends to remain in close proximity, and this is likely one of the initial directions I would take this project were I to resume it.

FtsQLB binding studies

I also performed Ni-NTA on-column binding assays to confirm direct interactions between some of the FtsLB and FtsQ constructs used for crystallization trials. As shown in Fig. A2.2, His-tagged FtsQ-short retained untagged NB + IL58-4fl on Ni-NTA resin in an approximately 1:1:1 ratio, which indicates formation of a complex containing all three

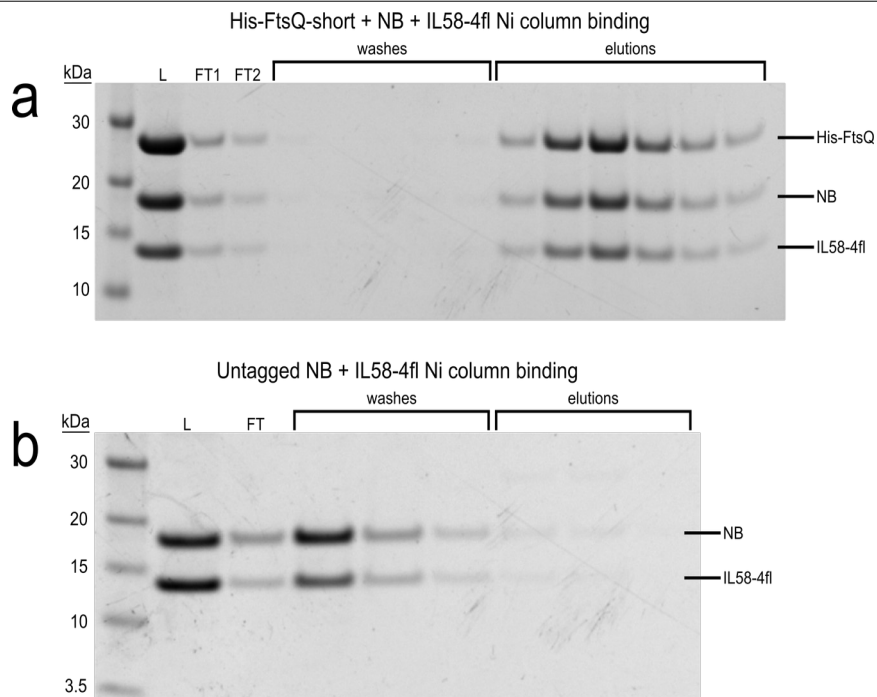


Figure A2.2. Ni-NTA binding experiments to show binding between soluble FtsLB and FtsQ constructs. a) His-tagged FtsQ-short retains untagged NEMO-FtsB(22-103) (NB) and IKK-GSGA-FtsL(58-121) (IL58-4fl) until the elution fractions, indicating formation of an FtsQLB complex. b) NB + IL58-4fl does not bind non-specifically to the column. “L” refers to column load; “FT” refers to flowthrough fraction. Molecular weight markers are included to the left.

proteins. I also performed similar experiments with NB + IL58-GS that gave essentially the same results (data not shown). Finally, I tested FtsQ binding with a series of soluble FtsLB constructs containing C-terminal truncations in FtsB (pSJC070 – pSJC072) or FtsL (pSJC073 – pSJC077). The FtsB truncations indicate that removing residues 85–103 of FtsB (pSJC071) results in loss of FtsQ binding (data not shown), which corresponds to prior *in vivo* work (3). The FtsL truncations, on the other hand, did not result in loss of FtsQ binding (data not shown), though the diminishing expression levels

for truncations of increasing severity made confirming this difficult. Previous research has shown that the FtsL C-terminal tail strengthens the interaction with FtsQ and is needed for cell division to occur (4), by my work indicates that it is not completely necessary for formation of FtsQLB *in vitro*.

References

1. Glas M, van den Berg van Saparoea HB, McLaughlin SH, Roseboom W, Liu F, Koningstein GM, et al. The Soluble Periplasmic Domains of Escherichia coli Cell Division Proteins FtsQ/FtsB/FtsL Form a Trimeric Complex with Submicromolar Affinity. *J Biol Chem.* 2015 Aug 28;290(35):21498–509.
2. Choi Y, Kim J, Yoon H-J, Jin KS, Ryu S, Lee HH. Structural Insights into the FtsQ/FtsB/FtsL Complex, a Key Component of the Divisome. *Sci Rep.* 2018 24;8(1):18061.
3. Gonzalez MD, Beckwith J. Divisome under construction: distinct domains of the small membrane protein FtsB are necessary for interaction with multiple cell division proteins. *J Bacteriol.* 2009 Apr;191(8):2815–25.
4. Gonzalez MD, Akbay EA, Boyd D, Beckwith J. Multiple interaction domains in FtsL, a protein component of the widely conserved bacterial FtsLBQ cell division complex. *J Bacteriol.* 2010 Jun;192(11):2757–68.